REPORT DOCUMENTATION PAGE

1. REPORT DATE *(DD-MM-YYYY)*	2. REPORT TYPE	3. DATES COVERED *(From - To)*
10-16-2008	Final Technical Report	9/15/2005 - 5-31-2008

4. TITLE AND SUBTITLE
Foundations of Isomer Physics for Energy Applications

5a. CONTRACT NUMBER

5b. GRANT NUMBER
FA9550-05-1-0486

5c. PROGRAM ELEMENT NUMBER

6. AUTHOR(S)
James J. Carroll

5d. PROJECT NUMBER

5e. TASK NUMBER

5f. WORK UNIT NUMBER

7. PERFORMING ORGANIZATION NAME(S) AND ADDRESS(ES)
Youngstown State University
One University Plaza
Youngstown, OH 44555

8. PERFORMING ORGANIZATION REPORT NUMBER
GC93-05-3

9. SPONSORING / MONITORING AGENCY NAME(S) AND ADDRESS(ES)
USAF, AFRL /NE
AF Office of Scientific Research
4015 Wilson Boulevard, Room 713
Arlington, VA 22203-1954
Dr Tatjana Curcic

10. SPONSOR/MONITOR'S ACRONYM(S)

11. SPONSOR/MONITOR'S REPORT NUMBER(S)

12. DISTRIBUTION / AVAILABILITY STATEMENT
Unlimited

13. SUPPLEMENTARY NOTES

14. ABSTRACT
Metastable excited nuclear states, isomers, have been of strong interest for decades, with studies motivated by their physical properties and the promise of high-energy-density applications. Much research has concentrated on induced depletion processes as a potential means of controlling the release of energy stored in these isomers. This research comprises a very specialized sub-field of nuclear physics and, as such, has often suffered from a lack of connection with the larger body of more traditional studies. The YSU isomer project has taken a broad view of induced depletion studies with the aim of providing a firm foundation to this maturing field. This report reviews work conducted by this project on induced isomer depletion and related issues of nuclear structure, as exemplified by peer-reviewed publications during the grant period.

15. SUBJECT TERMS

16. SECURITY CLASSIFICATION OF:			17. LIMITATION OF ABSTRACT	18. NUMBER OF PAGES	19a. NAME OF RESPONSIBLE PERSON
a. REPORT	b. ABSTRACT	c. THIS PAGE			Peter J. Kasvinsky
Unclassified	Unclassified	Unclassified	Unlimited	100	19b. TELEPHONE NUMBER *(include area code)* 330-941-3091

FINAL TECHNICAL REPORT

INTRODUCTION

Metastable excited nuclear states, isomers, have been a major subject of inquiry since their discovery in 1921, with studies motivated in different ways by their physical properties. Isomer halflives run the gamut from rather modest (like the $T_{1/2} \sim 14$ ms shape isomer of ^{242}Am) to extremely long (like the essentially stable spin isomer ^{180m}Ta, with $T_{1/2} > 10^{16}$ years). Quite short-lived isomers also exist. In all cases, the existence of an isomer reflects specific nuclear structure that creates some type of potential barrier against electromagnetic decay of the metastable level to lower-lying states. For so-called spin isomers, it is the angular momentum arising from a particular single-particle configuration that provides such a barrier, forcing electromagnetic decays to be restricted to high multipolarities. A further inhibition for K isomers of deformed nuclei comes from a need to significantly re-orient the angular momentum vector, whose projection on the body axis of nuclear symmetry is K. A full discussion of the underlying mechanisms of isomer formation may be found in the review of Ref. [1]. The population and decay of isomers can give considerable insight into nuclear structure, as discussed in [2].

Isomers have also been of great interest for potential applications, primarily due to the ability of some isomers to store tremendous amounts of energy, e. g. the K isomer ^{178m2}Hf stores 2.46 MeV per nucleus, or about 1.2 GigaJoules/gram, with a halflife of 31 years. Its natural decay follows a complex cascade of transitions that has been clarified [3] under a previous AFOSR grant (F49620-02-1-0187), terminating at the stable ground state. Harnessing this stored energy could give a source of "clean" nuclear energy for various applications [4], including, perhaps, a gamma-ray laser. Some other isomers do not have stable ground states, but might be valuable in providing a sequence of energy-releasing β or α decays [5].

Whatever the motivation, much effort has been expended to investigate the possibility of causing an induced depletion of long-lived isomers, releasing the stored energy as a burst of gamma rays or other nuclear radiations. A number of issues come to the fore when considering this topic: what isomers would be best to examine, what mechanism(s) would allow external control or bypass of the natural decay, and how would one experimentally measure an induced depletion from small isomer samples. Of course, the experimental goal would be to measure the energy required for the entity (photons, neutrons, etc.) that caused the induced depletion and the cross section for the reaction. The production of isomers in quantities sufficient for precision experiments is also an important goal.

In 2001, an extensive review [5] discussed the general topic with a focus on depletion induced by photons and a view of the related systematics as deduced from the closely-related "activation" of isomers. Just one isomer exists in nature (^{180m}Ta) and its induced depletion has been conclusively demonstrated, largely under previous AFOSR grants to the PI (see Refs. [6-8] and references therein). Up to now the main method of predicting possible depletion energies for other isomers was to consider their relationship to the systematics of isomer activation for neighboring isotopes and to depletion levels

found to depopulate ^{180m}Ta. This approach was most notably used in the case of the 31-year isomer of ^{178}Hf. It was suggested in 1995 that on this basis a trigger level might be found "near 2.8 MeV" [9] from the "speculation that [depletion] levels are prevalent and lie between 2.5 - 2.8 MeV" [10]. First depletion experiments were attempted in 1996 by inelastic scattering of alpha particles at Orsay, with a repeat in 1997, but as yet no firm results are known and the data are unavailable for analysis. The first photon depletion experiments began in late 1998 and the positive indications reported therefrom [11, 12] began an intense, and controversial, period of research as reviewed in Ref. [13].

The field of study of induced isomer depletion has now moved into a new era, defined by less reliance on systematics predictions and utilizing greatly improved spectroscopic level data. With the ability to identify and target specific potential depletion transitions, one can anticipate a greatly increased pace of research. Within this context, the work conducted by the YSU Isomer Physics Project under AFOSR support has provided a considerable base of fundamental knowledge and has significantly advanced the field. Such basic information as cross sections for different reaction mechanisms is central to any evaluation of the feasibility of isomers for applications.

A total of twelve manuscripts have been published during this grant. Also, three plenary, six invited and two contributed presentations by the PI resulted from grant sponsorship and a number of contributed presentations/posters were made by undergraduate students supported thereby.

The essential technical details of the papers may be found in Appendix A while Appendices B and C list Invited and Contributed Presentations, respectively, under this grant period.

HIGHLIGHTS OF PUBLISHED RESULTS

Experimental tests of induced isomer depletion occupy a rather narrow sub-field within nuclear physics. As such, this work is somewhat removed from the mainstream of nuclear physics and has suffered from a perceived lack of firm founding in traditional, experimentally-verified concepts of the larger field. Work conducted during this grant has contributed significantly to the foundations of induced isomer depletion and explored several new concepts. A few recent highlights will be given to indicate the breadth and depth of these efforts.

"Nuclear Forward Scattering vs. Conventional Mössbauer Studies of Atomically Tailored Eu-Based Materials," Konjhodzic, A. Adamczyk, F. Vagizov, Z. Hasan, E. E. Alp, W. Sturhahn, Jiyong Zhao and J. J Carroll, Hyperfine Int. 170, 83 (2006).

Summary:

This paper discussed experiments utilizing synchrotron radiation to perform Mössbauer spectroscopy on ^{151}Eu-doped magnesium sulfide. While the immediate impact was for the study of nano-scale devices composed of this or similar materials, the same physical processes may prove useful in coherent

control of nuclear processes, as discussed in detail in Kolesov, et al., Opt. Commun. 179, 537 (2000).

"Microsecond and nanosecond isomers populated in fission reactions," G. A. Jones, P. M. Walker, Zs. Podolyak, P. H. Regan, S. J. Williams, M. P. Carpenter, J. J. Carroll, R. S. Chakrawarthy, P. Chowdhury, I. J. Cullen, G. D. Dracoulis, A. B. Garnsworthy, G. Hackman, R. V. F. Janssens, T. L. Khoo, F. G. Kondev, G. J. Lane, Z. Liu, D. Seweryniak, N. J. Thompson and S. Zhu, FUSION06: International Conference on Reaction Mechanisms and Nuclear Structure at the Coulomb Barrier, AIP Conference Proceedings 853 (Springer, New York, 2006), p. 342.

Summary:

This paper provided an overview of an experiment performed to investigate electromagnetic transitions, and thus nuclear structure, of the isotope ^{178}Hf. In addition, incidental excitation of antimony and molybdenum nuclei was produced with resulting data on their structure. More detailed analyses followed later, but this paper illustrated the strength of fusion-fission reactions and coincidence gamma-ray spectroscopy as tools for the study of nuclear transitions. Such transitions in appropriate nuclei may provide the means for induced depletion of isomers.

"Design and characterization of a compact multi-detector array for studies of induced gamma emission: Spontaneous decay of ^{178m2}Hf as a test case," P. Ugorowski, R. Propri, S. A. Karamian, D. Gohlke, J. Lazich, N. Caldwell, R. S. Chakrawarthy, M. Helba, H. Roberts and J. J. Carroll, Nuclear Instruments and Methods A 565, 657 (2006).

Summary:

Some published reports (see the survey in Ref. [13]) have claimed evidence that induced depletion of the ^{178m2}Hf isomer could be caused by incident photons 10 keV. To investigate these claims with improved sensitivity, a final implementation of the YSU miniball array was utilized at the BL12B2 beamline at SPring-8. This paper gave a fully-detailed characterization of the miniball system based largely on using natural decay of ^{178m2}Hf. The purpose was to provided a baseline of natural events from which to compare measurements obtained during irradiations.

"Identification of a high-spin isomer in ^{99}Mo," G. A. Jones, P. H. Regan, P. M. Walker, Zs. Podolyak, P. D. Stevenson, M. P. Carpenter, J. J. Carroll, R. S. Chakrawarthy, P. Chowdhury, G. D. Dracoulis, A. B. Garnsworthy, G. Hackman, R. V. F. Janssens, T. L. Khoo, F. G. Kondev, G. J. Lane, Z. Liu, D. Seweryniak, N. J. Thompson, S. Zhu and S. J. Williams, Phys. Rev. C 76, 047303 (2007).

Summary:

This paper discussed the experimental identification of a new, high-spin isomer in ^{99}Mo based on nuclear spectroscopic data obtained in fusion-fission reactions with coincidence gamma-ray spectroscopy. Similar techniques may be valuable in searching for transitions that will permit an induced depletion of isomers.

"Nuclear structure and the search for induced energy release from isomers," J. J. Carroll, Nucl. Instrum. Meth. B 261, 960 (2007).

Summary:

This paper summarized the current state-of-the-art in experimental techniques available for the study of induced isomer depletion.

"Photon scattering experiments on the quasistable, odd-odd mass nucleus ^{176}Lu," S. Walter, F. Stedile, J. J. Carroll, C. Fransen, G. Friessner, N. Hollmann, H. von Garrel, J. Jolie, O. Karg, F. Käppeler, U. Kneissl, C. Kohstall, P. von Neumann-Cosel, A. Linnemann, D. Mücher, N. Pietralla, H. H. Pitz, G. Rusev, M. Scheck, C. Scholl, R. Schwengner, V. Werner and K. Wisshak, Phys. Rev. C 75, 034301 (2007).

Summary:

This paper reported the measurement of electromagnetic transition probabilities and energies for the isomeric nucleus ^{176}Lu.

SUMMARY

The feasibility of isomers for real applications will depend sensitively upon specific nuclear parameters, such as the energies of depletion levels. Nuclear theory cannot accurately predict the probabilities for transitions that would allow isomeric nuclei to be excited into depletion levels, nor branching ratios for decay of those levels. Thus, it remains for experimental studies to measure these important parameters using state-of-the-art techniques. In some instances, this may be accomplished by direct depletion tests made with samples already containing populations of isomers, while in other instances this may be accomplished by more traditional nuclear spectroscopic studies utilizing samples containing ground-state nuclei. The ability to connect the results from these different methods is critical to providing a firm foundation of fundamental knowledge from which the practical value of isomers may be assessed. This task is not yet complete. However, work performed under this grant has greatly improved the understanding of the mechanisms by which induced isomer depletion may be achieved for various nuclei, and has placed this field on a firm footing. The challenge of further advancing this field will fall to future research efforts.

REFERENCES

1. P. M. Walker and G. Dracoulis, Nature **399**, 35 (1999).

2. P. M. Walker and J. J. Carroll, Physics Today, 39 (June 2005).
3. M. B. Smith, P. M. Walker, G. C. Ball, et al., Phys Rev. C **68**, 031302(R) (2003).
4. H. Roberts, Hyperfine Int. **107**, 91 (1997).
5. J. J. Carroll, S. A. Karamian, L. A. Rivlin, et al., Hyperfine Int. **135**, 3 (2001).
6. D. Belic, C. Arlandini, J. Besserer, et al., Phys. Rev. Lett. **83**, 5242 (1999).
7. D. Belic, C. Arlandini, J. Besserer, et al., Phys. Rev. C **65**, 035801 (2002).
8. P. M. Walker, G. D. Dracoulis and J. J. Carroll, Phys. Rev C **64**, 061302 (2001).
9. C. B. Collins and J. J. Carroll, Laser Phys. **5**, 209 (1995).
10. C. B. Collins, J. J. Carroll, Yu. Ts. Oganessian, et al., Laser Phys. **5**, 280 (1995).
11. C. B. Collins, F. Davanloo, M. C. Iosif, et al., Phys. Rev. Lett. **82**, 695 (1999).
12. C. B. Collins, F. Davanloo, M. C. Iosif, et al., Laser Phys. 9, 8 (1999).
13. J. J. Carroll, Laser Phys. Lett. **1**, 275 (2004).

APPENDIX A

PUBLICATIONS DURING GRANT PERIOD

"Nuclear Forward Scattering vs. Conventional Mössbauer Studies of Atomically Tailored Eu-Based Materials," Konjhodzic, A. Adamczyk, F. Vagizov, Z. Hasan, E. E. Alp, W. Sturhahn, Jiyong Zhao and J. J Carroll, Hyperfine Int. 170, 83 (2006). **REPRINT**

"Microsecond and nanosecond isomers populated in fission reactions," G. A. Jones, P. M. Walker, Zs. Podolyak, P. H. Regan, S. J. Williams, M. P. Carpenter, J. J. Carroll, R. S. Chakrawarthy, P. Chowdhury, I. J. Cullen, G. D. Dracoulis, A. B. Garnsworthy, G. Hackman, R. V. F. Janssens, T. L. Khoo, F. G. Kondev, G. J. Lane, Z. Liu, D. Seweryniak, N. J. Thompson and S. Zhu, FUSION06: International Conference on Reaction Mechanisms and Nuclear Structure at the Coulomb Barrier, AIP Conference Proceedings 853 (Springer, New York, 2006), p. 342. **REPRINT**

"Design and characterization of a compact multi-detector array for studies of triggered gamma emission: spontaneous decay of ^{178m2}Hf as a test case," P. Ugorowski, R. Propri, S. A. Karamian, J. Lazich, D. Gohlke, N. Caldwell, S. C. Ravuri, M. Helba and J. J. Carroll, Nucl. Instrum. Meth. A 565, 657 (2006). **REPRINT**

"$K^{\pi} = 0^{+}$ 2.29 s isomer in neutron-rich ^{174}Tm," R. S. Chakrawarthy, P. M. Walker, J. J. Ressler, C. J. Pearson, G. C. Ball, D. Bandyopadhyay, E. F. Zganjar, M. B. Smith, A. N. Andreyev, S. Ashley, R. A. E. Austin, J. A. Becker, J. J. Carroll, D. S. Cross, D. Gohlke, J. J. Daoud, P. E. Garrett, G. F. Grinyer, G. Hackman, G. A. Jones, R. Kanungo, Y. Litvinov, A. C. Morton, W. J. Mills, R. Propri, C. E. Svensson, R. Wheeler and S. J. Williams, Phys. Rev. C 73, 024306-1 – 5 (2006). **REPRINT**

"Production of long-lived hafnium isomers in reactor irradiations," S. A. Karamian, J. J. Carroll, J. Adam, E. N. Kulagin, and E. P. Shabalin, High Energy Density Phys. 2, 48 (2006). **REPRINT**

"Identification of a high-spin isomer in ^{99}Mo," G. A. Jones, P. H. Regan, P. M. Walker, Zs. Podolyak, P. D. Stevenson, M. P. Carpenter, J. J. Carroll, R. S. Chakrawarthy, P. Chowdhury, G. D. Dracoulis, A. B. Garnsworthy, G. Hackman, R. V. F. Janssens, T. L. Khoo, F. G. Kondev, G. J. Lane, Z. Liu, D. Seweryniak, N. J. Thompson, S. Zhu and S. J. Williams, Phys. Rev. C 76, 047303 (2007). **REPRINT**

"Nuclear isomers: recipes from the past and ingredients for the future," P. M. Walker and J. J. Carroll, Nuclear Physics News 17, 11 (2007). **REPRINT**

"Nuclear structure and the search for induced energy release from isomers," J. J. Carroll, Nucl. Instrum. Meth. B 261, 960 (2007). **REPRINT**

"Weak *K*-hindrance manifested in alpha decay of the ^{178m2}Hf isomer," S. A. Karamian, J. J. Carroll, S. Iliev and S. P. Tretyakova, Phys. Rev. C 75, 057301 (2007). **REPRINT**

"Photon scattering experiments on the quasistable, odd-odd mass nucleus ^{176}Lu," S. Walter, F. Stedile, J. J. Carroll, C. Fransen, G. Friessner, N. Hollmann, H. von Garrel, J. Jolie, O. Karg, F. Käppeler, U. Kneissl, C. Kohstall, P. von Neumann-Cosel, A. Linnemann, D. Mücher, N. Pietralla, H. H. Pitz, G. Rusev, M. Scheck, C. Scholl, R. Schwengner, V. Werner and K. Wisshak, Phys. Rev. C 75, 034301 (2007). **REPRINT**

"Prospects for coherently driven nuclear radiation by coulomb excitation," S. A. Karamian and J. J. Carroll, Laser Physics 17, 80 (2007). **REPRINT**

"High-spin, multi-particle isomers in ^{121,123}Sb," G. A. Jones, S. J. Williams, P. M. Walker, Zs. Podolyak, S. Zhu, M. P. Carpenter, J. J. Carroll, R. S. Chakrawarthy, P. Chowdhury, I. J. Cullen, G. D. Dracoulis, A. B. Garnsworthy, G. Hackman, R. V. F. Janssens, T. L. Khoo, F. G. Kondev, G. J. Lane, Z. Liu, D. Seweryniak and N. J. Thompson, Phys. Rev. C 77, 034311 (2008). **REPRINT**

Hyperfine Interact (2006) 170:83–89
DOI 10.1007/s10751-006-9470-7

Nuclear forward scattering vs. conventional Mössbauer studies of atomically tailored Eu-based materials

A. Konjhodzie · A. Adamczyk · F. Vagizov · Z. Hasan · E. E. Alp · W. Sturhahn · Jiyong Zhao · J. J. Carroll

Published online: 9 January 2007

Abstract With the decrease in size of devices, rapid characterization of nano-devices is an inevitable necessity. It is shown that Mössbauer spectroscopy using synchrotron radiation from the advanced photon source provides such a tool of investigation. Results are presented and compared for conventional Mössbauer and Nuclear Forward Scattering for ^{151}Eu-doped magnesium sulfide as an example, especially at low concentrations.

Key words europium · nuclear forward scattering · Mössbauer spectroscopy · atomic tailoring · photonic materials · rare-earths

1 Introduction

Mössbauer spectroscopy is an extremely powerful technique of characterization for samples rich in iron and a few other isotopes. Using this method, different valence states of these isotopes as well as small variations in the crystalline field environment around them in a solid can be studied systematically and rapidly. As the size of the sample becomes microscopic, or the concentration of Mössbauer active nuclei decreases, the technique loses its effectiveness. In such cases, at least a lengthy data accumulation to enhance the signal to noise ratio becomes compulsory. However, for some experiments, the data accumulation time becomes prohibitively long. In this category, there are experiments performed on samples with extremely low concentrations of Mössbauer active ions or the ones that show extremely small effects resulting in the signal being buried in the noise. Nuclear Forward Scattering (NFS) using X-rays or γ-rays from a synchrotron source offers an alternative to

A. Konjhodzie · A. Adamczyk · F. Vagizov · Z. Hasan (✉)
Physics Department, Temple University, Philadelphia, PA 19122, USA
e-mail: zhasan@temple.edu

E. E. Alp · W. Sturhahn · J. Zhao
Advanced Photon Source, Argonne National Laboratory, Argonne, IL 60439, USA

J. J. Carroll
Department of Physics & Astronomy, Youngstown State University, Youngstown, OH 44555, USA

the conventional Mössbauer technique [1–3]. The radiation from the synchrotron source is intense, tunable in energy, and in the form of short pulses to provide the opportunity of time domain γ-ray spectroscopy.

This paper deals with the application of Mössbauer spectroscopy in identifying samples doped with Eu and its different valence states in extremely low concentrations in alkaline earth sulfides. We discuss the case of MgS in particular. Low concentrations of impurities are necessary for photonics applications where the impurity atoms or ions should be isolated from each other. These isolated atoms/ions have well defined energy levels that can be used for the desired applications. At high concentrations, however, pair effects arising from Coulomb or exchange interactions can significantly change the energy level structure from a single ion to a more complicated one. In general, these pairs are difficult to deal with theoretically and unpredictable for any practical use.

Typical impurity concentrations for photonics applications range around 0.01 mol% while the size of the Photonic devices can be as small as a few cubic microns. Using conventional Mössbauer spectroscopy, weeks or months of data accumulation time would be needed for such samples. This is partly because strong ^{151}Sm sources are not readily available. Therefore, synchrotron radiation offers a great opportunity to study the Mössbauer spectrum by nuclear forward scattering. A comparison of the Mössbauer spectroscopy between using a conventional ^{151}Sm source and the synchrotron radiation source is presented below.

2 Atomically tailored photonics materials

The size of photonic devices is always decreasing and in many cases has reached the quantum regime. In principle, the ultimate lower limit on the size of a photonic device is a single atom. However, to be useful this atom should be localized and optically addressable. Such is the case with optically active impurities in a wide bandgap semiconductor or an insulator. Therefore, in the future, only a few selected optically active atoms or ions in a solid will form the 'core' of the quantum photonic devices. Some fascinating applications that could work with only a few atoms in a solid host are: (1) spectral storage, where the information is stored in the optical spectrum of a small number of selected atoms in a solid, (2) quantum computing with a few optically addressable atoms, and, (3) coherent control of nuclear states with a laser [4–7]. In all these and similar atomic scale applications, there are severe constraints imposed on the energy level structure of the host, the optically active ion, its nucleus, and even the nuclei of the host material.

In spectral storage, for example, the electronic states should be tailored to strongly absorb the photons from a laser, the photons that are used for addressing or photo-transforming the ions. The energy of the optical transition should be tailored to be preferably in the range of commercial lasers. The electronic states should be suitably located in the bandgap of the host to enhance (or in some cases to suppress) two-photon ionization and other non-linear optical processes. And finally, the relative concentration of different ionization states of the active ion should be controlled to facilitate a particular photo-induced transformation.

For spectral storage, MgS and CaS were prepared with a very low concentration of Eu, 0.01 mol%. In these europium based II–VI sulfides, the information is stored in the spectrum of Eu^{2+} by photoionizing them with a laser. A relatively large concentration of Eu^{3+} is necessary for trapping the electrons liberated in the process of photoionization.

Therefore, doubly and triply positive valenee states and the electronie energy levels of Eu were tailored to meet the requirements of an ideal material for spcetral storage. It is not possible to determine the relative eoneentration of Eu^{2+}/Eu^{3+} in MgS using optieal techniques. This is partieularly true at low Eu eoneentrations. Eu^{3+} has weakly allowed optieal transitions within the states of $4f^6$ eonfiguration. Coineidently, very strongly allowed 4f–5d transitions of Eu^{2+} also lie around the samc energy range in this host. The two spectra overlap considerably and any quantitative determination of relative Eu^{2+}/Eu^{3+} eoneentrations is not possible. However, ^{151}Eu (nat. abun. ~48%) is a Mössbauer isotope. Therefore, this teehnique ean provide the information about the Eu^{2+}/Eu^{3+} eoneentration ratio.

Samples of MgS doped with varying concentrations of Eu wcrc prepared by the methods deseribed elsewhere [8, 9]. The laser-excited fluorescence spectra at ~15 K gave strong $4f^7$–$4f^65d^1$ emission eonfirming the presenee of Eu^{2+} in the sample. In MgS, Eu^{2+} substitutes for Mg^{2+} and therefore it is an encrgetieally more favored ionization state of Eu. Eu^{3+} ean also oeeupy a substitutional site with eharge eompensation provided by long-range displaeement of the lattiee ions. This displaeement maintains the eubie site symmetry and, therefore, both Eu^{2+} and Eu^{3+} oeeupy sites of oetahedral symmetry [10]. A slight variation from the eubie symmetry is there, whieh is expected due to the size mismateh between Eu^{2+}/Eu^{3+} and Mg^{2+}, the ion for whieh they substitute in the lattiee (Ionie radii: 1.17, 0.95 and 0.72 Å, respeetively, for Eu^{2+}, Eu^{3+} and Mg^{2+}). This relaxes the eubic seleetion rules for the 4f–5d electronie transition resulting in very strong Zero Phonon Lines (ZPL) in the optieal absorption spcetrum; an attribute of great importanee for quantum photonic applieations.

3 Mössbauer speetroseopy of ^{151}Eu in MgS

Mössbauer spectra of MgS:Eu samples, with naturally abundant Eu, (^{151}Eu:^{153}Eu, 0.478:0.522), were taken using a $^{151}SmF_3$ souree. Figure 1 shows the speetrum of $Mg_{0.8}Eu_{0.2}S$ at room temperature. The data aeeumulation was done in the eonstant velocity mode. It lasted for 14 h to give a signal of 8% absorption. The absorption speetrum shows a peak at 11.7 mm/s eorresponding to $^{151}Eu^{2+}$. A small shoulder is also elearly visible on the high velocity side, v=13.9 mm/s. The data has been fitted to two Lorentzian lines and has been resolved in thc diagram. Due to the broad linewidth of the SmF_3 source, ~2 mm/s, this feature eannot be further resolved, even at low temperature. The origin of this small peak has not been investigated in detail here. However, such features could arise from non-standard Eu^{2+} – eenters that could be formed due to the traee impurities. Our sample, MgS, is partieularly prone to sueh impurities – it readily absorbs water from the environment and is known to form oxygen-assoeiatcd Eu centers. Also, prolonged Mössbauer experiments expose the sample to such elements more easily. The sample is in the form of polyerystalline powder where the surfaee to volume ratio is high and small traees of water ean be absorbed readily.

The speetrum in Fig. 1 does not show any trace of Eu^{3+} resonanee whieh in this host should appear at ~0 mm/s. This elearly indieates that almost all Eu, 95(±5)% is in the form of Eu^{2+}. The uneertainty of ±5% is due to the poor signal to noise ratio of the absorption. The line-fitting of the speetrum in Fig. 1 shows that 88(±1)% of Eu^{2+} is at the normal substitutional site and the remaining 12(±1)% is at a site assoeiated with some impurity. In our ease, oxygen usually does not appear as an impurity. The appearanee of this shoulder, therefore, could be attributed to prolonged exposure of the sample to the environment. Optieal investigations on this sample are underway in our group.

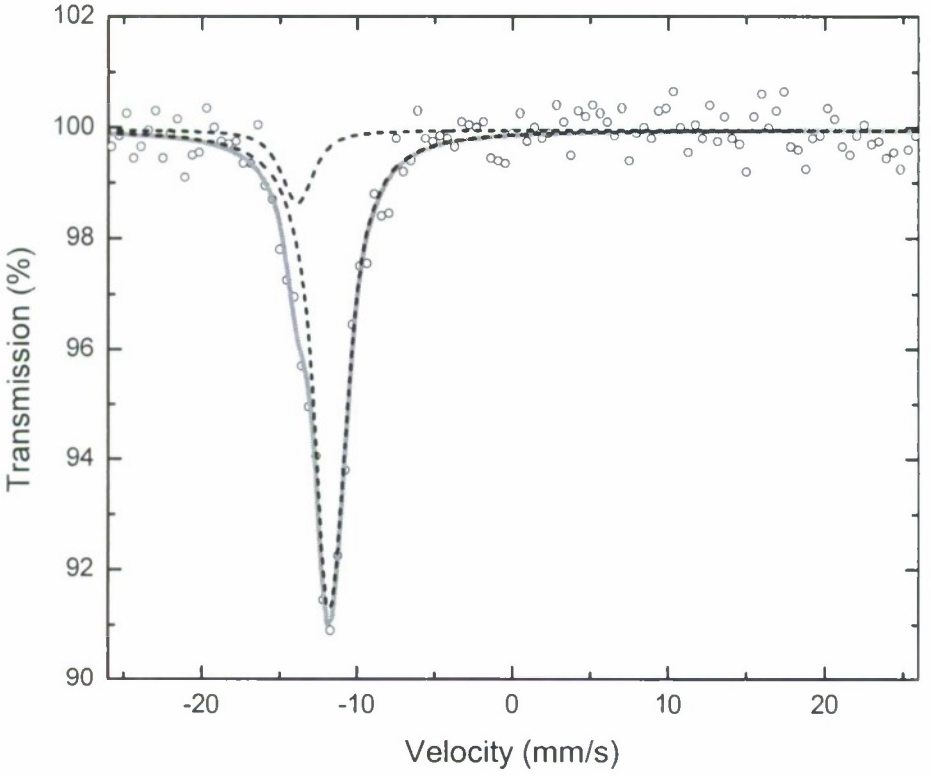

Fig. 1 Mössbauer spectrum of MgS:Eu (20%), data acquisition time 14 h. The data can be fitted to *two lines*, arising from two different Eu^{2+} centers as shown by the *dotted lines* (Isomer shifts: 13.9 and 11.7 mm/s, linewidths: 2.4 and 2.2 mm/s). The relative contribution of these two centers is 88% and 12%

Figure 2 shows the Mössbauer spectrum of MgS with 0.01 mol% of Eu. The spectrum was taken under exactly the same conditions as the experiment of Fig. 1. However, there were two exceptions: (1) the data accumulation was carried out for a period of 6 days. (2) the sample thickness was increased to 2 mm as opposed to ~0.5 mm for 20% Eu sample. The Eu^{2+} resonance at −12.6 mm/s is ~5% absorption above the noise level and the Eu^{3+} signal is clearly visible at +0.5 mm/s. Within the resolution of the absorption lines, the two lines appear as isolated single lines. By comparing the area under the two resonances, the ratio of $Eu^{2+/}$ Eu^{3+} is ~0.65/0.35 in this sample. A single line for Eu^{2+} further means that for this sample there is only one dominant Eu^{2+} site, i.e., the substitutional cubic site with Eu^{2+} replacing Mg^{2+}. The broadening of Mössbauer resonances could also be due to the temperature effects and quadrupole splittings of Eu^{3+} that are in the tens of MHz range. However, these effects are beyond the resolution of our SmF_3 source.

4 Nuclear forward scattering of MgS:Eu

Mössbauer studies, using the synchrotron at the Advanced Photon Source (APS), Argonne National Laboratory were performed on the same samples as used in Figs. 1 and 2.

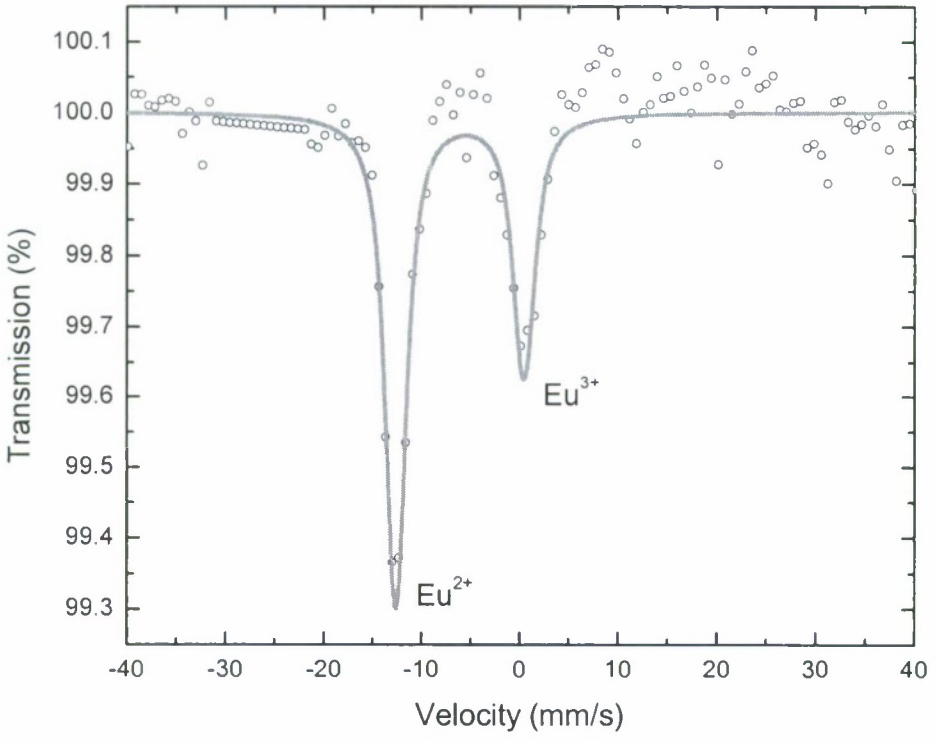

Fig. 2 Mössbauer spectrum of MgS:Eu (0.01 mol%) using a $^{151}SmF_3$ source, data acquisition time 6 days. Isomer shifts for Eu^{2+} and Eu^{3+} signals are, respectively, −12.6 and +0.5 mm/s. The corresponding linewidths are 2.4 and 2.6 mm/s, respectively

Figure 3 shows the nuclear forward scattering data on 20% Eu sample. The details of the experiments and the characteristics of the beam are described elsewhere [11]. To observe the beating of Eu^{3+} and Eu^{2+} signals over the time, a known amount of Eu_2O_3 was mixed in MgS:Eu (20 %) sample which predominantly had europium as Eu^{2+}. The CONUSS program [12] was used for fitting the decay of the beating signal. The fitting shown as the dashed curve in Fig. 3 used the relative Isomer Shift (IS=−12.8 mm/s), quadrupole splitting for Eu^{3+} (2.1 mm/s) and the relative concentration of Eu^{2+}: Eu^{3+} (0.35:0.65) from the known value from the data of Fig. 1. Only small variations, within the errors of determining these parameters were found to give the best fit. The isomer shift used in Fig. 3 is different from that used in Fig. 1, as we have not considered two different Eu^{2+} centers present in the sample as was clearly seen in Fig. 1. Secondly, in NFS (Fig. 3) we see relative isomer shift between Eu^{2+} in MgS and Eu^{3+} in Eu_2O_3 rather than SmF_3 (Fig. 1).

The total data accumulation time was 20 min for the spectrum of Fig. 3. This direct comparison between conventional Mössbauer and Nuclear Forward Scattering gives a ratio of 24. Roughly this is a factor by which the time of experiment is reduced from conventional Mössbauer to the Mössbauer studies using the time domain Nuclear Forward Scattering. In MgS samples with 0.01 mol% Eu the NFS experiment required a data collection time of about 6 h to give a good beating signal between the Eu^{3+} and Eu^{2+} resonances as opposed to 6 days of collection time for the conventional Mössbauer spectra of Fig. 2. Once again this is roughly a reduction by a factor of 24. However, note in these estimates, the ratio of the sizes of the samples is not taken into consideration. NFS is a very

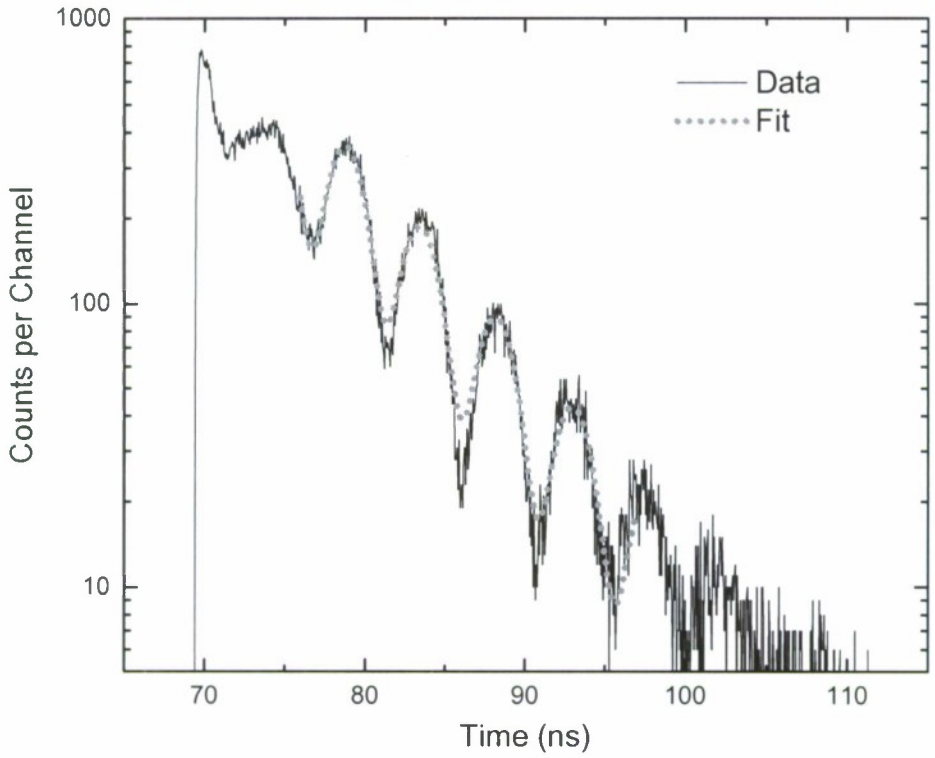

Fig. 3 Nuclear forward scattering using 21.54 keV radiation for ^{151}Eu from the APS. The sample was 70.7 μm thick and was composed of MgS:Eu (20%) mixed with Eu_2O_3 for observing the beating of the Eu^{3+} and Eu^{2+} signals. The relative concentration Eu^{3+}:Eu^{2+} was 0.65:0.35 and the data was accumulated for 20 min. The fitting of the decay with CONUSS program yielded relative isomer shift of −12.8 mm/s and the quadrupole splitting of 2.1 mm/s

sensitive technique and the sample thicknesses used were ~50–100 μm, smaller by an order of magnitude than what were used for the conventional Mössbauer experiments. If this is taken into consideration, then by using NFS assisted Mössbauer, the overall data collection times are reduced by more than two orders of magnitude. Thus, thin samples such as films, or samples with a very small concentration of Mössbauer isotopes are at a greater advantage with regard to the expediency of data accumulation in NFS assisted Mössbauer.

5 Conclusions

In conclusion, we have shown that Nuclear Forward Scattering using fast pulses from a synchrotron source has great promise for fast characterization. In MgS:Eu, the valence states of Eu and their electronic states have been tailored for extremely low concentration samples that are necessary for some photonic applications. We have presented and compared data on Mössbauer studies by the conventional technique and using nuclear forward scattering in this material. The main advantage of NFS is that it reduces the data collection times by orders of magnitude when compared to the conventional Mössbauer technique. This is hoped to enable quick characterization studies on samples that have extremely small

amounts of Mössbauer isotopes. Even more excitingly, with such reduction in data accumulation times it is hoped that some very novel experiments can be performed where small effects are supposed to give very weak observable signals. Such weak signals necessitate prohibitively long data acquisition times. One of these experiments is the laser control of nuclear states. In this experiment a strong laser is expected to pump the electronic state and by electron-nuclear coupling, the nucleus of the parent Eu ion can be coherently controlled that can be detected by Mössbauer spectroscopy. It is estimated that for a detectable signal months of data accumulation time may be required using conventional Mössbauer technique. NFS has potential to reduce this time to hours or even minutes.

Acknowlegment This work was made possible by grants from Temple University Office of Research, the Office of Naval Research (grant no. N00014-00-1-0371, N00014-02-1-0869), AFOSR (grant no. 49620-01-1-0279, 49620-96-1-0347) and DARPA (grant no. F49620-01-1-0566). We greatly appreciate the help from Mike Campanell in preparing the manuscript.

References

1. Leupold, O., Pollmann, J., Gerdau, E., Rüter, H.D., Faigel, G., Tegze, M., Bortel, G., Rüffer, R., Chumakov, A.I., Baron, A.Q.R.: Europhys. Lett. **35**, 671 (1996)
2. Koyama, I., Yoda, Y., Zhang, X.W., Ando, M., Kikuta, S.: Jpn. J. Appl. Phys. **35**, 6297 (1996)
3. Leupold, O., Chumakov, A.I., Alp, E.E., Sturhahn W., Baron, A.Q.R.: Hyperfine Interact. **123–124**, 611 (1999)
4. Hasan, Z., Mathur, V.K.: U.S. Patent Numbers: 6,528,234 (2003)
5. Mathur, V.K., Hasan, Z.: U.S. Patent Numbers: 6,514,435 (2003)
6. Basieva, I.T., Sekatskii, S.K., Pukhov, K.K., Basiev, T.T., Dietler, G.: Laser Phys. **14**, 1393 (2004)
7. Roman Kolesov, Yuri Rostovstev, Olga Kocharovskaya.: Opt. Commun. **179**, 537 (2000)
8. Hasan, Z., Biyikli, L., Macfarlane, P.I.: Appl. Phys. Lett. **72**, 3399 (1998)
9. Hasan, Z., Solonenko, M., Macfarlane, P.I., Biyikli, L., Mathur, V.K., Karwacki, F.A.: Appl. Phys. Lett. **72**, 2373 (1998)
10. Pandey, R., Sivaram, S.: J. Phys. Chem. Solids **52**, 211 (1991)
11. Toellner, T.S., Hu, M.Y., Sturhahn, W., Quast, K., Alp, E.E.: Appl. Phys. Lett. **71**, 15 (1997)
12. Sturhahn, W., Gerdau, E.: Phys. Rev. B **49**, 9285 (1994)

Microsecond and nanosecond isomers populated in fission reactions

G.A.Jones*, P.M.Walker*, Zs.Podolyák*, P.H.Regan*, S.J.Williams*, M.P.Carpenter†, J.J.Carroll**, R.S.Chakrawarthy‡, P.Chowdhury§, I.J.Cullen*, G.D.Dracoulis¶, A.B.Garnsworthy*, G.Hackman‖, R.V.F.Janssens†, T.L.Khoo†, F.G.Kondev††, G.J.Lane¶, Z.Liu*, D.Seweryniak†, N.J.Thompson* and S.Zhu†

*Dept. of Physics, School of Electronics and Physical Sciences, University of Surrey, Guildford, Surrey, GU2 7HX, UK
†Physics Division, Argonne National Laboratory, Argonne, IL 60439, USA
**Dept. of Physics and Astronomy, Youngstown State University, Youngstown, Ohio 44555, USA
‡TRIUMF, 4004 Westbrook Mall, Vancouver, British Columbia, V6T 2A3, Canada
§University of Massachusetts Lowell, Lowell, MA 01854, USA
¶Dept. of Nuclear Physics, RSPhysSE, Australian National University, Canberra 0200, Australia
‖TRIUMF, 4004 Westbrook Mall, Vancouver, British Columbia, V6T 2A3 Canada
††Nuclear Engineering Division, Argonne National Laboratory, Argonne, IL 60439, USA

Abstract. Fusion-fission reactions were induced by bombarding a thick ^{27}Al target with ^{178}Hf projectiles at a laboratory energy of 1150 MeV using the ATLAS accelerator at Argonne National Laboratory. The subsequent γ-ray decays were measured using the GAMMASPHERE germanium detector array. The beam was pulsed at two different ON/OFF cycles of 82.5/825 ns and 25/75 μs in order to observe the γ rays from the decay of isomeric states. In ^{121}Sb 2721+Δ keV, $I^{\pi}=(25/2^{+})$ and 2434 keV, $I^{\pi}=19/2^{-}$ states have measured half-lives of $T_{1/2}$=200(30) μs and 8.2(2) ns respectively. The 2614+Δ keV, $I^{\pi}=(27/2^{+})$ and 2486 keV, $I^{\pi}=19/2^{+}$ states in ^{123}Sb have measured half-lives of $T_{1/2}$=52(3) μs and 7.9(4) ns respectively. The positive parity isomers in these nuclei correspond to a $\pi d_{5/2}$ or $\pi g_{7/2}$ configuration, in ^{121}Sb and ^{123}Sb respectively, coupled to aligned $(h_{11/2})^2$ neutrons. The $I^{\pi}=19/2^{-}$ isomeric state in ^{121}Sb is proposed to have a $\nu h_{11/2} \otimes \nu d_{3/2} \otimes \pi d_{5/2}$ configuration. A previously unobserved isomer has been identified in ^{99}Mo at an energy of 3010 keV, decaying with $T_{1/2}$=18(5) ns. This state is interpreted as an energetically favoured 3 quasi-particle alignment of $\nu \begin{pmatrix} g_{7/2} \\ d_{5/2} \end{pmatrix} \otimes \pi(g_{9/2})^2$ configuration which is observed systematically in the even-Z N=57 isotones.

Keywords: gamma-ray spectroscopy, fusion-fission reactions, isomeric half-lives.
PACS: 23.30.-g, 23.20.En, 25.70.Jj, 27.50.+e, 27.60.+j

INTRODUCTION

In nuclei near closed shells, single-particle structure tends to dominate over rotational and vibrational collective effects. In medium and heavy (A>80) nuclei, high-j intruder orbitals play a very important role in the *yrast* structure. Particle-aligned states with configurations dominated by these high-j orbitals can be low enough in energy to form *yrast trap*, isomeric states [1]. Nuclei with a large number of isomers tend to decay via low multiplicity γ-ray cascades, and are difficult to study using high-spin, high-

CP853, *FUSION06*, edited by L. Corradi, D. Ackermann, E. Fioretto, A. Gadea, F. Haas, G. Pollarolo, F. Scarlassara, S. Szilner, and M. Trotta

multiplicity experimental techniques where only γ rays within a few nanoseconds of the *prompt* reaction time are considered. By contrast, one can achieve a great deal of clarity in experiments with extended times between reactions, in which low multiplicity, delayed transitions from isomeric decays can be studied.

EXPERIMENTAL DETAILS

Fusion-fission reactions were induced by bombarding a thick ^{27}Al target with ^{178}Hf projectiles at a laboratory energy of 1150 MeV, using the ATLAS accelerator at Argonne National Laboratory. Fission of the ^{205}At compound nucleus populated a broad swathe of nuclei with large yields, from $_{34}$Se to $_{54}$Xe. The resulting γ-ray decays from these products were measured using the GAMMASPHERE [2] array, comprising 101 high purity germanium detectors in this experiment. The beam delivered by ATLAS was bunched into pulses separated by 82.5 ns. This pulsing was utilised to deliver *short* and *long* pulsed beam conditions, enabling the study of metastable states in the $10^{-4} \rightarrow 10^{-9}$ s range. In the short beam pulsing, all but 1 from every 10 beam pulses was swept away from the target, resulting in a 825 ns period within which delayed γ-ray decays could be studied sensitively. Events where two or more coincident γ rays were detected were written to tape. In the long pulsing measurement, a 25 μs beam-on period preceded a 75 μs beam-off period, during which the data acquisition system was triggered by single γ-ray events, time stamped using an external 10 MHz oscillator.

RESULTS

The data were sorted into a variety of time-restricted symmetric and asymmetric cubes and matrices. They were tailored to search for γ-ray decays from isomers with a variety of different half-lives. Angular correlation measurements were made for pairs of γ rays using the prescription of Ref. [3], to help determine the multipolarities of transitions.

^{121}Sb

Figure 1 shows the updated level scheme from this experiment, extended from the work of Porquet *et al.* [4]. The 2057 keV state and 14 transitions (marked with asterisks) are reported for the first time in the present work. Figure 2(a) shows a spectrum of transitions from the decay of a long-lived isomer through the strongly-coupled rotational band built upon the $\pi g_{9/2}[404]$ configuration [4]. The isomer is also observed to decay through the single-particle structures (on the right side of Fig 1). Figure 2(b) illustrates the time projection of $\gamma - \gamma$ gates on the transitions depopulating this isomer. The isomeric half-life was measured to be $T_{1/2}$=200(30) μs, from a number of different gating conditions in both the collective and single-particle decay paths.

This metastable state appears to be just above the E_x=2721 keV, $I^{\pi}=21/2^+$ state and decays via an unobserved (probably E2) low-energy transition.

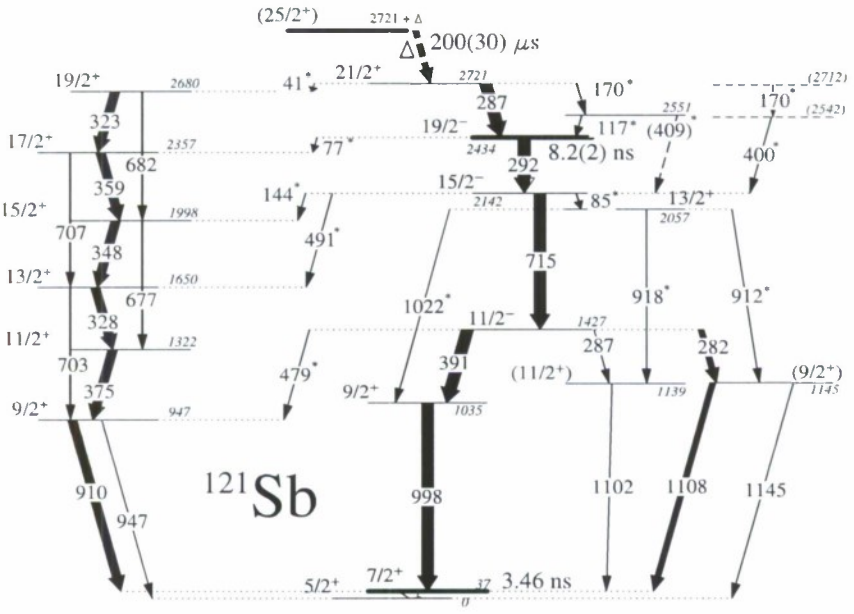

FIGURE 1. Level scheme for transitions in ^{121}Sb from the decay of a $T_{1/2}$=200μs isomer. Gamma-rays marked with asterisks* are those that have been observed for the first time. Widths do not represent absolute intensity measurements, but rather provide an indication to the relative strengths of different γ-ray decay paths.

The observation of the 41 keV transition (shown in a spectrum in the inset of Fig. 2(a)), which approaches the detectable limit of GAMMASPHERE, is a valuable link between the rotational band and the 2721 keV state. After taking into account the efficiency of the germanium detectors, the intensity of the 41 keV transition is found to be 12.4 times smaller than the 323 keV γ ray, using gates with no other feeding transitions. This corresponds to an internal conversion coefficient of α_{tot}=15(3). Calculations using Ref. [5] provide a theoretical value of α_{tot}=8.4 for an M1 transition, indicating that the 41 keV γ ray is an M1 with some E2 admixture. Similar calculations for the 287 and 292 keV γ rays require the 287 keV transition be of E1, M1 or E2 character.

Angular correlation measurements indicate that the 287 keV γ ray is a dipole transition. Figure 2(d) shows the angular correlation function for the 287 and 998 keV γ-ray pair. The A_2 and A_4 coefficients imply that the 287 keV transition is a dipole.

Based on this experimental evidence, the 2721 keV state is assigned $I^{\pi}=21/2^{+}$. Given that the 2721 keV state thus decays via 287 keV E1 and 41 keV M1 transitions, it is unlikely that it is the origin of the 200 μs isomer. The reduced matrix elements, B(E1) for 287 keV and B(M1) for 41 keV, with a 200 μs half-life, would require that the transitions are exceptionally hindered ($\sim 10^{-8}$ W.u.). It follows, that to account for such a long-lived isomer, there must exist another state that decays to the 2721 keV state via an unobserved, low-energy, highly converted transition. With consideration of the intensity of the isomeric decay, and the germanium detector efficiencies and internal conversion

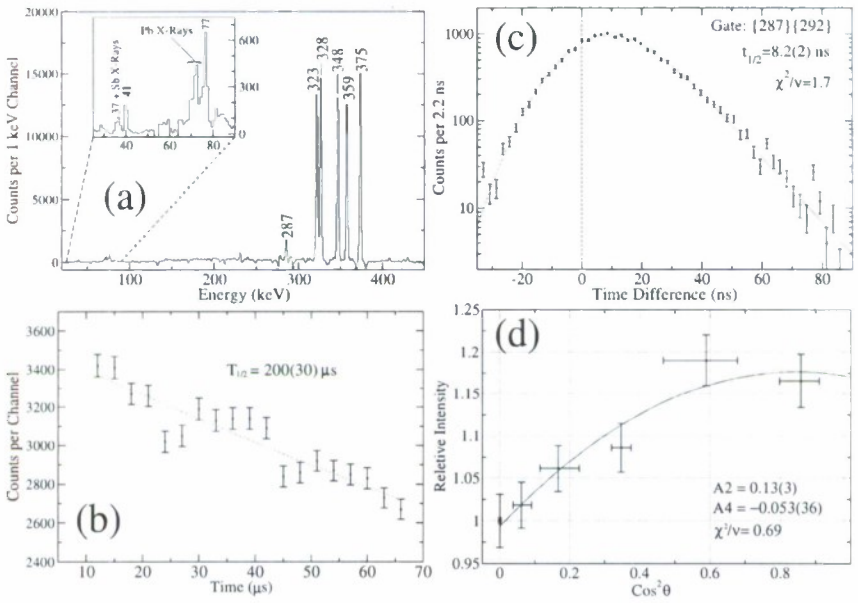

FIGURE 2. (a) A γ-ray spectrum double gated on each of the transitions in the strongly-coupled rotational band based on the $\pi g_{9/2}$ orbit, taken from the long-pulsing experiment. The inset shows an expansion of the low-energy part of the spectrum. Lead X-rays were observed, as the target included some ^{208}Pb. Time spectra in panels (b) and (c) show decays of the 200 μs and 8.2 ns isomers respectively in ^{121}Sb. The $\gamma-\gamma$ angular correlation of the 287 and 998 keV transitions is shown in panel (d), discussed in the text. The error bar on the x-axis expresses the range of θ for the detector pairs, where θ is the angle between the detectors.

coefficients of low energy γ rays, it is likely that the missing transition, Δ has energy $E_{\Delta(E2)}$<60 keV if it is considered to have E2 multipolarity.

In addition the E_x=2434 keV, $I^\pi=19/2^-$ state was observed to be isomeric. Figure 2(c) shows the time difference between 287 and 292 keV γ rays. A Gaussian plus exponential fit to these data results in a half-life of $T_{1/2}$=8.2(2) ns.

The 2542 and 2712 keV states have been inferred from the observation of weak 170 and 400 keV transitions in anti-coincidence with the 292 and 286 keV γ rays in the long-pulsing experiment. The ordering of the γ rays could not be established in the current work, so the state energies are marked as tentative in Fig. 1. An accurate lifetime for these delayed transitions could not be measured due to limited statistics, so it is unclear whether these γ rays are from the decay of the 200 μs isomer.

^{123}Sb

Figure 3(a) shows the partial level scheme of ^{123}Sb adapted from Ref. [4]. The transitions in this level scheme (up to $23/2^+$) were observed following the decay of an isomer in the long-pulsing experiment discussed above. Figure 3(b) shows a time

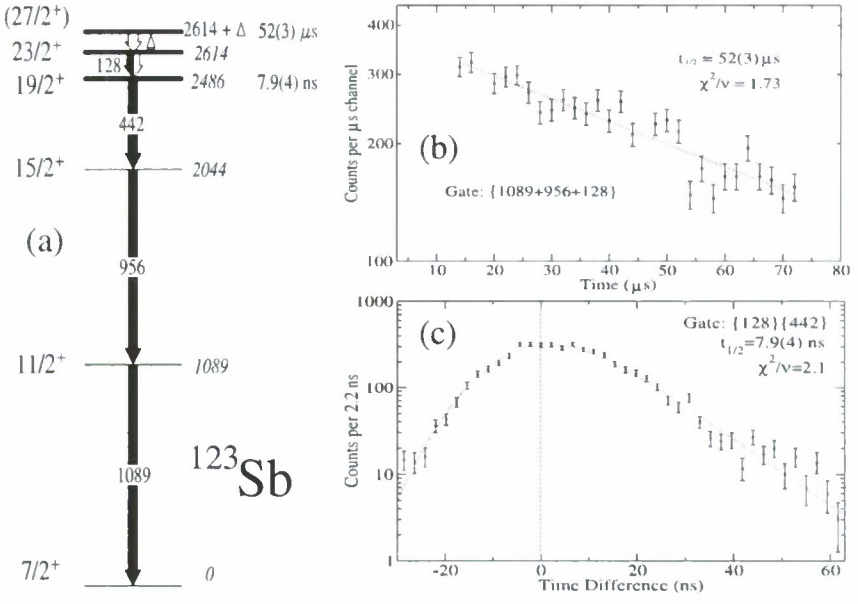

FIGURE 3. A partial level scheme for ^{123}Sb is displayed in panel (a). Time spectra showing the decay of the $T_{1/2}$=52 μs and 7.9 ns isomers in ^{123}Sb are shown in (b) and (c) respectively.

spectrum of the isomeric decay, with a measured half-life of $T_{1/2}$=52(3) μs. Initially it appears that the isomeric lifetime derives from the 2614 keV state. However, it is possible, as in the case of ^{121}Sb, that there is an unobserved transition from a higher-lying isomeric state (shown at 2614+Δ keV in Fig. 3(a)). It is shown later that this is the most likely scenario.

Combinations of $\gamma - \gamma$ angular correlations provide the spin assignments in Fig. 3(a) up to $23/2^+$. Intensity balance measurements, such as those outlined in the previous section, measure the internal conversion coefficient of the 128 keV γ ray as α_{tot}=0.69(13), corresponding to E2 multipolarity within the 2σ limit.

The 2486 keV state is observed to be isomeric. Figure 3(c) shows the time-difference between the 128 and 442 keV transitions. Using a Gaussian plus exponential fit, a half life of $T_{1/2}$=7.9(4) ns was measured.

^{99}Mo

Figure 4(a) shows a partial level scheme of ^{99}Mo extended from that established by Regan *et al.* [6]. In data from the short-pulsing experiment, transitions in the rotational band based on the $\nu h_{11/2}$ excitation were observed. Gamma rays from the $I^{\pi}=23/2^-$ state and below, were observed to be delayed (see Fig. 4(b)), and the 980 keV γ ray depopulating the $I^{\pi}=(27/2^-)$ state, was observed in the prompt gated spectra. A 305 keV γ ray was observed in coincidence with the delayed transitions, decaying from

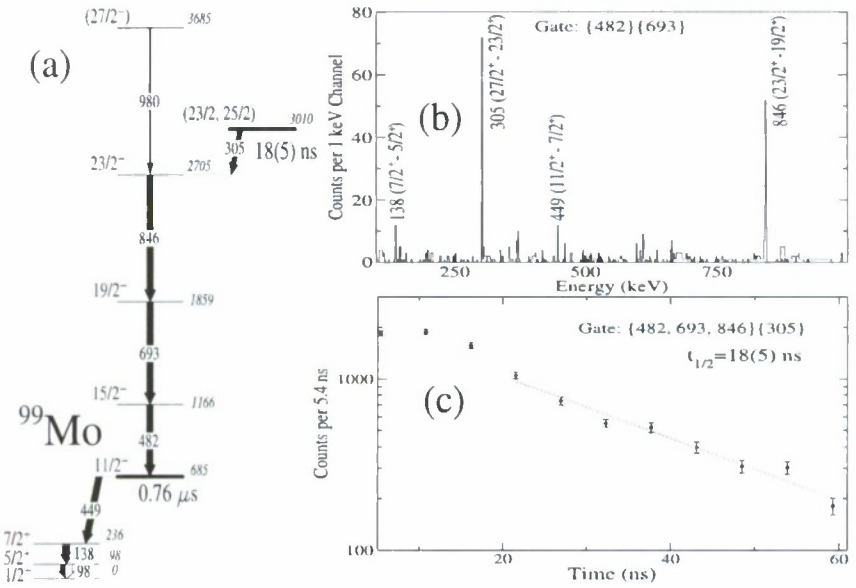

FIGURE 4. A partial level scheme of ^{99}Mo is shown in (a). Panel (b) shows a gate on delayed 482 and 693 keV transitions in the decay of the $T_{1/2}$=18(5) ns isomer. A time spectrum for the decay of the 3010 keV isomeric state is shown in (c). A prompt component (contamination) was subtracted using a time spectrum gated on γ rays with approximately the same energy, from non-isomeric states. The lifetime fit was performed over the range indicated.

a previously unreported state at E_x=3010 keV. No transitions feeding this state were observed in the current experiment and thus it was not possible to measure the lifetime of the state using the γ-γ time-difference technique used for isomeric states in the Sb nuclei. Figure 4(c) shows a germanium time spectrum of the double gated delayed transitions from the E_x=3010 keV state. Relative to the accelerator RF signal, the half-life of the decay is measured as $T_{1/2}$=18(5) ns. Data points close to the prompt part of the spectrum were not included in the fit due to uncertainties in the subtraction procedure. It was not possible to measure the multipolarity of the 305 keV transition with angular correlations, due to low statistics.

The E_x=3685 keV state was tentatively assigned $I^{\pi}=(27/2^{-})$ by Regan *et al.* [6]. The E_x=3010 keV isomeric state does not appear to be the yrast relative to the $I^{\pi}=(27/2^{-})$ state, from intensity measurements, and is thus unlikely to have the same spin. The spin of the E_x=3010 keV isomeric state is thus likely to be limited to I=(23/2, 25/2).

DISCUSSION

Figure 5 shows a comparison of states in ^{121,123}Sb with those in ^{120,122}Sn [7, 8] respectively.

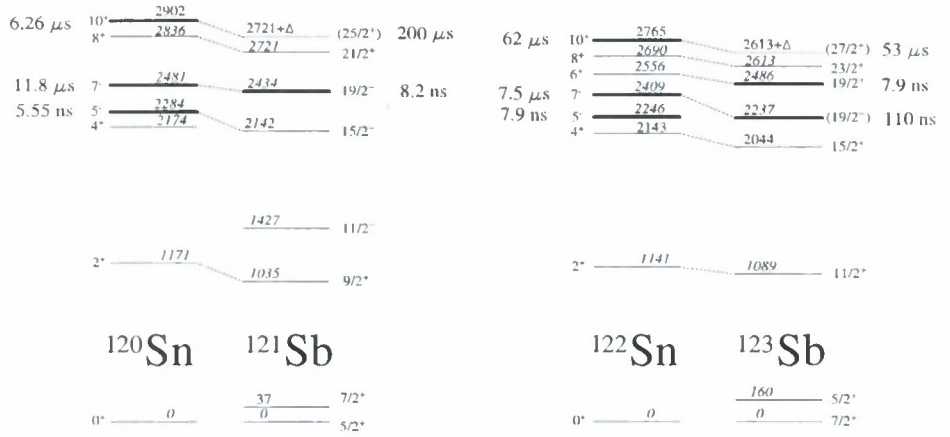

FIGURE 5. Energetic comparison of states in ^{121,123}Sb with those in isotonic Sn neighbours with the same neutron configurations.

^{121}Sb

The $19/2^-$ isomeric state observed in ^{121}Sb is consistent with sytematics of $19/2^-$ isomers in odd-mass antimony nuclei from A=113–131 [4, 7, 9, 10, 11, 12]. The transition rate of the 292 keV γ ray from the $19/2^-$ state is B(E2)=0.83(8) W.u. The $19/2^-$ isomers are analogous to the 7^-, $\nu h_{11/2} \otimes \nu d_{3/2}$ configuration isomers in neighbouring Sn nuclei (see Fig. 5), with the additional coupling of $\pi d_{5/2}$.

It has not been possible to ascertain the spin, parity and energy of the 200 μs isomer with certainty. Despite this, it is possible to infer the spin and parity using systematic considerations. Lighter odd-mass Sb nuclei with A$\geq$117 have isomeric $25/2^+$ states corresponding to the odd $d_{5/2}$ proton coupled to the fully aligned $\nu(h_{11/2})^2$ configuration, observed systematically as isomeric 10^+ states in neighbouring Sn nuclei. One can expect that a state of the same neutron configuration and spin is present in ^{121}Sb and, since the $\pi d_{5/2}$ orbital is more bound than the $\pi g_{7/2}$ [13], the isomer is expected to have $I^\pi=25/2^+$ character. It follows that such a state should decay to the $21/2^+$ level, which is part of the same $\pi d_{5/2} \otimes \nu(h_{11/2})^2$ multiplet, via a low-energy E2 transition.

^{123}Sb

The experimentally observed level structure of the positive parity band shown in Fig. 3(a) exhibits seniority coupling of $\pi g_{7/2} \otimes \nu(h_{11/2})^2$. However, the $I^\pi=27/2^+$ state corresponding to fully aligned $(h_{11/2})^2$ neutrons is not observed in this experiment. The $T_{1/2}$=7.9(4) ns half-life of the 2486 keV state corresponds to a transition rate of B(E2)=0.115(8) W.u. for the 442 keV γ ray. One would expect the decay of the $I^\pi=27/2^+$ state to be longer-lived than the $23/2^+$ state. It is therefore likely that an unobserved E_x=2614+Δ keV state is the origin of the 52 μs half-life, decaying via a

highly converted, low energy E2 transition. The energy of this transition can be limited experimentally, following similar arguments to the Δ transition in ^{121}Sb, to $E_{\Delta(E2)}$<60 keV. If one assumes the same transition rate for the $I^{\pi}=27/2^{+}$ state as the $19/2^{+}$, then this transition energy would be expected to be $E_{\Delta(E2)}$ ~30 keV. Also, if the $I^{\pi}=23/2^{+}$ state has a similar transition rate as the $19/2^{+}$, then one would expect an isomeric half-life of the order of 1μs. The half-life for this state was not observed experimentally.

^{99}Mo

The $I^{\pi}=21/2^{+}$ isomeric state in the N=57 isotone ^{105}Cd has a reported configuration of $\nu d_{5/2} \otimes \pi(g_{9/2})^{-2}$ as deduced from the g-factor measurement in Ref. [14]. The analogous maximally aligned coupling of the $(g_{9/2})^2$ protons with $\nu d_{5/2}$ and $\nu g_{7/2}$ should form states in ^{99}Mo with $I^{\pi}=21/2^{+}$ and $23/2^{+}$ respectively. Since we have restricted the spin of the isomeric state to I=(23/2, 25/2), the $I^{\pi}=23/2^{+}$, $\nu g_{7/2} \otimes \pi(g_{9/2})^2$ configuration seems more likely. In support of this assertion, if the E_x=3685 keV, $I^{\pi}=(27/2^{-})$ state corresponds to the alignment of the $(g_{9/2})^2$ protons coupled to the $\nu h_{11/2}$ (as suggested in Ref. [15]), the difference in energy between the $I^{\pi}=(27/2^{-})$ and isomeric E_x=3010 keV states (675keV) is qualitatively consistent with that between the yrast $I^{\pi}=11/2^{-}$ and the $7/2^{+}$ states (449 keV).

SUMMARY

Fusion-fission reactions using a pulsed beam have been successful in identifying γ-ray decays from a number of previously unobserved isomers in Sb and Mo nuclei. Shell-model calculations are the subject of current and future endeavours to compare with the empirical spectroscopy of mid-neutron-shell Sb nuclei.

REFERENCES

1. P. M. Walker, and G. D. Dracoulis, *Nature* **35**, 399 (1999).
2. I. Y. Lee *et al.*, *Nucl. Phys. A* **520**, 641c (1990).
3. G. D. Dracoulis *et al.*, *Phys. Rev. C* **71**, 044326 (2005).
4. M. G. Porquet *et al.*, *Eur. Phys. J. A* **24**, 39 (2005).
5. F. Rosel *et al.*, *At. Nucl. Data Tables* **21**, 91 (1978).
6. P. H. Regan *et al.*, *Phys. Rev. C* **68**, 044313 (2003).
7. S. Lunardi *et al.*, *Z.Phys.* **A328**, 487 (1987).
8. R. Broda et al., *Phys. Rev. Let.* **68**, 1671 (1992).
9. L. K. Kostov *et al.*, *Z. Phys.* **A337**, 407 (1990).
10. R. E. Shroy *et al.*, *Phys. Rev. C* **19**, 1324 (1979).
11. J. Genevey *et al.*, *Phys. Rev. C* **67**, 054312 (2003).
12. J. Genevey *et al.*, *Eur. Phys. J. A* **9**, 191 (2000).
13. M. G. Porquet *et al.*, *Eur. Phys. J. A* **25**, 319 (2005).
14. O. Hausser et al., *AECL-5614* **68**, 15 (1976).
15. P. H. Regan *et al.*, *J. Phys. G* **19**, L157 (1993).

Available online at www.sciencedirect.com
ScienceDirect
ELSEVIER
Nuclear Instruments and Methods in Physics Research A 565 (2006) 657–676
NUCLEAR INSTRUMENTS & METHODS IN PHYSICS RESEARCH Section A
www.elsevier.com/locate/nima

Design and characterization of a compact multi-detector array for studies of induced gamma emission: Spontaneous decay of ^{178m2}Hf as a test case

P. Ugorowski[a], R. Propri[a], S.A. Karamian[b], D. Gohlke[a], J. Lazich[a], N. Caldwell[a], R.S. Chakrawarthy[c,d], M. Helba[e], H. Roberts[e], J.J. Carroll[a,*]

[a]*Department of Physics and Astronomy, Youngstown State University, One University Plaza, Youngstown, OH 44555, USA*
[b]*Flerov Laboratory of Nuclear Reactions, Joint Institute for Nuclear Research, 141980 Dubna, Russia*
[c]*Department of Chemistry, Simon Fraser University, Burnaby, British Columbia, Canada V5A 1S6*
[d]*TRIUMF, Vancouver, British Columbia Canada V6 T 2A3*
[e]*SRS Technologies, Inc., Systems Technology Group, Huntsville, AL 35806, USA*

Received 20 January 2006; received in revised form 9 May 2006; accepted 12 May 2006
Available online 28 June 2006

Abstract

Reports that incident photons near 10 keV can induce the emission of gamma rays with concomitant energy release from the 31-year isomer of ^{178}Hf challenge established models of nuclear and atomic physics. In order to provide a direct and independent assessment of these claims, a multi-detector system was designed as a specialized research tool. The YSU miniball is unique in its combination of performance characteristics, compact size and portability, enabling it to be easily transported to and placed within the confines of beamline hutches at synchrotron radiation sources. Monochromatic synchrotron radiation was used in the most recent studies from which evidence of prompt triggering was claimed, suggesting similar sites for independent tests of these results. The miniball array consists of six high-efficiency BGO scintillators coupled with a single 65% Ge detector and provides time-resolved gamma-ray calorimetry rather than purely spectroscopic data. The need to record high detected folds from the array (up to seven-fold gamma coincidences) makes this system different in practice from standard spectroscopic arrays for which data is typically restricted to triples or lower folds. Here the system requirements and design are discussed, as well as system performance as characterized using the well-known natural decay cascades of ^{178m2}Hf. This serves as the foundation for subsequent high-sensitivity searches for low-energy triggering of gamma emission from this isomer.

PACS: 23.20.Lv; 27.70.+q; 29.30.−h; 29.30.Kv

Keywords: Multi-detector array; Gamma-ray calorimetry; Induced gamma emission; Isomer; ^{178m2}Hf

1. Introduction

The possibility that nuclear energy could be released in a relatively clean fashion from long-lived nuclear isomers has been under consideration for decades [1]. Such metastable states are capable of storing considerable energy for rather long durations. The archetype is ^{180m}Ta, being an excited state with a halflife greater than 10^{15} years and located 75 keV above the unstable ground state [2]. An induced depopulation of this isomer due to irradiation of samples with real photons (bremsstrahlung) was first observed in 1987 [3] with detailed confirmation and characterization of the process coming later (see Ref. [4] and references therein). The induced depopulation was accompanied by a release of the stored 75 keV, but was initiated by incident photons of at least 1 MeV, proving to be a sink rather than a source of energy. Nevertheless, the existence of transi-

*Corresponding author. Tel.: +330 941 3617; fax: +330 941 3121.
E-mail address: jjcarroll@cc.ysu.edu (J.J. Carroll).

0168-9002/$ - see front matter © 2006 Elsevier B.V. All rights reserved.
doi:10.1016/j.nima.2006.05.209

tions connecting the isomer to levels that decay toward the ground state provided intriguing insight into weak components in the wavefunctions [5].

Other isomers have been suggested as being potentially of greater practical value [1]. Principal among these is the 31-year-lived isomer ^{178m2}Hf, storing 2.446 MeV per nucleus, or about 1.3 GJ/g at natural density. Studies which attempted to replicate the induced depopulation of ^{180m}Ta for ^{178m2}Hf have concentrated so far on rather low energies, using real photons below 100 keV from bremsstrahlung and synchrotrons. Experiments using virtual photons via Coulomb excitation have been conducted on ground-state ^{178}Hf targets, providing results that support the possibility of induced depopulation of ^{178m2}Hf by transitions with energies greater than 300 keV [6,7]. Ref. [8] surveys the experimental landscape as of early 2004, and later results or additional details of previous results are described in Refs. [9–11]. The controversial nature of the positive results, in light of several carefully conducted null measurements, perhaps reached its zenith with the recent report [9] that induced depopulation of the ^{178m2}Hf isomer, with $J^{\pi} = K^{\pi} = 16^{+}$, proceeded through an intermediate, higher-lying state that subsequently decayed to the ground state in a single transition. Since only a modest-multipolarity transition from isomer to intermediate state could be expected, this would seem to require a $\Delta J > 10$ transition for the purported decay transition.

While the last claim [9] of induced depopulation of ^{178m2}Hf would appear to require little further consideration, other previous claims are not unphysical a priori, although theoretical analyses have cast doubt on the purported mechanism [12,13]. As in the case of ^{180}Ta and other nuclei (see, for example, Ref. [14]), the presence of K-forbidden transitions in ^{178}Hf, likely required for an induced depopulation, would provide important nuclear structure information. Depletion caused by incident photons of low energies, reported to be near 10 keV, would also have important implications to the understanding of nucleus–electron couplings and potential applications. Also, despite continued positive claims the magnitude of the effect remains rather small. Thus, improved experimental methods by which to better examine these claims will be valuable.

All of the most recent positive results (see the survey of Ref. [8] and Refs. [9,11]) were obtained using monochromatic synchrotron radiation (either from bending magnets or undulators) as the source of incident photons. Most null experiments were, in contrast, obtained using continuum radiation sources, including bremsstrahlung [15] or "white" synchrotron radiation [10,16,17] and thus presented unique experimental challenges that differed from the positive measurements. Also, in the null results of Refs. [10,16,17] no special timing instruments were used by which any relationship between pulses of synchrotron radiation and gamma rays emitted from the ^{178m2}Hf sample could have been recorded. It has been claimed that excess gamma-ray emission triggered by incident photons near 10 keV was prompt, coming within a few nanoseconds of the pulses of synchrotron radiation [11,18], and thus that the duty cycle of the synchrotron would lead to a washing out of the signal without timing information. Ref. [18] suggests (see p. 164) that this explains the null measurements. An independent examination of the positive reports of prompt triggered gamma emission, induced by monochromatic synchrotron radiation near 10 keV, requires a different approach than was taken in the works of Refs. [10,16,17]. For this purpose, a multi-detector gamma spectroscopic system was developed in a compact configuration that permitted its emplacement within the confines of the radiation hutch at the BL12B2 beamline of the SPring-8 synchrotron. This beamline was chosen as providing similar radiation characteristics to those utilized to obtain some positive results at SPring-8. These independent tests will be described in a future work [19].

This paper will first discuss the design requirements and implementation for the miniball system (Section 2) as needed to search for prompt triggered gamma emission from ^{178m2}Hf. Then the sensitivity of the array for detection of gamma-ray cascades will be covered, as measured from the well-known natural decay of this isomer. This will include determination of the system efficiency and detection limits for gamma-ray calorimetry (Section 3).

2. Detection system

2.1. Design requirements and configuration

Many multi-detector arrays have been constructed for high-resolution gamma-ray spectroscopy [20], such as the well-known Gammasphere system. The large value and physical size of these systems and their associated instrumentation make it infeasible to consider transporting them to sites such as SPring-8 and emplacing them within the confines of beamline hutches for experiments of short duration. Thus, it was necessary to develop a unique system of modest size that combined some spectroscopic capabilities with the essential ability to perform gamma-ray calorimetry. The latter aspect is similar in concept to that described in Ref. [21]. The present system was designated as the *YSU miniball*, stressing its similarities with much larger arrays, although its design is predicated on a very specific type of experiment. Initial design of the system occurred in 2001 [22] and an implementation was used in works described in Refs. [8,15].

Fig. 1 is a schematic energy-level diagram of the ^{178}Hf nucleus, which possesses several isomers. The long-lived (metastable) levels are those at 1147.4 keV, with a halflife of 4 s (*m1*), and at 2446.1 keV, with a halflife of 31 years (*m2*). The figure shows the main transitions resulting from the natural decay of the 31-year isomer [2,23]. Also depicted is a sketch of a general process of induced energy release that begins with excitation of a nucleus initially in the *m2* state to a higher-lying intermediate state. Back-decay (E) of the

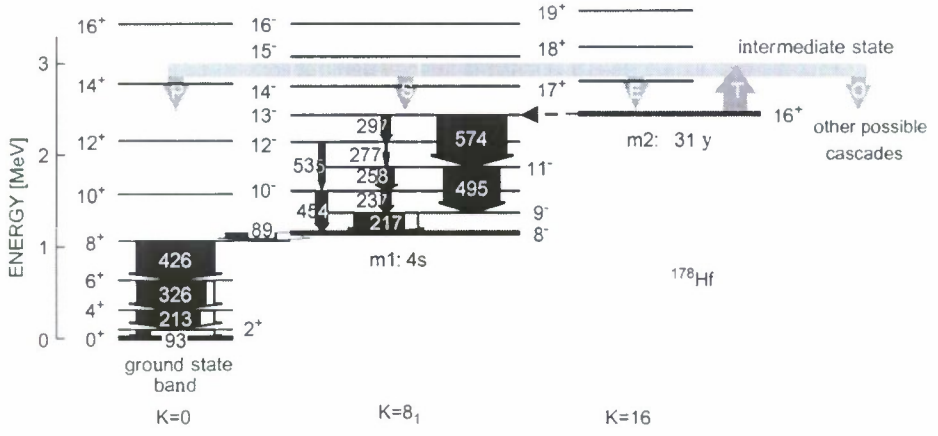

Fig. 1. Partial level diagram of ^{178}Hf, showing the dominant electromagnetic transitions occurring during spontaneous decay of the 31-year isomer [2]. The weak transitions found in the experiment of Ref. [23] are not shown. The total widths of cascade arrows represent the relative transition intensities, while their darkened widths indicate the gamma intensities. Transition energies are in keV. The primary initial step in the *m2* decay occurs by a completely converted 12.7-keV E3 transition and the corresponding arrow does not attempt to represent its intensity. Also shown is a depiction of a hypothesized triggering process by excitation of nuclei already in the 31-year isomeric state to a higher-lying intermediate level, as described in the text.

intermediate state to the isomer provides only elastic scattering of the incident entity, assumed to be real photons. Other decay branches of the intermediate state may bypass the *m2* level and initiate cascades that eventually reach the stable ground state. These branches would provide a means by which the 2446.1 keV stored by the 31-year isomer could be released via gamma rays and conversion electrons. These branches may be generally characterized as *prompt* (P), in which the cascade from the intermediate state reaches the ground-state band rapidly, *slow* (S), in which the cascade reaches the *m1* band, and *other* (O). The latter type of cascade bypasses the 4-s isomer, but may pass through some states that have significant halflives on the time scale of a detection system. Reports of induced energy release, so-called triggered gamma emission, have so far been restricted to incident photons energies near 10 keV. Below an energy of (2446.1 + 10) keV, known levels have halflives less than 1.5 ns with the exception of the *m1* metastable state and a shorter-lived isomer at 1554.0 keV ($T_{1/2} = 77.5$ ns) [2].

As mentioned above, recent reports of positive evidence of triggering indicated that the gamma emission was prompt, coming within 1 ns of the pulse of incident synchrotron radiation [11]. In that work, a small-volume Ge detector was used to measure gamma rays emitted from a sample containing ^{178m2}Hf as it was being irradiated with monochromatic synchrotron radiation near 10 keV. Spectroscopic information was recorded as well as the time between gamma detection and individual pulses of incident radiation. Those pulses were of 20–50 ps duration and were separated by several nanoseconds—the time of the pulses was determined by placing an avalanche photodiode in the beam (behind the sample) [11]. Although "1 GHz electronics" were employed for the photodiode [11], the true time resolution between pulses and gamma-ray detection was no doubt more on the order of 10 ns as is typical for Ge detectors. In any event, that report precludes cascades that are delayed by passage through the 77.5-ns isomer.

The ^{178}Hf nucleus provides a natural way of testing this claim of prompt gamma emission without the need to record the times for pulses of incident synchrotron radiation. As discussed in Refs. [15,22] and seen in Fig. 1, spontaneous decay of the *m2* isomer occurs via two bursts of gamma rays, each of which consists of a cascade with inter-transition delays less than 1.5 ns. The first burst occurs from transitions within the *m1* band, after decay of the *m2* state, and is stopped briefly by the 4-s isomer. The total energy released in the first cascade from the 16^+ *m2* isomer to the 8^- *m1* isomer is 1298.7 keV, while the energy released in the second cascade from the *m1* isomer to the ground state is 1147.4 keV. Within each cascade the gamma rays are simultaneous on the scale of the resolving time of Ge spectrometers. If the gamma rays were detected with sufficiently high efficiency by a large-solid-angle array, a summation of their energies would coincide with the total energies of the bursts, minus any energy lost into conversion electrons and therefore invisible to the Ge detectors. Conversely, prompt gamma emission due to the claimed induced energy release would produce a single burst of gamma rays with total energy of (2446.1 + 10) keV. Gamma-ray calorimetry would therefore distinguish clearly between prompt triggered events and those from natural decay. Such high-summed-energy cascades could only be due to triggering, so they would of necessity be correlated with incident pulses of synchrotron radiation without any need to explicitly record the time of those pulses.

The YSU miniball is designed to perform this function of time-resolved gamma-ray calorimetry using a compact array. A photograph of the miniball located with the BL12B2 hutch at SPring-8 is shown in Fig. 2. A balance between performance and portability was achieved by

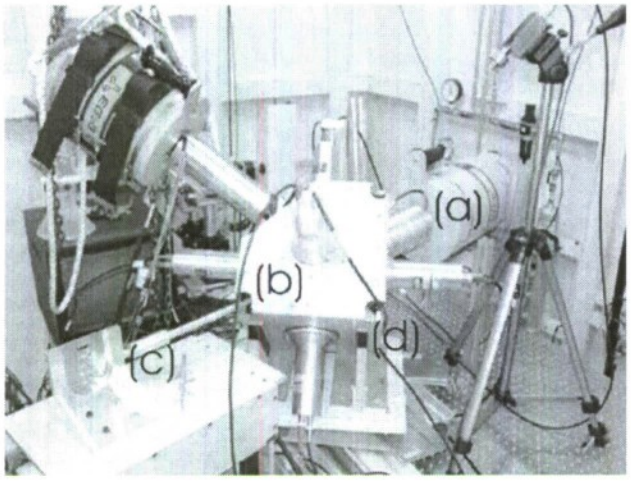

Fig. 2. YSU miniball array within the experimental hutch of the BL12B2 beamline at SPring-8. Labeled items are (a) a 65% Ge detector (part of miniball system), (b) a cubic support structure holding six BGO crystal/PMT assemblies, (c) a sample positioning arm, attached to a translation stage, and (d) exit port from the support structure for synchrotron radiation. The additional small-volume Ge and X-ray detectors are independent from the miniball instrumentation.

using six 3.0″ diameter × 2.5″ long BGO crystals to provide high solid angle (about 83% of 4π) and high intrinsic efficiency. NaI(Tl) crystals were employed in previous implementations [15,22], but the lower peak-to-Compton ratio of that scintillator material compared with BGO made interpretation of spectra more difficult, thus the change to BGO. Many reports of induced energy release indicated evidence of the emission of gamma rays at energies not part of the natural decay cascades (see the survey of Ref. [8]). High-resolution spectroscopy would be advantageous in identifying any such unusual gamma rays, but this would be precluded by the use of only BGO scintillators. In order to insure that every gamma-emission event observed by the array contained one gamma ray having a precisely determined energy, a 65% relative efficiency p-type Ge detector was coupled instrumentally to the BGO crystals. The large-volume Ge detector observed the sample through a gap between BGO detectors along one of the diagonals of a cubic support structure.

Use of a p-type crystal, with its associated thin Al-end window, was beneficial for spectra taken under irradiation in that the window would provide filtering of any incident radiation near 10 keV that was scattered toward the detector. Aluminum windows on the BGO crystal housings provided similar shielding, minimizing the chance of pile up between scattered synchrotron radiation and gamma rays.

Fig. 2 also shows the placement of a second Ge detector (10% efficiency n-type) and an X-ray detector, both of which observed the sample through other diagonals of the cube. These were used as parts of independent systems to obtain a separate singles spectrum (no coincidence) and a calibration of the scattered synchrotron radiation during exposures. They have no impact on the characterization of the miniball system and are not discussed further.

2.2. Instrumentation

A schematic of the pulse-processing instrumentation for the miniball is given in Fig. 3. Once data acquisition was enabled, recording of a gamma-emission event was initiated only when the Ge detector observed a gamma ray. One preamplifier output from the Ge detector was sent to an Ortec 579 Fast Filter Amplifier and then to an Ortec 583 constant-fraction (CF) discriminator to provide a master gate channel. The ARC method [24] was employed with this discriminator and its threshold set a minimum energy for recorded gamma rays into the Ge detector. The discriminator's NIM output was stretched and converted to TTL by a Stanford DG535 pulse generator. The output from the pulse generator served as the system gate and its width and delay could be adjusted over a wide range.

High voltage to the Ge detector was provided using a standard Ortec module that utilized manual front-panel controls. High voltage to each BGO's PMT was provided by a single octal NIM module from Radiation Technologies, Inc. that was computer controlled and allowed remote changes on the order of a few volts.

A FERA/CAMAC system was employed to record spectroscopic and time information from the detectors, chosen for its flexible programmability using the KMaxNT software [25] and for buffering and fast transfer of data. A customized toolsheet was built in this platform to control data acquisition, including operating parameters like ADC thresholds, data word sizes, use of zero-suppression, buffer size, etc., and to monitor individual detector energy and time spectra in real-time. The FERA hardware was managed by a CMC 203 driver that received the system gate and distributed it to two Ortec AD413A quad 8k peak-sensing ADC's and a Silena 4418/T octal TDC. Spectroscopic pulses from the Ge detector were input to an Ortec 672 linear amplifier with a shaping time of 2 μs and its unipolar output was digitized with one channel of an AD413A. Output from the BGO PMT's was routed first to an Ortec CF8000 octal CF discriminator. A buffered spectroscopic signal was available from each CF8000 channel whereby spectroscopic signals from the BGO detectors were fed to separate Ortec 672 amplifiers with shaping times of 2 μs. The bipolar signals from these amplifiers were digitized by other channels of the AD413A's after inversion, which provided the best linearity and resolution.

Negative NIM signals were output by each channel of the CF8000 as timing signals when the incoming PMT pulses exceeded adjustable thresholds. These timing signals were stretched by separate channels of an Ortec GG8010 and then converted to ECL standard signals by separate channels of a Phillips 7126 level translator prior to being input to the TDC. The leading edge of the gate distributed by the driver via the FERA bus served as a START pulse

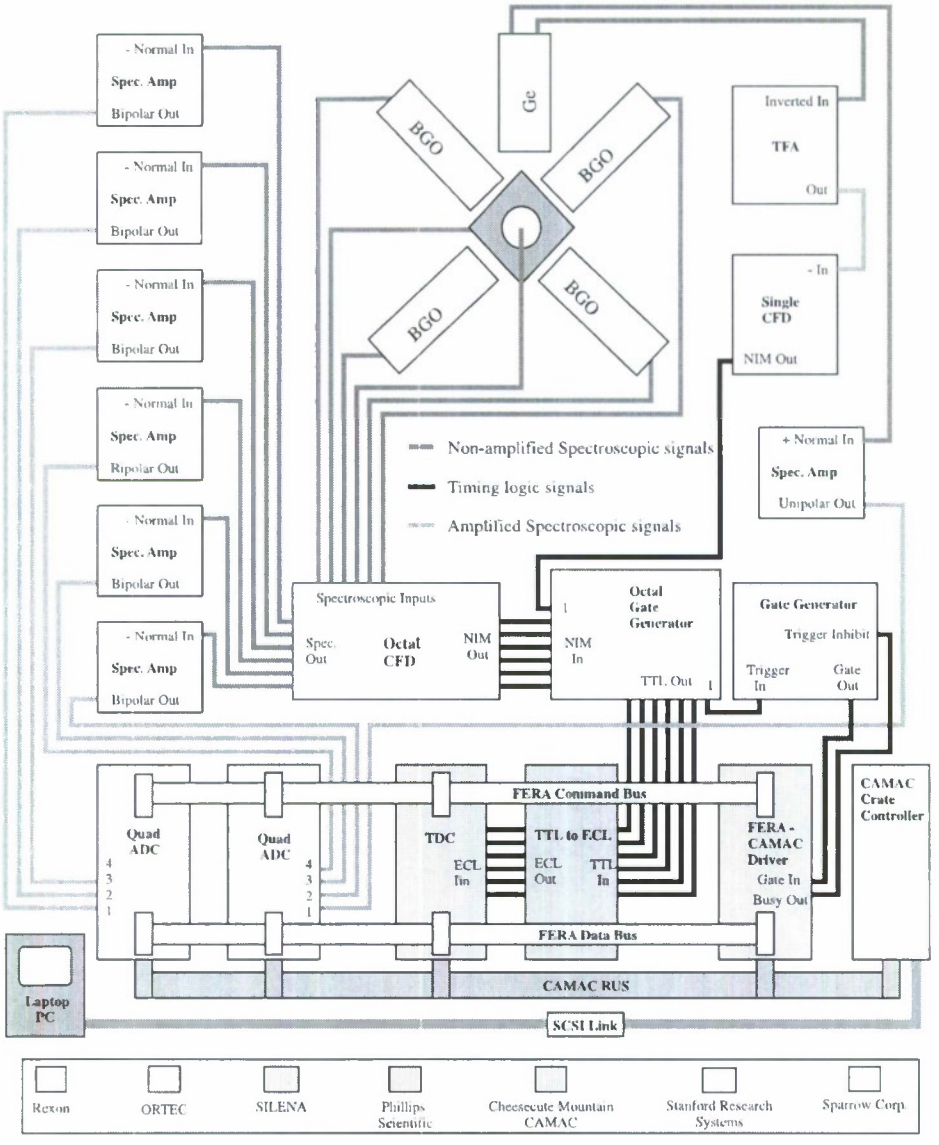

Fig. 3. Schematic of the pulse-processing instrumentation for the miniball array. The Ge detector provided the master gate for the system as described in the text.

to the TDC and the pulses originating from BGO PMT's served as STOP markers. This allowed recording of the relative time interval between a master Ge signal and those from each individual BGO detector. The TDC provided an active time window of 2.8-μs duration, during which START-STOP times were logged as distributed over 3840 channels—the module used an additional 256 channels for sliding-scale non-linearity compensation. The resolution of the TDC was 0.73 ns/channel, considerably shorter than the inherent time resolution obtainable from the Ge and BGO detectors after pulse processing, being both on the order of tens of ns. The temporal relationships between the gate, spectroscopic and timing pulses are shown in Figs. 4 and 5.

Although not suitable for extended discussion herein, it is worth noting that while CAMAC is an international standard this is not the case for the FERA system. The Fast Encoding and Readout ADC approach was developed by Lecroy to provide data transfers between CAMAC modules at rates in excess of that supported by the CAMAC backplane. FERA utilizes ECL signals on a front-panel bus distributed and managed by the driver module. Via handshakes the driver receives data from ADC's and TDC's and assembles these separate parameters (data pieces) into an event, then buffers many events either internally or in a separate memory module. In this system, when the internal buffer was 3/4 full, a Look At Me (LAM) was sent to the controlling computer to cause an upload of data. FERA handshake protocols are not fully standardized, therefore the amount of effort required to regularize communications between the driver and the Ortec and Silena modules should not go unrecognized. It is

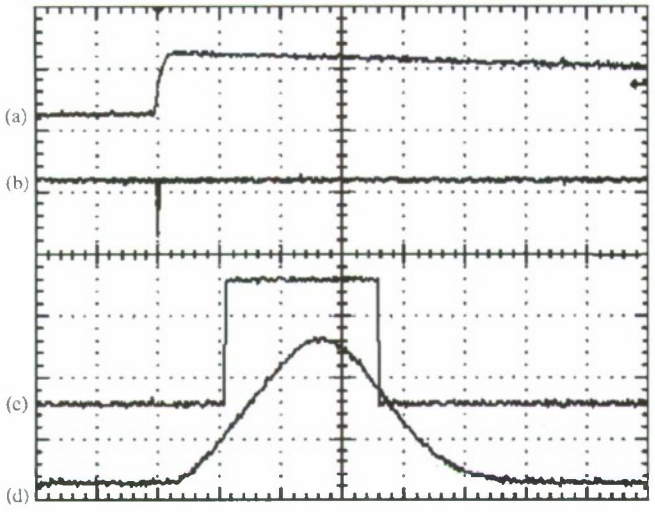

Fig. 4. Oscilloscope trace showing (a) the Ge detector preamp signal, (b) the Ge CFD timing pulse, (c) the system gate and (d) the output of the spectroscopy amplifier from the Ge signal. The time scale is 2 μs per division.

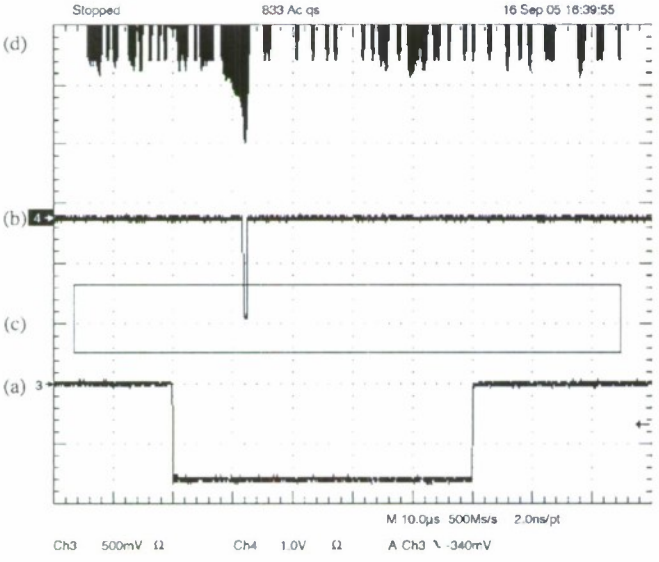

Fig. 5. Oscilloscope trace showing (a) inverted system gate, (b) a BGO timing STOP signal, (c) a histogramming box that determines the magnitude of negative-going STOP pulses that will be recorded and (d) a histogram showing the frequency of STOP pulses as a function of time. The histogram provides the coincidence curve used to set delays on the time channels. The time scale is 1 μs per division.

also worth noting that direct observation of signals on the FERA bus destabilized the communications between driver and other modules, an impediment to this regularization.

An absolute time for each event was assigned with 20-ns resolution by the CMC 203 CAMAC driver based on when it received a gate relative to the start of acquisition. Each parameter was a 32-bit word, two of which were used to record the absolute event time. This instrumental resolution was far better than that supported by the detectors themselves. A one-parameter header of constant digital value was inserted at the beginning of each event, so that events in which incomplete handshakes caused some parameters to be lost by the driver could be excluded as having too few parameters. A total of nineteen 32-bit parameters was recorded in each good event—off-line sorting of the data sets indicated that only 1 out of every 300 events was incomplete and such bad events were discarded off-line prior to data analysis.

Zero-suppression mode was not employed in the ADC's so as to avoid having events of varying lengths. Each ADC module possessed four inputs with a processing time of 6 μs per active input and 1.8 μs per inactive input. Readout of the ADC's to the driver was found experimentally to require 7.4 μs following the end of digitization. The total processing time for the ADC's could, therefore, vary in duration, but the TDC introduced a fixed deadtime of 33 μs that included digitization of the START–STOP delay and readout of the module. Output of additional gates from the DG535 was inhibited for a period chosen at 50 μs to avoid the possibility of interference with processing of the current event.

Proper digitization of spectroscopic and TDC STOP signals required use of the GG8010 and DG535 units to introduce appropriate delays at various points in the different channels. These modules also allowed matching of pulse widths to the demands of subsequent units in the data streams. For example, the Ge spectroscopic pulse was input into a linear amplifier set for triangular shaping with a 2-μs time constant. This shaping time had the added effect of introducing a delay of 5 μs between the peak of the initial pulse from the Ge preamplifier and the amplified pulse. The output of the DG535, serving as the system gate, was delayed and its width set to insure full digitization of the spectroscopic pulse by the ADC.

The use of preamplifiers for the BGO signals was considered, but rejected due to the inability to maintain a sufficiently fast risetime with available units. The PMT outputs were input directly into the CF8000, which produced both time marks and buffered spectroscopic signals. Tests showed that the best resolution for a BGO crystal was obtained by using the bipolar amplifier outputs and triangular shaping. The resulting resolution was found to be 8% for the ^{60}Co 1332 keV peak, as shown in Fig. 6. Proper digitization of peak heights by the ADC's required those peaks to not occur within 1 μs of the start or end of the gate. A gate duration of 5 μs was utilized to meet this condition based on the delays and widths of the spectroscopic pulses for the Ge and BGO channels.

As mentioned previously, timing pulses from the CF8000 were stretched, delayed and converted to ECL as needed for proper digitization by the TDC. Valid STOP signals had to reach the TDC during its 2.8-μs active period that began with the leading edge of the gate. Lack of a valid STOP pulse to the TDC during the active period was recorded as an increment of one count within the sliding-scale region. Invalid STOPs occurred for several reasons, as discussed later. The delays were selected so that true

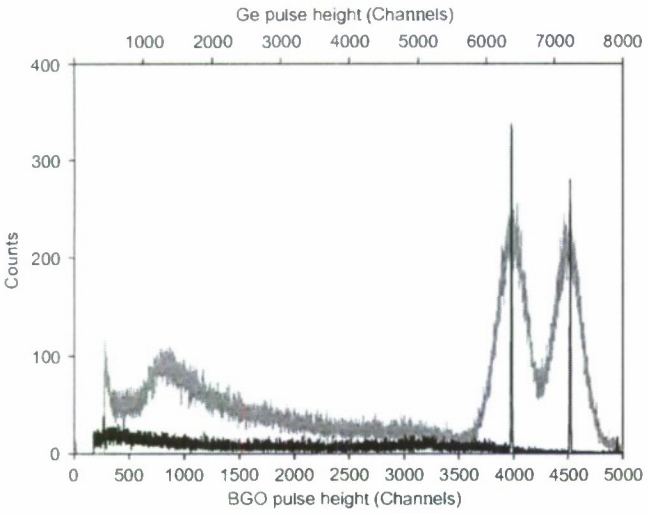

Fig. 6. Comparison of Ge (black) and BGO (grey) energy resolutions for a ^{60}Co calibration source (obtained at Youngstown State University during preliminary testing).

coincidence STOPs appeared at roughly channel 1500 for each TDC input by obtaining coincidence curves using the histogramming feature of the Tektronix TDS-5104 1-GHz digital oscilloscope. Fig. 5 shows a scope trace displaying the gate and STOP pulses from a single BGO, generated with a ^{60}Co source. Also shown in the figure is a histogram of the numbers of STOP pulses occurring as a function of time. The delay for this STOP stream was set so that coincidence between gamma rays entering the Ge (START) and this BGO produced a time marker within the gate.

Off-line sorting of data sets to extract singles or higher-fold spectra for any detector or combination of detectors was accomplished using an in-house software suite that was custom designed [26] for the miniball system. The software allowed sorting based on energy and timing parameters for each detector and determination of summed energy and detected fold from the BGO crystals.

Standard calibration sources were used to assess the basic performance of the miniball system as was done in earlier stages of its development [15]. Because the spontaneous decay of ^{178m2}Hf has been extensively characterized [2,23] and because the eventual aim was to perform trigger studies in subsequent experiments [19], it was decided to perform efficiency calibrations using a mixed ^{178m2}Hf/^{172}Hf sample. This approach benefited from the number and distribution of gamma lines, and the available coincidences.

One particular test with a standard calibration source was very valuable. A ^{137}Cs source was employed to investigate the possibility of Compton scattering in one detector causing coincident events in other detectors. Discriminator thresholds in the miniball instrumentation eliminated X-rays from recorded events, so that only random coincidences should have been in evidence from this single-line source. Fig. 7a shows a time spectrum obtained for one BGO crystal. A small coincidence peak

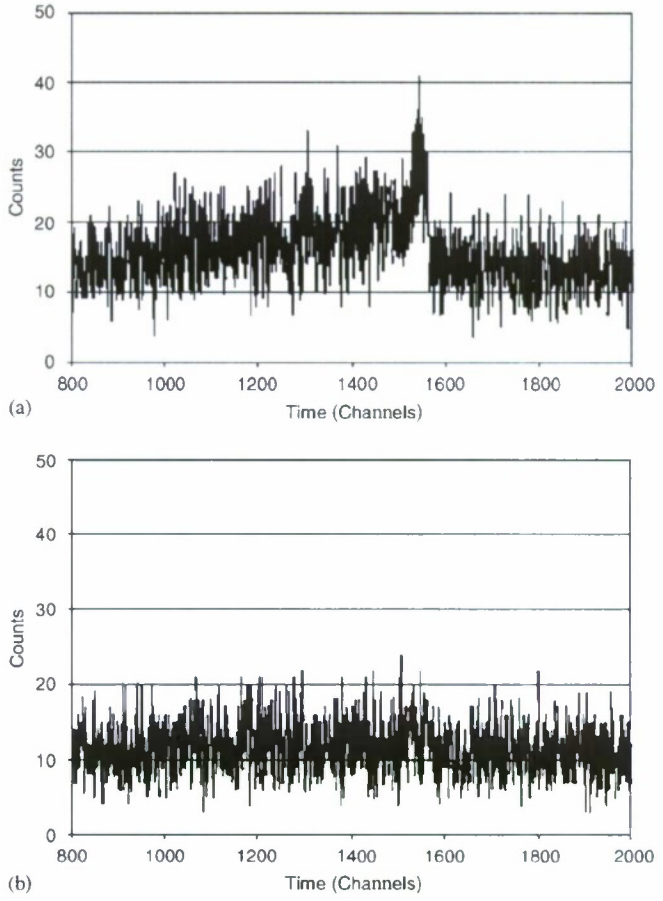

Fig. 7. (a) A TDC spectrum showing the distribution of STOP pulses from one BGO obtained from a ^{137}Cs source. Compton scattering between detectors results in a small coincidence curve, while in (b) this cross-talk between detectors has been eliminated by wrapping the detectors with 1 mm Pb.

was seen and interpreted as being due to Compton cross-talk between the Ge and that BGO. Such cross-talk could occur between any detectors. A 1-mm Pb wrap was applied around the BGO crystals as they extended within the cubic support structure, resulting in the time spectrum shown in Fig. 7b in which this cross-talk was eliminated. It should be noted that no filters were applied to the faces of any of the detectors, other than the thin Al detector housings.

3. Characterization using ^{178m2}Hf decay

3.1. Sample composition and configuration

The miniball performance was principally characterized by gamma rays emitted in spontaneous decays within a mixed ^{178m2}Hf/^{172}Hf source. This characterization was chosen, as mentioned above, to serve as the foundation for experiments conducted specifically to search for evidence of prompt-induced energy release during subsequent irradiations with synchrotron radiation.

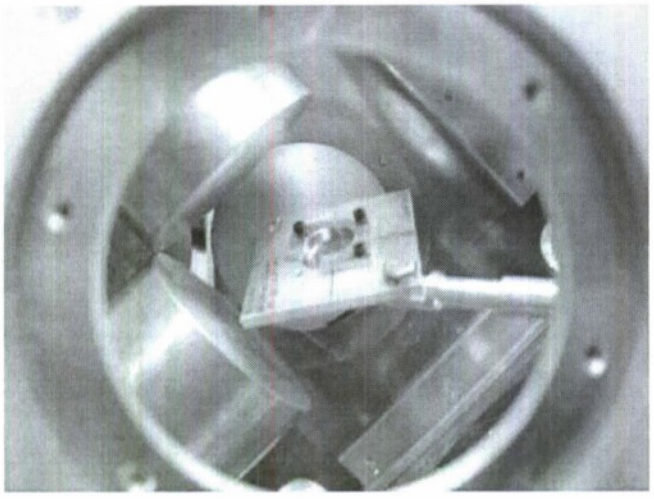

Fig. 8. Sample containing ^{178m2}Hf and ^{172}Hf, attached to the positioning arm and held in the central cavity of the miniball. Pb wraps around the BGO's were added after this picture. The diagonal of the cube containing the positioning arm is not perpendicular to the diagonal through which the synchrotron radiation was intended to pass in later experiments. The sample face was oriented at 15° with respect to the beam axis.

Fig. 8 shows a photograph of the sample employed in this work, attached to a positioning arm. The mechanical construction of the sample consisted of an Al frame that held together two 1-mm thick Be disks. The hafnium material was deposited by evaporation on one Be disk and occupied a roughly circular spot near the center of that disk.[1] The details of the distribution are not important for the present discussion, other than the fact that the radioactive Hf did not constitute a point source. The active content included 0.37 μCi of ^{178m2}Hf (2.0×10^{13} nuclei or 5.79 ng) and 0.29 μCi of ^{172}Hf (9.3×10^{11} nuclei or 0.26 ng) at the time of the tests in June 2004. It has been estimated [27] that the total hafnium content was approximately 2500 × that of the active ^{178m2}Hf material, which was produced by proton spallation [28]. The isomer-to-ground-state ratio for ^{178}Hf in the sample was also estimated [27] to be about 1:500. The hafnium material was deposited as a polycrystalline form by precipitation during 100% evaporation from solution in 1 N HCl. The sample was held within the miniball in the central cavity formed by the faces of the BGO crystals using the aluminum positioning arm that extended through one of the half diagonals of the cubic support structure. One full diagonal of the cube was reserved as the entrance and exit channels for synchrotron radiation. The large Ge detector coupled to the BGOs, an independent small Ge and an X-ray detector utilized separate half diagonals as viewing ports. The positioning arm was affixed outside the miniball structure to a translation table so that the sample could be moved remotely in a vertical plane. The orientation of the sample was determined by the eventual need to irradiate the largest possible area of the hafnium deposit with a beam spot of smaller dimensions.

[1]The distribution of hafnium material within the deposit was determined by passing a narrow (0.5 mm × 0.5 mm) beam of monochromatized synchrotron radiation set to the L_3 edge of Hf through the opening in the Al sample frame. Transmission of the radiation was recorded by pre- and post-sample ionization chambers as a function of sample position as it was raster-scanned across the fixed beam axis. (This procedure is discussed in detail in a forthcoming manuscript on searches for prompt-triggered gamma emission.)

3.2. Singles spectra, timing and detector efficiencies

Gamma radiation emitted due to natural decay of ^{178m2}Hf and ^{172}Hf within the mixed sample was recorded by the miniball system for a period of about 74 h. At regular intervals of about 12 h, the small dewar on the Ge detector was filled and data acquisition was halted for this period. The BGO PMT's were gain matched after each fill by minor adjustments to their operating voltages via software control. The Ge detector evidenced no gain drift and its voltage was maintained throughout the measurement. The data set consisted of 6831 3.5-MB files, each containing about 48,000 recorded events, from which a singles Ge spectrum was extracted as shown in Fig. 9. This was accomplished by first removing events of incorrect length, i.e. wrong number of parameters, which comprised about 0.3% of the data. Then the data were sorted without imposition of any conditions on coincidence between the Ge and BGO detectors or on detector pulse heights. The inset in the figure shows an expanded section of the spectrum that contains the doublet of lines at 213 and 217 keV that occur in the spontaneous decay of ^{178m2}Hf. The latter of these lines comes from the $9^- \rightarrow 8^-$ transition just above the *m1* isomer while the former originates with the $4^+ \rightarrow 2^+$ transition in the ground-state band (see Fig. 1). The doublet is well separated, indicating excellent performance for spectroscopy with this detector and confirming no measurable gain shift. All peaks in the spectrum were positively identified as corresponding to

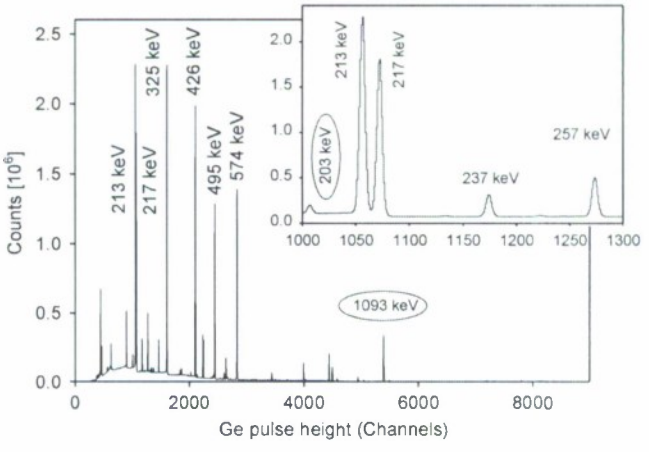

Fig. 9. Ge singles spectrum extracted from the miniball data without sort conditions and acquired for a total of about 74 h without irradiation. Major peaks from natural decay of ^{178m2}Hf (bare) and ^{172}Hf (ovals) are labeled.

gamma rays from spontaneous decay of ^{178m2}Hf, ^{172}Hf and its daughters, and natural background. The total event rate in the Ge was 1.2 kHz and deadtime resulting from this rate was on the order of 6%.

An initial question was the degree to which the efficiency of the large-volume Ge detector was influenced by the small gap through which it viewed the central cavity of the miniball. The restricted view was due to the BGO crystals and their Pb wraps and would partially shield the sample from view by the Ge detector. It was not possible to test this in the beamline hutch, so data were taken at Youngstown State University. Ge singles spectra were extracted from miniball data obtained using the hafnium source in two different geometric configurations: first, with the BGOs and Pb wraps in place and, second, with those BGOs and wraps removed which would otherwise have restricted the view of the Ge detector. Fig. 10a shows the "direct" efficiencies obtained from these measurements using the standard form

$$N_i = ATf_i\varepsilon_i^{\mathrm{Ge}} \tag{1}$$

where N_i is the number of counts contained within a given full-energy Ge peak, A is the sample activity, T is the acquisition live time, f_i is the fraction of decay events that emit γ_i and $\varepsilon_i^{\mathrm{Ge}}$ is the full-energy peak efficiency for detection of that specific gamma ray. The f_i values used in Eq. (1) were obtained from the ENSDF [2] as listed in Appendix A and peak fits were obtained using the commercial FitzPeaks program [29]. The effect of the gap between BGO crystals was to suppress the overall efficiency, but less so at higher gamma-ray energies where the cross section for photoelectric interactions decreases. Gamma rays entered only the central section of the Ge crystal and Compton-scattered photons therefrom had other opportunities to interact in the outer part of the detector. This produced the flattened efficiency curve shown in Fig. 10a when all BGO and wraps were in-place. Fig. 10b shows the actual Ge efficiency curve from data obtained at SPring-8, being about 0.35% near 1 MeV.

It was possible to provide an additional verification of the magnitude of the direct efficiency values. The method described in Appendix B was employed to obtain efficiencies based on the relationship between the number of counts in individual full-energy peaks and corresponding sum peaks appearing in the singles spectrum. Efficiencies determined in this way for specific pairs of gamma-ray energies are also plotted in Fig. 10b. It was not necessary for full-energy peaks in the Ge singles spectrum to be corrected for summing losses due to the small relative magnitude of this effect. The situation was different for the scintillators, as discussed below, which were closer to the sample and also had higher intrinsic efficiencies.

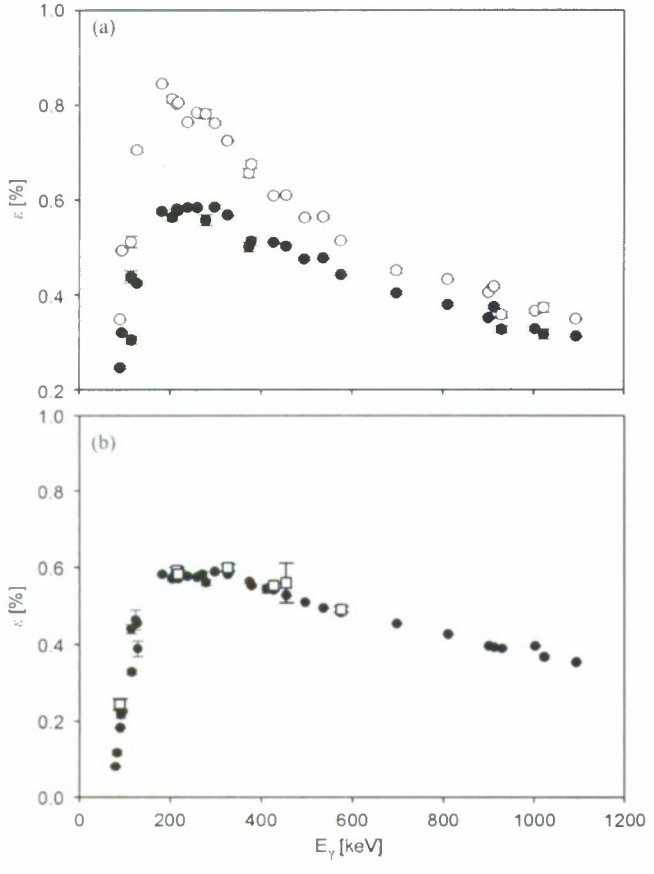

Fig. 10. (a) Plot showing measured efficiencies for the Ge detector using well-known gamma rays from ^{178m2}Hf and ^{172}Hf decays. Filled symbols indicate values obtained when the full miniball is assembled, including Pb wraps on the BGO crystals. The open symbols indicate values obtained when the BGO and their wraps are removed that would otherwise restrict the Ge detector's view of the central cavity. These measurements were made at Youngstown State University to determine the flattening of the efficiency curve due to the miniball configuration. (b) Plot showing measured efficiencies for the Ge detector using the hafnium source, taken at SPring-8 in the BL12B2 beamline hutch over a period of about 74 h. Efficiencies were determined directly from the counts within full-energy peaks (filled symbols) and also from selected sum peaks by the method of Appendix B (open symbols).

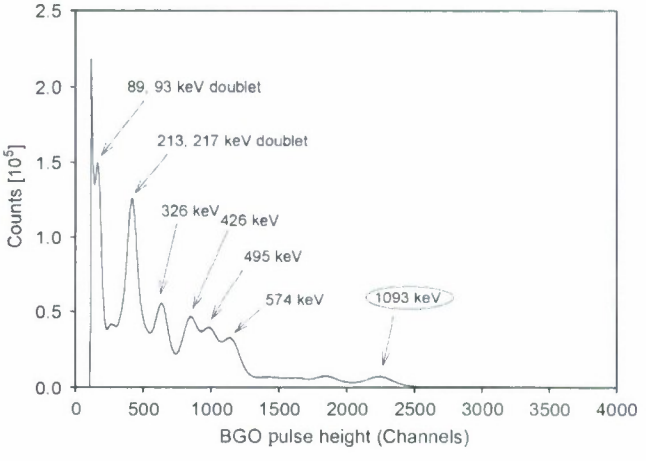

Fig. 11. Singles spectrum from a specific BGO detector and extracted without sort conditions from the full data set. Major peaks are labeled as in Fig. 9. The discriminator threshold for this BGO channel was significantly less than for other channels.

Singles spectra were also extracted for each BGO detector and one example is shown in Fig. 11. Again, no sorting conditions were imposed on the data, but the instrumentation required coincidence with a count from the Ge detector. The largest peaks in the spectrum were identified with intense gamma rays from ^{178m2}Hf and ^{172}Hf decays. The spectrum excludes the low-energy part of the 89/93-keV doublet due to the minimum thresholds in the CF discriminator. Clearly, spectroscopy with the BGO was severely inhibited due to the wide peaks, particularly for the many overlapping lines from the hafnium source. This same difficulty was found when attempting to determine the BGO efficiency using multi-line calibration sources such as ^{152}Eu. In no case could FitzPeaks provide meaningful fits for BGO spectra, but the well-known TV program [30] was able to provide accurate fits for singlets, with systematic errors on the order of 5% or less for sources such as ^{109}Cd or ^{137}Cs. It was also possible to obtain reasonable fits for the lines from ^{60}Co which were sufficiently resolved (see Fig. 6) and the efficiency for gamma-ray detection at 1332 keV in a single BGO crystal was about 3%. The paucity of points from single-line sources did not provide a suitable efficiency calibration over a wide range of energies, so a different procedure was employed.

A time spectrum obtained from a single BGO detector is shown in Fig. 12, extracted from the full data set. A START signal opened an active interval for the TDC such that STOP pulses occurring during this interval were distributed throughout the spectrum, as discussed above. Events in which (a) no gamma ray entered the BGO crystal, (b) no STOP pulse was generated because its energy was below the discriminator threshold, or (c) a STOP pulse was generated too late for the active window, were recorded in the sliding-scale section. Delays in the timing channels placed coincidence between Ge and BGO

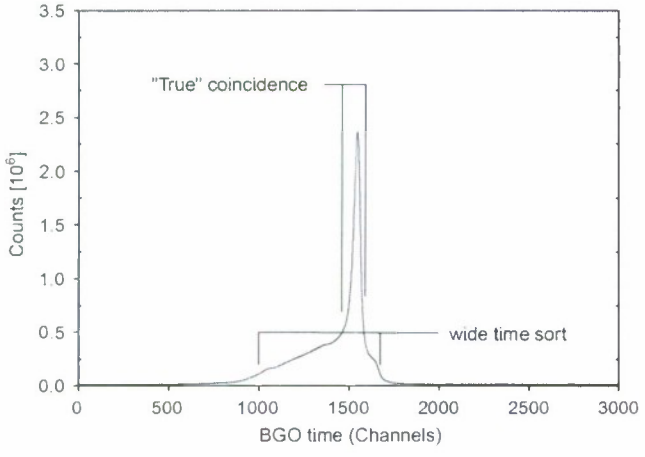

Fig. 12. Time spectrum for a specific BGO detector showing the distribution of STOP pulses. The "true" coincidence width is 51 ns, although a wider channel range was used in some time sorts to include the effects of walk of the Ge time mark (START) and BGO time mark (STOP).

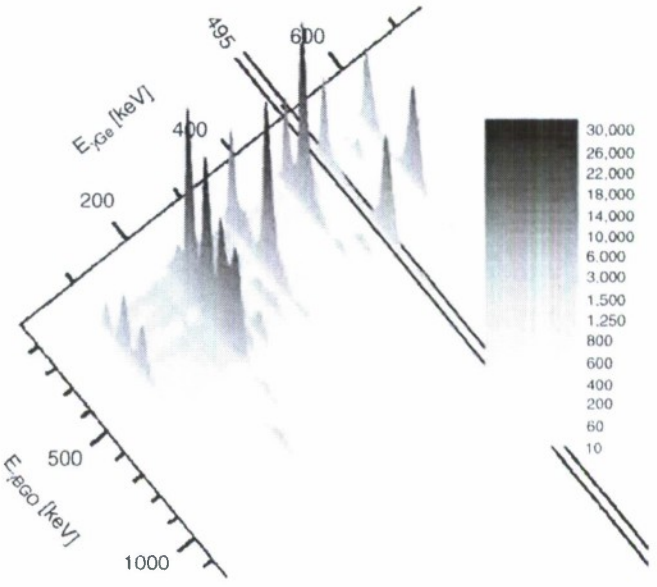

Fig. 13. Section of a bi-dimensional "doubles" spectrum displaying coincident events between the Ge detector and a specific BGO crystal. While full BGO singles spectra like that in Fig. 11 do not permit effective peak fitting, projections of slices ("cuts") of the doubles spectrum simplify the BGO spectra and do allow peak fitting. One cut is shown, made for events in which the full energy of the 495-keV gamma ray in ^{178m2}Hf→ ^{178m1}Hf decay is deposited in the Ge detector.

detectors at roughly the center of the active range. The shape of the coincidence curve in the figure indicated walk from low-energy pulses in the Ge channel as the origin of the shoulder to the left of the main coincidence peak. The smaller shoulder to the right was due to walk in the BGO channel. The full width of the narrow coincidence peak was 70 channels, corresponding to a resolving time of 51 ns. Based on the constant level of background far from the narrow peak, 0.72% of the counts within the 70-channel width corresponded to random coincidences with respect to the Ge START. Taking a larger width of 700 channels ensured inclusion of true coincidences with walk of either START or STOP signals and of those counts only 2.7% were due to random coincidences. Herein, a full sorting width of 700 channels was employed, but the effective resolving time for true coincidences was still on the order of 50 ns.

Fig. 13 shows a part of the γ–γ ("doubles") spectrum for the Ge and one specific BGO, extracted from the data set under the condition of coincidence as discussed above. While singles spectra (like that of Fig. 11) were too complex for fitting, projections of specific ranges in the γ–γ data allowed analysis using TV. Software gates (called cuts in TV) were made using this software,[2] such as the one shown in Fig. 13 around the 495-keV peak in the Ge projection. The BGO projection for this cut therefore

[2]Many other spectrum analysis programs were available, including the powerful Radware suite. The miniball system produces asymmetric data due to different detector types and so TV was chosen as being best suited to this application.

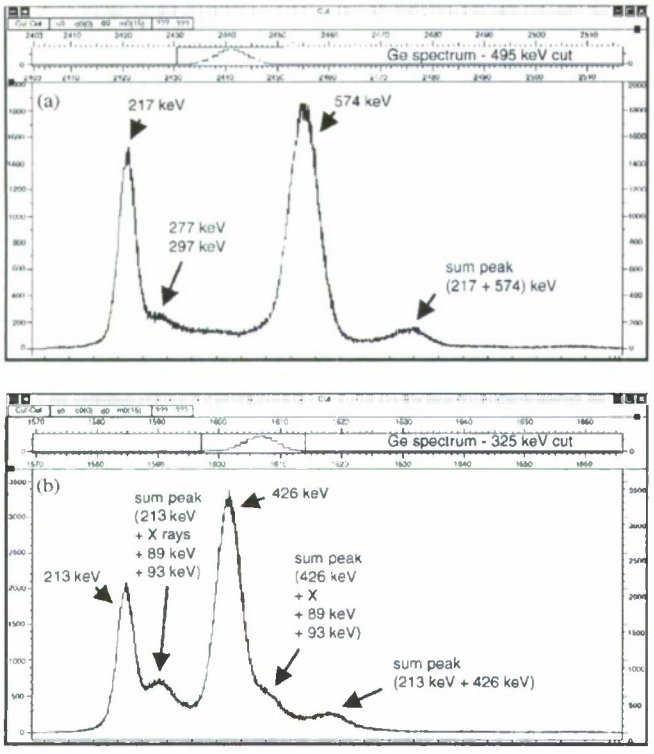

Fig. 14. (a) BGO projection (larger pane) obtained by a cut on the 495-keV photopeak in the Ge projection (short, top pane). The simplified structure in the BGO projection allowed identification and effective fitting of full-energy and sum peaks. (b) BGO projection obtained by a cut on the 325-keV Ge photopeak. Two coincident transitions are of too low energy to be recorded in the BGO due to discriminator levels. However, they appear as summations to the larger gamma-ray peaks at 213 and 426 keV, as do X-rays resulting from electron conversion.

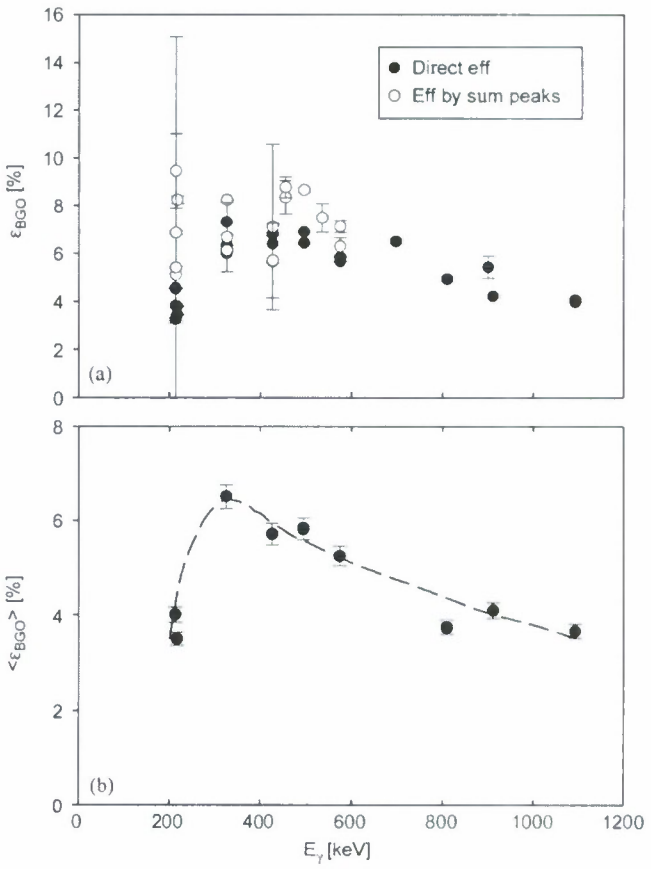

Fig. 15. (a) Plot showing measured efficiencies for a specific BGO detector using well-known gamma rays from ^{178m2}Hf and ^{172}Hf decays. Data were taken at SPring-8. Filled symbols indicate values obtained using the photopeak counts after inclusion of counts lost to summation. When possible, multiple values for the efficiency of each gamma ray were extracted from different cuts, providing an internal cross-check. Open symbols show values obtained by comparison of sum peaks from major gamma rays to the corresponding photopeak areas. (b) Effective single-BGO efficiency, obtained as the average of values from the six separate BGO detectors. Errors shown are systematic as statistical errors are comparable in magnitude to the size of the symbols. The curve is drawn to guide the eye.

contained coincident photopeaks and Compton events originating in the *m1* band of Fig. 1, and random coincidences. BGO spectra obtained from different cuts were quite sparse compared with a full projection and fits to the broad peaks were performed using the known energies of gamma rays emitted in ^{178m2}Hf and ^{172}Hf decays. Fig. 14 shows two BGO spectra corresponding to cuts on 495- and 325-keV lines in the Ge projection.

Efficiency values for gamma rays detected by a BGO and in coincidence with the Ge detector were obtained using the peak fits from cut spectra and are plotted in Fig. 15a. Considering a BGO spectrum that resulted from a specific Ge cut around γ_i, the number of counts N_{ji} in a full-energy peak therein was given by

$$N_{ji} = N_i f_{j|i} \varepsilon_j^{\mathrm{BGO}} \tag{2}$$

where N_i corresponds to the value in Eq. (1) provided that the cut process included standard background subtraction using channels in the continuum to the right and left of the Ge peak for γ_i. The $\varepsilon_j^{\mathrm{BGO}}$ denotes the photopeak efficiency for a specific γ_j in the BGO in coincidence with the given γ_i on which the cut was made in the Ge projection. The factor $f_{j|i}$ is the fraction of decay events that emit the particular γ_j provided that γ_i was also emitted (see Appendix A). A cut taken on the Ge 213-keV line provided BGO efficiencies for the coincident 325- and 426-keV lines. Likewise, a cut on the Ge 426-keV line provided BGO efficiencies for 213 and 325 keV. Thus, cross-checking was performed between efficiency values at each specific energy obtained using different cuts. It is worth noting that cut spectra corresponding to the ground state band did not include full-energy gamma-ray peaks at 89 and 93 keV from the $8^- \rightarrow 8^+$ and $2^+ \rightarrow 0^+$ transitions, respectively, or from X-rays following electron conversion. This was due to the small size of the corresponding unamplified BGO signals which were below most minimum discriminator thresholds. Nevertheless, the spectra evidenced summations between these gamma rays and the main features at 213, 325 and 426 keV. Also, summations appeared between X-rays emitted following conversion of the 89- and 93-keV transitions and the main gamma lines. These sum events

result from triple coincidences in which γ_i enters the Ge detector and both γ_j and γ_k enter a single BGO crystal. To determine the direct efficiencies from Eq. (2), counts in identifiable sum peaks within the BGO singles spectrum were added to the full-energy counts of individual gamma rays. The resulting efficiencies reflected values for hypothetical single-lines sources.

Efficiency values were also determined based on the relationship between individual and sum peaks using the method of Appendix B. Despite their larger statistical errors, their magnitudes confirm the direct efficiencies as shown in Fig. 15a. Systematic errors in fitting of the broad BGO peaks are not shown, but were estimated to be on the order of 10%.

Each scintillator evidenced a unique efficiency curve, as expected. The principal causes were that each detector lay at a slightly different spacing from the sample and that self-absorption was different for each specific sample orientation relative to a given detector. In one case (see Fig. 11), the CF8000 threshold could be set lower than for other BGO channels, but was increased to more closely match channels. For the following analysis, an averaged efficiency was determined as shown in Fig. 15b to represent the canonical single BGO response.

3.3. *Physical multiplicity and detected fold*

The miniball system was designed to perform time-resolved calorimetry for gamma-ray cascades resulting from natural decay of ^{178m2}Hf and from possible prompt induced energy release. Fig. 16 shows bi-dimensional plots of the Ge energy vs. the summed energy from the scintillators for different values of detected coincidence fold. Every event records at least one gamma ray, from the Ge crystal, so the total detected fold is designated as $(1+F)$, where F is the detected fold from the six BGO detectors. Sorting was performed as described above with F being the number of BGO's that produced a valid STOP pulse within the respective coincidence period of the individual detector. The summed gamma-ray energy registered from the BGO detectors was then obtained by adding the individual spectroscopic data from the separate scintillators.

Each natural decay of ^{178m2}Hf produces (see Fig. 1) two gamma-ray bursts from cascades separated by the 4-s *m1* isomer. Only a single cascade occurs below that isomer, releasing a total energy of 1147 keV and possessing a physical multiplicity M of five. However, the 93-keV transition is strongly converted ($\alpha_{93} = 4.74$) and it and the 89-keV transition are suppressed in the BGO spectra due to the discriminator levels. This means that the effective physical multiplicity is reduced to three unless the 89- or 93-keV gamma rays register in the Ge detector. The effective triplet cascade then contains the 213-, 325- and 426-keV transitions for a total energy of 964 keV. The cascade above the 4-s isomer releases 1298.7 keV and contains a number of branches, so that the physical multiplicity ranges from 4–6. The first step of the decay, the $16^+ \rightarrow 13^-$ transition at 12.7 keV, is completely converted with $\alpha_{12.7} = 1.39 \times 10^7$ so the effective physical multiplicity ranges from 3 to 5. The most intense branch (70.7%) occurs through the 574-, 495- and 217-keV transitions with a physical multiplicity of three (53.1% for the gamma-ray triplet). All gamma-ray triplets contribute a total of 72.2%.

Decay of ^{172}Hf nuclei in the sample produces gamma rays emitted in many different branched cascades from transitions in ^{172}Lu and ^{172}Yb. From the established nuclear data [2], on the order of 30 cascades correspond to a physical multiplicity of two, on the order of 140 cascades correspond to a physical multiplicity of three and on the order of 360 cascades correspond to a physical multiplicity of four. Higher multiplicity cascades are also possible. Beta decays of ^{172}Hf and ^{172}Lu can lead to different daughter levels, so cascades of identical physical multiplicity may represent various total energies released by the gamma-ray transitions. Despite the complexity of cascades following ^{172}Hf decay, a physical multiplicity of three represents a major component.

For a given physical multiplicity, the frequency with which a given detected fold F would occur could be modeled using a simple Monte Carlo code. Fig. 17a shows a histogram of the calculated detected fold F assuming an energy of 250 keV (with a measured BGO photopeak efficiency of 4.9% and therefore a total efficiency of about 5.7% used for this calculation, based on Ref. [31] and measured values) for all gammas in the cascade and a physical multiplicity of three. In this idealized case, the detected folds for the BGO detectors appear in the relative intensities listed in Table 1 and plotted in Fig. 17a. Also given are measured total counts within bi-dimensional Ge vs. summed BGO spectra for different coincident folds. The general agreement between measured and calculated intensities for different folds is surprisingly good, considering that the spectra contained contributions from different physical multiplicities. Another factor that reduced the accuracy of the calculation was that some coincidence counts in a BGO in coincidence were due to Compton rather than photopeak interactions. Some gamma rays reaching a BGO in coincidence did not provide a valid

Fig. 16. Bi-dimensional spectra showing events corresponding to different detected folds and displayed by the energy deposited in the Ge and the total energy deposited in all six BGO detectors: (a) corresponds to $F = 1$ with (b) being an expanded view; (c) corresponds to $F = 2$ with (d) being an expanded view; and (e) corresponds to $F = 3$ with (f) being an expanded view. Plots (a)–(f) were obtained by sorting the data on the wide time range. Plots (g) and (i) show data extracted using the wide time range for $F = 4$ and 5, respectively. Plot (h) shows a detected fold of $F = 4$ extracted using the narrow time range. Plots of $F = 5$ for the narrow time range and of $F = 6$ using either time range exhibit a small number of widely-scattered events that are not easily visible in print. The total counts in the $F = 5$ narrow-time sort spectrum is 53. The total counts in the $F = 6$ wide and narrow-time sort spectra are 38 and 0, respectively. Selected sum-energy loci are indicated as discussed in the text.

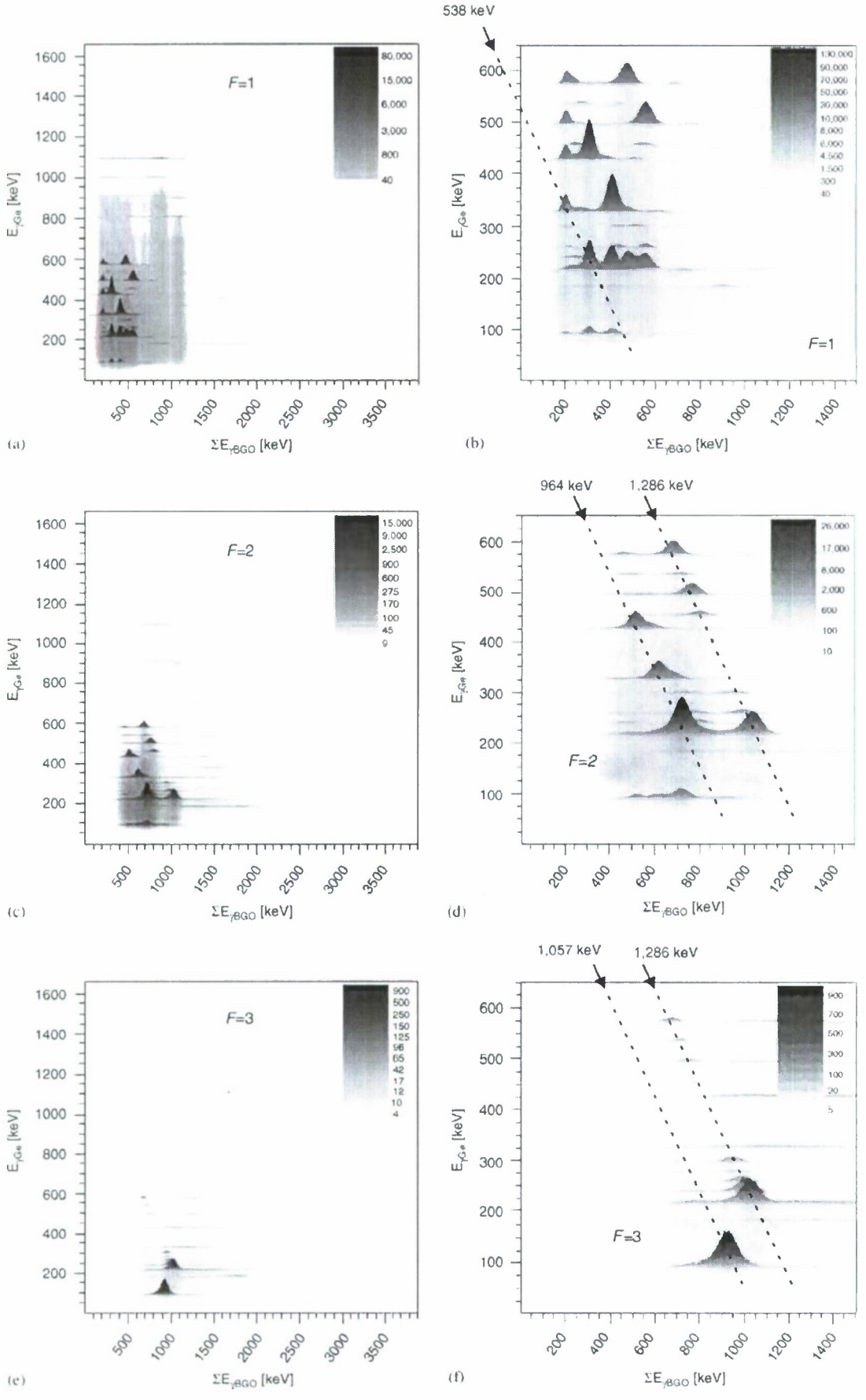
538 keV
964 keV
1,286 keV
1,057 keV
1,286 keV
F=1
F=2
F=3
(a)
(b)
(c)
(d)
(e)
(f)
$E_{\gamma Ge}$ [keV]
$\Sigma E_{\gamma BGO}$ [keV]

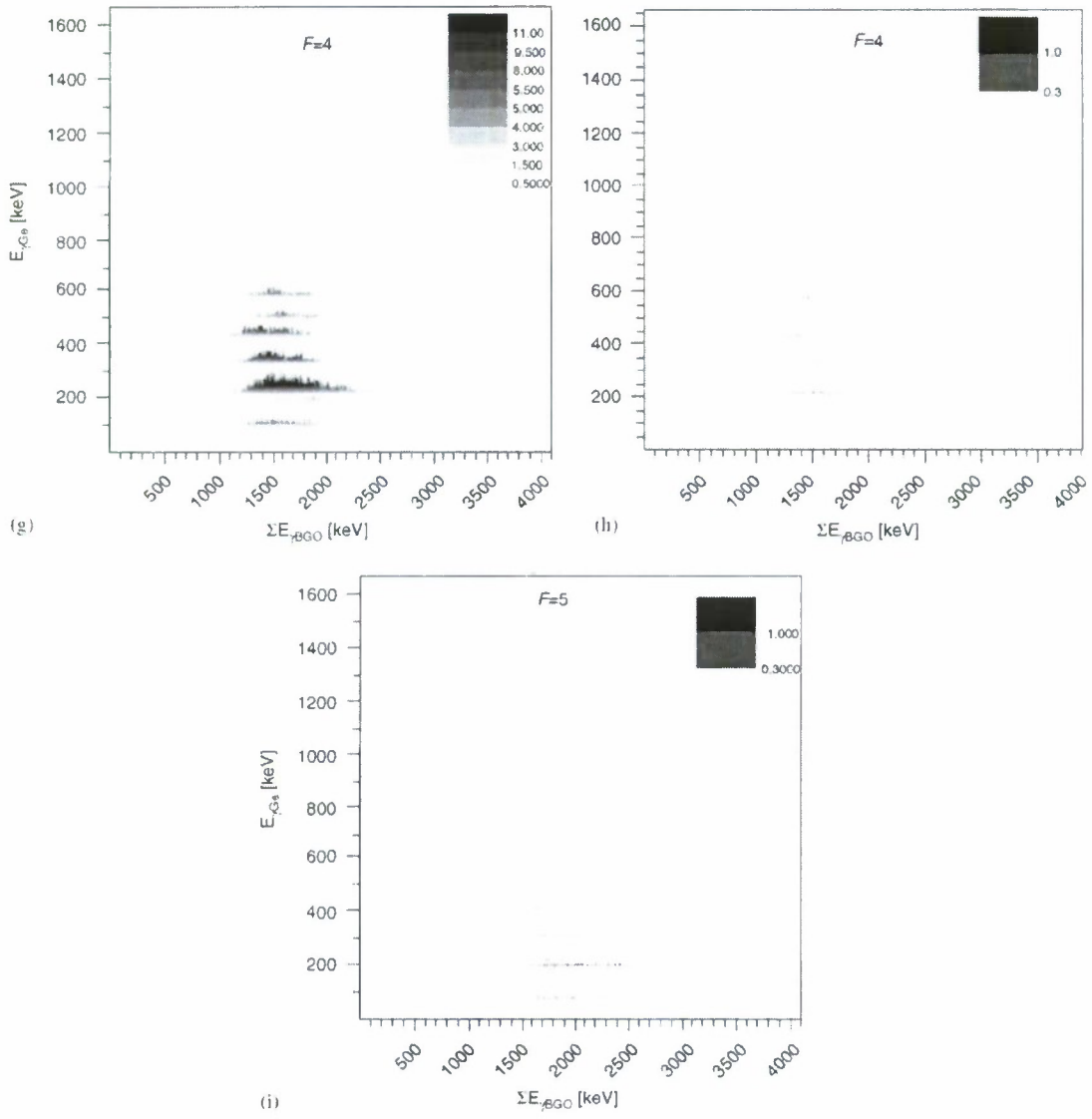

Fig. 16. (*Continued*)

STOP pulse due to their pulse height so that those events were recorded as having a detected fold of F—1 rather than F. This was also the case when coincident summing occurred within a single BGO. For prompt triggered gamma emission, the physical multiplicity will be on the order of eight so that the anticipated distribution of detected folds will be that of Fig. 17b.

3.4. Calorimetry

The spectrum of Fig. 16a, with expanded section in Fig. 16b, shows data for a detected fold of (1 + 1) (Ge + any one BGO[3]) and contains numerous paired gamma-ray peaks. In the case of ^{178m2}Hf decay in the cascade below the *m1* isomer, detection of 213 keV in the Ge coincident with detection of 325 keV in one BGO provides a peak while the converse (325 keV in the Ge, 213 keV in the BGO) provides its partner. A line drawn in Fig. 16a connecting these two peaks represents a locus of constant total deposited energy at 538 keV. This is significantly less than the total cascade energy since the physical multiplicity is five and the detected fold is only (1 + 1). Examination of the (1 + 2) spectrum of Fig. 16c, with expanded section in Fig. 16d, shows two loci of γ–γ–γ peaks corresponding to deposited energies of 964 and 1286 keV, representing nearly the full ^{178m1}Hf→^{178g}Hf and ^{178m2}Hf→^{178m1}Hf cascades, respectively.

The (1 + 3) spectrum of Figs. 16d and e also evidences a locus of 1286 keV from several cascade branches with

[3]This differs from Fig. 13 which shows doubles data between the Ge and one specific BGO, but without restrictions on what is recorded by the other BGO scintillators. Fig. 16a contains doubles between the Ge and any BGO for the case that exactly one of the BGO registers a coincident gamma ray.

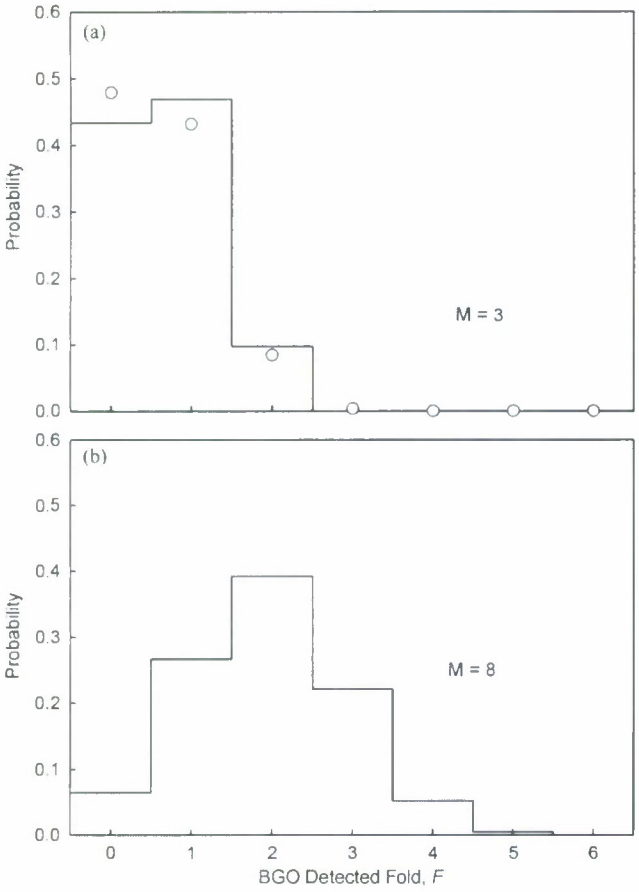

Fig. 17. Simulated distribution of BGO detected folds F for different physical multiplicities M for a cascade of 250-keV gamma rays and a corresponding total efficiency. The histogram of (a), with $M = 3$, represents the dominant cases for natural decay of ^{178m2}Hf and measured total counts in the spectra of Figs. 16c,d. The histogram of (b), with $M = 8$, represents the expected distribution of detected BGO folds for prompt triggered events, if any, from ^{178m2}Hf.

Table 1
Relative intensities for different BGO folds calculated for an idealized cascade of physical multiplicity three and based on the total BGO efficiency at a nominal 250 keV

F	Calculated intensity	Measured intensity
0	0.43	0.48
1	0.47	0.43
2	0.097	0.085
3	0	0.0038
4	0	0.00026
5	0	0.000011
6	0	0.00000014

Also given are relative intensities in measured bi-dimensional Ge vs. summed BGO spectra.

physical multiplicity of four above ^{178m1}Hf, while one peak is seen that corresponds to decay of ^{178m1}Hf to the ground state with summed energy of 1057 keV. The latter peak is actually a doublet of 89- and 93-keV lines in the Ge detector from events of physical multiplicity of four in the ground-state band. The peak corresponding to 93 keV in the Ge detector is smaller since the transition is heavily converted. No other peaks from the ground state band can appear with such high detected fold since the 89- and 93-keV peaks were suppressed from the BGO detectors due to discriminator thresholds.

In addition to features identified with ^{178m2}Hf, loci of constant summed energy appear in the spectra from cascades following ^{172}Hf decay. For a detected fold of (1 + 1) in Figs. 16a and b, paired peaks appear from 900- and 1093-keV transitions, giving a summed energy of 1993 keV. Many other peaks from ^{172}Hf decay contribute to the (1 + 1) spectrum, although in some instances both partners do not appear. This occurs when the energy of one of the gamma rays is too low to register in the BGO spectrum. For any detected fold, different summed energy loci exist from the numerous decay branches. Gamma-ray cascades in ^{172}Lu have summed energies less than 240 keV. Summed energies of ^{172}Yb cascades reach as high as 2343 keV (2.57%) after decay of ^{172}Lu, with a total of 9.59% exceeding 2200 keV.

If claims of prompt-triggered gamma emission from ^{178m2}Hf are correct, then the summed energy in an induced cascade would be about (2446 + 10) keV. The data shown in Fig. 16 evidenced no locus of coincident peaks at this summed energy and indeed none should occur for natural decays of the hafnium species in the sample. Fig. 16g shows a (1 + 4) spectrum with coincidence again determined by the wide (700-channel) time sort. The counts are quite low and distributed over a range of energies in the BGO dimension, suggesting a number of unresolved gamma-ray peaks. This is consistent with the numerous cascades of physical multiplicity five that occur in ^{172}Hf decay. The largest summed energy from these distributed counts would be about 2300 keV. It is interesting in Fig. 16g that the energies of coincident gamma rays from the Ge detector are those resulting from ^{178m2}Hf decay. Thus, these counts appear to be due to random coincidences between decays from the different hafnium species. Fig. 16h shows a (1 + 4) spectrum, but sorted on the narrow coincidence peak of Fig. 12 that contains a smaller fraction of random events. The number of counts is greatly reduced, confirming that random coincidences were the source of events in Fig. 16g. Random coincidences at a quite low level continue to appear for higher detected folds, such as $F = 5$ in Fig. 16i (wide time sort). A narrow time sort on $F = 5$ and wide and narrow sorts for $F = 6$ exhibit widely-scattered single events with total spectral counts of 53, 38 and 0, respectively.

In the subsequent experiment to examine gamma emission during irradiation with synchrotron radiation [19], it would be desired to determine the cross section for any prompt-triggered events. It is possible to foresee two possible outcomes from this experiment:

- Sufficient prompt induced gamma emission will occur so that identifiable peaks will appear in bi-dimensional Ge vs. summed-BGO spectra, or

- Insufficient prompt induced gamma emission will occur to produce identifiable peaks in bi-dimensional spectra and only scattered background counts appear.

In the first case, cuts in the $(1+F)$ spectra could be taken and the resulting peaks fitted in the summed-energy BGO projections. This would determine the measured rates for detection of specific $\gamma^{(1+F)}$ events and the placement of peaks along a locus of constant total deposited energy would allow the individual gamma-ray energies to be deduced. The reaction rate for induced events could then be determined from the detection rate of each peak by using the measured efficiencies for the different detectors at the appropriate energies and by assuming some value for f of the specific $\gamma^{(1+F)}$ cascade. An assumption of $f \approx 1$ would be reasonable for any prompt cascade through the ground-state band since there would be no branching and only a few transitions would be significantly converted. The cross section for prompt-induced gamma emission would finally be deduced from the reaction rate, the number of target ^{178m2}Hf nuclei and the incident photon flux.

To validate this approach, it was tested for various $(1+F)$ bi-dimensional spectra showing natural decay of ^{178m2}Hf. The analysis was performed only for *regular* peaks, i.e. those corresponding to deposition in the Ge of the full energy, E_i, of a single transition within a known cascade. Development of a general expression applicable to any regular peak for arbitrary detected fold and arbitrary summed energy is a complex problem that can be satisfactorily solved by Monte Carlo methods or the advanced approach of Ref. [21]. However, for the specific case of ^{178m2}Hf decay all the relevant cascade data are available. Thus, a relatively simple analytical approximation may be successfully applied to the observed intensities. To be consistent with the cuts of Figs. 13 and 14a, the case of $E_i = 495$ keV will be considered as resulting from a detected fold of $(1+2)$ and a summed energy of 1286 keV (see Figs. 16c and d).

Two cascades in the *m1* band can be identified that produce a 495 keV gamma ray (γ_i for the Ge detector): the $574 \rightarrow 495 \rightarrow 217$ keV sequence and the $297 \rightarrow 277 \rightarrow 495 \rightarrow 217$ keV sequence. Both cascades give a total energy of 1286 keV and thus will contribute to the number of counts in a regular peak resulting from a cut on 495 keV. A potential complication arises from the fact that $E_i = 495$ keV may also be produced by true coincidence summing (TCS) between 258 and 237 keV transitions[4] in two other cascades: $574 \rightarrow 258 \rightarrow 237 \rightarrow 217$ keV and $297 \rightarrow 277 \rightarrow 258 \rightarrow 237 \rightarrow 217$ keV. The probability of such TCS events occurring in the Ge crystal is lower than that for direct detection of the 495 keV gamma ray by about $(f_{258} f_{237|258}/f_{495})(\varepsilon^{Ge}_{258}\varepsilon^{Ge}_{237}/\varepsilon^{Ge}_{495})$. This factor is on the order of $(0.08)(0.005) = 0.0004$, so the probability of TCS in the Ge due to crossed-over transitions is negligible whenever the bridging transition is also detected.

For this regular peak, the number of counts $N_{i,F,\Sigma E} = N_{495,2,1286}$ is related to the rate of emission-causing events R and the measurement live time T by

$$N_{495,2,1286} = (RTf_{495}\varepsilon^{Ge}_{495})(30)[f_{574|495}\varepsilon^{BGO}_{574} f_{217|574,495}\varepsilon^{BGO}_{217} + 3f_{297|495}\varepsilon^{BGO}_{297} f_{277|297,495}\varepsilon^{BGO}_{277} f_{217|277,297,495}\varepsilon^{BGO}_{217}]. \quad (3)$$

The common combinatorial factor $30 = 6!/(6-F)!$ reflects that two of the six BGO scintillators exhibit full-energy deposition for this peak. The first term in the square brackets is an $M = 3$ cascade with γ_i, γ_j and γ_k caught in separate detectors while the second term is an $M = 4$ cascade in which one pair of gamma rays sum within a BGO detector. There are three possible pair-wise combinations for this cascade and for each of the 30 two-BGO combinations. One pair-wise combination, $297 + 277$ keV, is another example of crossed-over transitions, summing now within a scintillator. In Eq. (3) its contribution is negligible compared to that of the bridging 574 keV transition, but is included for completeness.

In the above example all of the M gamma rays from the cascades must be detected to contribute to the peak since it is partly defined by a total energy deposition of 1286 keV. Many possibilities exist for peaks to be produced with lesser total energies, such as when $(1+F) < M$ because one gamma ray misses all BGO detectors. This would require inclusion of a factor of the form $f(1 - 6\varepsilon^{BGO})$ where f is the joint probability for the missing gamma ray.

When applied to peaks corresponding to natural decays of ^{178m2}Hf, the rate R represents the sample activity. Using formulations like Eq. (3), the ^{178m1}Hf$\rightarrow$ ^{178g}Hf cascade in $(1+1)$ (Figs. 16a and b), $(1+2)$ (Figs. 16c and d) and $(1+3)$ (Figs. 16e and f) bi-dimensional spectra reproduce the known value of 0.37 μCi within ±15%. Application of the same procedure to peaks from the more complex ^{178m2}Hf$\rightarrow$ ^{178m1}Hf cascades reproduces the known activity to within ±30%.

An alternate means of determining the rate of prompt triggering would be required in the second case, where no identifiable peaks occurred in the bi-dimensional spectra. Then the detected rate for emitted gamma rays could only be determined from the total counts within a region of the spectra that corresponds to a specific summed BGO energy. For example, considering the width of peaks in the BGO dimension, events from a prompt-triggered cascade would reside between total energy lines of about 2380 and 2530 keV. Using effective efficiencies for Ge and BGO detectors averaged over this section of the bi-dimensional spectrum and an estimated f value, the reaction rate could be estimated. To determine if this procedure was feasible in practice, it was tested for regions in which natural decay of ^{178m2}Hf appears.

[4]The 495 keV transition bridges the two 258 and 237 keV transitions and represents the typical intraband case of a stretched E2 crossing over two component M1 transitions. In this case, the E2 branch is usually much more intense than the M1 branch since the former is of collective nature while the latter is more the result of single-particle changes.

Sum-energy ranges of 1200–1370 keV and 885–1040 keV were used in the (1 + 2) spectrum of Fig. 16b to count the total events from cascades above and below the 4-s isomer of ^{178}Hf, respectively. These were found to be 4,271,050 and 7,029,212 while in those same regions the counts within the full-energy peaks from ^{178m2}Hf cascades were 2,706,250 and 3,174,291. Thus, 63% and 45% of the total counts in the sum-energy ranges reside in full-energy peaks from this nuclide while the remaining counts are due to Compton events for ^{178m2}Hf gamma rays, photopeak and Compton events from ^{172}Hf decays, and other background. This background should include some contribution from cosmic rays, which will appear even with the shortest possible coincidence times. In order to estimate the activity based on the total counts within the ranges, and without basing this estimate on knowledge of specific peaks, it was necessary to employ some effective values for the joint emission probability and for the Ge and BGO efficiencies.

The estimated rate $R^{\mathrm{est}}_{(1+F)}$ of emission-causing events based on the total counts N_{101} within a sum-energy range from the (1 + 2) spectrum was determined using

$$R^{\mathrm{est}}_{(1+2)} = \frac{N_{101}}{T(3f)\left(30\left\langle \varepsilon_{\mathrm{Ge}}\varepsilon^{2}_{\mathrm{BGO}}\right\rangle\right)}. \tag{4}$$

Even without knowledge of specific peaks in the (1 + 2) spectrum, it is clear that triplet gamma-ray cascades will provide the dominant contribution to the total counts. Counts due to a triplet will appear spread over three peaks having the same sum-energy range due to the permutations of detection in the Ge and the scintillators. Taking the total counts in the sum-energy range means adding the contributions from all three peaks resulting from permutations for triplet detection. The Ge efficiency, however, was determined from Eq. (1) separately for each individual peak based on the full joint emission probability. Simply adding the numbers of events within all three permutations of the full-energy peaks overcounts the joint emission probability, thus the appearance of $3f$ in Eq. (4). For heavily branched cascades or when strong conversion occurs, the joint probability will differ significantly from unity. However, without knowledge of the specific cascades, a value of $f \approx 1$ is the only justifiable choice.

The Ge and BGO efficiencies for a (1 + 2) spectrum enter as a product of the form $\varepsilon^{\mathrm{Ge}}(\varepsilon^{\mathrm{BGO}})^2$ (see Eq. (3)). When employing the total counts within a sum-energy range, an average value over that range must be utilized. Using the total counts corresponding to ^{178m1}Hf→^{178g}Hf decay, an estimated rate of $R^{\mathrm{est}}_{(1+2)} = 33,670\ \mathrm{s}^{-1}$ was found, equivalent to an activity of 0.91 μCi. The sum-energy range corresponding to ^{178m2}Hf→^{178m1}Hf cascades provided $R^{\mathrm{est}}_{(1+2)} = 18,500\ \mathrm{s}^{-1}$, equivalent to 0.50 μCi.

Application of the same procedure to the (1 + 3) spectrum (Figs. 16d and e) gives rate estimates that are about a factor of 3–4 lower than the known ^{178m2}Hf activity of 0.37 μCi. For the ^{178m2}Hf→^{178m1}Hf sum-energy range, this was attributed to the use of $f \approx 1$ when the actual joint probability is about 0.1. The low value for the ^{178m1}Hf→^{178g}Hf sum-energy range was attributed to the fact that the low-energy gamma rays in the cascade (89 and 93 keV) do not register if they enter the scintillators, so that the total number of counts in the range is too low for the given multiplicity. Application of the procedure to the (1 + 4) spectrum (Figs. 16g and h) gives no estimate from the ground-state band (both 89- and 93-keV gamma rays must register for a total detected fold of five) and an estimate equivalent to 0.02 μCi for the ^{178m2}Hf→^{178m1}Hf cascades.

Prompt-induced gamma emission could be expected to exhibit little branching and few gamma rays out of the total multiplicity near 8 would have such low energies as to fail to register in the BGO detectors. Thus, the approach should provide a reasonable upper limit to the rate of such events should no peaks be in evidence in the bi-dimensional spectra.

The small number of counts within the summed-energy range of 2380–2530 keV, centered around (2446 + 10) keV, will serve as the background in the subsequent experiment [19]. Table 2 lists measured total counts due to natural decay and background in this region for bi-dimensional Ge vs. summed BGO spectra of different detected folds. The minimum detectable rates for gamma rays due to prompt triggering are also given, corresponding to three standard deviations of the background counts in the range for the specified fold.

Table 2
Measured total background counts (natural decay) and minimum detectable emission rates for the sum-energy range corresponding to prompt-induced emission, if any, from ^{178m2}Hf.

F	Total counts	Minimum gamma-ray detection rate [s^{-1}]
1 (wide sort)	32,180	2.56×10^{-3}
(narrow sort)	14,352	1.71×10^{-3}
2 (wide sort)	57,097	3.41×10^{-3}
(narrow sort)	7986	1.27×10^{-3}
3 (wide sort)	24,853	2.25×10^{-3}
(narrow sort)	1283	5.10×10^{-4}
4 (wide sort)	4342	9.39×10^{-4}
(narrow sort)	106	1.47×10^{-4}
5 (wide sort)	253	2.27×10^{-4}
(narrow sort)	2	2.02×10^{-5}
6 (wide sort)	3	2.47×10^{-5}
(narrow sort)	0	$< 1.01 \times 10^{-5}$

4. Summary

Claims of prompt gamma emission from ^{178m2}Hf induced by incident photons near 10 keV require confirmation by independent tests designed specifically for this type of event. The YSU miniball system is uniquely suited to such studies based on its capability for time-resolved gamma-ray calorimetry and is sufficiently compact and

portable to be transported to and placed within synchrotron radiation hutches. The system has been characterized by the natural decay of ^{178m2}Hf as a prelude to a search for low-energy prompt-induced gamma emission from this 31-year isomer. The sensitivity and detection limits for data obtained using the miniball were established.

Acknowledgments

The authors wish to thank Phil Walker (University of Surrey), Greg Lane (Australian National University) and Jo Ressler (Simon Fraser University) for valuable discussions. Special thanks go to M.-T. Tang, J.-J. Lee and K. Liang of the Taiwan National Synchrotron Radiation Research Center (NSRRC) and H. Suematsu of JASRI/SPring-8 for the gracious use of the BL12B2 contract beamline at SPring-8, and to SRS Technologies, Inc. for supplying the ^{178m2}Hf/^{172}Hf sample. Thanks also to Richard Sumner of CheeseCote Mountain CAMAC and Richard Laughlin of YSU Electronics Maintenance. Support for this work was provided by the DCI Postdoctoral Research Fellowship Program under contract 2002-H061400-000 and the US Air Force Office of Scientific Research under contracts F49620-03-1-0199 and F49620-02-1-0187.

Appendix A. Probabilities for individual and coincident gamma rays

The probability that an individual gamma is emitted following decay of ^{178m2}Hf is tabulated in the ENSDF [2] and adopted values are listed in Table A.1. Weak transitions found in Ref. [23] are not included as they could not be observed in this work.

Table A.1
Literature values [2] for emission probabilities and conversion coefficients for gamma rays resulting from decay of ^{178m2}Hf.

E_i [keV]	f_i	α_i	f_i^{calc}
12.7	7.178×10^{-8} (2)	1.39×10^{7}	7.181×10^{-8}
88.862	0.644 (10)	0.492	0.670
93.185	0.172 (3)	4.73	0.174
213.434	0.814 (11)	0.234	0.810
216.668	0.646 (10)	0.289	0.645
237.431	0.093 (2)	0.222	0.092
257.646	0.167 (4)	0.136	0.166
277.403	0.0138 (7)	0.13	0.0133
296.812	0.0969 (2)	0.090	0.0968
309.50	0.00019 (20)	8.66	0.00019
325.557	0.941 (11)	0.0626	0.941
426.360	0.970 (13)	0.0294	0.971
454.05	0.167 (3)	0.0249	0.164
495.013	0.713 (22)	0.0199	0.705
535.036	0.0941 (4)	0.0165	0.0908
574.215	0.879 (29)	0.0139	0.880

Errors on the adopted f values are given in the ENSDF format. Also given are calculated emission probabilities using the method described below

The above literature values were used in the determination of the efficiency for the Ge detector, from peak counts in the singles spectrum extracted without sort conditions from the miniball data and using Eq. (1) in the main text. Determination of efficiencies for gamma rays detected by single BGO scintillators requires the probabilities for double coincidences, since the instrumentation requires coincidence with the Ge detector. These probabilities may be calculated as follows based on the literature data.

Thirteen unique cascades from ^{178m2}Hf→^{178m1}Hf were identified as shown in Table A.2, again excluding the weak transitions found in Ref. [23]. The branching ratios for each transition were found from the f and α values according to

$$b_i = f_i(1+\alpha_i) \tag{A.1}$$

where b_i is the probability for a given branch from a given level, and f_i and α_i are the corresponding gamma probability and conversion coefficient. From these values it is possible to determine the total likelihood that any given cascade will occur. Based on Table A.2, the 574-keV transition is described by $b_{574} = (0.707 + 0.111 + 0.0741) = 0.892$, and from Eq. (A.1), $f_{574} = 0.880$. This agrees, as it should, with the literature value in Table A.1.

The joint probability that 574- and 495-keV gamma rays are emitted in coincidence is then found by

$$f_{574,495} = f_{574} f_{495|574} = f_{495} f_{574|495}. \tag{A.2}$$

It is straightforward from Table A.2 and Eq. (A.1) to find

$$f_{495|574} = \left(\frac{0.707}{0.707+0.111+0.0741}\right)\left(\frac{1}{1+0.0199}\right) = 0.777 \tag{A.3}$$

so that the joint probability $f_{574,495} = 0.684$. In a similar manner the joint probability for a triple coincidence may be found from Table A.2, as occurs when a single BGO exhibits sum peaks (γ_i detected by the Ge and both γ_j and γ_k detected by the BGO) or when two BGO detectors receive separate gamma rays. Only one cascade occurs in ^{178m1}Hf→^{178g}Hf decay and the joint probabilities then reduce to the product of the f values for the specific transitions. Other factors such as $f_{495|574,217}$, the joint probability that a 495 keV gamma rays is emitted given that 574 keV and 217 keV are also emitted, may be found in a similar manner.

While a tabular approach for enumerating possible cascades was simple for ^{178m2}Hf, it is not well suited for gamma rays resulting from decay of ^{172}Hf and its daughters. Among ^{172}Yb transitions there are 40 energy levels and about 2000 possible cascades following ^{172}Hf decay. The more general approach of Ref. [32] was used to determine f values needed to evaluate selected gamma rays following ^{172}Hf decay.

Table A.2
Unique cascades in decay of ^{178m2}Hf→ ^{178m1}Hf and their likelihood based on literature values

Cascade, E [keV]						Probability
12.7 →	574.2 →		495 →		216.7	0.707
12.7 →	574.2 →		257.6 →	454.1 →		0.111
12.7 →	574.2 →		257.6 →	237.4 →	216.7	0.0741
12.7 →	296.8 →	535 →		454.1 →		0.0544
12.7 →	296.8 →	535 →		237.4 →	216.7	0.0363
12.7 →	296.8 →	277.4 →	495 →		216.7	0.0118
12.7 →	296.8 →	277.4 →	257.6 →	454.1 →		0.00184
12.7 →	296.8 →	277.4 →	257.6 →	237.4 →	216.7	0.00123
309.5 →		535		454.1 →		0.000938
309.5 →		535		237.4 →	216.7	0.000626
309.5 →		277.4 →	495 →		216.7	0.000202
309.5 →		277.4 →	257.6 →	454.1 →		3.18×10^{-5}
309.5 →		277.4 →	257.6 →	237.4 →	216.7	2.12×10^{-5}

Appendix B. Determination of detector efficiencies via sum peaks of cascade gamma rays

Placement of the hafnium sample within the central cavity of the miniball represents a close geometry between source and detectors. The ^{178m2}Hf and ^{172}Hf radioisotopes emit cascades of gamma rays, so *true coincidence summing* (TCS) could be expected to impact the values of detector efficiencies determined from the counts within full-energy peaks. If the goal of the miniball system was to be able to compare the rates of emission at specific gamma energies from the natural decay, during and without irradiation by external photons, then efficiencies would not be required and TCS could be ignored. However, the possibility of emission of new gamma-ray lines from a prompt-triggered cascade required determination of the detector efficiencies and the role of TCS.

The general topic is discussed in Ref. [33] and numerous analytical, empirical and computational methods have been developed (see, for example, Refs. [32,34]). The methods all seek to correct the efficiencies determined directly from counts in full-energy peaks for events lost to summations. Herein it was desired to not only obtain such corrections, but also to determine the detector efficiencies based on comparison of the counts in sum peaks to the counts in the individual full-energy peaks. The latter would provide a verification of the direct efficiency values, and the radionuclide activities which enter the calculations in different order. No method has been applied previously to the hafnium nuclides of interest in this work, nor does the literature discuss the determination of efficiencies from the sum-to-individual-peak counts.

The present approach considers two gamma rays designated as γ_1 and γ_2, emitted in coincidence within a prompt cascade that may include other transitions. Entrance of both gamma rays into a single BGO detector causes a summation and a loss of counts from the respective photopeaks according to

$$N_j = N_i f_j \varepsilon_j^{\mathrm{BGO}} (1 - S_j) \tag{B.1}$$

where N_i is taken from Eq. (1) and N_j, f_j, and $\varepsilon_j^{\mathrm{BGO}}$ are the number of photopeak counts, the emission probability per decay, and the photopeak efficiency, respectively, corresponding to γ_j (recall that γ_i was already detected in coincidence in the Ge detector). The sample activity is A and T the acquisition live time. Self-absorption may occur as gamma rays emitted from the hafnium nuclei exit the sample through the Al frame (see Fig. 8), but this simply contributes to the real efficiency of a detector and does not appear explicitly in Eq. (B.1). All counts removed from the photopeak due to summations of any type are accounted for in the coefficient S_j. This includes, but is not limited to, summations with both full-energy and Compton events from γ_k and with both full-energy and Compton events from gamma rays other than γ_i , γ_j and γ_k in the same cascade. The number of counts appearing in a BGO sum peak, N_Σ, due to γ_j and γ_k is

$$N_\Sigma = (N_i f_j \varepsilon_j^{\mathrm{BGO}})(f_{k|ji} \varepsilon_k^{\mathrm{BGO}}) = (N_i f_k \varepsilon_k^{\mathrm{BGO}})(f_{j|ki} \varepsilon_j^{\mathrm{BGO}}) \tag{B.2}$$

reflecting the symmetry between peak-to-peak summations in the BGO crystal. The $f_{j|ki}$ is the conditional probability per decay that γ_j is emitted given that γ_k was emitted (to the same BGO) and γ_i was emitted for the Ge. These may be found as discussed in Appendix A.

In many instances, the parameter S_j will be approximately constant for a specific γ_j and γ_k pair. Then Eqs. (B.1) and (B.2) may be solved to obtain

$$\varepsilon_j^{\mathrm{BGO}} = \sqrt{\frac{N_j N_\Sigma}{\mathrm{ATN}_k f_j f_{j|ki}}} \tag{B.3}$$

and

$$1 - S_j = 1 - S_k = \sqrt{\frac{N_j N_k f_{j|ki}}{N_i N_\Sigma f_j}}. \tag{B.4}$$

The true efficiency value may also be determined from the apparent value, $\varepsilon_j^{\mathrm{BGO,app}}$, obtained directly from the

photopeak areas, using

$$\varepsilon_j^{\mathrm{BGO}} = \frac{\varepsilon_j^{\mathrm{BGO,app}}}{1 - S_j}. \tag{B.5}$$

In this approximation, the photopeak efficiencies for multi-line sources, such as ^{178m2}Hf and ^{172}Hf, may be determined through Eq. (B.3) or Eq. (B.5). Cascades emitted from ^{178m2}Hf satisfy the above approximation for a number of paired gamma rays that corresponded to sum peaks that did not exhibit contamination from actual transitions at that energy or from nearby ^{172}Hf lines. The values are plotted in Fig. 10b for the Ge detector and in Fig. 15a for a BGO detector. Direct efficiencies in Fig. 10 are uncorrected as S differs little from unity. The above method is similar to the more involved approach developed in Ref. [35] and efficiency values obtained by the two calculations typically agree to within less than 1%. Thus, the ^{178m2}Hf/^{172}Hf source may be valuable for efficiency calibrations of detectors even when TCS is significant.

References

[1] J.J. Carroll, S.A. Karamian, L.A. Rivlin, et al., Hyperfine Int. 135 (2001) 3.

[2] National Nuclear Data Center Online Evaluated Nuclear Structure Data File (ENSDF), www.nndc.bnl.gov, Brookhaven National Laboratory, 2005.

[3] C.B. Collins, C.D. Eberhard, J.W. Glesener, et al., Phys. Rev. C 37 (1988) 2267.

[4] D. Belic, C. Arlandini, J. Besserer, et al., Phys. Rev. C 65 (2002) 035801.

[5] P.M. Walker, G.D. Dracoulis, J.J. Carroll, Phys. Rev C 64 (2001) 061302.

[6] D. Cline, J. Modern Opt. Proceedings of the 35th Winter Colloquium on the Physics of Quantum Electronics 52 (2005) 2411.

[7] A.B. Hayes, D. Cline, C.Y. Wu, et al., Phys. Rev. Lett. 89 (2002) 242501;
A.B. Hayes, D. Cline, C.Y. Wu, et al., Phys. Rev. Lett. 96 (2006) 042505.

[8] J.J. Carroll, Laser Phys. Lett. 1 (2004) 275.

[9] C.B. Collins, N.C. Zoita, F. Davanloo, et al., Laser Phys. Lett. 2 (2005) 162.

[10] I. Ahmad, J.C. Banar, J.A. Becker, et al., Phys. Rev. C 71 (2005) 024311.

[11] C.B. Collins, N.C. Zoita, F. Davanloo, et al., Radiat. Phys. Chem. 71 (2004) 619.

[12] M.R. Harston, J.J. Carroll, Laser Phys 15 (2005) 487.

[13] E.V. Tkalya, Phys. Rev. C 71 (2005) 024606.

[14] G.D. Dracoulis, G.J. Lane, F.G. Kondev, et al., Phys. Rev. C 71 (2005) 044326.

[15] J.J. Carroll, J. Burnett, T. Drummond, et al., Hyperfine Int. 143 (2002) 37.

[16] I. Ahmad, J.C. Banar, J.A. Becker, et al., Phys. Rev. C 67 (2003) 041305(R).

[17] I. Ahmad, J.C. Banar, J.A. Becker, et al., Phys. Rev. Lett. 87 (2001) 0725031.

[18] C.B. Collins, N.C. Zoita, F. Davanloo, et al., Laser Phys. 14 (2004) 154.

[19] J.J. Carroll et al., Phys Rev. in preparation for 2006.

[20] I.Y. Lee, M.A. Deleplanque, K. Vetter, Rep. Prog. Phys. 66 (2003) 1095.

[21] M. Jääskeläinen, D.G. Sarantites, R. Woodward, et al., Nucl. Instr. Meth. 204 (1983) 385.

[22] J.J. Carroll, S.A. Karamian, M.K. Boyle, et al., Laser Phys 11 (2001) 6.

[23] M.B. Smith, P.M. Walker, G.C. Ball, et al., Phys. Rev. C 68 (2003) 031302(R).

[24] EG&G Ortec Modular Pulse-Processing Electronics and Semiconductor Radiation Detectors, 1997/1998, p 2.139, EG&G Ortec, 1998.

[25] KMaxNT, SPARROW Corporation, http://www.sparrowcorp.com/, 2006.

[26] R. Propri, S.A. Karamian, D. Gohlke, et al., in: Proceedings of the 7th AFOSR Workshop on Isomers and Quantum Nucleonics, Dubna, Russia, 2005 (JINR, Dubna, 2006).

[27] H. Roberts, G. Terry, M. Helba, et al., Analysis of Hf made at the LANL Nuclear Accelerator, Report prepared for the Army Research Laboratory, 2003.

[28] H.A. O'Brien, Nucl. Instr. Meth. B 40/41 (1989) 1126.

[29] FitzPeaks, JF Computing Services (http://www.jimfitz.demon.co.uk/fitzpeak.htm), 2005

[30] TV, Institute of Nuclear Physics, University of Cologne, Germany, www.ikp.uni-koeln.de/~fitz/, 2003

[31] Efficiency Calculations for Selected Scintillators, Saint-Gobain Ceramics & Plastics, Inc., 2005.

[32] K. Sinkko and H. Aaltonen, Calculation of the true coincidence summing correction for different sample geometries in gamma-ray spectroscopy, Finnish Centre for Radiation and Nuclear Safety Report STUK-B-VALO 40, 1985.

[33] G. Gilmore, J.D. Hemingway, Practical Gamma-Ray Spectrometry, Wiley, New York, 1995 (Chapter 7).

[34] S.H. Byun, W.V. Prestwich, K. Chin, et al., Nucl. Instr. Meth. A 535 (2004) 674.

[35] T. Vidmar, M. Korun, A. Likar, Nucl. Instr. Meth. A 508 (2003) 404.

$K^\pi = 0^+$ 2.29 s isomer in neutron-rich ^{174}Tm

R. S. Chakrawarthy,[1,2,*] P. M. Walker,[3] J. J. Ressler,[2] E. F. Zganjar,[4] G. C. Ball,[1] M. B. Smith,[1] A. N. Andreyev,[1] S. F. Ashley,[3] R. A. E. Austin,[5] D. Bandyopadhyay,[6] J. A. Becker,[7] J. J. Carroll,[8] D. S. Cross,[2] D. Gohlke,[8] J. J. Daoud,[1,3] P. E. Garrett,[1,6] G. F. Grinyer,[6] G. Hackman,[1] G. A. Jones,[3] R. Kanungo,[1] W. D. Kulp,[9] Y. Litvinov,[10] A. C. Morton,[1] W. J. Mills,[11] C. J. Pearson,[1] R. Propri,[8] C. E. Svensson,[6] R. Wheeler,[3,8] and S. J. Williams[3]

[1]*TRIUMF, 4004 Wesbrook Mall, Vancouver, British Columbia, V6T 2A3 Canada*

[2]*Department of Chemistry, Simon Fraser University, Burnaby, British Columbia, V5A 1S6 Canada*

[3]*Department of Physics, University of Surrey, Guildford, Surrey GU2 7XH, United Kingdom*

[4]*Department of Physics and Astronomy, Baton Rouge, Louisiana 70803, USA*

[5]*Department of Astronomy and Physics, St. Mary's University, Halifax, Nova Scotia, B3H 3C3 Canada*

[6]*Department of Physics, University of Guelph, Guelph, Ontario, N1G 2W1 Canada*

[7]*Lawrence Livermore National Laboratory, Livermore, California 94550, USA*

[8]*Department of Physics and Astronomy, Youngstown State University, Youngstown, Ohio 44555, USA*

[9]*School of Physics, Georgia Institute of Technology, Atlanta, Georgia 30332-0430, USA*

[10]*GSI, Planckstrasse 1, Darmstadt 64291, Germany*

[11]*Department of Physics, Simon Fraser University, Burnaby, British Columbia, V5A 1S6 Canada*

(Received 21 December 2005; published 8 February 2006)

Gamma-ray and conversion-electron spectroscopy have established the existence of a 2.29(1) s, $K^\pi = 0^+$, isomeric state in neutron-rich ^{174}Tm. The isomer deexcites via 100- and 152-keV electromagnetic transitions. First results from a newly commissioned Si(Li) detector array have established their $M1$ and $E3$ multipolarities, respectively. The single-particle configurations of the excited states suggest that the $E3$ transition originates from a $\pi h_{11/2}^{-1} \rightarrow \pi d_{3/2}$ configuration change, whereas the $M1$ transition occurs between members of a Gallagher-Moszkowski doublet. From the measured half-life, the deduced $B(E3)$ value of 0.024(2) W.u. is highly hindered. The reported measurements resolve ambiguities in the previously proposed β decay scheme of ^{174}Er to ^{174}Tm.

DOI: 10.1103/PhysRevC.73.024306 PACS number(s): 21.10.Tg, 23.20.Lv, 23.20.Nx, 27.70.+q

I. INTRODUCTION

Models of exotic neutron-rich nuclei predict interesting, as yet unexplored, new physics [1]. However, these nuclei are largely difficult to access in experiments. Isomeric states are proving to be a convenient tool to access and explore excited states in neutron-rich nuclei [2]. In well-deformed nuclei, isomerism can usually be ascribed to K-forbidden and/or high-multipolarity transitions [3]. After accounting for these aspects, the reduced hindrance then depends primarily on "local" nuclear-structure K-mixing effects, such as density of states, deviations from axial symmetry, and Coriolis mixing [3]. Taken together, these many influences severely complicate the prediction of isomer decay rates. Nevertheless, the experimental identification of isomeric states has a pivotal role in studies of nuclei approaching the drip-lines [2,4] and even of some of the heaviest nuclei synthesized to date [5]. Although there is evidence for exotic proton and two-proton decay modes of isomers near the proton drip-line [6], analogous questions regarding the neutron decay mode of isomers in the neutron-rich region are still open [7]. Additionally, one of the goals of a future study of neutron-rich nuclei in the Dy-Hf region is to search for the possible existence of an "island" of β-decaying high-K isomers [3,8]. Furthermore, isomer production, especially with high-energy proton-induced reactions, is still poorly understood, and will be important for future radioactive-beam projects. There are open questions on the reaction mechanism and production cross sections of isomers in even-even, odd-even, and odd-odd nuclei [9]. Additional complications arise because of the unknown release times of isomers and exotic nuclei from, for example, surface-ionization ion sources. Thus, experiments form a crucial component to address these issues.

A new program of research in the deformed, isomer-rich, 170–190 mass region [3,8,10] has been launched at the Isotope Separator and Accelerator (ISAC) facility sited at TRIUMF, Vancouver, Canada. In the present work we report on the characterization of a new 2.29 s isomer in neutron-rich ^{174}Tm ($Z = 69$). The motivation to study such deformed odd-odd nuclei is based on their level structures, whose excitation spectra are among the most intricate and poorly characterized in nuclear structure physics [11]. This is associated with partially blocked pairing, high level density (resulting in a multitude of low-lying configurations), and complex decay patterns. The high probability of isomeric states is a key feature in the spectra of these nuclei, and their identification can lead to unambiguous temporal ordering of excited states. Such is the case with ^{174}Tm, as presented here.

II. EXPERIMENTAL PROCEDURE AND RESULTS

In the present series of experiments, nuclei far from the line of β stability are produced at the ISAC facility using 30-μA 500-MeV proton-induced reactions on a Ta target. The reaction products deexcite during transit, whereas long-lived

*Electronic address: rsc1@triumf.ca

isomers ($T_{1/2} \geqslant$ a few milliseconds) allow a fraction of the isotopes to be delivered in an excited state. The reaction products are extracted using a surface ionization source and accelerated to an energy of 30 keV. A high-resolution mass analyzer separates species with different mass number, which are then transported to experimental stations such as the 8π spectrometer. This spectrometer has been reconfigured in a close-packed configuration [12] and is comprised of 20 Compton-suppressed high-purity germanium detectors. The low-energy beams from ISAC are focused at the center of the 8π array and stopped in a 12.7-mm-wide continuous-loop collector tape that is fed from a large aluminum storage chamber. The movable tape transport facility removes long-lived activity from the focus of the 8π array and minimizes the contaminating activity present in an isobaric beam. Within the 8π array, an aluminum hemispherical mounting houses five Si(Li) detectors in a pentagonal geometry, cooled to liquid-nitrogen temperatures. Typically, the off-line intrinsic resolution of the (cooled) Si(Li) detectors is 2.9-keV at 975-keV (K-shell converted electron of the 1063-keV transition in ^{207}Bi); whereas the in-beam resolution is 1.85-keV at 302-keV (K-shell converted electron of the 364-keV transition in ^{174}Tm β decay). Each of the five Si(Li) detectors, 5 mm thick, circular in shape, and with an area of 200 mm^2, was mounted at a distance of 2.2 cm from the beam focus. The Pentagonal Array for Conversion Electron Spectroscopy (PACES) covers 8% of the solid angle [13].

In two sets of experiments several of the known high-K isomers in the Dy-Hf region, with half-lives ranging from a few milliseconds to several minutes, have been accessed [14]. We report here the spectroscopy of a new 2.29(1) s isomer in the neutron-rich nucleus ^{174}Tm. An initial study measuring only the γ transitions was presented at ENAM04 [15]. The $A = 174$ isobaric beam was implanted into the movable tape transport facility, with beam-off/beam-on/beam-off cycling times of 2s/2s/2s, 2s/3s/3s, 5s/10s/10s, and 10s/100s/50s. Any remnant radioactive decay from the beam particles missing the tape were monitored in the initial beam-off period after moving the tape.

Singles and coincidence γ-γ, γ-electron, and electron-electron data were acquired and sorted off-line into several matrices; these include γ-time, electron-time, γ-γ, γ-electron, and electron-electron coincidence matrices. Standard radioactive sources of ^{152}Eu, ^{133}Ba, ^{207}Bi, as well as the known γ-ray and electron peaks from ^{174}Tm ground-state β decay, were utilized to calibrate the spectra. The accumulated γ-ray data were dominated by the ground-state β decay of ^{174}Tm ($T_{1/2} = 5.4$ min). The detection of new isomers is compounded by the presence of multiple decay sources of varying intensities in the form of (here, $A = 174$) isobaric contaminants as well as ionized fluoride/oxide molecular beams (leading to decays from the $A = 158$ and $A = 155$ mass chains). Despite contamination, a judicious choice of cycling times enabled rather clean separation of, especially, short-lived isomers. The yields of the $A = 174$ oxide beam, mainly emanating from the decay of ^{158}Er and ^{158}Tm, were measured to be 13 and 1% of the ^{174}Tm$_{g.s.}$ yield, respectively; whereas the decays from the $A = 174$ fluoride beam, primarily from ^{155}Tm, was measured to be at a 0.03% level. Figure 1 shows the singles γ-ray spectrum, after subtracting the dominant ^{174}Tm$_{g.s.}$ activity. The inset shows the growth and decay curve of the 2.29(1) s isomer in the 2s/3s/3s tape cycle [15]; the prominent peaks are the 100.3- and 152.1-keV γ-ray transitions and the Tm K x rays. The ground-state-to-isomer ratio (later corrected for electron conversion) is 200:1 and demonstrates the device sensitivity. The two coincident γ-ray transitions were, in addition, also known to be present in the ground-state β decay of ^{174}Er, which has a half-life of 3.3 min [16,17]. From the γ-γ coincidence data, K-conversion coefficients of 3.1(1) and 1.13(6) were extracted, respectively, for these two transitions and were the basis for $M1$ assignments in the previous works [15,17].

The ground-state spin and parity of ^{174}Tm are known to be $I^\pi = 4^-$, as deduced from the ground-state systematics of the odd-proton Tm isotopes and the $N = 105$ isotones, and the allowed-unhindered β decay proceeding to the lowest two excited 5^- states in ^{174}Yb [18]. However, the excited states in ^{174}Tm populated in the $I^\pi = 0^+$ ground-state β decay of ^{174}Er

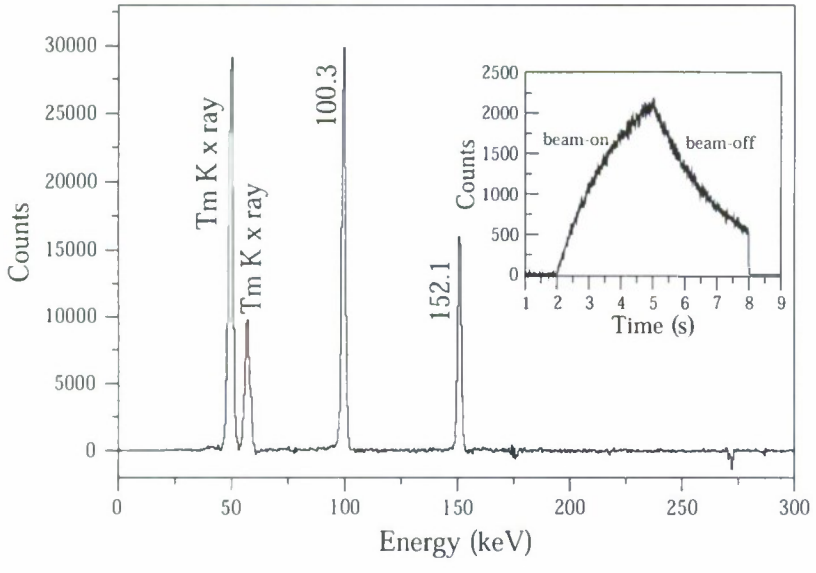

FIG. 1. The short-lived singles γ-ray spectrum showing prominently the Tm K x rays and the 100- and 152-keV γ-ray transitions. The 5.4-m ^{174}Tm ground-state β-decay component has been subtracted. The inset shows the growth and decay of the isomer gated by the 100-keV γ-ray transition.

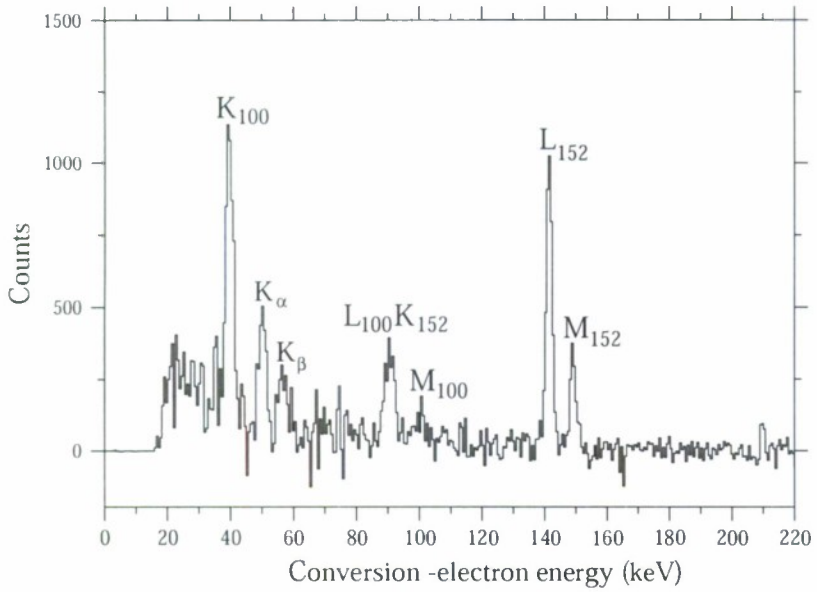

FIG. 2. The singles conversion-electron spectrum obtained by subtracting the 5.4-m ^{174}Tm ground-state β-decay component. K_γ denotes the conversion-electron corresponding to the γ-ray transition, whereas the Tm x rays are labeled K_α/K_β.

must be of low spin. Hence an unobserved low-energy, high-multipolarity transition was postulated between the low-spin states observed following β decay and the high-spin ground state [17]. However, several issues could not be resolved from γ-ray spectroscopy alone. These relate to the large intensity difference between the two, seemingly $M1$, γ-ray transitions at 100 and 152 keV; the absence of a 252-keV crossover $E2$ transition; and speculation that the isomeric state could be a new excited state, the decay of which could not itself be established, requiring population from a hypothesised high-K β-decaying isomer in ^{174}Er [15].

A closer examination of the K-electron conversion coefficient for the 152-keV transition, extracted from x-ray and γ-ray intensities [15,17], reveals that it agrees, within error, with the values expected [19] for a $M1$ multipolarity ($\alpha_K = 0.81$) and an $E3$ multipolarity ($\alpha_K = 1.18$). Furthermore, a $E3$ multipolarity for the 152-keV transition would explain the large intensity imbalance with the 100-keV transition that arises from the earlier deduction of $M1$ multipolarity for both transitions. However, the L-conversion coefficients would differ greatly ($\alpha_L = 0.12$ and 4.1 for $M1$ and $E3$ multipolarity, respectively), motivating a measurement involving a conversion-electron spectrometer. Therefore, in a follow-up experiment, a new conversion-electron spectrometer, PACES, was brought on-line at the 8π-spectrometer station. The singles conversion-electron spectrum obtained by subtracting (with appropriate time restrictions) the transitions from the 5.4 m ^{174}Tm ground-state β decay is depicted in Fig. 2. This clearly illustrates electrons from K-, L-, and M-converted transitions that are involved in the isomer decay, in addition to the Tm K_α and K_β x rays. The conversion-electron spectrum, gated by the 100-keV γ-ray transition, is shown in Fig. 3. The key feature is

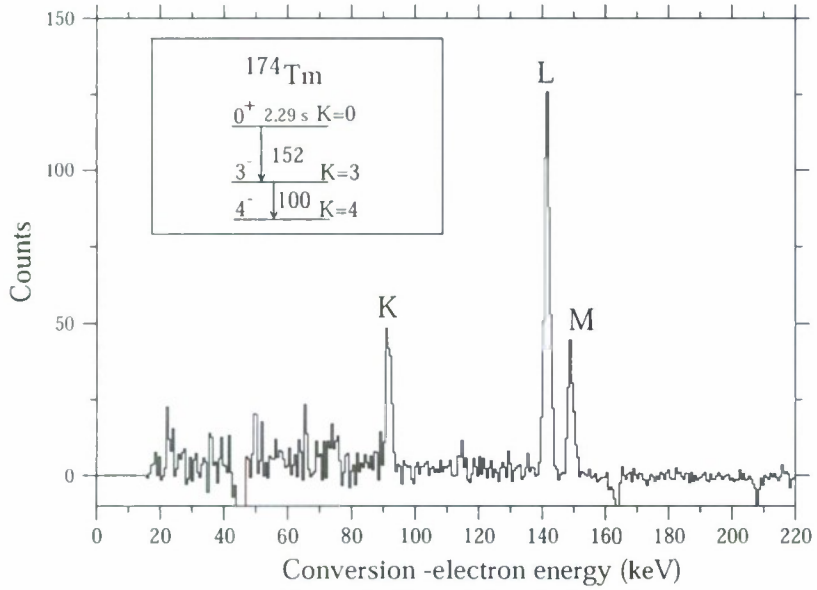

FIG. 3. The conversion-electron spectrum gated by the 100-keV γ-ray transition. The earlier [15,17], incorrect, $M1$-multipole assignment for the 152-keV transition would have given rise to strong K conversion and very little L and M conversion. The inset depicts the isomer decay scheme as a result of the present work.

TABLE I. Relative γ-ray intensities, experimental and theoretical internal conversion coefficients (ICC).

E_γ keV	I_γ	ICC (present expt.)	ICC (Ref. [17])	ICC(theo., Ref. [19])	Multipolarity
152.1	66.5(6)	α_K 1.13 ± 0.06	α_K 0.54 ± 0.06	$\alpha_K(E3)$ 1.18	$E3$
		α_L 3.31 ± 0.48	—	$\alpha_L(E3)$ 4.10	
		α_M 1.10 ± 0.12	—	$\alpha_M(E3)$ 0.99	
100.3	100.0(6)	α_K 3.1 ± 0.01	α_K 1.7 ± 0.3	$\alpha_K(M1)$ 2.66	$M1$
		α_L 0.45 ± 0.10	—	$\alpha_L(M1)$ 0.40	
		α_M 0.14 ± 0.03	—	$\alpha_M(M1)$ 0.09	

the prominent peak at 142-keV because of L conversion, with the K- and M-conversion peaks being of relatively low intensity in this spectrum. The deduced conversion coefficients, as well as the K/L- and L/M intensity ratios, compare very well with an $E3$ multipolarity assignment for the 152-keV transition and rule out the $M1$ alternative. Similarly, the conversion electron data unambiguously assign $M1$ multipolarity to the 100-keV transition. The K-, L-, and M-conversion coefficients from the present and the previous data are shown in Table I. The deduced isomer decay scheme is depicted in the inset of Fig. 3. Analysis of the electron-electron coincidence matrix shows the expected coincidence relationships between the K and L conversions emanating from the two coincident transitions.

III. DISCUSSION

As discussed, the ground-state spin-parity of ^{174}Tm was deduced to be 4^-. In view of the lack of a crossover γ-ray transition (I_γ 252-keV $\leqslant$ 0.34% I_γ 100-keV) or a highly converted $M4$ transition, in the "singles" conversion-electron spectrum (Fig. 1), it is reasonable to infer that the 100- and 152-keV transitions are of stretched $M1$ and $E3$ character, respectively. A 100-keV $M1$ transition would not give rise to such a long half-life, so the 152–100 keV transition ordering is well defined. Accordingly, the spin-parity sequence is (in increasing energy order) either $4^- - 5^- - 8^+$ or $4^- - 3^- - 0^+$. Only the 0^+ assignment for the 252-keV isomer is consistent with the known indirect feeding from the β decay of ^{174}Er [16,17].

Because this is one of the most deformed regions of the nuclear chart, the levels can be classified by the K quantum number, equal to the value of the spin of each intrinsic state. Thus, the isomer acquires a $K^\pi = 0^+$ assignment. The identification of the isomer contradicts the previous claim of observing the 100- and 152-keV γ-ray transitions in coincidence with β particles from the ^{174}Er ground-state decay [16,17]. Transitions with energies of 637, 643, 708, 714, 766, and 773 keV were observed in both the LBNL and GSI ^{174}Er β decay data [16,17], though not in the present work, as an erbium beam is not produced efficiently by the ion source. These γ-ray transitions likely feed the $K^\pi = 0^+$ isomer and originate from low-spin levels, consistent with a scenario of allowed Gamow-Teller β decay. Indeed, the summed singles intensities of all these transitions [17] is 94(4)% of the total ($\gamma + e^-$) intensity of each of the 100- and 152-keV transitions (from the deduced $M1$ and $E3$ assignments, respectively). Furthermore, a direct $^{174}\mathrm{Er}(I^\pi = 0^+_{\mathrm{g.s}}) \rightarrow {}^{174}\mathrm{Tm}(I^\pi = 0^+_{\mathrm{isomer}})$ Fermi transition will be strongly suppressed because of the nonanalog nature of the orbitals involved, consistent with the observed intensity flow.

The same selection rule also forbids β decay of the ^{174}Tm isomer to ^{174}Yb $K^\pi = 0^+$ levels. An upper limit of 1.0(5)% β-decay branch could be deduced for such a forbidden decay. This limit was determined from the peak-free region of the electron spectrum from the 2s/3s/3s tape cycle after background subtraction from the e^- time data. (A significant branch would indicate the importance of the so-called correction terms [20].)

A simple structural description of the observed states can be obtained purely by considering the available single-particle orbitals near the Fermi surface. For ^{174}Tm, the relevant proton single-particle Nilsson orbitals have quantum numbers $1/2^+[411]$ and $7/2^-[523]$, at a calculated quadrupole deformation of $\beta_2 \sim 0.28$ [21]. These orbitals couple with the neutron Nilsson orbitals, namely $7/2^-[514]$, $5/2^-[512]$, and $1/2^-[521]$, to produce a set of low-lying intrinsic states in ^{174}Tm. By comparison to the odd-A neighbors, the odd proton of ^{174}Tm is likely to be in the $1/2^+[411]$ Nilsson orbital (^{173,175}Tm $I^\pi_{\mathrm{g.s.}} = 1/2^+$), and the odd neutron in the $7/2^-[514]$ Nilsson orbital (^{173}Er,^{175}Yb $I^\pi_{\mathrm{g.s.}} = 7/2^-$). Following the empirical Gallagher-Moszkowski (GM) rules [22], a coupling of the orbitals $\pi 1/2^+[411] \otimes \nu 7/2^-[514]$, a spin-parallel triplet state, is especially energetically favored and gives rise to the ground-state spin-parity of $K^\pi = 4^-$. The observation of allowed-unhindered β decay to the $K^\pi = 5^-$ states in ^{174}Yb lends further support to this assignment [18].

The $K^\pi = 3^-$ state at 100-keV is suggested to be the singlet coupling of the GM-doublet arising out of the same orbitals, $\pi 1/2^+[411] \otimes \nu 7/2^-[514]$. The 100-keV $M1$ transition is then a K-allowed transition between the GM-doublet members. Indeed, calculations based on the quasiparticle phonon model (QPM) predict the two lowest lying intrinsic states in ^{174}Tm as a result of such a coupling, and the calculated splitting of 94-keV is very close to the observed splitting of 100-keV (neglecting zero-point rotational motion) [11]. The contribution of this quasiparticle configuration is about 66 and 63% in the triplet and singlet states, respectively; a small contribution of 12% is calculated to arise from a Q_{22} collective vibration.

The $K^\pi = 0^+$ state at 252 keV is seen to result from a favored coupling of the $\pi 7/2^-[523] \otimes \nu 7/2^-[514]$ Nilsson orbitals. The 152-keV $E3$ transition is then a K-allowed proton-hole transition from the intruder $h_{11/2}(\otimes h_{9/2})$ orbital to the normal-parity $d_{3/2}$ orbital. Incidentally, for this

configuration the protons and neutrons occupy the spin-orbit partners of the $1h$ orbital; such states are, supposedly, highly favored because of an attractive proton-neutron interaction. The 152-keV transition occurs between two intrinsic states differing only in the proton orbital, whereas the neutron orbital is a spectator. Likewise, the 100-keV transition involves a proton spin-flip. Thus, the two observed transitions in the decay scheme of the 2.29 s isomer can be explained as being K-allowed transitions that occur between three deformed intrinsic states involving only proton excitations. In well-deformed odd-odd nuclei, in addition to the usual K-selection rule, there is a two-particle transition selection rule involving the so-called nonoverlap forbidenness such that a simultaneous change of proton and neutron intrinsic configurations is severely hindered [23]. The proposed excitation scheme is consistent with the requirements of these two selection rules. From the measured half-life of 2.29 s, a $B(E3)$ value of 0.021(1) W.u. [using theoretical value of $\alpha(\text{theo})_{(\text{total})} = 6.61$] or, using the measured conversion electron coefficient $\alpha(\text{expt.})_{(K+L+M)} = 5.5(5)$, a $B(E3)$ value of 0.024(2) W.u. could be deduced for the 152 keV, $K^\pi = 0^+ \rightarrow K^\pi = 3^-$, transition. In terms of the hindrance factor, defined as [24]

$$F_W = \frac{T_{1/2\gamma}\,(\text{experiment})}{T_{1/2\gamma}\,(\text{Weisskopf})}, \tag{1}$$

the $E3$ transition is calculated to have $F_W = 42(4)$ [$\alpha(\text{expt.})_{(K+L+M)} = 5.5(4)$] or 48.7(2) [$\alpha(\text{theo})_{(\text{total})} = 6.61$], which is well within the prescribed range for a K-allowed $\Delta K = 3$, $E3$ decay [24].

IV. CONCLUSION

In summary, through γ-ray and conversion electron spectroscopy the excitation energy and decay properties of the 2.29 s isomeric level in ^{174}Tm have been firmly established. The results of three different experiments [15–17] can be combined to explain all the data consistently with a minimum number of states. The isomeric level is characterized by a $K^\pi = 0^+$ assignment and the two coincident γ-ray transitions involve mainly proton excitations. The deduced transition rate is hindered but well within the prescribed limits of K-allowed $E3$ decays. It is important for future experiments on heavy neutron-rich nuclei that there should be simultaneous measurements of both γ rays and conversion electrons, to derive unambiguous level schemes.

ACKNOWLEDGMENTS

We are grateful to the hard work put in by the TRIUMF accelerator personnel for a smooth operation of the Cyclotron-ISAC facility during the experiments. This work was supported in part by NRC/NSERC Canada, U.K. EPSRC, U.S. Department of Energy (DOE), and DARPA Microsystems Technology Office through U.S. AFOSR contract F49620-03-C-0024 with Brookhaven Technology Group, Inc. USA. J.J.C., D.G., and R.W. acknowledge support by the U.S. AFOSR under contract F49620-02-1-0817, and R.P. was supported by the Army Research Laboratory via contract W911CX-05-C-0081 to Ecopulse, Inc. USA. W.D.K. is supported through a U.S. DOE grant DE-FG02-96ER40958. JAB's work is supported under a US Dept. of Energy contract with UC-LLNL (nr. W-7405-Eng-48).

[1] J. Dobaczewski, I. Hamamoto, W. Nazarewicz, and J. A. Sheikh, Phys. Rev. Lett. **72**, 981 (1994).
[2] M. Caamano *et al.*, Eur. Phys. J. A **23**, 201 (2005).
[3] P. M. Walker and G. D. Dracoulis, Nature (London) **399**, 35 (2001).
[4] H. Grawe, A. Blazhev, M. Górska, I. Mukha, C. Plettner, E. Roeckl, F. Nowacki, R. Grzywacz, and M. Sawicka, Eur. Phys. J. A **25**, 357 (2005).
[5] F. R. Xu, E. G. Zhao, R. Wyss, and P. M. Walker, Phys. Rev. Lett. **92**, 252501 (2004).
[6] I. Mukha *et al.*, Phys. Rev. Lett. **95**, 022501 (2005); I. Mukha *et al.*, Nature (London) **439**, 298 (2006).
[7] P. M. Walker and J. J. Carroll, Phys. Today **58**, 39 (2005).
[8] P. M. Walker and G. D. Dracoulis, Hyperfine Interact. **135**, 83 (2001).
[9] B. L. Zhuikov, M. V. Mebel, V. M. Kokhanyuk, A. S. Iljinov, A. Y. Zyuzin, and J. S. Vincent, Phys. Rev. C **68**, 054611 (2003).
[10] K. Jain, O. Burglin, G. D. Dracoulis, B. Fabricius, N. Rowley, and P. M. Walker, Nucl. Phys. **A591**, 61 (1995).
[11] A. K. Jain, R. K. Sheline, D. M. Headly, P. C. Sood, D. G. Burke, I. Hrivnacova, J. Kvasil, D. Nosek, and R. W. Hoff, Rev. Mod. Phys. **70**, 843 (1998).
[12] G. C. Ball *et al.*, J. Phys. G **31**, S1491 (2005).
[13] E. Zganjar *et al.*, to be published.
[14] M. B. Smith *et al.*, Nucl. Phys. **A746**, 617 (2004).
[15] R. S. Chakrawarthy *et al.*, Eur. Phys. J. A **25**, 125 (2005).
[16] R. M. Chasteler, J. M. Nitschke, R. B. Firestone, K. S. Vierinen, P. A. Wilmarth, and A. A. Shihab-Eldin, Z. Phys. A **332**, 239 (1989).
[17] K. Becker, F. Meissner, W.-D. Schmidt-Ott, U. Bosch, V. Kunze, H. Salewski, R. Kirchner, O. Klepper, E. Roeckl, D. Schardt, and K. Rykaczewski, Nucl. Phys. **A522**, 557 (1991).
[18] N. Kaffrell and W. Kurcewicz, Nucl. Phys. **A255**, 339 (1975).
[19] F. Rösel, H. M. Fries, K. Alder, and H. C. Pauli, At. Data Nucl. Tables **21**, 91 (1978); http://ie.lbl.gov/programs/icc/icc.html.
[20] S. Raman, T. A. Walkiewicz, and H. Behrens, At. Data Nucl. Tables **16**, 451 (1975).
[21] W. Nazarewicz, M. A. Riley, and J. D. Garrett, Nucl. Phys. **A512**, 61 (1990).
[22] C. J. Gallagher and S. A. Moszkowski, Phys. Rev. **111**, 1282 (1958).
[23] C. J. Gallagher, Nucl. Phys. **16**, 215 (1960).
[24] K. E. G. Löbner, Phys. Lett. **B26**, 369 (1968).

Available online at www.sciencedirect.com
SCIENCE DIRECT
High Energy Density Physics 2 (2006) 48–56
High Energy Density Physics
www.elsevier.com/locate/hedp

Production of long-lived hafnium isomers in reactor irradiations

S.A. Karamian [a,*], J.J. Carroll [b], J. Adam [a,1], E.N. Kulagin [a], E.P. Shabalin [a]

[a] Joint Institute for Nuclear Research, Flerov Laboratory of Nuclear Reactions (FLNR), Joliot-Curie Str., 6, Dubna 141980, Moscow Region, Russia
[b] Youngstown State University, Youngstown, OH 44555, USA

Received 15 December 2005; revised 21 February 2006; accepted 8 March 2006
Available online 5 April 2006

Abstract

Experiments on production of long-lived ^{178m_2}Hf isomer in reactor irradiations are described. Properties of this nuclide are promising for its potential application as a relatively safe power source characterized by high density of accumulated energy. Metal ^{nat}Hf samples were activated in the Dubna IBR-2 reactor at positions corresponding to different neutron fluxes. Samples were bare or shielded by Cd and B_4C layers. The gamma activity of the samples was analyzed with Ge gamma spectrometers during a two-year period following their irradiation. In the presence of dominant activation products ^{175}Hf and ^{181}Hf, the high-spin isomers ^{178m_2}Hf and ^{179m_2}Hf were also detected despite relatively low levels. The isomer-to-ground state ratios and cross-sections were determined from the measured yields. For ^{178m_2}Hf, the cross-section for burnup (destruction) by neutron capture after its production was also estimated, clarifying the results from earlier experiments. In the context of suggestions for use of ^{178m_2}Hf for applications, the results confirm that large-scale production of this isomer by reactor irradiations is not feasible. In contrast, the efficiency of production of ^{179m_2}Hf is much higher and an amount of about 10^{16} atoms may be produced in standard reactor irradiations. For ^{178m_2}Hf, more productive methods are known, in particular fast neutron irradiations at $E_n \geq 14$ MeV and spallation reactions at intermediate energies. Neutron cross-sections for isomers may also be significant in astrophysics.

PACS: 28.20-v; 29.25.Rm; 84.60.Ve

Keywords: Energy storage; Isomer nuclide; Production; Reactor neutrons; Cross-sections

1. Introduction

High-energy density sources are needed for modern aerospace devices and for other applications. A compact, portable and safe source can attract attention of engineers of different specializations. The isotopes, like ^{238}Pu and ^{210}Po were used since many years, but their disadvantage was entirely clear because such a source being destructed should create a biologically dangerous α-radioactive pollution. Other nuclear power sources are ecologically dirty as well. During recent years, an interest has appeared in the energy stored by nuclear isomers. The ^{178m_2}Hf isomer is recognized in literature as most promising because it does not create daughter radioactive products that longer-lived than 4 s, emits only photons and soft electrons and is characterized by high-energy density of 1.3 GJ/g. This would be a source of relatively clean nuclear energy, which is not very dangerous even in a view of accidental destructions.

Possible use of ^{178m_2}Hf isomer as an energy reservoir was proposed in 1995 and discussed in the special issue of the "Hyperfine Interaction" journal [1]. In more detail, the advantageous properties of ^{178m_2}Hf and of some other isomers – candidates for triggered decay, were reviewed in Ref. [2]. Different ways for energy release due to a triggering of ^{178m_2}Hf by some external stimulus (like X-rays) have been tested beginning from 1999. More than 10 articles are published and the results are analyzed and commented in Ref. [3]. Unfortunately, some promising observations have not been reproduced and confirmed by other researchers and the problem remains

* Corresponding author. Tel.: +7 496 216 4668; fax: +7 496 216 5083.
E-mail address: karamian@nrmail.jinr.ru (S.A. Karamian).
[1] Permanent address: Inst. Nuc. Phys., Řez., CZ-25068, Prague, Czech Republic.

1574-1818/$ - see front matter © 2006 Elsevier B.V. All rights reserved.
doi:10.1016/j.hedp.2006.03.001

not yet well clarified until now. However, even without stimulation this long-lived ($T_{1/2} = 31$ y) source can find an application as a power supply unit for microelectronics devices in systems restricted in the size and weight. Therefore, it would be important to find relatively simple and inexpensive method for massive production of ^{178m_2}Hf. Reactor irradiations are known to be most productive for accumulation of radioactive isotopes, thus the reactor yield of ^{178m_2}Hf isomer has to be measured in reliable experiment.

On the other hand, the ^{178m_2}Hf production in the first wall of a fusion reactor was discussed in Ref. [4]. Fusion neutrons should be productive for the synthesis of ^{178m_2}Hf in stellar conditions, as well. Let us remind that the radioactive products of nucleosynthesis define the stable isotope abundances. For instance, the production and survival of ^{180m}Ta isomer in the cosmogenic radiation bath was described in Ref. [5] and in the references therein. The γ-radiation of radionuclides plays important role in the energy balance of stars. By the methods of γ-astronomy, some emission lines of nuclides, like ^{56}Ni–^{56}Co, were successfully detected, and one can suppose similar success in future for the ^{178m_2}Hf characteristic lines provided that the sensitivity of γ-telescopes is significantly improved. Such manifestations of ^{178m_2}Hf are defined by its production and destruction cross-sections with fast and slow neutrons. The present article is devoted to this problem.

Total and activation cross-sections as well as resonance parameters for slow neutron radiative capture may be found for stable Hf isotopes in the tabulations of Refs. [6,7]. It is well-known that the main activity induced in natural hafnium targets is due to the production of ^{175}Hf (70-day halflife) and ^{181}Hf (42-day halflife) after (n,γ) reactions. In addition, the short-lived first metastable (m_1) isomers of ^{178}Hf, ^{179}Hf and ^{180}Hf are also formed with cross-sections that are sufficient for successful detection. However, the production of high-spin second metastable (m_2) isomer via (n,γ) reactions in isotopes like ^{178}Hf and ^{179}Hf are more problematic. Only recently has a measurement appeared in the literature for the production of $J^{\pi} = (25/2^-)$ ^{179m_2}Hf [8]. The production of the famous $J^{\pi} = 16^+$ isomer ^{178m_2}Hf was reliably detected from its activity in 1973 [9], but the cross-section was deduced using some assumptions that deserve additional investigation.

The population of high-spin states following neutron capture may be expected to have a rather low probability due to the need for their population by stretched cascades of many γ rays. This type of cascade is characterized statistically by a relatively low yield. High-fluence irradiations are normally required in order to produce an observable activity for such low-yield products, but this introduces another complication in that a significant "burnup," or depletion, of the produced nuclei may occur.

For some products the destruction cross-section can be higher than 1000 barns. Therefore, fluences above 0.5×10^{21} n/cm^2 should be avoided to produce negligible burnup, or the remaining activity after irradiation would suggest a production cross-section that was significantly underestimated. With restricted fluences, a larger amount of the target material should be exposed for higher sensitivity of measurements. But, significant self-absorption of thermal and resonance neutrons in targets must also be avoided and this restricts a target thickness. In addition, fast neutrons within a reactor spectrum are sometimes useful for isomers production via $(n,n'\gamma)$ reactions, and their contribution may complicate the analysis of the experiment. All these factors must be kept in mind when designing experiments for the measurement of low-yield exotic radionuclides by reactor irradiations. In the present work, the production of the high-spin isomers ^{178m_2}Hf and ^{179m_2}Hf isomers was observed and quantitatively characterized. These measurements therefore serve to augment the existing data obtained in high-flux irradiations for the former isomer [9] and to provide new information for the latter [8]. The burnup of ^{178m_2}Hf by (n,γ) reactions was also investigated, expanding the results of Ref. [9] and comparing it with the present measurements.

2. Experimental detail

In a first series of experiments, metal Hf samples of about 20 mg were irradiated in an outer channel of the IBR-2 Dubna reactor of the Frank Laboratory of Neutron Physics, Joint Institute for Nuclear Research. Metal Hf targets of natural isotopic composition are advantageous as compared to an enriched target in their chemical purity and lower resonance-absorption factors. The standard method of Cd difference was applied for the isolation of the separate effects of thermal and epi-Cd neutrons. The neutron spectrum at the location of the targets was well-known from previous experiments, but NiCr-alloy samples were nevertheless irradiated as spectators. The activity of ^{51}Cr served to calibrate the slow neutron flux while ^{58}Co was produced in a reaction with fast neutrons at $E_n > 0.8$ MeV and was used for calibration of the fast neutron flux.

Following their irradiation, the activity of the samples was studied using a 20% efficiency HPGe gamma detector. The spectroscopic system allowed a count rate up to 15 kHz while preserving a reasonable dead time less than 25% and a spectral resolution on a level of 1.8 keV for the ^{60}Co lines. Standard test sources (^{152}Eu and others) were used for energy and efficiency calibrations of the γ spectrometer.

In measured spectra from the activated Hf samples, γ lines were observed and their peak areas quantitatively determined for the following radionuclides: ^{175}Hf, ^{179m_2}Hf, ^{180m}Hf and ^{181}Hf. The bulk of the activity was due to ^{175}Hf (70 d) and ^{181}Hf (42.4 d) formed in (n,γ) reactions. Negligible activity was contributed by admixtures of other elements in the Hf material. Only Zr was present in a quantity of about 3%, while the concentration of other elements was estimated to be on the level of less than 1 ppm. The detected yields of ^{175}Hf and ^{181}Hf were used as additional, intrinsic calibrators of the neutron fluxes and then the thermal cross-section $\sigma_{th} = (0.44 \pm 0.02)$ b and resonance integral $I_\gamma = (5.8 \pm 0.7)$ b were deduced for ^{180m}Hf production in the ^{179}Hf(n,γ) reaction. The resulting values were in good agreement with the tabulated data [6], confirming the accurate calibration of the neutron flux in these irradiations.

A yield of the high-spin ^{179m_2}Hf isomer was detected and clearly originated from reactions with fast neutrons, since the effect of thermal neutrons was found to be insignificant for its production. This conclusion was definite because bare and Cd-shielded samples showed the same activity of ^{179m_2}Hf within the standard error. No γ lines from ^{178m_2}Hf were observed in this first series of irradiations, reflecting its low production yield and the presence of much higher activities of other nuclides.

A second series of experiments were performed in order to significantly improve the sensitivity of the measurements for detection of the low-yield isomers. At the same position in the outer channel, a larger Hf sample was placed for a longer duration. The sensitivity was improved by three orders-of-magnitude, but this was still insufficient for observation of ^{178m_2}Hf. A strong increase in the neutron flux was then sought to increase the production of this isomer. In the reactor, an inner channel was available that allowed an irradiation near, but outside, the active core within a cylindrical region was shielded by a 3-mm layer of B_4C. A Hf sample was exposed there for 18 days, after which decay of the resulting activity was followed for two years. Finally, activity of ^{178m_2}Hf was successfully observed and its yield determined after the third series of irradiations.

At the inner location, the thermal flux was determined in earlier experiments to be about 0.5×10^{12} neutrons/(cm^2 s), thus during the 18-day irradiation a fluence near 10^{18} n/cm^2 could be accumulated. In the present experiments, the value of flux was not used explicitly since all measurements were carried out in a relative mode by comparing the activities of ^{178m_2}Hf, ^{179m_2}Hf and ^{180m}Hf nuclei to those of spectators and intrinsic calibrators ^{175}Hf, ^{181}Hf and ^{95}Zr which were present within the targets. Such a method is reliable and accurate in the presence of shields. Data processing requires special care for high-sensitivity measurements of neutron-production cross-sections. The burnup of isomeric nuclei produced during the irradiation must be taken into account when the neutron fluence exceeds 10^{20} n/cm^2. In the present irradiations, however, even in the inner channel the fluence was 100 times lower. This is due to the fact that IBR-2 is a pulsed reactor constructed specially for time-of-flight spectroscopy, not to achieve a high mean power. With this fluence, burnup of high-spin hafnium isomers or other double neutron-capture reactions may be expected to have a probability below 10^{-3} compared to the probability for single neutron capture. Nevertheless, some excess activity of ^{182}Ta was detected beyond that which could be attributed to single neutron capture on a small admixture of ^{181}Ta in the target. This excess production of ^{182}Ta was likely due to the double neutron-capture process: ^{180}Hf(n,γ) ^{181}Hf $\rightarrow$ ^{181}Ta$(n,\gamma)^{182}$Ta.

Also, in order to achieve a higher absolute yield of ^{178m_2}Hf in the second and third experimental series, relatively thick metal samples were used. Self-absorption of thermal and resonance neutrons could not be neglected for these thicker samples, which were rods of 1-mm cross-sectional dimension.

The well-known equation describing the reaction rate per target nucleus when exposed to comparable fluxes of thermal and resonance neutrons is:

$$r = \left(\sigma_{\text{th}} + \frac{I_\gamma}{k}\right) F_{\text{th}}, \tag{1}$$

where F_{th} is the thermal neutron flux. The coefficient k reflects the particular characteristics of the spectrum of irradiating neutrons, being a fixed constant for a definite location of each irradiation station in a specific reactor. It may be defined approximately as:

$$k = \frac{F_{\text{th}}}{F_{\text{res}}} \ln(E_2/E_1), \tag{2}$$

where $E_1$and E_2 define the "resonance" range of neutron energies and F_{res} is the flux of resonance neutrons. For simplicity, one can introduce the notation:

$$\sigma_{\text{eff}} = \left(\sigma_{\text{th}} + \frac{I_\gamma}{k}\right). \tag{3}$$

In the first series of experiments, the numerical value $k = 5$ was determined and this was in agreement with extensive previous measurements carried out in the outer channel of the IBR-2 reactor. The outer and inner channels used in this work are separated by only air and a shutter is opened when the outer channel is used. Thus, the same value of k was used for irradiations at the inner location, while the effect of B_4C and self-shielding was considered separately as described below.

The production rate of some nuclide in a target of definite composition and mass can be expressed as follows:

$$\frac{dN}{dt} = \frac{N_A c a m}{M}\left(\sigma_{\text{th}}\tau_{\text{th}} + \frac{I_\gamma}{k}\tau_{\text{res}}\right) F_{\text{th}}, \tag{4}$$

where N_A is Avogadro's number, c is the mass concentration of the element of interest in g/g, a is the abundance of a particular isotope of that element, m is the total mass of the irradiated target and M is the atomic mass of the element. The τ_{th} and τ_{res} factors are dimensionless attenuation coefficients reflecting self-absorption in the target layer for thermal and resonance neutrons, respectively. Each may reach a maximum value of unity for targets of negligible thickness or be significantly smaller for thick targets.

Eq. (4) describes the (n,γ) capture reaction with slow neutrons. The F_{th} and k parameters represent characteristics of the reactor, while all but one of the other parameters must be specified for a definite nuclide in the target, i.e. the capturing isotope. The lone exception is the factor τ_{th}, which is a unique parameter characteristic of all reactions with thermal neutrons in a target of specific composition and thickness and is independent of the particular capturing isotope. Unlike τ_{th}, τ_{res} is individualized because the resonance energies and peak cross-sections are extremely specific to each isotope and vary irregularly from one nuclide to another. Strong absorption near the resonance peak for one isotope may produce

absolutely no influence on the resonances of other nuclides. The partial thickness of the target corresponding to the individual isotopes will also depend on c, a and M, and this is important for resonance neutron absorption.

In the outer channel, neither the first nor the second series of irradiations were sufficiently intense to produce a detectable yield of ^{178m_2}Hf. However, the dominant activities of ^{175}Hf, ^{181}Hf and ^{95}Zr were measured with high accuracy. Using Eq. (4), the concentration of Zr was evaluated numerically, as well as the τ_{th} coefficient specific to the target and the resonance-absorption coefficient τ_{res} specific to ^{181}Hf production via the ^{180}Hf(n,γ) reaction. For ^{175}Hf and ^{95}Zr, resonance-absorption was insignificant due to the low concentration of ^{174}Hf and ^{94}Zr nuclides within the target. These evaluated parameters were then employed in the analysis of the measurements carried out following the irradiation near the active core that had much higher flux.

In the inner location, the thermal neutron flux was strongly attenuated (almost absorbed entirely) by the 3-mm thick B_4C shield, while the transmission of neutrons was also influenced at other energies below 20 eV. No sharp cut-off occurs since the total cross-section of boron varies smoothly with neutron energy. Therefore, activation by thermal neutrons could be excluded and the effect of resonance neutrons was characterized by a corrected resonance integral I_γ(corr) as follows:

$$I_\gamma(\mathrm{corr}) = I_\gamma \frac{\int_0^{E_{max}} E_n^{-1}\chi(E_n)g\Gamma_n \mathrm{d}E_n}{\int_0^{E_{max}} E_n^{-1} g\Gamma_n \mathrm{d}E_n}, \quad (5)$$

where I_γ is the tabulated resonance integral, $\chi(E_n)$ is the calculated transmission function through the B_4C filter, and $g\Gamma_n$ is the resonance strength obtained from the data of Ref. [6]. Using so-calculated I_γ(corr) values, one can calibrate the resonance neutron flux inside the B_4C shield, again determined from the measured activities of high-yields of ^{175}Hf and ^{181}Hf. For both isotopes the self-absorption coefficients τ_{res} are known from the outer-channel experiment described above, but the τ_{res} value corresponding to the production of ^{178m_2}Hf in the ^{177}Hf(n,γ) reaction was not calibrated. Although one may assume stronger absorption for ^{177}Hf than for ^{180}Hf, taking into account the resonance strengths for both nuclides. A more precise estimate for the τ_{res} of ^{177}Hf was obtained on the basis of the resonance excitation function given in Ref. [7], as compared to ^{180}Hf.

Finally, the total number of resonance neutron-capture events by ^{177}Hf nuclei in the target was deduced. From this value the isomer-to-ground state ratio σ_m/σ_g may be determined for ^{178}Hf whenever activity of ^{178m_2}Hf is measured.

3. Results

In gamma spectra measured after two years of cooling of the Hf sample exposed to a fluence of about 10^{18} n/cm^2 (in the inner channel), characteristic lines from ^{178m_2}Hf decay were found as shown in Fig. 1. Their intensities were still much lower than the lines resulting from the dominant ^{175}Hf and ^{181}Hf activities. This could be expected for the 31-year-lived isomer, which should be produced with a low yield that is suppressed by its high angular momentum and resulted in an isomer-to-ground state ratio on the level of about 10^{-8} or less. The spectrum contains many lines of different origin, including those from activated admixtures within the sample, from natural background and from summations of the gamma rays with characteristic X-rays of the emitting atoms within the sample and the Pb within the detector shield. The panels in Fig. 1 show gamma lines from ^{178m_2}Hf decay as well as some other lines that are not related to this analysis.

Table 1 gives the number of counts detected for gamma transitions from ^{178m_2}Hf decay at 426.4, 495.0 and 574.2 keV, in comparison with the major lines of ^{175}Hf and ^{181}Hf. Lines from ^{178m_2}Hf at lower energies were completely obscured by the large Compton background despite the cooling period. The statistical error in the peak area of the line at 574.2 keV is poor because this lies near the strongly manifested Compton ridge due to γ lines from ^{95}Zr and ^{95}Nb detected at energies of about 750 keV. Better accuracy was reached for the other two lines and the observed intensities were sufficient to define the number of ^{178m_2}Hf nuclei within the activated target, taking into account all necessary factors of efficiency and decay. By comparing this number to the calculated total number of ^{177}Hf(n,γ) events, as described above, gave the experimentally measured σ_{m_2}/σ_g ratio for ^{178}Hf. The latter value was determined for resonance neutrons transmitted through the B_4C filter. However, a similar σ_{m_2}/σ_g ratio should be valid for slow neutrons in general, including thermal neutrons. Such regularity has been experimentally confirmed in many cases when the σ_m/σ_g ratio was determined both from measured σ_{th} and I_γ values, e.g. the case of the ^{180m}Hf isomer [6].

Taking the σ_{m_2}/σ_g ratio so-obtained and then using the known [6] σ_{th} and I_γ parameters for the ^{177}Hf(n,γ) reaction, the partial σ_{th} and I_γ for population of ^{178m_2}Hf were deduced. The accuracy of this result cannot be expected to be very high due to the modest statistics (see Table 1). In principle, however, the present data were taken under more clean conditions than in previous measurements reported in the literature and should be reliable.

Neutron-capture cross-sections for Hf nuclides are summarized in Table 2 with literature data taken from Ref. [6]. The present results are given for the reactions of particular interest, ^{177}Hf$(n,\gamma)^{178m_2}$Hf, ^{178}Hf$(n,\gamma)^{179m_2}$Hf and ^{178m_2}Hf$(n,\gamma)^{179g,m_2}$Hf. The latter reaction which is responsible for ^{178m_2}Hf destruction (burnup) may be especially exotic and is discussed in more detail below.

More than 30 years ago, activity of the ^{178m_2}Hf isomer was observed [9] from isotopically enriched hafnium targets irradiated within a high-power reactor. Gamma spectra of this isomer were carefully studied using state-of-the-art techniques available at that time. However, the production cross-section given in Ref. [9] may not be very accurate because it was determined by only considering the effect of thermal neutrons,

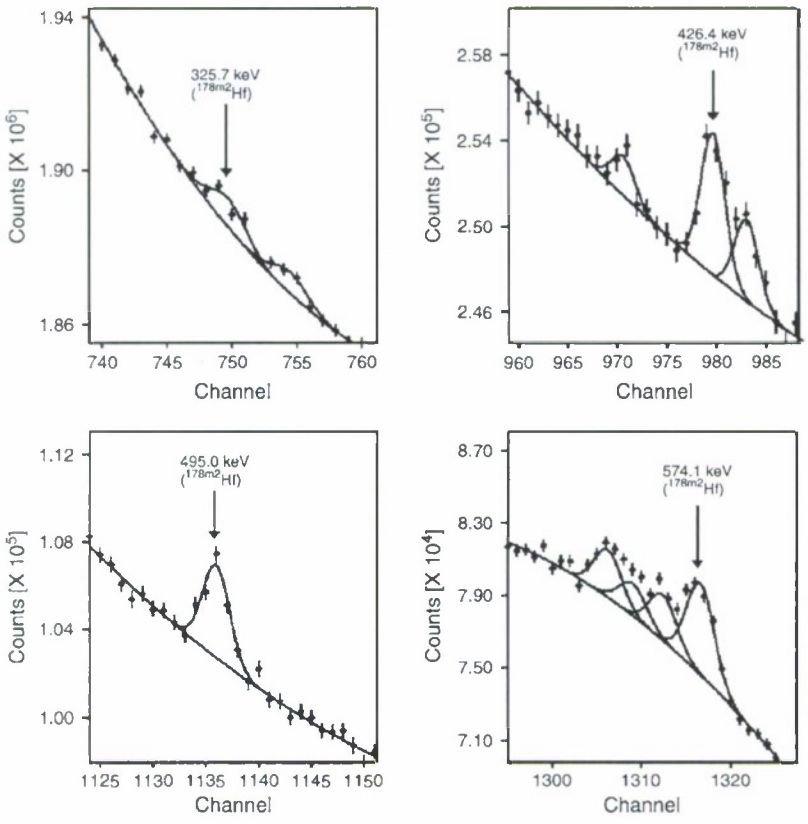

Fig. 1. Panels show sections of the gamma spectrum collected from the metal ^{nat}Hf sample after neutron irradiation in the inner channel of the IBR-2 reactor, and after two years of cooling time. Lines corresponding to decay of ^{178m_2}Hf isomer are identified and peak fits are shown from which the counts of Table 1 were determined.

neglecting the resonance neutron flux, and assuming that the "burnup" (destruction) cross-section was at a rather low level of less than 20 b. It is well-known that a purely thermal flux does not exist in any reactor near its active core and the presence of resonance neutrons changes the yields of reaction products. Also the ^{178m_2}Hf yield could be strongly reduced due to the burnup process at the fluences applied in the work of Ref. [9], $\geq 10^{21}$ n/cm^2. The degree of burnup definitely depends on the values of σ_{th} and I_γ for the isomeric nucleus, but the relatively low σ_{th} given in Ref. [9] was unexpected.

Values of σ_{th} and I_γ for neutron capture show for many nuclei a correlation with the level density of neutron resonances. Standard estimations using the Gilbert–Cameron formula [11], verified by known neutron resonance densities for various nuclides, predict a much higher resonance density for ^{178m_2}Hf than that known for the ^{178g}Hf nucleus. The former nucleus may be characterized by a level density comparable with the measured resonance density for ^{177}Hf, or perhaps even larger. Thus, similar values of σ_{th} and I_γ can be expected for ^{178m_2}Hf and ^{177}Hf nuclei and these are much larger than the 20 b used in Ref. [9]. Recently, the burnup cross-section due to thermal neutrons was measured in Ref. [12] for the ^{177m}Lu isomer and a value of $\sigma_{th} = 590$ b was obtained, including both neutron capture and superelastic scattering components. Noting that ^{177m}Lu also possesses high spin and excitation energy similar to ^{178m_2}Hf, one may expect them to have comparable burnup cross-sections. Such arguments motivated the present independent measurements of the ^{178m_2}Hf production cross-section in reactor irradiations and an evaluation of the role of burnup which depends on neutron flux.

There is no doubt that the number of produced ^{178m_2}Hf nuclei was determined correctly in the earlier experiment [9], although the cross-section was underestimated by a factor of 10 using an incorrect approximation. Now that yield [9] may be taken and combined with appropriate corrections so that it can be compared with the present cross-sections. To make

Table 1
Number of peak counts in the γ lines from ^{178m_2}Hf compared to the lines of ^{175}Hf and ^{181}Hf (see Fig. 1)

Nucleus	E_γ (keV)	Counts	Statistical error (%)
^{178m_2}Hf	426.4	19,321	6.3
	495.0	12,461	7.6
	574.2	16,627	10.4
^{175}Hf	343.4	1.086×10^9	0.2
	432.8	1.599×10^7	0.3
^{181}Hf	482.0	1.487×10^8	0.3

The gamma spectrum was taken after two years of "cooling" of a metal ^{nat}Hf sample activated with reactor neutrons.

Table 2
Neutron capture cross-sections for hafnium isotopes

Target	J_t^π	Product	J_p^π	σ_{th} (b)	I_γ (b)	σ_m/σ_g	Reference
^{174}Hf	0^+	^{175}Hf	$5/2^-$	561	436	–	[6]
^{176}Hf	0^+	^{177}Hf	$7/2^-$	23.5	880	–	[6]
^{177}Hf	$7/2^-$	^{178g}Hf	0^+	373	7173	–	[6]
		^{178m_1}Hf	8^-	0.96	–	2.6×10^{-3}	[6]
		^{178m_2}Hf	16^+	2.6×10^{-6}	5×10^{-5}	$(7 \pm 2) \times 10^{-9}$	Present
^{178}Hf	0^+	^{179g}Hf	$9/2^+$	84	1950	–	[6]
		^{179m_1}Hf	$1/2^-$	53	–	0.63	[6]
		^{179m_2}Hf	$25/2^-$	$\leq 2 \times 10^{-4}$	$\leq 1.3 \times 10^{-3}$	$\leq 2.4 \times 10^{-6}$	Present
^{178m_2}Hf	16^+	^{179g}Hf	$9/2^+$	190	4500	(0.24 ± 0.07)	Present[a]
		^{179m_2}Hf	$25/2^-$	45 ± 5	1060 ± 60	–	[10]
^{179}Hf	$9/2^+$	^{180g}Hf	0^+	41	630	–	[6]
		^{180m}Hf	8^-	0.45	6.9	1.1×10^{-2}	[6]
^{180}Hf	0^+	^{181}Hf	$1/2^-$	13.04	35.0	–	[6]

[a] Obtained by comparison of present results with those of Ref. [9].

this recalculation of the cross-section corresponding to the earlier experiment, the following assumptions are made:

1. The effective cross-section of Eq. (3) is, in general, appropriate to account for the contribution of resonance neutrons.
2. An effective, or net, production cross-section, σ_{pro}, calculated with the σ_{th} and I_γ from the current experiment, should be valid for the conditions of Ref. [9] when an appropriate value of $k = 20$ (suitable for a well-thermalized spectrum as would be expected for that experiment) is taken.
3. The yield of ^{178m_2}Hf measured in Ref. [9] in a high-fluence irradiation may then be reproduced with the calculated σ_{pro} by taking into account a much larger burnup effect than was assumed in the earlier work.

Following this approach, the effective cross-section for burnup in the ^{178m_2}Hf(n,γ) reaction was deduced. The accumulation of a given product nucleus in the presence of burnup is given by

$$N_{net}(\Phi) = \frac{N_t \sigma_{pro}}{(\sigma_1 - \sigma_{burn})}\left[e^{-\sigma_{burn}\Phi} - e^{-\sigma_1 \Phi}\right], \quad (6)$$

where N_{net} and N_t are the net number of product nuclei and the number of target nuclei at the start of the irradiation, respectively, Φ is the neutron fluence, σ_{burn} and σ_1 are the capture cross-sections that take into account the burnup of the product and target nuclei, respectively. The σ_{pro} value is the physical production cross-section without burnup. All σ values are defined to be effective, as in Eq. (3).

Combining the present production cross-section results with the yield measurements of Ref. [9] as described above, the effective burnup cross-section, σ_{burn}, was deduced for ^{178m_2}Hf isomer using Eq. (6). This effective cross-section is a linear combination of σ_{th} and I_γ values summed for two exit channels of the capture reaction, together corresponding to the formation of ^{179}Hf product nuclei in either its ground state (g) or its 25-day-lived m_2 state.

Fortunately, decomposition of σ_{burn} was possible because σ_{th} and I_γ parameters have already been directly measured for production of ^{179m_2}Hf after irradiation of ^{178m_2}Hf in Ref. [10]. The ground state yield may also be determined by subtraction of ^{179m_2}Hf contribution from the total burnup yield of ^{178m_2}Hf. It was assumed that the ratio σ_{m_2}/σ_g for production of ^{179m_2}Hf and ^{179g}Hf nuclei in neutron capture by ^{178m_2}Hf should be approximately the same for both thermal and resonance neutrons. The partial σ_{th} and I_γ for the ^{178m_2}Hf$(n,\gamma)^{179g}$Hf branch are therefore deduced and should be added to the previously known values for the branch of the reaction that populates ^{179m_2}Hf. Thus, the burnup of ^{178m_2}Hf due to neutron-capture reactions is now characterized by the total σ_{th} and I_γ values, although with only modest accuracy. Nevertheless, the general behavior of production and burnup processes has been clarified by the present experiment.

Table 3 compares the cross-sections for ^{178m_2}Hf production in reactions with slow and fast neutrons. The upper limit therein for the ^{178}Hf$(n,n'\gamma)$ reaction was determined based on the present measurements. Fast neutrons with $E_n \geq 3$ MeV

Table 3
Summary of the production of ^{178m_2}Hf via different neutron-induced reactions

Reaction	Energy	ΔJ	Cross-section (mb)	σ_m/σ_g	Reference
^{177}Hf(n,γ)	Thermal	12	2.6×10^{-3}	–	Present
	Resonance	12	$I_\gamma = 5 \times 10^{-2}$	$(7 \pm 2) \times 10^{-9}$	Present
^{178}Hf$(n,n'\gamma)$	$E_n \geq 3$ MeV	31/2	$\leq 7 \times 10^{-3}$	$\leq 2.5 \times 10^{-6}$	Present
^{179}Hf$(n,2n)$	$E_n = 14.5$ MeV	11	7.3	3.5×10^{-3}	[4]

could, in principle, activate the ^{178m_2}Hf state located at a 2.446-MeV excitation energy. Fast neutrons can certainly penetrate through the B_4C shield without significant absorption and their flux was measured by activation of a Ni spectator. Thus, a cross-section can be deduced for fast neutron production of ^{178m_2}Hf if its production is attributed to the $(n,n'\gamma)$ reaction. However, the values of σ_{m_2} and σ_{m_2}/σ_g obtained in such a manner are unphysically large when the reaction's spin deficit of $\Delta J = 31/2$ is considered for a hypothetical ^{178}Hf$(n,n'\gamma)^{178m_2}$Hf reaction. Recall that $\Delta J = J_m - J_t - 1/2$. Finally, it was assumed that the deduced cross-section for fast neutron production of ^{178m_2}Hf is just an upper limit, while the dominant means of producing this isomer is due to slow neutron capture. The ^{179}Hf$(n,2n)$ reaction with 14.5-MeV neutrons was characterized in Refs. [4,13]. The efficient production of ^{178m_2}Hf in that reaction makes it one of the best methods for accumulation of this isomer, but the achievable flux of 14-MeV neutrons restricts the real use of this reaction for large-scale manufacture. In the case of reactor irradiations, neutrons with energies greater than 10 MeV appear with very low probability.

Table 4 summarizes cross-sections for ^{179m_2}Hf production which are described in more detail in Ref. [8]. In that work it was explained that the main production mechanism was the $(n,n'\gamma)$ reaction, unlike the situation found now for ^{178m_2}Hf production. The difference may be attributed primarily to the spin deficit (ΔJ) values, which causes a preference in the (n,γ) reaction for ^{178m_2}Hf, but in the $(n,n'\gamma)$ reaction for ^{179m_2}Hf. The absolute cross-section for ^{179m_2}Hf production is not particularly low and in standard reactor irradiations quantities as large as μg ^{179m_2}Hf could be accumulated. Nanogram amounts are achievable for ^{178m_2}Hf, but this would appear to be insufficient for applications or for using the isomer as target or beam nuclei in experiments.

According to Refs. [4,13], ^{178m_2}Hf and ^{179m_2}Hf isomers are produced with much higher cross-sections in the $(n,2n)$ reaction with 14.5 MeV neutrons, see in Tables 3 and 4. For massive production of ^{178m_2}Hf in USA, the spallation reaction was applied using thick Ta targets exposed to high-power 800 MeV proton beam available at Los Alamos [20]. The physical cross-sections for high-spin isomer production via spallation of different targets by 600 MeV proton beam have been systematically measured at Dubna, Refs. [21,22]. Definitely, the high yield characterizing spallation reactions was confirmed and quantitatively specified. The ^{176}Yb(^{4}He, $2n$) reaction at 36 MeV He-ion beam seemed attractive in another aspect, namely in the sense of the best purity of the produced ^{178m_2}Hf activity [23], as compared to the spallation and other reactions. Recently, a productivity of high-energy bremsstrahlung for the ^{178m_2}Hff accumulation has been tested [24] using the Ta sample irradiated with electrons at 5 GeV synchrotron. The analysis and comparison of different methods is given in Ref. [25].

4. Discussion

The results summarized in Tables 2–4 permit the plot of Fig. 2, showing the systematics of the isomer-to-ground ratio versus spin deficit for production of hafnium isomers. This plot leads to some interesting points and, perhaps, a general conclusion. It can be seen in Fig. 2 that the σ_m/σ_g ratio follows a regular exponential decrease with increasing ΔJ. The (n,γ), $(n,n'\gamma)$ and $(n,2n)$ reactions demonstrate separate curves with individual slopes in the log plot. A natural explanation for the appearance of different curves is that the projectile angular momentum increases with the neutron kinetic energy. In general, the systematics does not demonstrate any unexpected behavior, but the plot allows a quantitative definition of real values for specific reactions. It can, therefore, be used to make estimates of σ_m/σ_g values for other cases. It is important to note is that the systematics cover a wide range in angular momentum, as high as $J = 16$ for isomers populated in the (n,γ) reaction and corresponding to a σ_m/σ_g ratio lower than 10^{-8}. Such values are not typical in comparison with other measurements known in the literature for neutron-induced reactions.

The conclusion that ^{179m_2}Hf is produced via $(n,n'\gamma)$ reactions while, conversely, ^{178m_2}Hf is produced via (n,γ) reactions is supported by Fig. 2 in addition to the arguments given above. In this plot the upper limits determined for ^{178m_2}Hf production via the $(n,n'\gamma)$ reaction and for ^{179m_2}Hf production via the (n,γ) reaction deviate from the systematic pattern, both lying far above the curves corresponding to the respective reactions. The limit was deduced from the measured yield attributing it either to the (n,γ) or to the $(n,n'\gamma)$ reaction. Good agreement with the regular pattern for the definite-type reaction confirms a negligible contribution from the another one, especially if the latter one is characterized in systematics by much lower yield. This was the case for both ^{178m_2}Hf and ^{179m_2}Hf isomers allowing us to differentiate between possible producing reactions.

The present result that there are significant cross-sections for burnup of ^{178m_2}Hf in the ^{178m_2}Hf$(n,\gamma)^{179m_2,g}$Hf reaction equal in total $\sigma_{th} = 235$ b and $I_\gamma = 5600$ b is worth further discussion. Such large values are known for many other nuclei, e.g. the ^{177}Hf nucleus with odd-neutron number is characterized by even higher values, as is known from Ref. [6]. In the even–even ^{178}Hf nucleus, a pair of neutrons is decoupled

Table 4
Summary of the production of ^{179m_2}Hf via different neutron-induced reactions

Reaction	Energy	ΔJ	Cross-section (mb)	σ_m/σ_g	Reference
^{178}Hf(n,γ)	Thermal	12	≤ 0.2	$\leq 2.4 \times 10^{-6}$	Present
	Resonance	12	$I_\gamma \leq 13$	$\leq 7 \times 10^{-6}$	Present
^{179}Hf$(n,n'\gamma)$	$E_n \geq 1.5$ MeV	15/2	4.5 ± 0.5	$(1.6 \pm 0.2) \times 10^{-3}$	Present
^{180}Hf$(n,2n)$	$E_n = 14.8$ MeV	12	25	7×10^{-3}	[4]

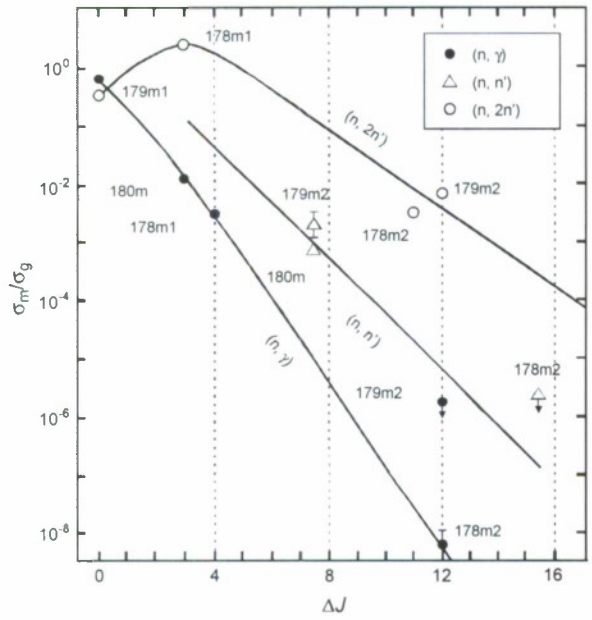

Fig. 2. Measured values of the isomer-to-ground state ratio versus spin deficit (ΔJ) parameter for hafnium isomers produced in neutron-induced reactions. Numerical data and references are given in Tables 2–4. For simplicity, points according to the literature are given without error bars.

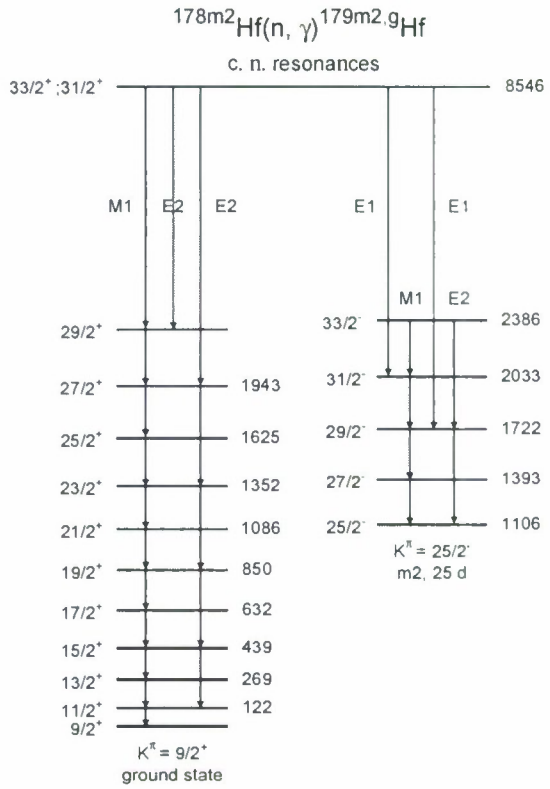

Fig. 3. Partial level scheme depicting population of the m_2 and ground states in ^{179}Hf after the ^{178m_2}Hf(n,γ) reaction with slow neutrons. The cascades shown illustrate the discussion in the text.

in the m_2 state, so that the isomeric nucleus can manifest itself for as equivalent in behavior to an odd-neutron nucleus. Thus, the observed large burnup cross-section is not out of scale [6], unlike the extremely large (n,γ) cross-section for burnup of ^{178m_2}Hf reported in Ref. [14]. That value was deduced by indirect method basing on the resonance parameter evaluation.

Table 2 shows that the population of the ground state appears with 4× higher probability than the m_2 state, but stronger selectivity was not manifested. This can be understood in the following way. Fig. 3 shows a partial level scheme for ^{179}Hf, the daughter of the burnup reaction of ^{178m_2}Hf. Compound-nucleus states of ^{179}Hf are excited after neutron capture by ^{178m_2}Hf and possess $J^\pi = 31/2^+$ or $33/2^+$ and a fixed excitation energy near 8546 keV. For the lower-lying structure, the important features are the m_2 isomer in ^{179}Hf with $J^\pi = 25/2^-$ at 1106 keV and the two rotational bands built on the ground and isomeric states. Many other bands exist [15] and the population of m_2 and g states may initially proceed via such bands near the top of the cascade that follows neutron capture. However, these decay paths will eventually reach the bands shown in Fig. 3. Direct transitions can also take place from the compound-nucleus state to the ground or m_2 bands, but, of course, many different cascade paths contribute to the population of a given final state because the level density above $E^* = (4–5)$ MeV is high in hafnium nuclei.

There is no spin deficit for the burnup reaction of ^{178m_2}Hf leading to the high-spin ^{179m_2}Hf state and it should be strongly populated. It is possible that some preference for this final state may arise due to its high K value and the fact that there is a similar structure of the target and product m_2 isomers. However, this experiment demonstrated a preference for population of the ground state. A first conclusion is that the K quantum number and structure tagging do not survive past neutron capture at E^* above 8 MeV. This may explain the nearly equal population of the m_2 and ground states.

A similar lack of selectivity to structure details at $E^* > B_n$ was concluded from the measurements of Ref. [16] on depopulation of the ^{180m}Ta isomer by fast neutron inelastic scattering, in accordance with the basic ideas of the statistical model. In that work, no preferential population of the ground state was observed, unlike the present case of capture on ^{178m_2}Hf. The question remains why there exists even a modest preference for ground state population following the (n,γ) reaction on ^{178m_2}Hf. One must take into account the presence of many levels of appropriate spin near and below the compound-nucleus state and these will be populated after neutron capture with equal probability without any influence of structure effects. Thus, selectivity for reaching either the ground or m_2 states cannot appear near the top of the cascades. One must speculate that the modest preference for the ground state arises due to the position of the m_2 level at 1.1 MeV. Some cascades proceeding to the ground state may obtain a higher probability simply because they possess a larger reserve of energy above the ground state than those reaching the isomer, thus providing more possibilities for branching. This idea has not yet been developed in detail.

The above interpretation can be modified if superelastic scattering (SES) [17] contributes a significant part of the observed total burnup cross-section. Until now, SES for ^{178m_2}Hf was not measured and theoretical estimates allow a wide range for this cross-section. This process was not accounted for in the present analysis. There is a lack of sufficiently developed simulation procedures for reactions with high-spin isomers, despite interesting experimental data may be found in the literature [5,12,16–19].

5. Summary

Production of high-spin ^{178m_2}Hf isomer in ^{nat}Hf targets was successfully observed after their activation with the reactor neutrons at fluences lower than 10^{18} n/cm^2. It was established that ^{178m_2}Hf is mainly produced due to the capture of slow neutrons in (n,γ) reaction, while ^{179m_2}Hf is produced in the $(n,n'\gamma)$ reaction with fast neutrons. The production cross-sections are very different, so that it is possible to accumulate ^{179m_2}Hf in a microgram amount after standard irradiations, but only nanograms of ^{178m_2}Hf. Comparing the present measurements with the published data, the destruction (burnup) cross-section was deduced for ^{178m_2}Hf due to a second neutron capture from the reactor flux. The partial $\sigma_{th}$and I_γ values were specified for the burnup process leading to both m_2 and g states in ^{179}Hf. Also, the isomer-to-ground state ratios for hafnium isomers in neutron-induced reactions were systematized. The potential application of ^{178m_2}Hf isomer as a reservoir for energy storage and pulsed release has already been discussed extensively in the literature. However, the present results, as well as those in the literature, do not support an optimistic view of reactors as a source of large-scale manufacture of ^{178m_2}Hf. Other reactions may prove more efficient for production of this long-lived isomer. Spallation reactions with protons of intermediate energy, or neutron irradiations at an energy of 14 MeV and higher must be the most productive as is discussed recently in the review of methods in Ref. [25].

Acknowledgements

The authors gratefully acknowledge support from the United States Air Force Office of Scientific Research under contract F49620-02-01-0187.

References

[1] Hyperfine Interact. 107 (1997) 3–68, 91–183.
[2] J.J. Carroll, S.A. Karamian, L.A. Rivlin, et al., Hyperfine Interact. 135 (2001) 3.
[3] J.J. Carroll, Laser Phys. 1 (2004) 275.
[4] M.B. Chadwick, P.G. Young, Nucl. Sci. Eng. 108 (1991) 117.
[5] D. Belic, C. Arlandini, J. Besserer, et al., Phys. Rev. C65 (2002) 035801.
[6] S.F. Mughabghab, Neutron resonance parameters and thermal cross sections, part b, Z = 61–100, In: Neutron Cross Sections, vol. 1, Academic Press, 1984.
[7] V. McLane, C.L. Dunford, P.F. Rose, Curves, In: Neutron Cross Sections, vol. 2, Academic Press, 1988.
[8] S.A. Karamian, J.J. Carroll, J. Adam, et al., Laser Phys. 14 (2004) 438.
[9] R.G. Helmer, C.W. Reich, Nucl. Phys. A211 (1973) 1.
[10] S.A. Karamian, Y.T. Oganessian, J. Adam, et al., in: Proc. VI International School-Seminar "Heavy-Ion Physics", Dubna, Russia, World Scientific, Singapore, 1998. p. 565.
[11] A. Gilbert, A.G.W. Cameron, Can. J. Phys. 43 (1965) 1446.
[12] O. Roig, G. Bélier, J.-M. Daugas, et al., Nucl. Instrum. Methods A521 (2004) 5.
[13] Y. Weixiang, L. Hanlin, Z. Wenrong, Chin. J. Nucl. Phys. 14 (1992) 326.
[14] G.V. Muradian, O.Y. Shatrov, M.A. Voskanian, et al., Phys. At. Nucl. 66 (2003) 6.
[15] S.M. Mullins, G.D. Dracoulis, A.P. Byrne, et al., Phys. Rev. C61 (2000) 044315.
[16] S.A. Karamian, C.B. Collins, J.J. Carroll, et al., Phys. Rev. C59 (1999) 755.
[17] G. Reffo, M.H. MacGregor, Nucl. Sci. Eng. 114 (1993) 124.
[18] I.A. Kondurov, Y.V. Petrov, E.M. Korotkikh, et al., Phys. Lett. B106 (1981) 383.
[19] Y.T. Oganessian, S.A. Karamian, Hyperfine Interact. 107 (1997) 43.
[20] H. O'Brien, Nucl. Instrum. Methods B40/41 (1989) 1126.
[21] S.A. Karamian, J. Adam, D.V. Filossofov, et al., Nucl. Instrum. Methods A489 (2002) 448.
[22] S.A. Karamian, J. Adam, P. Chaloun, et al., Nucl. Instrum. Methods A527 (2004) 609.
[23] Y.T. Oganessian, S.A. Karamian, Y.P. Gangrski, et al., J. Phys. G18 (1992) 393.
[24] S.A. Karamian, J.J. Carroll, J. Adam, N.A. Demekhina, Nucl. Instrum. Methods A530 (2004) 463.
[25] S.A. Karamian, Phys. At. Nucl. (Moscow) 68 (2005) 1827.

Identification of a high-spin isomer in ^{99}Mo

G. A. Jones,[1,*] P. H. Regan,[1] P. M. Walker,[1] Zs. Podolyák,[1] P. D. Stevenson,[1] M. P. Carpenter,[2] J. J. Carroll,[3] R. S. Chakrawarthy,[4] P. Chowdhury,[5] A. B. Garnsworthy,[4] R. V. F. Janssens,[2] T. L. Khoo,[2] F. G. Kondev,[6] G. J. Lane,[7] Z. Liu,[1] D. Seweryniak,[2] N. J. Thompson,[1] S. Zhu,[2] and S. J. Williams[1,4]

[1] *Department of Physics, University of Surrey, Guildford GU2 7XH, United Kingdom*

[2] *Physics Division, Argonne National Laboratory, Argonne, Illinois 60439, USA*

[3] *Department of Physics and Astronomy, Youngstown, Ohio 44555, USA*

[4] *TRIUMF, 4004 Westbrook Mall, Vancouver, British Columbia V6T 2A3, Canada*

[5] *University of Massachusetts Lowell, Lowell, Massachusetts 01854, USA*

[6] *Nuclear Engineering Division, Argonne National Laboratory, Argonne, Illinois 60439, USA*

[7] *Department of Nuclear Physics, RSPhysSE, Australian National University, Canberra 0200, Australia*

(Received 16 February 2007; revised manuscript received 26 April 2007; published 2 October 2007)

A previously unreported isomer has been identified in ^{99}Mo at an excitation energy of $E_x = 3010$ keV, decaying with a half-life of $T_{1/2} = 8(2)$ ns. The nucleus of interest was produced following fusion-fission reactions between a thick ^{27}Al target frame and a ^{178}Hf beam at a laboratory energy of 1150 MeV. This isomeric state is interpreted as an energetically favored, maximally aligned configuration of $\nu h_{\frac{11}{2}} \otimes \pi(g_{\frac{9}{2}})^2$.

DOI: 10.1103/PhysRevC.76.047303 PACS number(s): 21.10.Dr, 23.20.Lv, 27.60.+j, 25.70.Jj

The near-yrast structure of the $A \sim 100$ region with $N \geqslant 56$ is dominated by excitations associated with the high-j "unnatural parity" proton $g_{\frac{9}{2}}$ and neutron $h_{\frac{11}{2}}$ orbitals. Decoupled, rotational sequences built on a single $\nu h_{\frac{11}{2}}$ orbital are observed in all $N = 57$ isotones from $^{99}_{42}$Mo up to $^{109}_{52}$Te [1–7] with associated weakly deformed, prolate shapes. At medium spins, these single-quasiparticle rotational bands are crossed by multi-quasiparticle configurations, which have been interpreted in the framework of the Cranked Shell Model to be associated with either $\nu h_{\frac{11}{2}} \otimes \pi(g_{\frac{9}{2}})^2$, $\nu h_{\frac{11}{2}} \otimes \nu(g_{\frac{7}{2}})^2$, or $\nu h_{\frac{11}{2}} \otimes \nu(h_{\frac{11}{2}})^2$ configurations, depending on the proton number and the associated core deformation [1–3]. These collective rotational bands can compete with single-particle excitations formed by the favored, maximally aligned couplings of high-j proton ($g_{\frac{9}{2}}$) and neutron ($h_{\frac{11}{2}}$ and $g_{\frac{7}{2}}$) orbitals. This Brief Report describes the identification of a high-spin isomeric state that feeds the previously reported $h_{\frac{11}{2}}$ decoupled-rotational structure, at $I^\pi = \frac{23}{2}^-$, in ^{99}Mo [1].

The experiment was performed at Argonne National Laboratory using the Argonne Tandem Linear Accelerator System (ATLAS), which delivered a ^{178}Hf beam at a laboratory energy of 1150 MeV, with an average beam intensity of 2 particle nA. The main experimental focus was to study long-lived isomers in hafnium-like nuclei, using deep-inelastic reactions with a thick ^{208}Pb target; the results from this work are reported in Ref. [8]. The data on ^{99}Mo described in this Brief Report were obtained from incidental fusion-fission reactions between the ^{178}Hf projectiles and the ^{27}Al support frame for the ^{208}Pb target. Nuclei synthesized in fusion-fission reactions were identified as such from the observation of γ rays associated with the decay of binary products, consistent with the fission of the ^{178}Hf + ^{27}Al fusion-compound nucleus. The beam delivered by the ATLAS was bunched into short pulses of width ~0.5 ns, separated by periods of 82.5 ns. This pulsing was utilized to study metastable states in the $10^{-9} < T_{1/2} < 10^{-4}$ s range; nine out of ten beam pulses were swept away from the target, resulting in a 825 ns period within which delayed γ-ray decays could be studied. Events where two or more coincident γ rays were detected within a 2μs range were written to tape for subsequent off-line analysis. A total of 2.1×10^9 events were recorded over the course of a 5-day experiment.

The nature of the fusion-fission reaction process leads to the detection of a plethora of γ rays emitted from excited states in a broad range of nuclei, resulting in a highly complex data set. The γ-ray decays from all the reaction products were measured using the Gammasphere [9] array, comprised of 101 Compton-suppressed germanium detectors in this experiment. Because of this level of complexity it was necessary to utilize multidimensional γ-ray coincidence techniques to correlate γ-ray decays associated with particular nuclides. A variety of coincidence cubes corresponding to different γ-ray time and energy conditions were created; Table I provides details of cubes created, which are relevant to this report. These were analyzed with standard software packages described in Refs. [10–12].

A high-spin isomer in ^{99}Mo has been observed for the first time using these data. Figure 1 provides a level scheme of transitions in ^{99}Mo deduced from the current work. The isomeric state at $E_x = 3010$ keV is observed to decay directly into the negative-parity sequence, reported in Ref. [1], by the emission of a 305 keV transition to the $I^\pi = \frac{23}{2}^-$ member of the decoupled rotational band. Figure 2(a) shows the promptly fed decays of the negative-parity band in ^{99}Mo; the 980 and 1064 keV transitions are observed from the previously reported $I^\pi = (\frac{27}{2}^-)$ and $(\frac{31}{2}^-)$ states, respectively. Figure 2(b) shows delayed transitions associated with double gates in ^{99}Mo. This spectrum clearly identifies the 482, 693, and 846 keV transitions associated with decays from the $I^\pi = \frac{15}{2}^-$, $\frac{19}{2}^-$,

*Corresponding author: G.Jones@Surrey.ac.uk

TABLE I. Three-dimensional cubes used to create the level scheme in Fig. 1 and spectra in Fig. 2. Prompt and delayed γ rays (γ_p and γ_d, respectively) are defined by the time difference, $\mathrm{TD}_{p\,or\,d}$, between the γ-ray, T, and that of the beam, RF. The time difference between γ rays, TD_γ, is used to define transitions that are prompt with respect to each other.

	Conditions			Spectrum (see Fig. 2)	Gates ($\{x\}\{y\}$)
	x	y	z		
1[a]	γ_p	γ_p	γ_p	(a)	{846}{482, 693}
2[b]	γ_{d1}	γ_{d1}	γ_{d1}	(b)	{846}{482, 693}
3[c]	γ_{d1}	γ_{d1}	γ_p	(c)	{482}{305, 693}
4[d]	γ_{d2}	γ_{all}	$T_{\gamma_{all}}$	(d)	{138, 449}{305}

[a]1 - $\mathrm{TD}_\gamma(=|T_1 - T_2|) < 30$ ns; $\mathrm{TD}_p(=|\mathrm{RF} - T|) < 20$ ns (at $E_\gamma = 300$ keV).
[b]2 - $\mathrm{TD}_\gamma(=|T_1 - T_2|) < 30$ ns; $\mathrm{TD}_{d1}(=|\mathrm{RF} - T|) > 20$ ns (at $E_\gamma = 300$ keV).
[c]3 - TD_γ, TD_{d1}, & TD_p, as defined above.
[d]4 - $\mathrm{TD}_{d2}(=|\mathrm{RF} - T|) > 90$ ns.

and $\frac{23}{2}^-$ states, respectively; there is no evidence for a 980 keV γ ray in delayed coincidence with any transitions in ^{99}Mo. A previously unreported 305 keV transition is apparent in this spectrum; it is interpreted as the direct decay from an isomeric state at $E_x = 3010$ keV. No transition from the isomer to the $I^\pi = \frac{19}{2}^-$ state was observed in this experiment. This is consistent with intensity measurements for delayed transitions below the isomer, which indicate 100% feeding through the 305 keV decay.

The spectrum shown in Fig. 2(c) illustrates promptly fed γ rays above the $E_x = 3010$ keV state, using double gates on delayed transitions (see Table I). A weak 1739 keV transition is observed in this spectrum, which fits energetically with a decay from the $E_x = 4749$ keV, $I^\pi = (\frac{31}{2}^-)$ state to the isomeric level. Table II shows Weisskopff estimates of the 1739 keV transition for different multipolarities. For this transition to compete with the collective-$E2$, 1064 keV γ ray, one would expect it to decay between states with $|I_i - I_f| = \Delta L \leqslant 2$. The 1739 keV transition is placed tentatively in the level scheme provided in Fig. 1. Other γ-ray photopeaks at 685, 764, and 842 keV are identified in this spectrum, associated with prompt transitions that possibly populate the isomeric state. Because of the complexity of the data set, particularly with γ rays of energy $E_\gamma < 1$ MeV, these transitions could not be linked confidently to the decay of specific states above the $E_x = 3010$ keV isomer in ^{99}Mo.

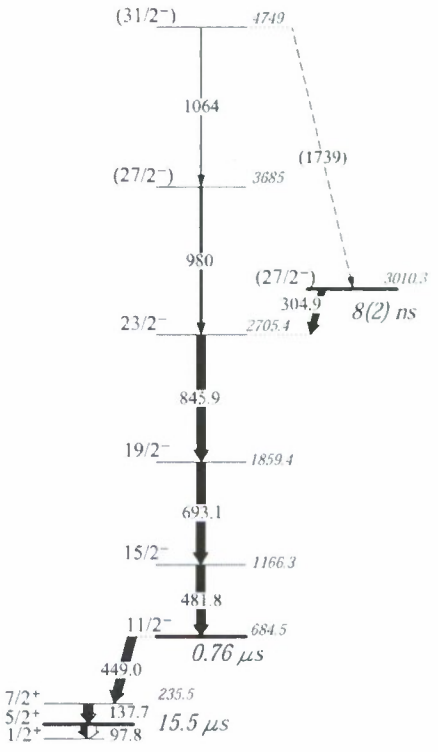

FIG. 1. Partial level scheme for transitions observed in ^{99}Mo. Arrow widths provide an indication of the relative strengths of different γ-ray decay paths. The γ-ray energies from states with $E < 3685$ keV have an error of 0.3 keV; the 980, 1064, and 1739 keV γ rays are accurate to 1 keV.

Figure 2(d) provides a γ-ray time spectrum of the double-gated delayed transitions from the isomeric $E_x = 3010$ keV state. Relative to the accelerator RF signal, the half-life of the decay is measured as $T_{1/2} = 8(2)$ ns, using a folded Gaussian plus exponential fit.

The spin-parity assignment for this previously unreported state is based on (i) the observed decay to the $I^\pi = \frac{23}{2}^-$ member of the negative-parity collective sequence in ^{99}Mo; (ii) the measured lifetime associated with the 305 keV decaying transition; and (iii) the tentatively observed 1739 keV, $\Delta L \leqslant 2$ transition that links the $E_x = 4748$ keV state with the $E_x = 3010$ keV isomer.

Weisskopf single-particle transition rates for a 305 keV transition with $E1$ or $M1$ multipolarity are $B(E1) = (1.4 \pm 0.4) \times 10^{-6}$ W.u. or $B(M1) = (9.6 \pm 2.4) \times 10^{-4}$ W.u., respectively. Such a retarded $M1$ transition is unlikely [13];

TABLE II. Weisskopf single-particle estimates for γ-ray decays in ^{99}Mo.

γ (keV)	Weisskopff estimate (s)					
	$E1$	$E2$	$E3$	$M1$	$M2$	$M3$
305	1.1×10^{-14}	7.9×10^{-9}	8.5×10^{-3}	7.8×10^{-13}	5.5×10^{-7}	5.9×10^{-1}
1152	2.1×10^{-16}	1.0×10^{-11}	7.7×10^{-7}	1.4×10^{-14}	7.1×10^{-10}	5.4×10^{-5}
1739	6.0×10^{-17}	1.3×10^{-12}	4.3×10^{-8}	4.2×10^{-15}	9.1×10^{-11}	3.0×10^{-6}

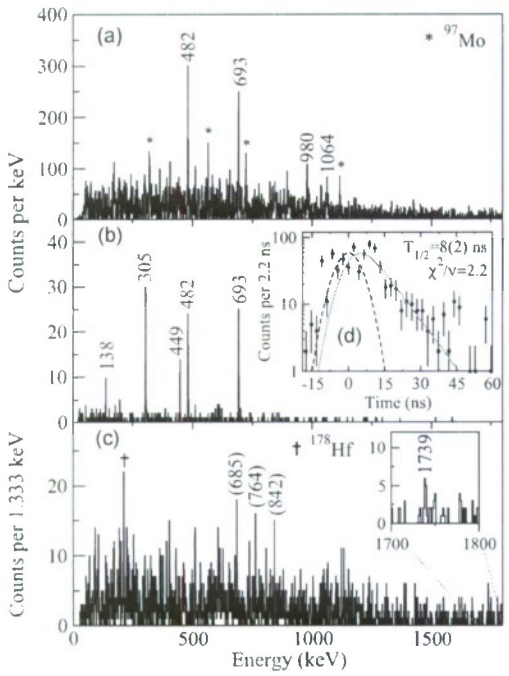

FIG. 2. (Color online) Spectra of γ-ray decays in ^{99}Mo from the short-pulsing experiment; details of the coincidence gates used to produce spectra are provided in Table I. Panels (a) and (b) show transitions associated with ^{99}Mo in prompt and delayed projections, respectively. The γ rays in (c) illustrate candidates for transitions decaying from states above the $E_x = 3010$ keV isomer. Panel (d) gives the time evolution of the isomeric decay, including a folded Gaussian plus exponential fit; the dashed line is the prompt Gaussian used in the fit (with FWHM = 12.5(10) ns), obtained from a fit to a prompt γ ray with $E_\gamma \sim 300$ keV. Contaminants (^{97}Mo and ^{178}Hf) are indicated in each spectrum where applicable.

however, Endt [13] shows that $E1$ transitions in this region can be hindered to this magnitude. Examples of such hindered $E1$ transitions can also be seen in Ref. [14]. An $E1$, 305 keV transition would imply $I^\pi = \frac{23}{2}^+$ or $\frac{25}{2}^+$ for the isomer. Under such circumstances, one might expect to observe a 1152 keV transition from the isomer to the $I^\pi = \frac{19}{2}^-$ state; Weiskopff estimates in Table II indicate that a 1152 keV, $M2$ or $E3$ transition is likely to compete with the $E1$, 305 keV decay. The fact that no competing $E_\gamma = 1152$ keV decay is observed to the $I^\pi = \frac{19}{2}^-$ (or lower spin) member of the negative-parity sequence suggests that the spin of the isomeric state is at least $I = \frac{25}{2}$.

A stretched-$E2$, 305 keV transition provides $I^\pi = \frac{27}{2}^-$ spin-parity assignment for the $E_x = 3010$ keV state, corresponding to a Weisskopf single-particle transition rate of $B(E2) = 0.96(24)$ W.u. Weiskopff estimates for the 1739 keV transition are also consistent with a $I^\pi = \frac{27}{2}^-$ assignment for the isomer. On the basis of these arguments, we suggest an $E2$ assignment for the 305 keV transition and thus a tentative $I^\pi = (\frac{27}{2}^-)$ spin-parity assignment for the isomeric state.

An $I^\pi = \frac{21}{2}^+$ isomeric state in the $N = 57$ isotone $^{105}_{48}$Cd has a reported configuration of $\nu d_{\frac{5}{2}} \otimes \pi(g_{\frac{9}{2}})^{-2}$, as deduced from the g-factor measurement in Ref. [15]. The analogous maximally aligned coupling of the $(g_{\frac{9}{2}})^2$ protons with $\nu d_{\frac{5}{2}}$, $\nu g_{\frac{7}{2}}$, and $\nu h_{\frac{11}{2}}$ would be expected to form energetically favored multiparticle states in ^{99}Mo with $I^\pi = \frac{21}{2}^+$, $\frac{23}{2}^+$, and $\frac{27}{2}^-$, respectively. A simple estimate for the excitation energies of such states can be made with $E_x = [\varepsilon_i + 2\Delta_p]$, assuming no residual interactions. The single-quasiparticle energy, ε_i, is taken from the low-lying single-quasiparticle states in ^{99}Mo; the proton-pair gap, $\Delta_p = 2.12$ MeV, is estimated using an empirical mass formula [16] with binding energies taken from Ref. [17]. An empirical comparison of the proton-pair gap shows that the estimate is accurate to within a few hundred keV; the excitation energy of the aligned $\nu d_{\frac{5}{2}} \otimes \pi(g_{\frac{9}{2}})^2$, $I^\pi = \frac{21}{2}^-$ state in ^{93}Mo is $E_x = 2.4$ MeV. Table III shows the energy estimates for the expected $I^\pi = \frac{21}{2}^+$, $\frac{23}{2}^+$, and $\frac{27}{2}^-$ states associated with the simple $(d_{\frac{5}{2}})$, $(g_{\frac{7}{2}})$, or $(h_{\frac{11}{2}})$ neutron, coupling to the maximally aligned $\pi(g_{\frac{9}{2}})^2$ configuration. The calculated state energy for the maximally aligned $\nu h_{\frac{11}{2}} \otimes \pi(g_{\frac{9}{2}})^2$ configuration appears to be within 200 keV of the observed isomeric-state energy. The experimentally suggested spin-parity for the isomer is also consistent with this assessment.

TABLE III. Multiparticle estimates for states in ^{99}Mo.

I^π	Configuration	E_x (MeV)
$\frac{27}{2}^-$	$\nu h_{\frac{11}{2}} \otimes \pi(g_{\frac{9}{2}})^2$	2.805
$\frac{23}{2}^+$	$\nu g_{\frac{7}{2}} \otimes \pi(g_{\frac{9}{2}})^2$	2.356
$\frac{21}{2}^-$	$\nu d_{\frac{5}{2}} \otimes \pi(g_{\frac{9}{2}})^2$	2.257

This interpretation assumes a spherical shape; however, preliminary potential-energy-surface calculations [18], which follow the prescription of those presented in Ref. [19], indicate a shallow oblate-triaxial minimum for the isomeric state. Whilst the spherical pairing estimate offers an impressive correlation with experimental data, a deformed shape for the isomeric state could be a possibility. In the absence of further data on the isomeric state and/or the observation of collective states associated with its configuration, it is not possible to make a firm conclusion in this respect. Nevertheless, this low-lying spherical or oblate-triaxial isomer is distinct from the prolate-triaxial structure of the $\nu h_{\frac{11}{2}}$ band, which undergoes a bandcrossing at higher spin [1] and forms a rotation-aligned $\nu h_{\frac{11}{2}} \otimes \pi(g_{\frac{9}{2}})^2$ sequence.

In summary, a previously unidentified isomeric state in ^{99}Mo has been reported here for the first time. The isomer was identified from the study of γ-ray spectroscopy in a pulsed-beam experiment. Using systematic arguments and a simple pairing estimate, the state is interpreted as a maximally aligned $\nu h_{\frac{11}{2}} \otimes \pi(g_{\frac{9}{2}})^2$ configuration.

This work is supported by the U.S. Department of Energy, Office of Nuclear Physics, under Contract DE-AC02-06CH11357 (A.N.L.); the U.S. AFOSR under Contract F49620-02-1-0187; the AWE (U.K.); and the EPSRC (U.K.).

[1] P. H. Regan, A. D. Yamamoto, F. R. Xu, C. Y. Wu, A. O. Macchiavelli, D. Cline, J. F. Smith, S. J. Freeman, J. J. Valiente-Dobón, K. Andgren, R. S. Chakrawarthy, M. Cromaz, P. Fallon, W. Gelletly, A. Gorgen, A. Hayes, H. Hua, S. D. Langdown, I.-Y. Lee, C. J. Pearson, Zs. Podolyák, R. Teng, and C. Wheldon, Phys. Rev. C **68**, 044313 (2003).

[2] A. D. Yamamoto, P. H. Regan, C. W. Beausang, F. R. Xu, M. A. Caprio, R. F. Casten, G. Gurdal, A. A. Hecht, C. Hutter, R. Krucken, S. D. Langdown, D. Meyer, J. J. Ressler, and N. V. Zamfir, Phys. Rev. C **66**, 024302 (2002).

[3] P. H. Regan, G. D. Dracoulis, G. J. Lane, P. M. Walker, S. S. Anderssen, A. P. Byrne, P. M. Davidson, T. Kibedi, A. E. Stuchbery, and K. C. Yeung, J. Phys. G **19**, L157 (1993).

[4] B. M. Nyako, J. Gizon, A. Gizon, J. Timar, L. Zolnai, A. J. Boston, D. T. Joss, E. S. Paul, A. T. Semple, N. J. O'Brien, C. M. Parry, A. V. Afanasjev, and I. Ragnarsson, Phys. Rev. C **60**, 024307 (1999).

[5] D. Jerrestam, B. Fogelberg, A. Kerek, W. Klamra, F. Liden, L. O. Norlin, J. Kownacki, D. Seweryniak, Z. Zelazny, C. Fahlander, J. Nyberg, M. Guttormsen, J. Rekstad, T. Spedstad-Tveter, A. Gizon, J. Gizon, R. Bark, G. Sletten, M. Piiparinen, Z. Preibisz, T. F. Thorsteinsen, E. Ideguchi, and S. Mitarai, Nucl. Phys. **A593**, 162 (1995).

[6] T. Ishii, A. Makishima, K. Koganemaru, Y. Saito, M. Ogawa, and M. Ishii, Z. Phys. A **347**, 41 (1993).

[7] A. J. Boston, E. S. Paul, C. J. Chiara, M. Devlin, D. B. Fossan, S. J. Freeman, D. R. LaFosse, G. J. Lane, M. Leddy, I. Y. Lee, A. O. Macchiavelli, P. J. Nolan, D. G. Sarantites, J. M. Sears, A. T. Semple, J. F. Smith, and K. Starosta, Phys. Rev. C **61**, 064305 (2000).

[8] G. A. Jones, Ph.D. thesis, University of Surrey, 2006, unpublished.

[9] I.-Y. Lee, Nucl. Phys. **A520**, 641c (1990).

[10] W. Urban, Ana Software (private communication).

[11] D. Radford, Nucl. Instrum. Methods A **361**, 297 (1995).

[12] D. Radford, Nucl. Instrum. Methods A **361**, 306 (1995).

[13] P. Endt, At. Data Nucl. Data Tables **26**, 47 (1979).

[14] W. Andrejtscheff, L. K. Kostov, H. Rotter, H. Prade, F. Stary, M. Senba, N. Tsoupas, Z. Z. Ding, and P. Raghavan, Nucl. Phys. **A437**, 167 (1985).

[15] O. Hausser, J. R. Beene, H. R. Andrews, and G. D. Sprouse, AECL-5614 **68**, 15 (1976).

[16] A. Bohr and B. R. Mottelson, *Nuclear Structure* (Benjamin, Elmsford, NY, 1969), Vol. 1.

[17] G. Audi, A. H. Wapstra, and C. Thibault, Nucl. Phys. **A729**, 337 (2003).

[18] F. R. Xu (private communication).

[19] F. R. Xu, P. M. Walker, J. A. Sheikh, and R. Wyss, Phys. Lett. **B435**, 257 (1998).

Nuclear Isomers: Recipes from the Past and Ingredients for the Future

PHILIP M. WALKER[1] AND JAMES J. CARROLL[2]
[1]*Department of Physics, University of Surrey, Guildford, Surrey GU2 7XH, UK*
[2]*Department of Physics and Astronomy, Youngstown State University, Youngstown, Ohio 44555, USA*

Introduction

"But you've no idea what a difference it makes, mixing it with other things" [1].

In this new age of radioactive beams for nuclear physics research, it is timely to reflect on the enduring role of nuclear isomers, that is, excited, metastable states of nuclei. Heroic experiments with tiny quantities of isomer targets point the way toward the wide vistas of isomer beams, and new possibilities confront our ingenuity at the interface between nuclear and atomic physics. It is the relatively long half-lives of isomers that lead to their special status.

The prediction by Soddy in 1917 [2] that a single nuclide might have states that are "different in their stability and mode of breaking up" was soon followed by Hahn's observations in 1921 of UZ and UX_2, now known as ^{234}Pa and ^{234m}Pa. However, isomers only became well recognized in 1936, with von Weizsäcker's explanation in terms of angular momentum: high angular momentum transitions are slow. So successful were isomers at accounting for multiple half-lives that, it can be argued, the discovery of uranium fission in 1938 had been significantly delayed. Isomers went on to be cornerstones of the nuclear shell model, and even the collective model owes much to isomers. A classic example is ^{180m}Hf, which decays through a sequence of states, interpreted by Bohr and Mottelson [3] as having energies characteristic of a quantum rotor. The energy gap associated with isomers in even-even nuclides also tells us much about the pairing interaction.

The place of isomers in contemporary nuclear structure investigations is illustrated in the following paragraphs. Other recent reviews include those of Walker and Dracoulis [4,5] and Walker and Carroll [6].

Extreme Isomers

Most isomers can be characterized as shell-model states involving one or two—but even up to about ten—specific, unpaired nucleon orbitals. The isomer-related orbitals typically couple to make higher-spin states than other couplings at similar energy, so that isomer decay necessitates the emission of high-spin and/or low-energy radiation, resulting in their long half-lives. In the case of deformed nuclei with an axis of symmetry, a key feature is the orientation of the angular-momentum vector, with a projection, K, on the symmetry axis that is approximately conserved, leading to the occurrence of K isomers. The close connection with shell-model orbits means that an isomer can be considered to be a "simple" state, with the bulk of the wavefunction being well defined. The blocking of pairing correlations in multi-particle isomers leads to them being, in a sense, even simpler than ground states. Nevertheless, the observed radiations from isomers frequently violate selection rules, and there is a sensitive dependence on low-amplitude wavefunction admixtures [7]. Some of these features are schematically illustrated in Figure 1. The remaining principal class of isomers is that of shape isomers, exemplified by fission isomers, where it is a shape change rather than an angular-momentum change that is responsible for the long half-life. Using an energy-spin representation, as shown in Figure 2, the different isomer types can be broadly separated by their general origins, although there are overlaps, such as K traps being also yrast traps if they lie on the yrast line (the locus of states with lowest energy at each spin value).

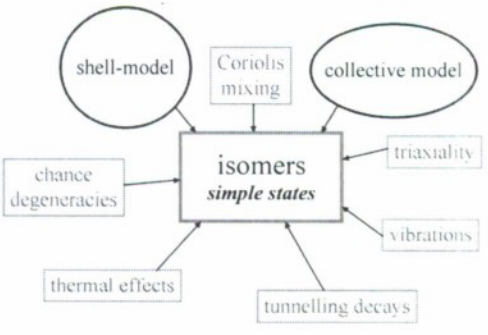

Figure 1. *Although isomers can be considered to have simple shell-model configurations, their decay radiations are sensitive to many influences.*

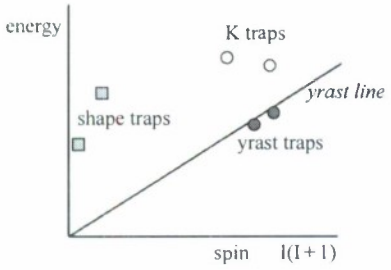

Figure 2. *Schematic representation of isomer types in energy-spin space.*

In order to appreciate the range of isomers found in nature, we will discuss some extreme examples (see Table 1). First, however, a comment is needed as to what half-life is necessary for an excited nuclear state to be called an "isomer". This half-life is ill-defined, but is usually taken to be long enough to permit an isomer and its decay radiations to be separated from the plethora of "prompt" radiations from nuclear reactions. For the purposes of the present discussion, the minimum half-life is taken to be 5 ns.

The half-life range in Table 1 covers 33 orders-of-magnitude. The observed decay modes, even from this short list, include α (^{270}Ds), β (^{94}Ag), γ (^{152}Er), p (^{94}Ag) and 2p (^{94}Ag) emission. Note the absence of neutron emission. The ^{152}Er isomer at 13 MeV is neutron (and proton) unbound, but such decay is inhibited by the centrifugal barrier. We can speculate that neutron radioactivity may soon be discovered from as-yet-unknown long-lived isomers in neutron-rich nuclides.

The extremely low energy, ~7.6 eV, of the ^{229}Th isomer has attracted considerable attention. One possible application is to test the constancy of fundamental constants [14].

An isomer can be longer lived than its ground state. For example, there is a factor of about sixty between the ~6 ms isomer in ^{270}Ds and its ~100 μs ground state. Indeed, this feature may apply more widely to superheavy nuclides [15] and thus could provide significant experimental advantages. Conversely, at the predicted superheavy "island of stability," if ground-state half-lives are too long (e.g., 1 hour) for the detection of time-correlated single-atom decays, it may yet be possible to identify decays from short-lived isomers. Perhaps there are already cases where superheavy isomers, rather than their ground states, have unknowingly been detected.

From this brief discussion, it is evident that, aside from interest in the structure of isomers themselves, they can serve as "tools" or "stepping stones" as we reach out to search for exotic phenomena, especially as we explore the limits of nuclear stability. Another example is ^{254}No [16] where highly excited isomers provide information about orbitals that may form the ground-state structure of heavier nuclides; and a wealth of new information is coming from projectile-fragmentation reactions, as performed at GANIL, GSI, and NSCL. These reactions produce a vast range of nuclides, both proton rich and neutron rich, which can be identified by their mass-to-charge (A/q) ratio on an ion-by-ion basis, within about 500 ns of their formation. The best sensitivity to nuclear structure, through measuring the subsequent decay radiations, is for isomers that decay on a μs time scale, which minimizes random events. Early work of this kind was already sensitive to isomeric-ion rates of less than one per second, and experimental techniques are improving rapidly [17].

Isomer Targets

In principle, isomers can be used for the full range of nuclear reactions that are open to ground states. However, there is only one naturally occurring, effectively "stable" isomer, ^{180m}Ta, and this is nature's rarest stable nuclide. On the positive side for isomer experiments, the ground state is unstable and β decays with an 8-hour half-life, but natural tantalum is only 0.01% ^{180m}Ta, the remainder being ^{181}Ta. Despite the difficulties, enriched targets have been made, even in sufficient quantities for photon scattering experiments. Because the stellar nucleosynthesis and survival of ^{180m}Ta present a long-standing puzzle, the laboratory photo-destruction of the isomer, through its ground state, gives vital information regarding possible stellar synthesis environments. Belic et al. [18] identified single-step photo-destruction resonances at photon energies down to 1010 keV. This was subsequently shown to fit well with level-scheme information, enabling the details of the photo-destruction pathway to be identified [19], as illustrated in Figure 3. Note that the minimum photon energy of 1010 keV is, in this case, much higher than the

Table 1. Examples of extreme isomers.

Nuclide	Half-life	Spin (ħ)	Energy	Attribute	Ref.
^{12}Be	~500 ns	0	2.2 MeV	low mass	[8]
^{94}Ag	300 ms	21	6 MeV	proton decay	[9]
^{152}Er	11 ns	~36	13 MeV	high spin and energy	[10]
^{180}Ta	>10^{16} y	9	75 keV	long half-life	[11]
^{229}Th	~5 h	3/2	~7.6 eV	low energy	[12]
^{270}Ds	~6 ms	~10	~1 MeV	high mass	[13]

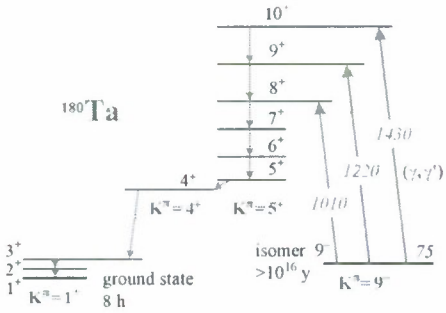

Figure 3. *Simplified scheme showing ^{180m}Ta photo-excitation, with decay to the ground state [19]. Energies (in italics) are in keV.*

isomer energy of 75 keV. In addition, multi-step photo-destruction at lower photon energies has been predicted to be important in stellar environments [20].

Radioactive isomer targets have also been made. A remarkable case is ^{178m2}Hf, a 31-year isomer at an excitation energy of 2.45 MeV. This has a unique combination of high energy and long half-life, arising from a K=16, 4-quasiparticle configuration. Targets with more than 10^{14} atoms of ^{178m2}Hf have been used for several nuclear physics experiments, such as deuteron scattering [21], but target impurities have limited the quality of the data obtained. Attempts at photo-destruction of the isomer have been controversial [22], but so far only upper limits have been reliably determined [23] in the photon energy range 5–100 keV.

Isomer Beams

The question naturally arises, in view of the high intensities of radioactive beams soon to be available, as to whether isomers would make better beams than targets. Compare the background of 10^5 decay/s from 10^{14} atoms of ^{178m2}Hf, making up some small fraction of a target, with the near-zero background that could be obtained from 10^6 ^{178m2}Hf ion/s in a purified beam. It may then be possible, for example, to look for Coulomb excitation, through a 0.33 MeV, E2 transition, to the I=14 member of the ground-state band [24], and thereby test the high degree of K mixing that has been inferred by Hayes et al. [25]. This would be a form of isomer photo-destruction, but now with a substantial energy release (2.45 MeV) compared to the energy of excitation (0.33 MeV).

However, a different perspective should also be considered. Once isomer *beams* are under discussion, then ^{178m2}Hf is not so special from an experimental point of view. There are numerous highly excited isomers with $T_{1/2} > 500$ ns, surviving long enough for mass separation and/or ion-by-ion A/q identification. A selection of such isomers, with energy >2 MeV, is illustrated in Figure 4.

Pioneering experiments at RIKEN, Japan, have been performed with isomer beams, produced using inverse heavy-ion, fusion-evaporation reactions in conjunction with a recoil filter. Measurements include the Coulomb excitation of a 2 μs, K=8 isomer in ^{174}Hf [26], and secondary fusion reactions with a 1 μs, I=49/2 isomer in ^{145}Sm [27]. However, to date, the limitations of low beam intensity, low beam purity and poor beam optics have placed severe restrictions on the quality of the information that can be obtained. Now we are entering a new era for radioactive beams in general, and for isomer beams in particular. A key aspect for isomer beams will be the ability to separate the isomeric states from their respective ground states, and several methods are available.

An outstanding capability has already been demonstrated at ISOLDE, CERN. Copper isomers and ground states have been separated by laser resonance ionisation. In the case of ^{68}Cu, a purified beam of the I=6 isomer ($T_{1/2}$=4 m, 722 keV) was accelerated to 200 MeV and Coulomb excited by ^{120}Sn target nuclei [28]. A notable feature was the detection of a γ-ray cascade back to the ground state, bypassing the isomer. This ISOL method is best for isomer with $T_{1/2} \geq 1$ s.

Also requiring second or longer half-lives is the storage-ring technique developed at GSI for fragmentation reaction products [29]. The different orbits of electron-cooled beams

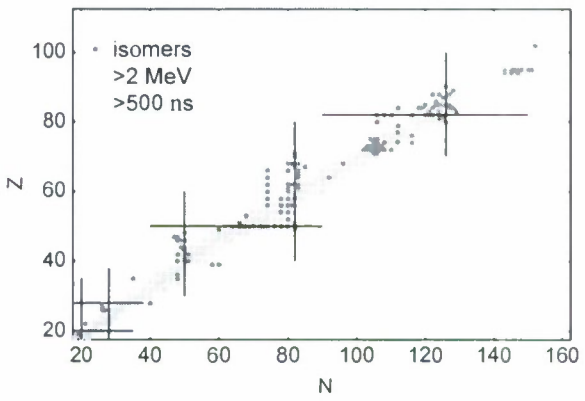

Figure 4. *Chart of nuclides, illustrating a selection of highly excited isomers (dots) that are long enough lived for secondary-reaction measurements. Naturally occurring nuclides are shown as faint squares.*

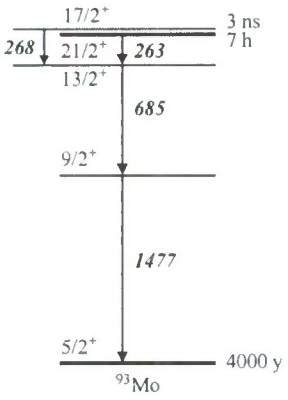

Figure 5. *Energy levels of ^{93}Mo, with a 7 hour isomer at 2.43 MeV.*

have been shown to give the capability of isomer separation by insertion of a mechanical "scraper." Alternatively, there are special cases such as ^{212}Po, where the ground state is short lived (0.3 μs) compared to the isomer (45 s) so that a ^{212m}Po beam would already be purified by the time it was cooled. Finally, for μs isomers it is possible to use delayed-coincidence techniques to select isomer-related events, for example by requiring Coulomb excitation γ rays to be time correlated with γ rays that come from the isomer decay. The many possibilities need careful evaluation.

Atomic–Nuclear Interface

The 7 hour, I = 21/2 isomer in ^{93}Mo, at 2.43 MeV, presents an unusual situation, illustrated in Figure 5. The structurally related 17/2 state is just 5 keV higher in energy than the isomer. It has been estimated that, in a plasma at a temperature above 5×10^6 K, the isomer decay rate would be enhanced by a factor of $\sim 10^6$, largely due to the predicted NEEC (nuclear excitation by electron capture) process [30]. NEEC is the inverse of electron conversion, which is well known often to dominate over γ-ray emission for low-energy transitions, but NEEC itself has yet to be observed in any nuclide. The 7 hour isomer in ^{93}Mo seems to be a candidate for a radioactive beam with which to explore such a process. Indeed, the release of 2.43 MeV isomer energy initiated by a 5 keV excitation could have wider interest. This is just one example of using an isomer to give a prominent signal (several high-energy γ rays) when excited by relatively low-energy photons. There are many more possibilities represented in Figure 4.

Gamma-Ray Laser

Isomers have been associated with the quest for a γ-ray laser, a long-standing dream that is perhaps as challenging as the search for controlled fusion power. The first concrete suggestions for a laser that utilized nuclear excited states as upper and lower lasing levels appeared in the literature in 1963 [31], following an earlier, previously classified Russian patent [32]. It is interesting how soon these works came after the first demonstration of optical lasing, but perhaps more amazing is that the fundamental recognition that stimulated emission was possible in nuclei came as early as 1926 [33].

A γ-ray laser would require a difficult synthesis of natural parameters and technical achievements, a challenge that has not yet been surmounted. In any laser, the most basic requirement is a population inversion between paired quantum states that serve as upper and lower laser levels. Stimulated emission of the corresponding electromagnetic decay transition gives the laser radiation, with repeated re-excitation of the upper laser level "pumping" the inversion and repeated stimulation of the emission increasing the amplification. Such a repetition is unlikely for a γ-ray laser, due to the difficulty in providing efficient reflection of high-energy photons.

It is in the preparation of a population inversion that isomers have been proposed to play a major part. The greatest impediment to the creation of a γ-ray laser has been the inherent conflict (the "graser dilemma" [34]) between the pumping of a population inversion and the requirement that the linewidth for the lasing transition be maintained as close to the natural width as possible. Various methods have been suggested by which to preserve the natural transition linewidth, such as using the Mössbauer effect or laser-cooled ensembles, but strong irradiation of a laser material to provide an inversion could easily destroy the narrow linewidth. A nuclear analogue of the standard four-level laser scheme, with nuclei beginning in a long-lived isomer instead of the ground state, might reduce the pump fluxes (by photons, neutrons, or ions) to a level that preserves the linewidth. So far, no system of suitable levels with the necessary transition probabilities and lifetimes has been found in any nuclide. It is worth mentioning that an extension of atomic processes like quantum interference might be possible, eliminating the competing absorption of laser photons by the lower laser level in a process called gain without inversion [35].

The field of γ-ray lasers thus remains dependent on further innovation. One key step would be the demonstration of isomer energy release induced by low-energy ($<<$ 1 MeV) photons [36]. This is where, as discussed earlier, radioactive beams may be needed.

Outlook

It is well recognized that radioactive beams are opening up the nuclear landscape. In this brief review, we have tried to show that isomers give an added dimension to these radioactive-beam developments, further extending the nuclear physics horizons. Moreover, isomer beams will offer unique possibilities to explore new physics at the atomic–nuclear interface. We must expand our mental horizons, not just our physical horizons, if we are fully to exploit the opportunities, and there is plenty of scope for new ideas.

Acknowledgments

This work has been supported by the UK EPSRC and AWE, and by the US AFOSR under contract FA9550-05-1-0486.

References

1. L. Carroll, *Through the Looking Glass* (Macmillan and Co., London, 1872).
2. F. Soddy, *Nature* 99, 433 (1917).
3. A. Bohr and B. R. Mottelson, *Phys. Rev* 90, 717 (1953).
4. P. M. Walker and G. D. Dracoulis, *Nature* 399, 35 (1999).
5. P. M. Walker and G. D. Dracoulis, *Hyperfine Interactions* 135, 83 (2001).
6. P. M. Walker and J. J. Carroll, *Physics Today* 58, 39 (June 2005).
7. G. D. Dracoulis et al., *Phys. Rev. Lett.* 97, 122501 (2006).
8. S. Shimoura et al., *Phys. Lett.* B560, 31 (2003).
9. I. Mukha et al., *Phys. Rev. Lett.* 95, 022501 (2005); Nature 439, 298 (2006).
10. A. Kuhnert et al., *Phys. Rev.* C46, 484 (1992).
11. M. Hult et al., *Phys. Rev.* C74, 054311 (2006).
12. B. R. Beck et al., *Phys. Rev. Lett.* 98, 142501 (2007).
13. S. Hofmann et al., *Eur. Phys. J. A10*, 5 (2001).
14. V. V. Flambaum, *Phys. Rev. Lett.* 97, 092502 (2006).
15. F. R. Xu et al., *Phys. Rev. Lett.* 92, 252501 (2004).
16. R.-D. Herzberg et al., *Nature* 442, 896 (2006).
17. P. H. Regan et al., *Nucl. Phys. A*, 787, 491c (2007).
18. D. Belic et al., *Phys. Rev. Lett.* 83, 5242 (1999).
19. P. M. Walker, G. D. Dracoulis and J. J. Carroll, *Phys. Rev.* C64, 061302R (2001).
20. P. Mohr, F. Käppeler and R. Gallino, *Phys. Rev.* C75, 012802R (2007).
21. S. Deylitz et al., *Phys. Rev.* C53, 1266 (1993).
22. E. V. Tkalya, *Phys. Rev.* C71, 024606 (2005).
23. I. Ahmad et al., *Phys. Rev.* C71, 024311 (2005).
24. S. A. Karamian and J. J. Carroll, *Laser Phys.* 17, 80 (2007).
25. A. B. Hayes et al., *Phys. Rev. Lett.* 96, 042505 (2006).
26. T. Morikawa et al., *Phys. Lett.* B350, 169 (1995).
27. H. Watanabe et al., *Nucl. Phys.* A746, 540c (2004).
28. G. Georgiev et al., *Int. J. Mod. Phys.* E15, 1505 (2006); I. Stefanescu et al., *Phys. Rev. Lett.* 98, 122701 (2007).
29. F. Bosch et al., *Int. J. Mass Spec.* 251, 212 (2006).
30. G. Gosselin and P. Morel, *Phys. Rev.* C70, 064603 (2004).
31. G. C. Baldwin, J. P. Neissel and L. Tonks, *Proc. IEEE* 51, 1247 (1963); V. Vali and W. Vali, *Proc. IEEE* 51, 182 (1963).
32. L. A. Rivlin, Soviet Inventor's Certificate No. 621265, 10 January 1961.
33. A. S. Eddington, *The Internal Constitution of the Stars* (Cambridge University Press, London, 1926).
34. G. C. Baldwin and J. C. Solem, *Rev. Mod. Phys.* 69, 1085 (1997).
35. O. Kocharovskaya, R. Kolesov, and Y. Rostovtsev, *Laser Phys.* 9, 745 (1999).
36. J. J. Carroll et al., *Hyperfine Interactions* 135, 3 (2001).
37. O. Hahn, *Chem. Berichte* 54, 1131 (1921).
38. C. F. von Weizsacker, *Naturwissenschaften* 24, 813 (1936).

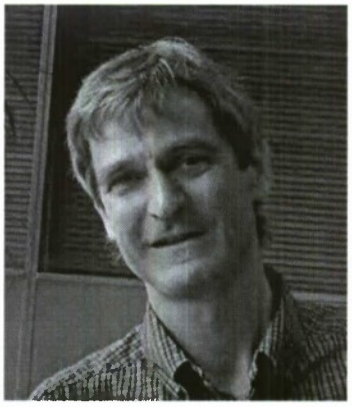

PHILIP M. WALKER

JAMES J. CARROLL

Available online at www.sciencedirect.com
ScienceDirect
Nuclear Instruments and Methods in Physics Research B 261 (2007) 960–964
NIM B
Beam Interactions with Materials & Atoms
www.elsevier.com/locate/nimb

Nuclear structure and the search for induced energy release from isomers

James J. Carroll *

Department of Physics and Astronomy, Youngstown State University, One University Plaza, Youngstown, OH 44555, USA

Available online 18 April 2007

Abstract

Metastable nuclear isomers are central to the study of nuclear structure and their energy storage capability has suggested a variety of applications. The feasibility of applications depends sensitively on the efficiency of any process that can deplete an isomer upon demand. This work surveys how the state-of-the-art in nuclear level and transition data impacts the search for induced energy release from isomers using recent advances in experimental techniques.

PACS: 21.60.−n; 25.20.−x; 27.70.+q; 27.90.+b

Keywords: Nuclear structure; Isomer; ^{180m}Ta; ^{178m2}Hf; ^{177m}Lu; ^{242m}Am; Induced depletion

1. Background

Metastable isomers, long-lived[1] nuclear excited states, can store large amounts of energy for significant periods. The longest halflife for any known isomer is more than 10^{16} years [1] (^{180m}Ta) while the largest stored energy[2] is 2.446 MeV (^{178m2}Hf), corresponding to a specific energy of 1.2 GJ/g. Many metastable isomers, particularly those in $A \sim 180$ nuclei, are characterized by large values of angular momentum. This reflects the presence of nucleon orbitals of high intrinsic angular momentum near the corresponding Fermi levels, so that high spins can be obtained at relatively low excitation energy. The result is that these long-lived isomers are typically yrast[3] and the paucity of levels to which they can decay through low multipolarity transitions leads to their metastable nature [3].

Isomer decays and transitions feeding isomers can provide valuable insight into nuclear structure (see, for example [4]). In general, isomers are central to the study of nuclei and have been instrumental in many important discoveries (see the review of [5]). In addition, the energy-storing capability of isomers has led to their consideration for various potential applications [6]. This has given added impetus to studies of electromagnetic transitions involving isomers [7].

The consideration of applications for isomers begins with the question: What could one do with a "clean" source of nuclear energy? No doubt this question was first posed long before the discovery of nuclear isomerism in 1921, but nevertheless motivates the search for induced energy release from isomers. Such an energy release may also be termed induced isomer depletion or triggered gamma emission. The answer to this question is beyond the present scope, but clearly leads to other questions: Is natural decay sufficient? If not, how could a release of nuclear energy be caused upon demand? What does "clean" mean when considering some particular application? Even

* Tel.: +1 330 941 3617; fax: +1 330 941 3121.
E-mail address: jjcarroll@cc.ysu.edu

[1] Isomers of interest herein are excited states with half-lives longer than one day.

[2] Nuclear data herein are taken from [2] unless indicated otherwise.

[3] The lowest-energy state of a given angular momentum is defined to be *yrast*, a standard term from nuclear structure physics. As such, an yrast state has only levels of lower angular momentum to which it can decay, limiting the number of available decay branches.

0168-583X/$ - see front matter © 2007 Elsevier B.V. All rights reserved.
doi:10.1016/j.nimb.2007.04.128

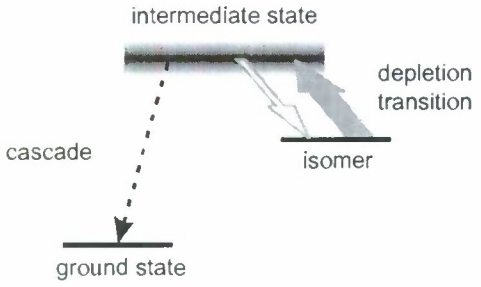

Fig. 1. Schematic depicting a process of induced isomer depletion. An isomeric nucleus is first excited to a higher-lying intermediate state. In addition to the back-decay to the isomer, the intermediate state must possess a decay branch that leads to a cascade that bypasses the isomer.

without a full definition, it would seem that a "clean" energy release would likely exclude fission and fusion reactions, producing numerous radioactive by-products, and leads to a consideration of other forms of energy storage in nuclei.

As early as 1926 [8] the possibility of stimulated emission of nuclear transitions was recognized. This was followed much later by more direct proposals for a γ-ray laser [9]. It was realized that the well-known four-level laser scheme might be obtained in nuclei by starting with a population in an isomeric state. Thus, isomers became a focus as the possible basis for controlled, on-demand energy release from nuclei via electromagnetic radiation. Analogous to optical pumping of lasers, there was also a concentration on inducing isomer depletion with photons.

The proposed mechanism of energy release, which would deplete the population of an isomer, is shown in Fig. 1. The process would not enhance isomer decay, but would bypass the metastable state's slow decay transitions. It might be expected that the necessary transitions could be identified simply by going to the existing nuclear databases. This is, unfortunately, the exception instead of the rule.

2. "Storage" isomers

About 30 isomers are known with half-lives longer than one day, as given in [7]. These may be considered as "storage" isomers. The metastable state of ^{180}Ta is the archetype of the spin isomer, where electromagnetic decays are inhibited by large changes in the magnitude of angular momentum needed to reach lower-lying levels. The isomer is characterized by $J^\pi = 9^-$ while the ground state possesses $J^\pi = 1^+$. An electromagnetic decay from isomer to ground-state would therefore be a magnetic 2^8-pole transition, with corresponding small probability. The excitation energy of the isomer is 75 keV above the unstable ground-state ($T_{1/2} = 8.2$ h), which decays by electron capture or β^- emission.

The $T_{1/2} = 31$ year isomer ^{178m2}Hf is an example of a K isomer. The ^{178}Hf nucleus is prolate with axial symmetry, as is typical mid-shell. Thus, the relative orientation of the angular momentum vector is quantized by K, its projection along the symmetry axis. Natural decay of ^{178m2}Hf occurs through electromagnetic transitions beyond the dipole, but which also require larger changes in the orientation of angular momentum. Intrinsic (single-particle) excitations in deformed nuclei form rotational bands as in diatomic molecules. The ^{178m2}Hf isomer is an intrinsic level with $J^\pi = K^\pi = 16^+$ and its dominant decay branch is a 12.7 keV transition to the $J^\pi = 13^-$ level in the rotational band built upon a $J^\pi = K^\pi = 8^-$ intrinsic state. The decay multipolarity is $L = 3$, but the E3 transition is K-forbidden since $\Delta K = 8$, giving an excess $\nu = \Delta K - L = 5$ orientation change. Due to mixing mechanisms, the transition is not truly forbidden, but is instead hindered by a factor of $f^\nu = (66)^5$. The reduced hindrance, f, varies among nuclei and even for different transitions in the same nucleus, but is typically on the order of 100 for $A \sim 180$. Large changes in K provide the dominant cause of metastability for isomers like ^{178m2}Hf, thus the term K isomer.

In all cases, metastable isomers serve as reservoirs of energy and may prove to be useful as batteries of high intrinsic energy density. With the exception of naturally-occurring isomers like ^{180m}Ta or those arising in the decay of terrestrial ores, isomers must be produced artificially and thus are not true energy sources.

3. Experimental search for induced isomer depletion

Due to its exceptional halflife, ^{180m}Ta is present in all naturally-occurring tantalum and thus is available for study. The ^{180}Ta ground-state is unstable and exists only in equilibrium with the long-lived isomer, so this material is a fully-inverted medium in the parlance of laser physics. The first concrete demonstration of induced depletion was obtained in 1987 [10] using 6 MeV bremsstrahlung.

The convenient halflife of ^{180g}Ta makes activation experiments possible, in which spectroscopy is performed out-of-beam. It was found [10] that after irradiation, the sample exhibited radiation signatures from the daughters of ^{180g}Ta and that this radiation decayed with a halflife of 8.2 h. In 1990, the variable-energy S-DALINAC electron accelerator was utilized to investigate the energy and cross-section required for this process. Within the experimental limits, it was demonstrated [11] that the depletion was induced strongly by photons near 2.8 MeV, with an integrated cross-sections on the order of 100 eV b. Later experiments [12] increased the sensitivity of the measurement, confirming the previous result and adding seven other energies at which the depletion occurred. Although a surprising result, the cross-sections were in agreement with nuclear systematics [13].

Induced depletion of ^{180m}Ta has been conclusively demonstrated and confirmed by independent experiments (for example [14]). The conclusion for applications of this isomer is straightforward: the lowest energy needed to induce the depletion is about 1 MeV while the energy stored in the isomer is 75 keV. Even considering the additional energy released by ^{180g}Ta decay, the process cannot provide an

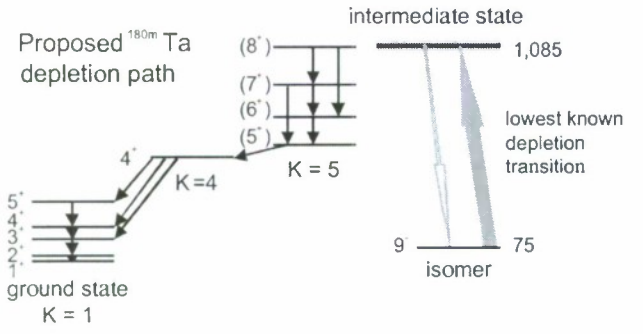

Fig. 2. Partial level scheme for ^{180}Ta, adapted from [14,15], showing the proposed identification of a known excited state with the lowest-energy intermediate state for isomer depletion [11]. Energies are in keV.

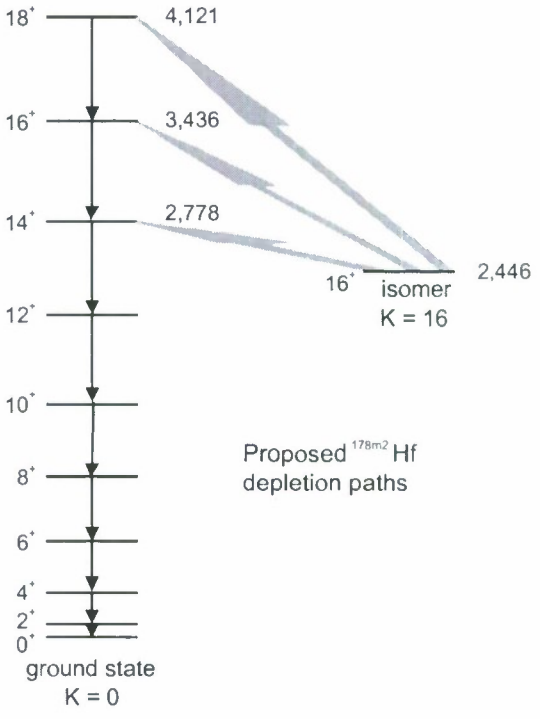

Fig. 3. Partial level scheme for ^{178}Hf, adapted from [4], showing the proposed identification of intermediate states for depletion of the 31-year isomer. Energies are in keV.

energy source. The results nevertheless proved the general scheme of Fig. 1 and suggested looking at higher-energy isomers. From the perspective of nuclear structure, the results are more difficult to understand.

At the time of the 1987 and 1990 experiments, level data for ^{180}Ta were not sufficiently detailed to provide significant *a priori* guidance as to what states might participate in isomer depletion. The situation is not much different today, despite tremendous advances in nuclear spectroscopy. The most complete examination of ^{180}Ta to-date is that of [15] and Fig. 2 shows a partial level scheme adapted from that work and [16]. Also shown is the lowest-energy intermediate state for isomer depletion [12] at 1085 keV. The proposed identification of a known level with this intermediate state may comprise a real connection between nuclear structure and isomer depletion. Even so, experiments have thus far failed to detect the back decay that must occur from intermediate state to isomer. The transition probability appears to correspond to a quite low K hindrance [16] despite $\nu = 3$, suggesting significant mixing of the K quantum number for the intermediate state.

The 31-year isomer ^{178m2}Hf stores far more energy than ^{180m}Ta. Not naturally-occurring, samples containing ^{178m2}Hf trace their lineage to two productions, by fusion evaporation [17] and proton spallation [18]. The former material is of far greater purity (about 5% isomer-to-ground-state ratio), but in lesser quantity. First experiments to search for induced isomer depletion were performed at CSNSM, Orsay, France, in 1996 and 1997. Results have not been released to-date from either test.[4]

Beginning in 1998, experiments were conducted to test depletion of ^{178m2}Hf by real photons with energies less than 100 keV. Many papers in the literature claim positive evidence of an induced energy release initiated by real photons near 10 keV. As surveyed in [20], all such claims originated from one group while independent studies by other groups found no evidence of this effect. Further reports in support of this effect (again, by the same group) and detecting no effect (independent groups) since [20] may be found in [21–24]. Additional tests were performed in 2003 and 2004 at the SPring-8 synchrotron, site of many of the claimed positive results and have found no evidence of an induced depopulation of ^{178m2}Hf by photons at the reported energy.[5] The question has been raised as to why independent groups have failed to observe the claimed effect. The inverse question is equally valid: why does one group continue to see the claimed effect? The interested reader is encouraged to examine the literature and form an independent assessment.

Available nuclear structure information for ^{178}Hf does not indicate a level within about 17 keV above the 31-year isomer, but this does not completely preclude the existence of such a state. Highly K-forbidden transitions would be expected to be small branches and therefore difficult to identify in spectroscopic experiments even with the most advanced gamma arrays. Only recently have experiments been conducted [4,25] that identify potential intermediate states and depopulation paths for ^{178m2}Hf, as shown in Fig. 3. Coulomb excitation (i.e. virtual photons) was used to study the population of excited states in ^{178}Hf from a ground-state target and determined that some levels in the ground-state band had small γ-ray branches directly

[4] The experimental scheme was proposed in [19] and supported on-site at Orsay in 1996 and 1997 by co-authors Carroll, Collins and Karamian. Recorded data were retained by the Orsay group.

[5] Results being prepared for submission in 2007 to PRL.

to the 31-year isomer. The reduced transition probabilities were near 1 W u, implying strong mixing of high-K components into low-K levels in the ground-state band above $J = 12$. These transitions would permit depletion of ^{178m2}Hf if an isomeric target was irradiated. The results are a triumph of modern nuclear structure research as related to a search for induced energy release from isomers. Nevertheless, no depletion experiment has been performed so far to test these transitions. The potential depletion transition of lowest-energy requires 332 keV.

Similar situations may be found for other metastable isomers of interest, such as ^{177m}Lu ($E^* = 970$ keV, $T_{1/2} =$ 160 days) and ^{242m}Am ($E^* = 49$ keV, $T_{1/2} = 141$ years). The most detailed structure information for ^{177}Lu was obtained in 2004 [26] and three transitions were observed that feed the isomer directly from higher levels. For possible intermediate states, these higher levels unfortunately have no known decay branches that bypass the isomer. As in many cases, nuclear structure information provides only limited guidance to the design of experiments on induced depletion of this isomer.

The long-lived ^{242m}Am isomer is interesting for a number of reasons. The isotope is odd-odd, so its level structure should be very rich, yet the available nuclear data is rather sparse. Decay of the 16-h ground-state would initiate a series of energy-releasing transmutations. And an excited state is known to exist just 4.3 keV above the isomer, reachable by a thus-far unobserved E2 transition. The corresponding transition probability should be very small due to K hindrance, but there may be a close match in energy between this 4.3 keV nuclear transition and an atomic transition [27]. The well-known NEET process might concentrate a broad atomic excitation into the narrow nuclear transition. Recently, an experiment was performed to study the nuclear structure of ^{242}Am using Argonne National Laboratory's ATLAS accelerator and Gammasphere, coupled to the CHICO charged-particle detector. Preliminary analysis [28] suggests some possible depletion paths, resulting from the observation of numerous new levels and transitions.

4. New approaches

Research into nuclear structure is only beginning to provide real guidance to the search for induced isomer depletion. This is largely due to the use of advanced detector arrays with greater sensitivity to weak transitions. In the future, more direct tests of isomer depletion will likely take place, but must rely on the ability to obtain either isomeric targets or isomeric beams of sufficient purity. Pure isomeric targets are extremely difficult to obtain, so the next major step will probably rely on the production of isomeric beams. One recent proposal [29] describes an experimental scheme utilizing a ^{178}Hf beam enriched in the 31-year isomer to perform Coulomb excitation. And the most exciting possibilities lie with pure isomer beams produced by ISOL or other methods, as reviewed in [30]. A major advance was made recently at REX-ISOLDE, where ^{68m}Cu was separated by selective photoionization. Coulomb excitation of the resulting isomer beam demonstrated an induced depletion [31].

5. Summary

The techniques of modern nuclear structure studies are very advanced, yet are only now reaching the level of sensitivity necessary to support investigations of induced energy release from isomers. Only in a few instances is it possible to predict *a priori* what levels might serve as intermediate states for isomer depletion. The next generation of experiments, using isomer beams, will allow more direct tests of these processes and the underlying physical mechanisms.

Acknowledgements

The author wishes to thank Drs. Sarkis Karamian, Phil Walker, Doug Cline and others for valuable discussions. Support for this work was provided by the Air Force Office of Scientific Research under Contract FA9550-05-1-0486.

References

[1] M. Hult, J. Gasparro, G. Marissens, P. Lindahl, U. Wätjen, P.N. Johnston, C. Wagemans, M. Köhler, Phys. Rev. C 74 (2006) 054311.
[2] Evaluated Nuclear Structure Data File, www.nndc.bnl.gov, Brookhaven National Laboratory, 2006.
[3] P.M. Walker, G. Dracoulis, Nature. 399 (1999) 35.
[4] A.B. Hayes, D. Cline, C.Y. Wu, J. Ai, H. Amro, C. Beausang, R.F. Casten, J. Gerl, A.A. Hecht, A. Heinz, et al., Phys. Rev. Lett. 96 (2006) 042505.
[5] P.M. Walker, J.J. Carroll, Phys. Today (June) (2005) 39.
[6] H. Roberts, Hyperfine Int. 107 (1997) 91.
[7] J.J. Carroll, S.A. Karamian, L.A. Rivlin, A.A. Zadernovsky, Hyperfine Int. 135 (2001) 3.
[8] A.S. Eddington, The Internal Constitution of the Stars, Cambridge Univ. Press, London, 1926.
[9] L.A. Rivlin, Soviet Inventor's Certificate No. 621265, January 10, 1961.
[10] C.B. Collins, C.D. Eberhard, J.W. Glesener, J.A. Anderson, Phys. Rev. C 37 (1988) 2267.
[11] C.B. Collins, J.J. Carroll, T.W. Sinor, M.J. Byrd, D.G. Richmond, K.N. Taylor, M. Huber, N. Huxel, P.v. Neumann-Cosel, A. Richter, et al., Phys. Rev. C 42 (1990) 1813.
[12] D. Belic, C. Arlandini, J. Besserer, J.D. Boer, J.J. Carroll, J. Enders, T. Hartmann, F. Käppeler, H. Kaiser, U. Kneissl, et al., Phys. Rev. C 65 (2002) 035801.
[13] S.A. Karamian, J.J. Carroll, Laser Phys. 11 (2001) 23.
[14] I. Bikit, L. Lakosi, J. Safar, L. Conkic, Astrophys. J. 522 (1999) 419.
[15] G.D. Dracoulis, T. Kibédi, A.P. Byrne, R.A. Bark, A.M. Baxter, Phys. Rev. C 62 (2000) 037301.
[16] P.M. Walker, G.D. Dracoulis, J.J. Carroll, Phys. Rev. C 64 (2001) 061302.
[17] Y.T. Oganessian, S.A. Karamian, Y.P. Gangrski, B. Gorski, B.N. Markov, Z. Szeglowski, C. Briançon, D. Ledu, R. Meunier, M. Hussonnois, et al., J. Phys. G 18 (1992) 393.
[18] H.A. O'Brien, Nucl. Instr. and Meth. B 40/41 (1989) 1126.
[19] C.B. Collins, J.J. Carroll, Y.T. Oganessian, S.A. Karamian, Laser Phys. 5 (1995) 280.
[20] J.J. Carroll, Laser Phys. Lett. 1 (2004) 275.

[21] C.B. Collins, N.C. Zoita, F. Davanloo, S. Emura, Y. Yoda, T. Uruga, B. Patterson, B. Schmitt, J.M. Pouvesle, I.I. Popescu, et al., Radiat. Phys. Chem. 71 (2004) 619.
[22] C.B. Collins, N.C. Zoita, F. Davanloo, Y. Yoda, T. Uruga, J.M. Pouvesle, I.I. Popescu, Laser Phys. Lett. 2 (2005) 162.
[23] N.C. Zoita, F. Davanloo, C.B. Collins, J.M. Pouvesle, S. Emura, I.I. Popescu, V.I. Kirischuk, N.V. Strilchuk, T. Uruga, Y. Yoda, J. Phys. IV France 127 (2005) 163.
[24] I. Ahmad, J.C. Banar, J.A. Becker, T.A. Bredeweg, J.R. Cooper, D.S. Gemmell, A. Kraemer, A. Mashayekhi, D.P. McNabb, G.G. Miller, et al., Phys Rev. C 71 (2005) 024311.
[25] A.B. Hayes, D. Cline, C.Y. Wu, M.W. Simon, R. Teng, J. Gerl, C. Schlegel, H.J. Wollersheim, A.O. Macchiavelli, K. Vetter, et al., Phys. Rev. Lett. 89 (2002) 242501.
[26] G.D. Dracoulis, G.J. Lane, F.G. Kondev, A.P. Byrne, T. Kibédi, I. Ahmad, M.P. Carpenter, S.J. Freeman, R.V.F. Janssens, N.J. Hammond, et al., Phys. Lett. B 584 (2004) 22.
[27] A.A. Zadernovsky, J.J. Carroll, Hyperfine Int. 143 (2002) 153.
[28] A.B. Hayes, D. Cline, K.J. Moody, C.Y. Wu, J.A. Becker, M.P. Carpenter, J.J. Carroll, D. Gohlke, J.P. Greene, A.A. Hecht, et al., Laser Phys. 17 (2007) 745.
[29] S.A. Karamian, J.J. Carroll, Laser Phys. 17 (2007) 80.
[30] P.M. Walker, Int. J. Modern Phys. E 15 (2006) 1637.
[31] G. Georgiev, I. Stefanescu, D.L. Balabanski, P. Butler, J. Cederkäll, T. Davinson, P. Delahaye, V.N. Fedosseev, L.M. Fraile, S. Franchoo, et al., Int. J. Modern Phys. E 15 (2006) 1505.

Weak K hindrance manifested in α decay of the $^{178}Hf^{m2}$ isomer

S. A. Karamian,[1] J. J. Carroll,[2] S. Iliev,[1] and S. P. Tretyakova[1]
[1] *Flerov Laboratory of Nuclear Reactions, Joint Institute for Nuclear Research, Dubna, RU-141980, Russia*
[2] *Department of Physics and Astronomy, Youngstown State University, Youngstown, Ohio 44555, USA*
(Received 18 July 2006; published 10 May 2007)

An experiment has been performed to detect the α emission mode in $^{178}Hf^{m2}$ isomer decay and a partial half-life of $(2.5 \pm 0.5) \times 10^{10}$y was measured. It was concluded that α decay is strongly retarded by the centrifugal barrier arising due to the high spin of this isomeric state. Additional analysis shows, however, that the K-hindrance in this α decay is relatively weak, despite the strong manifestation of spin-hindrance.

DOI: 10.1103/PhysRevC.75.057301 PACS number(s): 23.60.+e, 21.10.Tg, 27.70.+q

Electromagnetic decay of the noted 31-year-lived isomer $^{178}Hf^{m2}$ has been studied extensively (see Ref. [1] and references therein). The level structure of this isotope was also examined using spectroscopic techniques in many reaction studies, such as those of Refs. [2,3]. Until now, however, α decay of this isomer has not been observed.

A scheme of the process according to the tabulated data of Refs. [4,5] is given in Fig. 1. A maximum energy release in the α decay corresponds to the transition from the isomeric level to the ground state in the daughter ^{174}Yb nucleus. The value of $Q_\alpha = 4.53$ MeV allows α decay with a half-life on the order of days, much shorter than that due to electromagnetic decay. However, the isomer-to-ground state α decay spans a 16-unit change in angular momentum and should be strongly suppressed by the centrifugal barrier. Additional structure hindrance may arise due to the K quantum number as $\Delta K = 16$ for this transition. The total Q_α for decay of the ground and first isomeric (m1) states of ^{178}Hf are relatively low and should correspond to very long α decay half-lives according to the known systematics.

For mid-Z elements, alpha decay is typically observed for short-lived neutron-deficient isotopes. Considering elements ranging from Nd to Pb and isotopes thereof bounded by the magic numbers $N > 82$ and $Z \leqslant 82$, α decay energies E_α to specific daughter states are known. In many cases the corresponding partial α decay half-lives have been measured [5]. The hafnium isotopes lie in the center of this range of nuclides, having well-deformed axially symmetric prolate shapes, and it can be expected that they should obey the semi-empirical systematics.

A Geiger-Nuttall plot [6] is shown in Fig. 2 for even-Z nuclei, evidencing a nearly linear dependence of $\log(T^\alpha_{1/2})$ on the square root of Q_α. There is a small curvature to the plots, but this occurs over many orders-of-magnitude. The systematic behavior is valuable for estimating the unmeasured half-life of a nuclide for which Q_α is known. This is the initial basis for a prediction of the α decay half-life of $^{178}Hf^{m2}$. Geiger-Nuttall systematics, however, reflect well-allowed decays and do not account for structure or angular momentum hindrances. In α decay of $^{178}Hf^{m2}$, the high-spin of the initial state should strongly influence $T^\alpha_{1/2}$.

Hindrance factors in α decay of odd-mass nuclei were discussed in Ref. [7], being given by the ratio of the measured $T_{1/2}$ to an expected magnitude based on known values for α transitions without spin change, typically in neighboring even-even nuclei. This approach combines hindrances arising due to different physical reasons. However, in principle, one may distinguish "macroscopic" and "spectroscopic" hindrances. The first hindrance arises in the case of particle emission with non-zero orbital momentum due to the centrifugal barrier. The second one reflects a structure hindrance due to the re-arrangement of single-particle orbits and of the nuclear spin orientation.

For electromagnetic decay, structure hindrances are typically isolated in reference to the standard decay rate theoretically predicted for transitions of known energy and multipolarity. In deformed nuclei such "K hindrances" were determined successfully for many transitions and the reduced hindrance factors were systematized. The latter parameter describes, in definition, the retardation factor reduced to one unit of the $(\Delta K - \lambda)$ value, where λ is a multipolarity of the transition.

Here we extend this scheme to α decay. The α decay of $^{178}Hf^{m2}$ seems ideal for this development, having strong changes of both spin and K in α transitions to the yrast band of ^{174}Yb. Such transitions are selected as they possess the highest Q_α values (see Figs. 1 and 2). We first use the empirical systematics of Fig. 2 to estimate α decay half-lives without hindrances, next construct a systematic description for the spin hindrance from the centrifugal barrier, and then compare the "predicted" half-life with the measured one to determine the K hindrance.

A centrifugal barrier arises for any α transition with spin change. For isolation of a corresponding retardation factor, consider experimental data on α decay when the K quantum number makes no effect. Recall that K is defined as the projection of the angular momentum vector I on the symmetry axis. It does not exist in near-magic spherical nuclei or in nuclei with nonaxial shapes. For evaluation of the spin-hindrance, we assume that K does not exist and the α decay rate for transitions between initial I_i and final I_f states may be expressed as

$$R = \frac{N_{at} \ln 2}{T^\alpha_{1/2}(Q^{if}_\alpha)} \sum_{m=-I_f}^{I_f} \frac{1}{F(|I_i - m|)}, \quad (1)$$

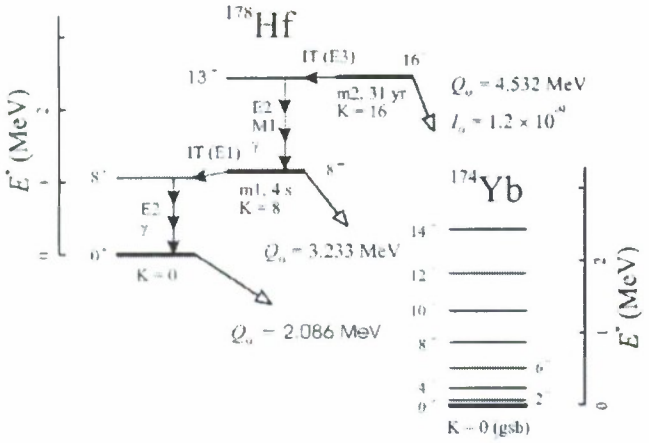

FIG. 1. α decay scheme for ^{178}Hf nuclei in the ground and isomeric states. The Q_α values were deduced from the nuclear mass tables [4] and the level energies and angular momenta from Ref. [5]. The presently measured absolute intensity is given for α decay of the $m2$ level to be 1.2×10^{-9}.

where Q_α^{if} is the transition energy, m is the projection of $\vec{I}_f$ along the direction of $\vec{I}_i$, N_{at} is the number of decaying nuclei and $T^{\alpha}_{1/2}(Q^{if}_{\alpha})$ corresponds to a value from Fig. 2 that depends only on Q_α^{if} and assumes zero spin change. The $F(|I_i - m|) = F(\ell)$ is defined as the spin-hindrance factor and depends only on the difference in spins between initial and final states. If $I_i = 0$, the sum in Eq. (1) may be replaced by the spin volume factor $(2I_f + 1)$ divided by $F(I_f)$.

Data exists in the literature on the relative intensities for branches of α decay for ground states of even-even nuclei that reach levels in the ground-state band of the daughter nuclide. The initial and final states are characterized by $K = 0$ so it was possible to isolate the spin-hindrance factor at $\Delta I = I_f$. Data [5] for ^{230}Th and ^{238}Pu were analyzed using Eq. (1) and the corresponding Geiger-Nuttall curves. With this procedure, values of the spin hindrance function $F(\ell)$ were characterized up to $\ell = 8$.

For α decay of ^{178}Hf^{m2}, the spin difference could be as high as $\Delta I = 16$, so the $F(\ell)$ values extracted from Th and Pu are insufficient. To extend $F(\ell)$ to higher spin differences, data were used for α decay of the high-spin isomers ^{211m}Po $(25/2^+)$, ^{212m}Po (18^+) and ^{214m2}Rn (8^+). These nuclei demonstrate pure manifestation of spin hindrance in α decay. They are near-magic nuclei so their α decays proceed without structure retardation.

For each of these nuclei, a ratio was taken between the isomer's half-life for α decay giving a specific ΔI and the ground state's α decay halflife for a specific ΔI. This ratio of half-lives was then related to the difference between the spin changes caused by the isomer and ground-state α decays to determine $F(\ell)$. The difference between spin changes was not so large for ^{211}Po: even though a branch of the isomer's α decay provides as much as $\Delta I = 12$, the ground state α decay causes $\Delta I = 4$. However, for ^{212}Po and ^{214}Rn the spin difference is equal to the spin released in the isomer decay. In this manner, Eq. (1) was used to obtain $F(\ell)$ up to $\ell = 18$ and confirming the $\ell \leqslant 8$ values.

Figure 3 shows the extracted $F(\ell)$ function. The magnitude of this hindrance is very high for ℓ up to 16, of importance for the estimation of α decay of the $I^\pi = 16^+$ ^{178}Hf^{m2} isomer. By analogy with electromagnetic decay, one can introduce a reduced hindrance factor f for α decay according to $F(\ell) = f^\ell$, also given in Fig. 3; despite the scatter the trend suggests a choice of $f = 6.8$ for high ℓ numbers. Thus, the necessary components are now available to obtain a reliable

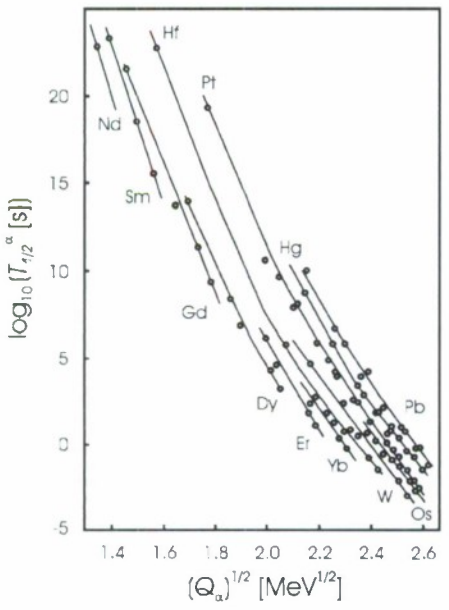

FIG. 2. Geiger-Nuttall systematics of α decay half-lives for nuclei in the range of $Z = 60$–82.

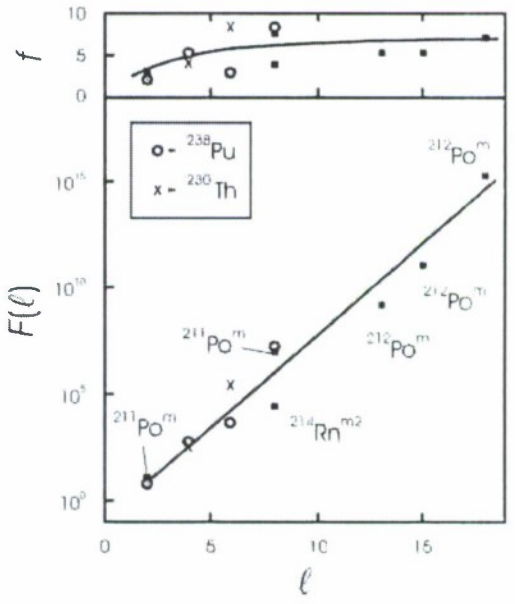

FIG. 3. Spin hindrance $F(\ell)$ versus angular momentum taken by the emitted α particle (bottom panel) and the reduced hindrance f (top panel). Three points marked as ^{212m}Po correspond to different branches of its α decay.

TABLE I. Estimated partial half-lives for α decay of the $^{178}Hf^{m2}$ isomer to levels in the ground-state band of ^{174}Yb. The calculations are discussed in the text.

Transition $I_i \rightarrow I_f$	E_α [MeV]	$T_{1/2}^{\alpha,f}$ [yr]
$16^+ \rightarrow 0^+$	4.43	8.6×10^{10}
$16^+ \rightarrow 2^+$	4.35	3.0×10^{9}
$16^+ \rightarrow 4^+$	4.18	3.4×10^{8}
$16^+ \rightarrow 6^+$	3.91	1.2×10^{8}
$16^+ \rightarrow 8^+$	3.56	2.8×10^{8}
$16^+ \rightarrow 10^+$	3.12	2.7×10^{9}
$16^+ \rightarrow 12^+$	2.61	7.2×10^{10}
$16^+ \rightarrow 14^+$	2.03	5.5×10^{13}

estimate of the α decay half-life of $^{178}Hf^{m2}$ based on empirical information.

The partial α decay half-lives, $T_{1/2}^{\alpha,f}$, are given in Table I for the transitions from the $I_i^\pi = 16^+$ ^{178}Hf isomeric state to levels in the ground-state band of ^{174}Yb with $I_f^\pi = 0^+$–14^+. The values in the table were obtained using Eq. (1) where the dominant contribution in the summation corresponds to the minimum ΔI. This occurs because $F(\ell)$ is a very steep function. The shortest half-life is expected for decay that reaches the 6^+ level of the daughter, giving the optimum product of $T_{1/2}^{\alpha,f}(Q_\alpha^{if})$ and $F(\ell)$. Using the partial half-lives, the total α decay half-life is estimated to be $T_{1/2}^{\alpha} = 6.4 \times 10^7$ y. The α decay represents a low-intensity branch compared to electromagnetic decay of the isomer, thus requiring a sensitive measurement.

A source of $^{178}Hf^{m2}$ containing about 3.5×10^{13} atoms with isomeric nuclei was prepared about ten years ago [8] at the Flerov Laboratory of Nuclear Reactions, JINR. The hafnium fraction was chemically isolated from the enriched ^{176}Yb target after exposing it to a 36-MeV ^{4}He-ion beam. The hafnium fraction containing $^{178}Hf^{m2}$ activity was deposited onto a Be foil and formed a hafnium oxide layer; no hafnium carrier was used in the chemical preparation. The thickness of the layer was small, definitely allowing small energy losses for transmission of α particles. The only hafnium in the material was that produced by nuclear reactions within the high-purity and highly-enriched ^{176}Yb target. The purity of the hafnium material was guaranteed by several methods [8], including neutron activation analysis.

A first measurement was performed using a Si surface barrier (SSB) detector with active area of 14-mm diameter. The $^{178}Hf^{m2}$ source was placed in vacuum at 10 mm from the SSB detector. The absolute efficiency of the detector was calibrated using a ^{nat}U sample and the energy resolution was found to be better than 50 keV. The $^{178}Hf^{m2}$ source was kept for two weeks in the chamber, pumped twice per week by a dry system. A spectrum of α particles was collected and a background spectrum was also measured during a two-week period under identical conditions, but without a source.

Single events were observed in both spectra. An α energy range from 2.0–4.5 MeV was selected so as to cover all branches listed in the table. The total number of events within the selected range was obtained for the "effect" spectrum (with source) and the "background" spectrum (without source). Subtracting the "background" number from the "effect" value gave $N_\alpha = (-17 \pm 25)$ as the number of α decays from the $^{178}Hf^{m2}$ source during the two-week period. Correcting to the detector efficiency, one obtains an upper limit for α emission from the source at $\leqslant 1$ alpha per 3 hours. This gives $T_{1/2}^{\alpha} > 6.6 \times 10^9$ y for $^{178}Hf^{m2}$ and a K-hindrance factor >100.

No statistically-significant emission, above background, was detected within the entire range of energies from 2 to 9 MeV. The background level must be attributed to contamination of the vacuum chamber, etc., which were composed of regular technical materials like stainless steel. It was decided to employ a more sensitive detection method rather than to attempt an improvement of sensitivity with SSBs by increasing the acquisition time, installing multiple detectors or preparing a more purified vacuum chamber.

Low-background charged-particle detection has been known for decades using solid-state track detectors. This approach is well-developed and has been calibrated by many groups, including at JINR (see Refs. [9,10]). In the present experiment for α detection, CR-39 foils were used as produced by "Track Analysis Systems Ltd, UK." These detector-quality foils were produced from very pure materials and contain no α active contaminants. Thus, in measurements with these foils the only source of background could be by penetration of radon. The track detector foil is provided with a clean polyethylene film cover to exclude radon. The film is removed prior to use. During experiments, the foils must remain isolated from the surrounding air. Thus, the $^{178}Hf^{m2}$ source was pressed between two clean CR-39 foils and carefully wrapped by plastic. The sandwich was then sealed for months within a plastic box since plastic materials contain less contamination from U and Th than metal packing.

Tracks due to α particles appeared in the exposed detector foil after etching the foil to develop those tracks. The tracks were counted by visual registration using an optical microscope. The foil facing the source had an α detection integral efficiency of about 80% from 2π, according to previous calibrations. The rear-positioned foil was useful to determine the background.

After seven-months exposure to the source, the surfaces of the exposed CR-39 detector foils showed moderate damage. A rough spot was present on the foil past etching, seen directly by the naked eye in the region where the active material was placed. This diffuse damage was interpreted as being caused by a high flux of low-energy electrons emitted from the source. Tracks of α particles were nevertheless discerned and counted, but it was decided to reduce the electron-induced damage to the foil surface.

Additional series were carried out in which detector foils were exposed to the hafnium source for shorter periods of 1 and 3.5 months. The etching time was slightly shortened as well to minimize the development of the diffuse damage spot. Under these conditions the degree of damage on the surface of the detector foil due to electrons was significantly reduced. Tracks of α particles were observed clearly and in accordance with their standard configuration. The total number of tracks within the area in contact with the active spot of the source

was integrated and was consistent with the number found in the first experiment with CR-39 when normalized for time. The region in the facing foils away from the source, without exposure to α particles, was also examined to determine the level of background.

Complementary background measurements were performed with similar CR-39 foils kept in the same environment and placed in contact with various non-α active foils including a Be foil similar to that which served as substrate for the hafnium source. The background was also measured without any material in contact with a detector. In all cases, the background track densities were statistically identical and also identical to the value obtained from the detector foil used with the hafnium sample (facing the sample), but away from the active spot.

The background track number was measured with good statistical accuracy to be 160 events and was then used to define the excess of counts due to the presence of the $^{178}Hf^{m2}$ activity. The three exposure runs covered a total duration of about one year and the results were integrated to deduce 307 excess counts due to α activity of the source, giving 2.1α/day after time and efficiency correction. During the measurement period, the number of $^{178}Hf^{m2}$ nuclei was about 2.8×10^{13}, so that

$$T^{\alpha}_{1/2} = (2.5 \pm 0.5) \times 10^{10} y. \quad (2)$$

This significantly improves the estimate of Ref. [11] of $T^{\alpha}_{1/2} > 6 \times 10^{8}$ y for $^{178}Hf^{m2}$. The present measurement error exceeds a 10% statistical error since systematical errors could not be excluded, for instance, due to the uncertainty in the efficiency of detection. Spectral information on $^{178}Hf^{m2}$ α decay is based only on the theoretical values given in the table as the experiments did not allow groups to be distinguished in the α spectrum.

The measured $T^{\alpha}_{1/2}$ is larger than the estimated value by a factor of 390. One can interpret this as a manifestation of K hindrance in α decay. A K hindrance of only 4×10^2 is quite low for α decay of $^{178}Hf^{m2}$. For example, one of the dominant decay branches seen in the table reaches the 6^+ level in ^{174}Yb via a transition with degree of K forbiddenness $\nu = (\Delta K - \Delta I) = 6$. In comparison, the corresponding spin hindrance $F(\ell = 6) \sim 10^5$ is seen in Fig. 3. This suggests that in reality K hindrance is weakly manifested in α decay of $^{178}Hf^{m2}$ and the K quantum number plays a relatively small role.

A theoretical analysis of α decay half-lives is given in Refs. [12,13]. For the ground state of ^{178}Hf, $T^{\alpha}_{1/2} \sim 5 \times 10^{23}$ y was found [12]. The measured value for the $^{178}Hf^{m2}$ isomer is much shorter, $T^{\alpha}_{1/2} = 2.5 \times 10^{10}$ y. This is the sustained manifestation of the gain in Q_{α} value due to the 2.446-MeV excitation energy of the isomer as shown in Fig. 1. The retardation of α decay by angular momentum creates a factor of many orders-of-magnitude and, after accounting for this effect, a relatively weak K hindrance was deduced from the experimental $T^{\alpha}_{1/2}$ value.

This work was supported by Youngstown State University as part of Battelle contract TCN04177 from the U.S. Army Research Laboratory (contract DAAD19-02-D-0001).

[1] M. B. Smith, P. M. Walker, G. C. Ball *et al.*, Phys. Rev. C **68**, 031302(R) (2003).
[2] S. M. Mullins, G. Dracoulis, A. P. Byrne *et al.*, Phys. Lett. **B393**, 279 (1997); **B400**, 401 (1997).
[3] A. Aprahamian, R. C. de Haan, H. G. Börner *et al.*, Phys. Rev. C **65**, 031301(R) (2002).
[4] P. Möller, J. R. Nix, W. D. Myers, and W. J. Swiatecki, At. Data Nucl. Data Tables **59**, 185 (1995).
[5] R. B. Firestone and V. S. Shirley, *Table of Isotopes*, 8th ed. (Wiley, New York, 1996).
[6] H. Geiger and J. M. Nuttall, Phil. Mag. **22**, 613 (1911).
[7] M. R. Schmorak, Nucl. Data Sheets **31**, 283 (1980).
[8] Yu. T. Oganessian, S. A. Karamian, Yu. P. Gangrsky *et al.*, in *Proceedings of the International School-Seminar "Heavy-Ion Physics,"* Dubna, Russia, (JINR, Dubna, 1993). Vol. 1, p. 365.
[9] S. P. Tretyakova, Yu. S. Zamiatnin, V. N. Kovantsev *et al.*, Z. Phys. A **333**, 349 (1989).
[10] S. A. Karamian, F. Grüner, W. Assmann *et al.*, Nucl. Instrum. Methods B **193**, 144 (2002).
[11] J. van Klinken, W. Z. Venema, R. V. F. Janssens *et al.*, Nucl. Phys. **A339**, 189 (1980).
[12] C. Xu and Z. Ren, Phys. Rev. C **69**, 024614 (2004).
[13] V. Yu. Denisov and H. Ikezoe, Phys. Rev. C **72**, 064613 (2005).

Photon scattering experiments on the quasistable, odd-odd mass nucleus ^{176}Lu

S. Walter,[1,*] F. Stedile,[1] J. J. Carroll,[2] C. Fransen,[3] G. Friessner,[3] N. Hollmann,[3] H. von Garrel,[1,†] J. Jolie,[3] O. Karg,[4,‡] F. Käppeler,[5] U. Kneissl,[1] C. Kohstall,[1,§] P. von Neumann-Cosel,[4] A. Linnemann,[3] D. Mücher,[3] N. Pietralla,[4] H. H. Pitz,[1] G. Rusev,[6] M. Scheck,[1,‖] C. Scholl,[3] R. Schwengner,[6] V. Werner,[3,¶] and K. Wisshak[5]

[1] *Institut für Strahlenphysik, Universität Stuttgart, D-70569 Stuttgart, Germany*

[2] *Department of Physics and Astronomy, Youngstown State University, Youngstown, Ohio 44555, USA*

[3] *Institut für Kernphysik, Universität zu Köln, D-50937 Köln, Germany*

[4] *Institut für Kernphysik, Technische Universität Darmstadt, D-64289 Darmstadt, Germany*

[5] *Institut für Kernphysik, Forschungszentrum Karlsruhe, D-76021 Karlsruhe, Germany*

[6] *Institut für Strahlenphysik, Forschungszentrum Dresden-Rossendorf, D-01314 Dresden, Germany*

(Received 18 December 2006; published 2 March 2007)

The quasistable odd-odd-mass nucleus ^{176}Lu is of special interest in nuclear structure physics and, above all, in nuclear astrophysics. Systematic photon scattering experiments have been performed at the bremsstrahlung facility of the 4.3-MV Stuttgart Dynamitron accelerator with bremsstrahlung end-point energies of 2.3 and 3.1 MeV to determine the low-energy dipole strength distribution in the s-only isotope ^{176}Lu. The main goal was to pin down possible intermediate states (IS) for the photoactivation of the short-lived 123-keV isomer, which is the key process determining the effective lifetime of ^{176}Lu in a stellar photon bath and hence for the use of this isotope as a stellar chronometer. Using an enriched sample, 29 transitions ascribed to ^{176}Lu were detected below 2.9-MeV excitation energy. The corresponding excitation strengths were determined. For the previously proposed lowest IS at 839 keV, an upper limit for the excitation strength corresponding to a lifetime of $\tau \geq 1.5$ ps can be given. Astrophysical consequences, also in view of new Stuttgart photoactivation experiments, are discussed. The fragmentation of the dipole strength is compared to those in neighboring even-even and odd-even nuclei.

DOI: 10.1103/PhysRevC.75.034301 PACS number(s): 25.20.Dc, 21.10.Re, 23.20.Lv, 27.60.+j

I. MOTIVATION AND INTRODUCTION

The isotope ^{176}Lu is one of the only nine known stable or quasistable naturally occurring odd-odd mass nuclei. It has a ground-state spin of $J_0^\pi = 7^-$ ($K = 7$) and decays by β^- decay with a long half-life of about 4×10^{10} yr [1,2] to ^{176}Hf; see Fig. 1. In addition, a low-lying $J^\pi = 1^-$, $K = 0$ isomer occurs in ^{176}Lu at an excitation energy of 123 keV with a half-life of only 3.635 h, which decays also by β^- transitions to ^{176}Hf. Such large spin differences of low-lying levels are a common characteristics in heavy odd-odd nuclei and originate from aligned and antialigned couplings of the unpaired protons and neutrons in high-spin Nilsson orbits. In the case of ^{176}Lu these are the $\pi 7/2^+[404]$ and $\nu 7/2^-[514]$ orbits [3].

Due to the long half-life of about 40 Gyr and the fact that the isotope is shielded against an r-process synthesis, ^{176}Lu was suggested as an appropriate s-process chronometer [5–7]. However, answering the question to what extent ^{176}Lu can serve as a cosmic clock or represents more a stellar thermometer is complicated due to its nuclear structure and depends critically on a possible photoexcitation of the 1^- isomer, and its subsequent short-lived 3.635 h β decay, within the photon bath of a stellar s-process scenario [7–12]; see Fig. 2. Therefore, the electromagnetic coupling between the ground state and the low-lying isomeric level via low-lying intermediate states (IS) is of fundamental importance for the nucleosynthesis of ^{176}Lu and for tests of stellar models [7,13–15].

IS can be determined from the kinks in the yield curves observed in photoactivation experiments using bremsstrahlung photon beams (see, e.g., Ref. [16]). However, in such experiments the energy determinations are limited to an accuracy of about ±30 keV [16]. Moreover, in photon scattering experiments (nuclear resonance fluorescence (NRF)) the excitation energies of such IS can be measured with accuracies of better than 1 keV. Therefore, as a first part of joint efforts to investigate the photo-induced population of the 123-keV isomer in ^{176}Lu (photon scattering and photoactivation experiments), systematic NRF studies on ^{176}Lu were performed at the Stuttgart facility to measure the strength distributions of low-lying dipole modes and of possible IS. In addition, the combination of photoactivation and photon scattering experiments provides new information on the branching ratio Γ_{iso}/Γ_0, for the population of the isomer via the IS, and the IS decay back to the ground state, even without knowledge of the spin J_{IS} and the total width Γ of the IS.

*Present address: Institut für Kernphysik, Forschungszentrum Karlsruhe, D-76021 Karlsruhe, Germany.

†Present address: Daimler Chrysler AG, D-71013 Sindelfingen, Germany.

‡Present address: Fachbereich Material-und Geowissenschaften, Technische Universität Darmstadt, D-64287 Darmstadt, Germany.

§Present address: Phywe Systeme, D-37079 Göttingen, Germany.

‖Present address: Departments of Physics & Astronomy, University of Kentucky, Lexington, Kentucky 40506-0055, USA.

¶Present address: WSNL, Yale University, 272 Whitney Ave, New Haven, CT 06520-8124, USA.

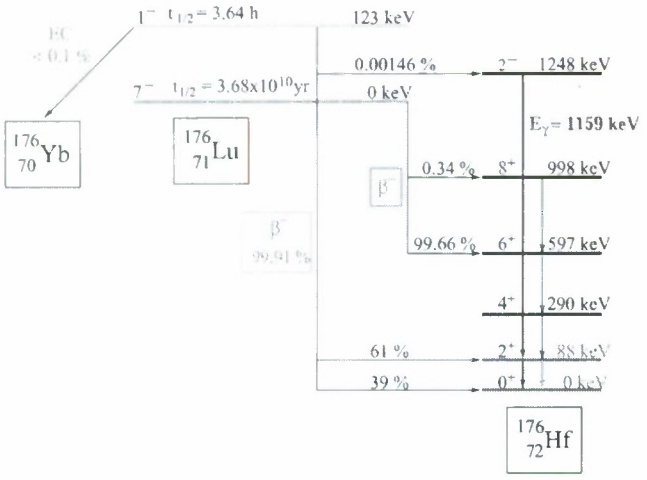

FIG. 1. (Color online) Decay scheme of ^{176}Lu. The isomeric state as well as the ground state both decay by β^- decay primarily to ^{176}Hf [2,4].

A further goal of the present investigations was to study for the first time the fragmentation of the low-lying dipole strength in an odd-odd nucleus with a high ground-state spin as compared to those in its neighboring even-even and even-odd nuclei.

The present NRF measurements were complemented by photoactivation experiments of highest sensitivity to study directly the population of the low-lying 1^- isomer at 123 keV. The obtained results will be presented and discussed in a forthcoming article [17].

II. EXPERIMENTAL TECHNIQUES

A. The nuclear resonance fluorescence method

Photon scattering of bound states, nuclear resonance fluorescence, represents the most sensitive technique to study low-lying dipole excitations. The formalism describing photon scattering is summarized in previous reviews (e.g., Refs. [18–20]). In experiments using continuous bremsstrahlung as a photon beam the total cross section integrated over one resonance and the full solid angle is measured:

$$I_{S,f} = g \cdot \left(\pi \frac{\hbar c}{E_\gamma}\right)^2 \cdot \frac{\Gamma_0 \Gamma_f}{\Gamma}. \tag{1}$$

Here Γ_0, Γ_f, and Γ are the decay widths of the photo-excited state with spin J to the ground state, to a final lower-lying state, and its total width, respectively. The statistical factor $g = (2J + 1)/(2J_0 + 1)$ is called spin factor. The product $g \cdot \Gamma_0$, which can be directly extracted from the measured scattering intensities, is proportional to the reduced excitation probabilities $B(E1)\uparrow$ or $B(M1)\uparrow$:

$$B(\Pi 1)\uparrow = g\, B(\Pi 1)\downarrow = \frac{9}{16\pi}\left(\frac{\hbar c}{E_\gamma}\right)^3 \cdot (g\Gamma_0). \tag{2}$$

Whereas in the favorable cases of even-even nuclei model-independent spin and parity assignments to the photo-excited states are possible from angular distribution and polarization measurements, the angular distributions of the scattered photons for odd-mass and odd-odd target nuclei are rather isotropic. Therefore, in general no unambiguous spin assignments to the photo-excited states are possible. In addition, the vanishing anisotropy in the angular distributions leads to rather weak polarizations of the scattered photons. This implies that no parity assignments are possible by polarization measurements as in the case of even-even nuclei. For the comparison with the dipole strengths in even-even nuclei the quantity

$$g \cdot \Gamma_0^{\text{red}} = g \cdot \frac{\Gamma_0}{E_\gamma^3} \tag{3}$$

is introduced, which is proportional to the reduced dipole excitation probability [see Eq. (2)]. These quantities can be extracted even without knowledge of the spins of the photo-excited states.

Decay branching ratios R_{expt} defined by

$$R_{\text{expt}} = \frac{B(\Pi L;\, J \to J_f)}{B(\Pi L;\, J \to J_0)} = \frac{\Gamma_f}{\Gamma_0} \cdot \frac{E_{\gamma J_0}^3}{E_{\gamma J_f}^3} \tag{4}$$

may contain valuable information on the spin J and, in the case of deformed nuclei, on the K quantum number of the photoexcited state.

If all decay branches of the photo-excited states can be measured and hence the total decay widths Γ are determined, lifetimes τ can be extracted via the uncertainty relation:

$$\tau = \frac{\hbar}{\Gamma}. \tag{5}$$

It should be emphasized that these lifetime determinations are complementary to direct lifetime measurements because the shorter the lifetimes the larger the widths and hence the easier the measurements in NRF.

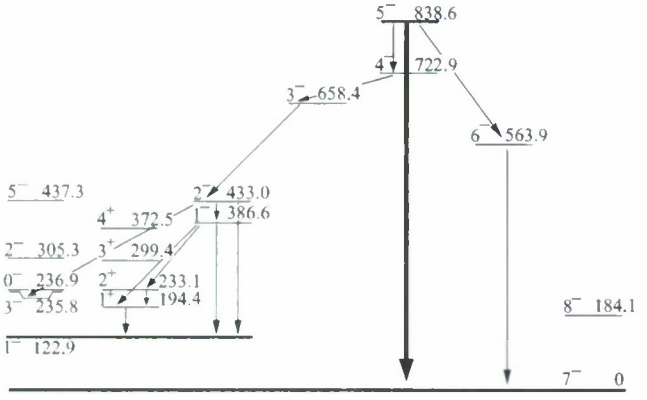

FIG. 2. This level scheme shows a possible coupling between the ground state of ^{176}Lu and the isomer at 123 keV via the IS at 838.6 keV with a spin of 5^- and quantum number $K = 4^-$ (see Ref. [9]).

B. Experimental details and setup at the Stuttgart Dynamitron

The present NRF experiments on ^{176}Lu were performed at the well-established Stuttgart bremsstrahlung facility [19].

Measurements using bremsstrahlung end point energies of 2.3 and 3.1 MeV were carried out to achieve an optimal sensitivity, in particular in the low-energy range of astrophysical interest. The DC electron currents used in the present experiments had to be limited to about 250 μA, due to the thermal capacity of the radiator target of about 1 kW. The measuring times were 171 and 125 h for the runs at 2.3 and 3.1 MeV end point energies, respectively.

Because ^{176}Lu has a natural abundance of only 2.6% [21], the use of very expensive enriched target material was imperative. Due to the kind loan by Forschungszentrum Karlsruhe, a target consisting of 2.001 g of Lu_2O_3 enriched to 72.5% in ^{176}Lu was available for the present experiments. The residual impurity of 27.5% consisted of ^{175}Lu. Because this isotope has been studied in previous NRF experiments at Stuttgart [22], an unambiguous distinction of excitations in ^{176}Lu and ^{175}Lu was possible. The targets were attached to aluminum sheets. The isotope ^{27}Al, with some very well-known excitations, serves generally in bremsstrahlung-induced NRF experiments as a photon flux monitor [23].

The scattered photons were detected by three high-resolution HPGe γ-ray spectrometers installed at angles of about 90°, 127°, and 150° with respect to the incoming bremsstrahlung beam. Each of the detectors had an efficiency of about 100% relative to a standard 7.6 × 7.6 cm NaI(Tl) detector. The energy resolutions were typically about 2 keV at a photon energy of 1.3 MeV and about 3 keV at 3 MeV. The detector at 127° was additionally surrounded by a bismuth germanate (BGO) anti-Compton shield to improve its response function. With this arrangement the peak-to-background ratio could be improved by a factor of about 2. This gain in sensitivity is of particular importance at photon energies near the end point energy. A part of a spectrum from 2.5 to 3.2 MeV is shown in Fig. 3. Both spectra were measured with the detector at 127°. The end point energy of 3.1 MeV can be clearly seen.

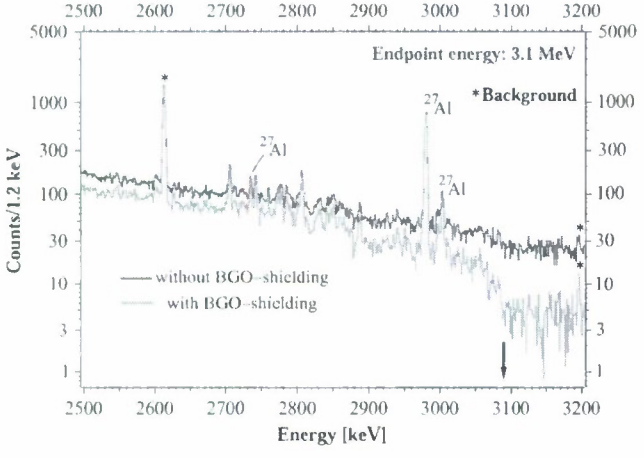

FIG. 3. (Color online) (γ, γ') spectrum with an end point energy of 3.1 MeV. Note the improvement in the peak-to-background ratio by a factor of 2–3 due to the active BGO anti-Compton shielding.

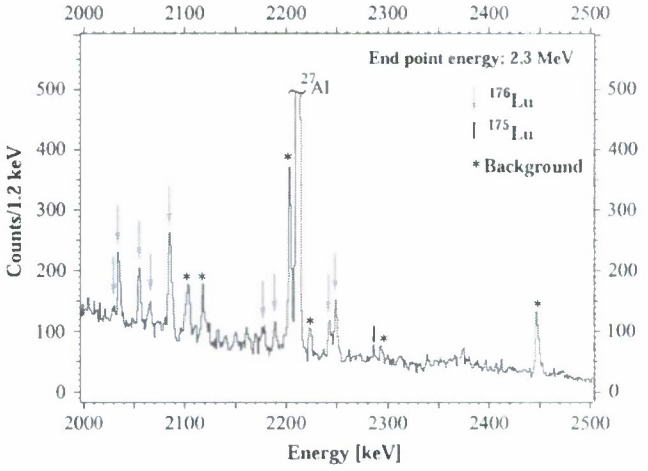

FIG. 4. (Color online) (γ, γ') spectrum with an end point energy of 2.3 MeV. The peak at 2212 keV stems from ^{27}Al, used for photon flux calibration. For further explanations, see text.

III. RESULTS

Due to the limited experimental sensitivity and the large number of possible transitions, it was impossible to deduce information about spins or mixing parameters δ. Therefore, an isotropic angular distribution of $W(\theta) \equiv 1$ for the calculation of the integrated cross section $I_{S,0}$ and the other values listed in Table I was assumed.

A. Measurement with 2.3 MeV end point energy

The data presented here result from a measurement performed with an end point energy of 2.3 MeV, 171 h measuring time, and an average electron beam current at the target of 200 μA. A small part of the spectrum in the energy range from 2.0–2.5 MeV is shown in Fig. 4. Transitions in ^{176}Lu are marked with green arrows. The other peaks are due to background (marked by asterisks) or are transitions from the ^{175}Lu impurity in the sample (marked by a black bar). The latter transitions are known from earlier experiments at Stuttgart [22]. The peak at 2212 keV stems from ^{27}Al and was used for photon flux calibration.

In this measurement, 14 transitions have been identified—although the lowest in energy may eventually prove to be from ^{175}Lu, because the previous NRF measurements on ^{175}Lu [22] started only at 1545 keV. However, neither of these two transitions are listed in the compilation of Ref. [24].

The lowest-lying 1S at 838.6 keV [9] could not be detected with the current experimental sensitivity. However, an upper limit for the integrated cross section $I_{S,0}$ of 1.5 eV b can be given from the analysis of the detection limits. Using the uncertainty principle, this corresponds to a minimum lifetime τ of about 1.5 ps, which, considering the experimental uncertainty, is consistent with a GRID measurement performed by Doll *et al.* [10] obtaining $\tau_{839} \geq 10$ ps. For more experimental details of this 1S, see Table II.

TABLE I. Combined results of the measurements at end point energies of 2.3 and 3.1 MeV. Quoted are exeitation energies E_x, integrated eross seetions $I_{S,0}$, the produet of spin faetor g and ground-state transition width Γ_0, branching ratios $R_{\exp,i}$, the produet of spin faetor g and the reduced ground-state transition width $\Gamma_{0,\mathrm{red}}$, and the exeitation probabilities $B(M1)\uparrow$ and $B(E1)\uparrow$.

E_x (keV)	$I_{S,0}$ (eV b)	$g\cdot\Gamma_0$ (meV)	$R_{\exp,i}$	$g\cdot\Gamma_{0,\mathrm{red}}$ (meV/MeV^3)	$B(M1)\uparrow$ (μ_N^2)	$B(E1)\uparrow$ (10^{-3}e^{2}fm^2)
1332	2.58(70)	1.19(24)	–	0.50(10)	0.043(9)	0.48(10)
1497[b]	1.38(41)	0.80(19)	–	0.24(6)	0.021(5)	0.23(5)
1671[b]	1.86(43)	1.35(23)	–	0.29(5)	0.025(4)	0.28(5)
1739	2.00(55)	1.57(32)	–	0.30(6)	0.026(5)	0.29(6)
1760[b]	4.25(145)	3.42(89)	–	0.63(16)	0.054(14)	0.60(16)
1902[a]	0.62(33)	0.58(25)	–	0.08(4)	0.007(3)	0.08(4)
2030	0.75(39)	0.80(35)	–	0.10(4)	0.008(4)	0.09(4)
2036[b]	3.37(53)	3.63(40)	–	0.43(5)	0.037(4)	0.41(5)
2056[b]	3.07(51)	3.39(40)	–	0.39(5)	0.034(4)	0.37(4)
2067[a,b]	2.16(42)	2.41(35)	–	0.27(4)	0.024(3)	0.26(4)
2086[b]	7.12(97)	8.49(80)	0.18(10)	0.93(9)	0.081(8)	0.89(8)
2178[b]	2.63(48)	3.28(44)	–	0.32(4)	0.027(4)	0.30(4)
2190[b]	1.83(38)	2.29(35)	–	0.22(3)	0.019(3)	0.21(3)
2243[b]	4.14(69)	5.46(65)	–	0.48(6)	0.042(5)	0.46(6)
2249[b]	7.47(113)	16.59(148)	0.51(9) 1.32(56)	1.46(13)	0.126(11)	1.39(12)
2266	1.11(43)	1.48(45)	–	0.13(4)	0.011(3)	0.12(4)
2315	1.33(64)	1.85(74)	–	0.15(6)	0.013(5)	0.14(6)
2359	0.94(40)	1.36(47)	–	0.10(4)	0.009(3)	0.10(3)
2559	0.83(53)	1.42(78)	–	0.08(5)	0.007(4)	0.08(4)
2566	1.28(94)	2.19(140)	–	0.13(8)	0.011(7)	0.12(8)
2602	1.79(62)	3.15(83)	–	0.18(5)	0.015(4)	0.17(5)
2628	1.02(41)	1.83(58)	–	0.10(3)	0.009(3)	0.10(3)
2775	5.21(130)	10.44(188)	–	0.49(9)	0.042(8)	0.47(8)
2790	3.87(129)	7.83(199)	–	0.36(9)	0.031(8)	0.34(9)
2803	2.48(71)	5.08(108)	–	0.23(5)	0.02(4)	0.22(5)
2807	8.70(161)	17.85(235)	–	0.81(11)	0.07(9)	0.77(10)
2848	1.58(46)	3.33(73)	–	0.14(3)	0.012(3)	0.14(3)
2852	2.42(61)	5.12(93)	–	0.22(4)	0.019(3)	0.21(4)
2860	1.18(57)	2.50(99)	–	0.11(4)	0.009(4)	0.10(4)

[a]This peak, also possibly being an inelastie transition, is treated as a ground-state transition here.
[b]Error-weighted average of the measurements at 2.3 and 3.1 MeV.

B. Measurement with 3.1 MeV end point energy

A second experiment was performed at a higher energy ($E_0 = 3.1$ MeV) for 125 h and with an average electron beam current at the target of 210 μA. A spectrum in the energy range from 2.0 to 2.5 MeV is shown in Fig. 5. Because the end point energy is higher compared to that in Fig. 4, the number of high energetic γ rays is larger, but the low-energy nonresonant background is increased as well. The combined numerical results of the measurements at end point energies of 2.3 and 3.1 MeV are presented in Table I.

TABLE II. Experimental limits for the properties of the IS at 839 keV: integrated cross section, decay widths, lifetime, and transition strength.

E_x (keV)	$I_{S,0}$ (eV b)	Γ_0 (meV)	$\Gamma_{0,\mathrm{red}}$ (meV/MeV^5)	τ ps	$B(E2)\uparrow$ (e^{2}fm^4)
839	<1.5	<0.37	<0.9	$\gtrsim$1.5	<820

IV. DISCUSSION

In case of the measurement with a 2.3 MeV end point energy, 6 possible inelastic transitions were found, whereas before in the run with a 3.1 MeV end point energy, 28 eandidates for inelastic transitions, transitions of photo-excited states to lower-lying states, were found based on the Ritz combination principle and on the knowledge of the low-energy level scheme. To reduce the large number of possible correlations, the Alaga rules [25] were taken into account. For strongly deformed nuclei, the ratio of the reduced transition probabilities of a transition with multipole order L from a state i within one rotational band (with K_i) to the states f, f', ... of other rotational bands depends only on geometrical factors

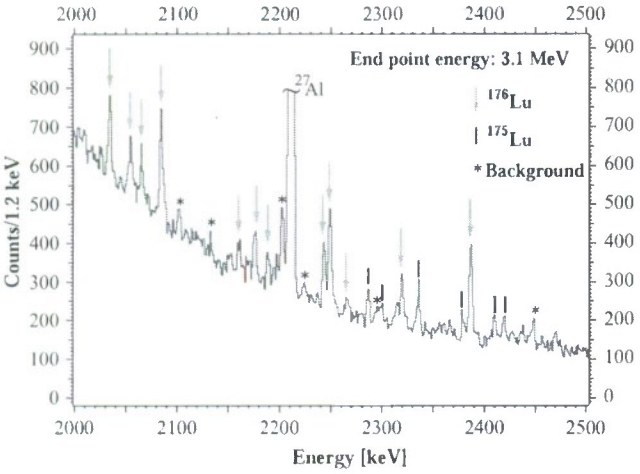

FIG. 5. (Color online) (γ, γ') spectrum with an end point energy of 3.1 MeV. The higher end point energy leads to an increase in the nonresonant background at low energies.

and can be expressed by means of the ratio of Clebsch-Gordan coefficients:

$$R_f^{\text{theo}} = \frac{B(L, J_i \to J_f)}{B(L, J_i \to J_{f'})} = \left| \frac{\langle J_i, L, K_i, K_f - K_i | J_i, L, J_f, K_f \rangle}{\langle J_i, L, K_i, K_0 - K_i | J_i, L, J_0, K_f \rangle} \right|^2 . \quad (6)$$

Whenever the experimental data were sufficient to calculate R_f^{theo}, the experimental value R_f^{exp} was compared with the theoretical one. If the ratio R_f^{exp} was larger than 5, the possiblity that there is an inelastic transition was eliminated. The adopted criterion seems to be reasonable, because states exhibiting such a high decay branching ratio hardly can be populated by a dipole excitation from the ground state due to their low ground-state decay widths. Hence, in case of the 2.3 MeV measurement, two levels at 2086 and 2249 keV were determined, each with one possible inelastic transition (to the $J^\pi = 6^-$ level at 184 keV) whereas the 3.1 MeV measurement exhibited a further decay branch of the upper level at 2249 keV to a state at 1760 keV, unknown so far.

A comparison of the strength distribution of ^{175}Lu and ^{176}Lu is shown in Fig. 6. The detected total transition strength in ^{176}Lu is lower than expected, due to a stronger fragmentation in this nucleus, so that probably a larger part of the strength lay below the sensitivity limit of the present experiment.

Especially when comparing ^{176}Lu with the isobars ^{176}Yb and ^{176}Hf, the stronger fragmentation can be easily seen in Fig. 7: in the energy range between 1 and 3 MeV, the total

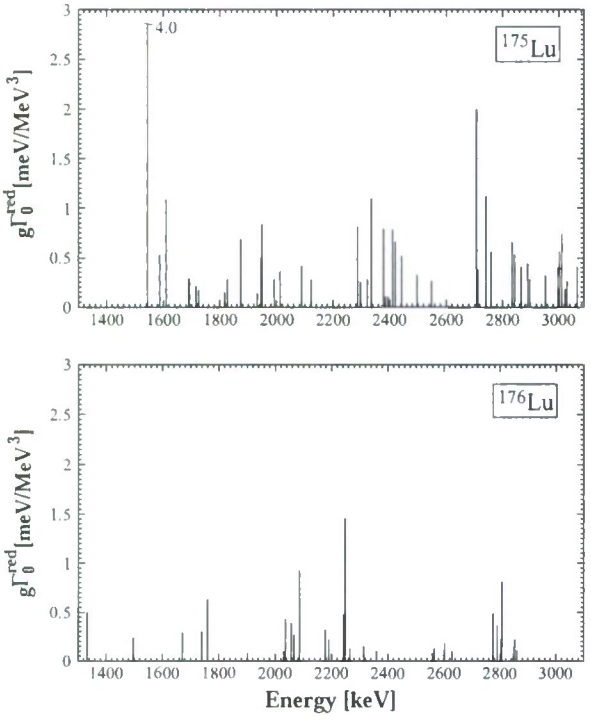

FIG. 6. Strength distributions in ^{175}Lu [22] and ^{176}Lu.

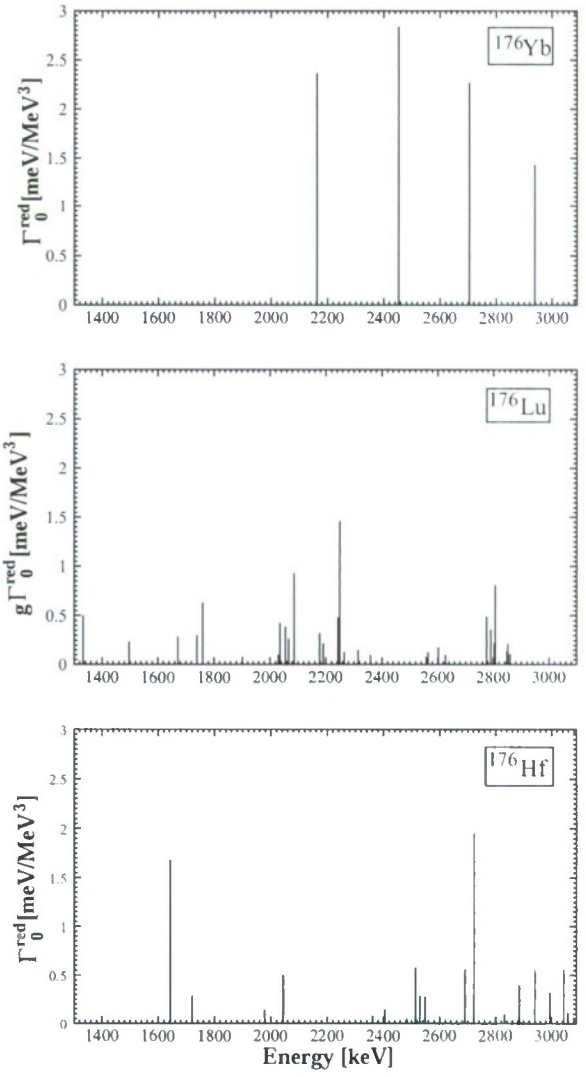

FIG. 7. Strength distributions in the neighboring isobars ^{176}Yb [26] and ^{176}Hf [27], compared with that of ^{176}Lu.

dipole strengths, assuming $M1$ character for the excitations in ^{176}Lu and ^{176}Yb, are 0.852(154) μ_N^2 for ^{176}Lu, compared to 2.32(60) μ_N^2 for ^{176}Yb and 1.347(112) μ_N^2 for ^{176}Hf. Because the Yb and Hf isobars are even-even nuclei, they show fewer transitions, however, with a stronger total transition strength. In case of Yb, it is possible that weaker transitions could not be detected due to the limited sensitivity of that older measurement.

V. CONCLUSIONS

Two photon scattering experiments on the odd-odd nucleus ^{176}Lu have been performed, using end point energies of 2.3 and 3.1 MeV, respectively. In total 29 transitions, ascribed to this nucleus, have been found in the energy range from 1.3 to 2.9 MeV, and their transition strengths have been determined. For the lowest proposed 1S at 839 keV, an upper limit of $I_{S,0} < 1.5$ eV b, corresponding to a minimum lifetime of $\tau \gtrsim 1.5$ ps, can be given. This is consistent with the GRID measurement by Doll *et al.* [10].

The combined results of these NRF measurements and photoactivation experiments will be presented and discussed in a forthcoming article [17].

ACKNOWLEDGMENTS

This work was partially supported by the Deutsche Forschungsgemeinschaft (DFG) under contracts Kn 154/31, Br 799/11, Jo 391/3-1, and SFB 634. J.C. acknowledges support from the U.S. Air Force Office of Scientific Research under contract FA9550-05-1-0486. N.P. thanks the Department of Energy for his support under grant DE-FGO2-04ER41334.

[1] G. F. Grinyer, J. C. Waddington, C. E. Svensson, R. A. E. Austin, G. C. Ball, G. Hackman, J. M. O'Meara, C. Osborne, F. Sarazin, H. C. Scragga, and H. D. H. Stöver, Phys. Rev. C **67**, 014302 (2003).
[2] Y. Nir-El and G. Haquin, Phys. Rev. C **68**, 067301 (2003).
[3] M. S. Basunia, Nucl. Data Sheets **107**, 791 (2006).
[4] R. B. Firestone, *Table of Isotopes*, 8th edition (John Wiley and Sons, Inc. New York, 1996).
[5] J. Audouze, W. A. Fowler, and D. N. Schramm, Nature Phys. Sci. **238**, 8 (1972).
[6] M. Arnould, Astron. Astrophys. **22**, 311 (1973).
[7] F. Käppeler, H. Beer, and K. Wisshak, Rep. Prog. Phys. **52**, 945 (1989).
[8] N. Klay, F. Käppeler, H. Beer, G. Schatz, H. Börner, F. Hoyler, S. J. Robinson, K. Schreckenbach, B. Krusche, U. Mayerhofer, G. Hlawatsch, H. Lindner, T. von Egidy, W. Andrejtscheff, and P. Petkov, Phys. Rev. C **44**, 2801 (1991).
[9] N. Klay, F. Käppeler, H. Beer, and G. Schatz, Phys. Rev. C **44**, 2839 (1991)
[10] C. Doll, H. G. Börner, S. Jaag, F. Käppeler, and W. Andrejtscheff, Phys. Rev. C **59**, 492 (1999).
[11] K. T. Lesko, E. B. Norman, R.-M. Larimer, B. Sur, and C. B. Beausang, Phys. Rev. C **44**, 2850 (1991).
[12] J. Vanhorenbeeck, J. M. Lagrange, M. Pautrat, J. S. Dionisio, and Ch. Vieu, Phys. Rev. C **62**, 015801 (2000).
[13] F. Käppeler, Prog. Part. Nucl. Phys. **43**, 419 (1999).
[14] D. Belic, C. Arlandini, J. Besserer, J. de Boer, J. J. Carroll, J. Enders, T. Hartmann, F. Käppeler, H. Kaiser, U. Kneissl, M. Loewe, H. J. Maier, H. Maser, P. Mohr, P. von Neumann-Cosel, A. Nord, H. H. Pitz, A. Richter, M. Schumann, S. Volz, and A. Zilges, Phys. Rev. Lett. **83**, 5242 (1999).
[15] D. Belic, C. Arlandini, J. Besserer, J. de Boer, J. J. Carroll, J. Enders, T. Hartmann, F. Käppeler, H. Kaiser, U. Kneissl, E. Kolbe, K. Langanke, M. Loewe, H. J. Maier, H. Maser, P. Mohr, P. von Neumann-Cosel, A. Nord, H. H. Pitz, A. Richter, M. Schumann, F.-K. Thielemann, S. Volz, and A. Zilges, Phys. Rev. C **65**, 035801 (2002).
[16] D. Belic, J. Besserer, C. Arlandini, J. de Boer, J. J. Carroll, J. Enders, T. Hartmann, F. Käppeler, H. Kaiser, U. Kneissl, M. Loewe, H. Maser, P. Mohr, P. von Neumann-Cosel, A. Nord, H. H. Pitz, A. Richter, M. Schumann, S. Volz, and A. Zilges, Nucl. Instrum. Methods A **463**, 26 (2001).
[17] F. Stedile *et al.*, publication in preparation (2007).
[18] U. E. P. Berg and U. Kneissl, Annu. Rev. Nucl. Part. Sci. **37**, 33 (1987).
[19] U. Kneissl, H. H. Pitz, and A. Zilges, Prog. Part. Nucl. Phys. **37**, 349 (1996).
[20] Ulrich Kneissl, Norbert Pietralla, and Andreas Zilges, J. Phys. G: Nucl. Part. Phys. **32**, R217 (2006).
[21] J. R. de Laeter and N. Bukilic, Phys. Rev. C **73**, 045806 (2006).
[22] R.-D. Herzberg, C. Fransen, R. Fischer, O. Beck, D. Belic, J. Besserer, P. von Brentano, Th. Eckert, U. Kneissl, B. Krischok, J. Margraf, H. Maser, A. Nord, N. Pietralla, H. H. Pitz, A. Wolpert, and A. Zilges, Phys. Rev. C **56**, 2484 (1997).
[23] N. Pietralla, I. Bauske, O. Beck, P. von Brentano, W. Geiger, R.-D. Herzberg, U. Kneissl, J. Margraf, H. Maser, H. H. Pitz, and A. Zilges, Phys. Rev. C **51**, 1021 (1995).
[24] A. O. Macchiavelli and E. Browne, Nucl. Data Sheets **69**, 903 (1998).
[25] G. Alaga, K. Alder, A. Bohr, and B. R. Mottelson, K. Dan. Vidensk. Selsk. Mat. Fys. Medd. **29(9)**, 1 (1955).
[26] A. Zilges, P. von Brentano, R. D. Heil, U. Kneissl, S. Lindenstruth, H. H. Pitz, U. Seemann, R. Stock, and C. Wesselborg, Nucl. Phys. **A507**, 399 (1990).
[27] M. Scheck, D. Belic, P. von Brentano, J. J. Carroll, C. Fransen, A. Gade, H. von Garrel, U. Kneissl, C. Kohstall, A. Linnemann, N. Pietralla, H. H. Pitz, F. Stedile, R. Toman, and V. Werner, Phys. Rev. C **67**, 064313 (2003).

ISSN 1054-660X, Laser Physics, 2007, Vol. 17, No. 2, pp. 80–86.

Prospects for Coherently Driven Nuclear Radiation by Coulomb Excitation

S. A. Karamian[a, *] and J. J. Carroll[b]

[a] *Joint Institute for Nuclear Research, Dubna, Moscow oblast, 141980 Russia*
[b] *Youngstown State University, Youngstown, Ohio, 44555 United States*
*e-mail: karamian@nrmail.jinr.ru

Received September 2, 2006

Abstract—Possible experiments are discussed in which Coulomb excitation of nuclear isomers would be followed by sequential energy release. The possibility of coherent Coulomb excitation of nuclei ensconced in a crystal by channeled relativistic heavy projectiles is considered. The phase shift between neighbor-nuclei excitations may be identical to the photon phase shift for emission in the forward direction. Thus, the elementary string of atoms may radiate coherently with emission of characteristic nuclear γ rays, and the intensity of the radiation would be increased due to the summation of amplitudes. Mössbauer conditions should be important for this new type of collective radiation, which could be promising in the context of the γ-lasing problem.

PACS numbers: 25.70.De, 42.55.Vc

DOI: 10.1134/S1054660X07020053

1. INTRODUCTION

The creation of an externally driven γ-ray source using triggered decay of nuclear isomers has been proposed and discussed in the special volume of [1]. The idea was suggested even earlier [2] for nuclear Coulomb excitation applied to the pumping of a nuclear ensemble in future schemes for a γ-ray laser. Experimentally, triggering of the ^{178m2}Hf isomer in inelastic scattering reactions was tested in 1996–1997 by the "Hafnium Collaboration" using an in-beam multidetector system and an α-particle beam of the Orsay Tandem accelerator. Due to the restricted thickness and purity of the isomeric target, conclusive results were not obtained or published, but partial analysis indicated that an excitation energy of about 300 keV is needed for successful triggering of this isomer. Many subsequent efforts were spent to find triggering of ^{178m2}Hf with low-energy X-rays or synchrotron photons at $E_\gamma < 100$ keV, but definite evidence reproducible by different groups was not obtained. A review of these experimental attempts is given in [3] for the ^{178m2}Hf isomer, most attractive for applications due to its long half-life, 31 y, and the high density of stored energy, 1.3 GJ/g. Nuclear spectroscopy with the Coulomb excitation technique has proven over many years to be very valuable for measurements of strengths of nuclear transitions, and it can be applied to search for and to quantitatively study triggering transitions in ^{178}Hf. In the present work, such an experiment is proposed and described in some detail, including the general scheme, background conditions, expected count rate, and the absolute sensitivity.

Coulomb excitation may also be valuable in another mode of application, i.e., for coherent nuclear excitation by relativistic heavy projectiles. It should be stressed immediately that such a process can provide coherence both in excitation and radiation of the nuclei ensconced in a crystal lattice. An elementary string of atoms in the lattice may radiate coherently at a frequency corresponding to the characteristic nuclear γ line. Mössbauer conditions will clearly play an important role for this collective radiation. In the literature, many kinds of coherent radiation generated by charged particles in crystals were described, e.g., parametric radiation and channeling radiation. In addition, the idea of a γ-lasing scheme has been described using short bursts of a crystallized ion beam in a cooler ring [4]. The multiple resonance excitation of each projectile nucleus by regular collisions in a crystal was considered in detail in [5]. In the present work, the idea of coherent radiation emitted by the lattice nuclei due to Coulomb excitation by channeled relativistic heavy ions is discussed.

2. SEARCH FOR TRIGGERING LEVELS ABOVE THE ^{178m2}Hf ISOMER

In the experiment described in [6], the population of levels in bands built on isomers was successfully observed via Coulomb excitation reactions acting on the stable ^{178}Hf isotope in its ground state. Surprisingly, the cross-section for this population was moderately high; this was attributed to strong K mixing of different structure configurations at high angular momentum, i.e., between the band built on the $K = 16$ isomer and the ground-state $K = 0$ band. Interband transitions were eventually deduced from the results of [6], and they are displayed in Fig. 1, where the partial level scheme of ^{178}Hf is shown.

This observation suggests a special experiment by which to observe triggering of the ^{178m2}Hf isomer into the levels of the ground-state band via Coulomb excitation, essentially as an inverse of the reaction observed in [6]. The magnitude of the cross-section for the population of ^{178}Hf isomers [6] likewise promises significant probabilities for the reversed process of triggering. A successful new experiment will quantify parameters such as the energies, multipolarities, and reduced matrix elements for energy-releasing trigger transitions. These parameters are needed to assess the feasibility of inducing a release of isomeric energy under an intense photon flux, as suggested for some applications [7].

At this time, technical challenges restrict the availability of samples containing ^{178m2}Hf in an amount sufficient for preparation of a target suitable for standard in-beam γ-spectroscopic experiments. Therefore, it is necessary to consider the possibility of performing an experiment with ^{178m2}Hf nuclei as projectiles. Radioactive ion-beam facilities operate routinely at many laboratories, and the long-lived ^{178m2}Hf nuclide should not be extraordinarily difficult for beam production.

The most critical issues which define the cost of an experiment and the quality of the measurements are the consumption rate for and total available amount of ^{178m2}Hf. Taking into account the production parameters achieved for ^{178m2}Hf in the best reactions, one deduces that 10^{15} isomeric atoms can be accumulated by moderate-cost irradiations (for details, see [2]). Thus, about 10^{13} ions of ^{178m2}Hf may be delivered to the target in a Coulomb excitation experiment because of a typical 1% efficiency of accelerators. The isomer production is typically characterized by a relatively poor isomer-to-ground state ratio, lower than 5% in the best case. Therefore, the accelerated beam will contain mostly stable ^{178}Hf nuclei in the ground state with a little admixture of ^{178m2}Hf. A total beam current of about 1 particle nA is considered, as it would not destroy a target foil.

It is important to understand why the consumption of isomeric material in the form of a beam is preferable to the use of a small isomeric target. In-beam experiments provide the possibility of Coulomb excitation of each accelerated nucleus as they impinge upon a thick target made of some material which can be obtained in sufficient quantity. A ^{178m2}Hf isomeric target would be restricted to about 1 μg/cm^2 thickness, and this will provide an interaction probability that is a factor of 10^{-3}–10^{-4} lower than in typical Coulomb excitation experiments. The gain factor for the isomer beam experiment is reduced by the efficiency of acceleration for the available material, about 10^{-2}, but an order-of-magnitude overall gain of interaction probability remains over an experiment with such a thin isomeric target. An additional advantage arises because the ^{178m2}Hf target creates a high-intensity background in γ detectors due

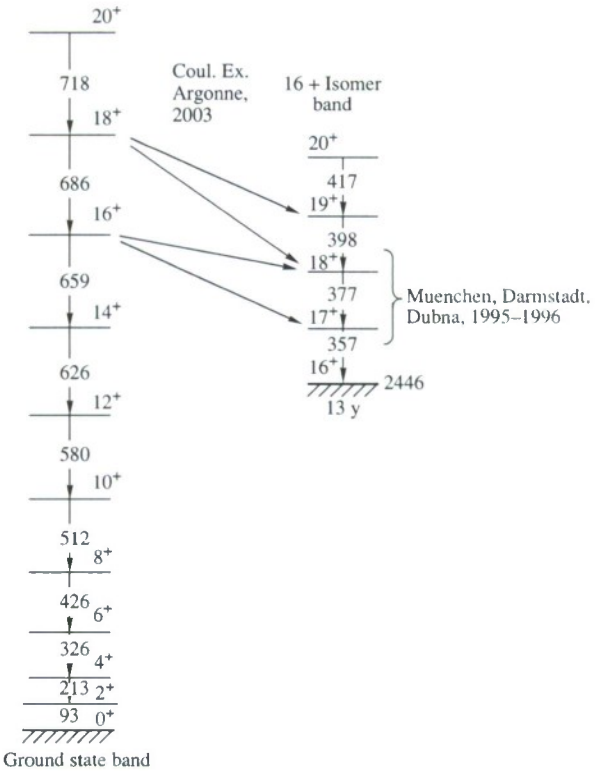

Fig. 1. Partial energy-level scheme for the ^{178}Hf nucleus.

to the spontaneous decay, while, in the mode of an in-beam excitation experiment, the radioactive nuclei are collected downstream, beyond the target and out of the detection area. In the end, much better background conditions and much higher sensitivity of trigger detection may be provided in the latter version. Contaminant activities can be removed without special efforts, because the accelerator serves as a high-resolution mass analyzer.

The schematic of the experiment is as follows. A target made of low-background material like ^{208}Pb is irradiated by a ^{178m2}Hf ion beam at an energy much lower than the Coulomb barrier of interaction. The projectile-target γ spectrum due to Coulomb excitation should be recorded in coincidence with the scattered ions. Use of a multidetector γ array is needed to obtain γ–γ and higher coincidences. The spectrum collected with the 5% "isomeric" beam must be compared with that obtained from a pure ground-state ^{178}Hf beam and the difference spectrum obtained. This difference spectrum may contain cascades corresponding to the population of high-spin levels both within the band built on the isomer and within the ground-state band (gsb). In the latter case, the population of high-spin members of the gsb may take place due to single-step Coulomb excitation from the isomer if K mixing is indeed significant, as discussed in [6]. Observation of the corresponding

γ cascades would then serve as a signal of isomer triggering.

As is the usual case in any experiment, the background intensity plays a significant role. One may analyze some restrictions on the scheme that accrue from the presence of different backgrounds:

(1) The beam energy should be relatively low, about 4 MeV/nucleon, in order to prevent population of $J \geq 14$ members of the gsb due to excitations of $J = 0$ ground states present in the beam. The probability for such multiple Coulomb excitations is drastically reduced at this low beam energy [6], and triggering can therefore be clearly isolated.

(2) The need to obtain coincidences between γ signals and the scattered projectile does not allow the use of a thick target that stops the beam. Detection of the scattered projectile defines the direction of the emitter motion, but the absolute speed varies due to energy losses in the target. The target thickness should be optimized for successful Doppler correction; for a Pb target, a value of 4 mg/cm^2 is found to be satisfactory.

(3) Doppler correction is absolutely necessary. Otherwise, it would be difficult to observe narrow γ lines when those gammas are emitted in flight.

For the count rate estimation, single-step $E2$ Coulomb excitations from the 16^+ isomeric level to the 14^+, 16^+, and 18^+ levels of the gsb are calculated. The respective transition energies are known to be 331, 990, and 1675 keV. Weisskopf strength was assumed for these transitions due to the observation in [6] of strong K mixing in the gsb at spins $J \geq 10$. Following this, $B_W(E2)\uparrow = 0.0297\ e^2b^2$ is taken as the Weisskopf value for all transitions. With a mean projectile energy of 740 MeV, one finds values of the Coulomb excitation parameter of $\xi = 0.489$ for 331 keV, $\xi = 1.46$ for 990 keV, and $\xi = 2.47$ for 1675 keV transitions.

Assuming the c.m. solid angle for detection of scattered ions to be 5 sr and using the parameters described above, an excitation rate of about 245 events/s is found for the 331 keV transition, about 3.2 events/s for the 990 keV, and about 1.5×10^{-2} events/s for 1.675 keV transition. These values correspond to an isomeric ion-beam intensity of 3×10^8 s^{-1}; high statistics of the events can be collected using a total of 10^{13} ions containing isomeric nuclei. The gamma background due to Coulomb excitation starting from the 0^+ ground state would not be significant and, in addition, can be removed by subtracting a spectrum taken under the same conditions but with a pure ^{178}Hf ground-state beam. Thus, the triggering events can be reliably selected and the corresponding cross-section deduced.

Direct observation of such transitions and characterization of their cross-sections is essential for basic scientific knowledge and to assess the feasibility of applications.

3. COHERENT COULOMB EXCITATION IN CRYSTALS

Relativistic heavy-ion beams are available today at some accelerator facilities, and additional possibilities will appear in the future. The status of such facilities will eventually change from exotic to more regular as tools for experimental physics. The enormous cost of these scientific instruments does not restrict progress in experimental methods. Recall, for instance, neutrino telescopes or free-electron lasers at teraelectronvolts accelerators. Thus, without apology, a new application is proposed here for heavy-ion beams at energies >1 GeV/nucleon for the generation of coherent nuclear γ radiation.

A channeled particle may produce a regular consequent excitation of nuclei ensconced in one elementary string in a crystal. At relativistic energies, the phase shift in excitation of neighbor nuclei is almost the same as the phase shift of the de-excitation photons emitted in the forward direction. Accordingly, the coherent excitation and radiation of a whole string of atoms with emission of a characteristic nuclear γ line may occur. Such a possibility exists, in principle, but it's amplitude depends on many concrete parameters and conditions. Below, some of these are characterized.

As is well known, channeling requires that $\Psi \leq \Psi_{cr}$, where Ψ is the angle of a particle's trajectory relative to the plane or axis of crystal. The critical angle of axial channeling Ψ_{cr} is normally estimated by the Lindhard equation. In the relativistic case, this has the form

$$\psi_{cr} = 2.4 \times 10^{-4} \sqrt{\frac{Z_1 Z_2}{Wd}}, \quad (1)$$

where Ψ_{cr} is expressed in radians, the total energy W in gigaelectronvolts, and the interatomic distance d in angstrems. The planar channeling wavelength in the harmonic approximation can be estimated with the expression

$$\lambda = \frac{\pi d_p}{\psi_{cr}}, \quad (2)$$

where the interplane spacing d_p is expressed in angstrems. One can combine Eqs. (1) and (2) when the axial channeling trajectory has zero orbital momentum and its plane is perpendicular to the crystal plane. At the trajectory maximum, the projectile moves most closely to the atomic plane and rows. For individual atomic collisions, the impact parameter varies slowly in this part of the trajectory. Numerical estimates indicate that a length of the trajectory of about $\lambda/10$ near the trajectory maximum can provide consequent collisions for coherent excitation of nuclei. At a larger longitudinal coordinate, a transversal deviation appears and increases the impact parameter of collisions.

The experiment's main idea is illustrated in Fig. 2: a channeled projectile passes near some individual atomic string and excites the nuclei in a series of subse-

quent collisions. A flat trajectory is typical for channeling at high energies, and many collisions will be characterized by a similar impact parameter b. Finally, the whole string accumulates an excitation at the nuclear frequency mode and may radiate coherently with an intensity proportional to $(aN)^2$, where N is the number of excited nuclei and a is the excitation amplitude for an individual nucleus. A natural condition for coherence would be phase matching between excitation and radiation processes, and this can be satisfied for the forward-angle photon emission along the string which was excited by the relativistic projectile. To provide an acceptable yield of radiation, the individual amplitude a must not be very small even though coherent enhancement takes place.

The impact parameter of atomic collisions in channeling conditions is normally restricted by the inequality of $b \geq u$, where $u \approx 5 \times 10^{-10}$ cm corresponds to the mean amplitude of thermal vibrations of atoms in the crystal. The probability of nuclear Coulomb excitation is drastically reduced for distant collisions. But there exists an exception: in the case of $E1$ excitation, the cross-section becomes very large at small angles of scattering, i.e., with an increase in b. In Fig. 3, the Coulomb excitation functions for $df/d\Omega$ and f shown as given by the quasi-classical calculations of [8]. The basic parameters used in Coulomb excitation theory and the cross-section expression for $E1$ excitation are

$$\eta_i = \frac{Z_1 Z_2 e^2}{\hbar v}; \quad \xi = \eta_i \frac{\Delta E'}{2E}; \tag{3}$$

$$\sigma = 2.5 \times 10^{-2} \frac{Z_1^2 A_1}{E} B(E1) f_{E1}(\eta_i, \xi), \tag{4}$$

where the projectile is characterized by atomic number Z_1, velocity v, and kinetic energy in the c.m. system E. The recalculated excitation energy of a level is $\Delta E' = \Delta E(1 + A_1/A_2)$, and Z_2 and A_2 define the target nucleus. The cross-section σ is expressed in barn, E in megaelectronvolts, and the reduced probability of nuclear transition $B(E1)$ in e^2 barn. One can see in Fig. 3 that the differential function calculated with $\xi = 0$ diverges at angles $\vartheta \longrightarrow 0$. Divergence also appears for total cross-section values at $\xi \longrightarrow 0$.

An infinite cross-section is unphysical, and the solution must lie in the used approximations implicit in the calculation of Eq. (4) [8]. It is important to note that the quasi-classical condition $\eta \gg 1$ is satisfied well in the case of very heavy ions even at high energies. Essentially relativistic collisions with $\gamma \gg 1$ require some modification of the theory, but it was already shown that, in the typically used Born approximation, such a modification does not reduce the cross-sections from that calculated within the standard theory [8]. Thus, it can be expected that the $E1$ cross-section will remain quite large even if more accurate approximations for relativistic ions are used.

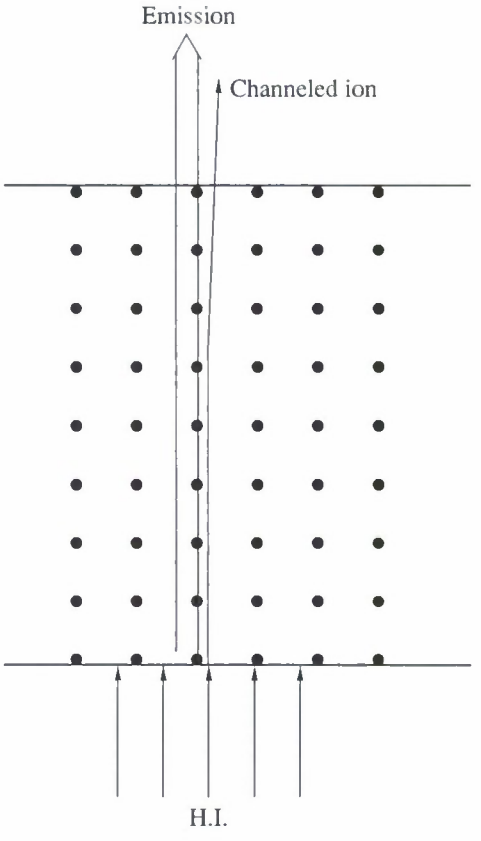

Fig. 2. Schematic picture of the coherent nuclear excitation and radiation in a crystal by a channeled heavy ion.

For the present purposes, it is only important that the cross-sections for small-angle scattering are high and, consequently, that the total σ is high as well. Large cross-sections were experimentally confirmed in Darmstadt [9] for the $E1$ giant dipole resonance when excited in collisions of heavy nuclei at a moderate relativistic factor $\gamma = 1.45$ and with $\xi = 0.05$. In the current problem, the parameters are even more favorable: ξ must really be almost zero, and higher γ values are defined by the other conditions. Thus, the cross-sections should be orders of magnitude higher as compared to the value of 5 barns observed in [9].

Coherence of neighbor nuclei in the crystal string depends on the phase shift between the radiation they emit. The starting point of the excitation is defined by the time mark due to arrival of the channeled ion, and the radiation phase shift is defined by the time of flight of photons from one nucleus to another for forward-angle emission. The following equation can be derived:

$$\Delta\varphi = 5.068 \times 10^2 E_\gamma d \frac{(1 - \beta)}{\beta}, \tag{5}$$

where the phase shift $\Delta\varphi$ is expressed in radians, the interatomic distance d in angstrems, the photon energy E_γ in megaelectronvolts, and $\beta = v/c$. A relatively small

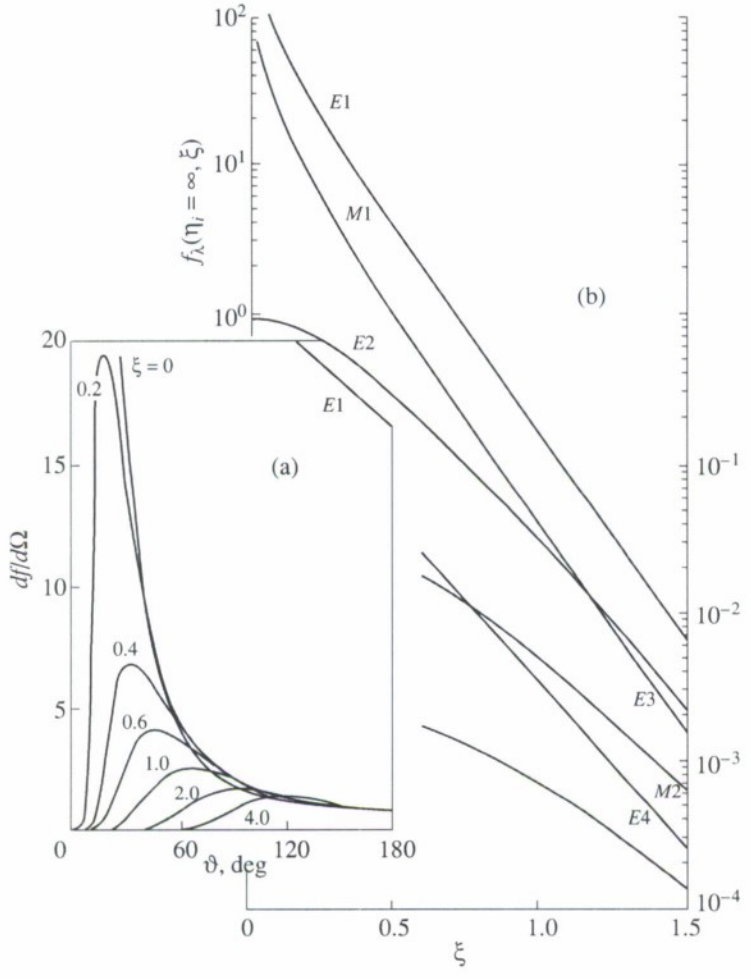

Fig. 3. Differential (a) and integral (b) Coulomb-excitation functions taken from [8]. In (a) the $E1$ excitation angular distribution is normalized to unity at $\vartheta = 180°$.

phase shift of about 5 mrad may be reached for photon energies $E_\gamma \leq 30$ keV at a β value very close to unity. However, the phase shift is periodic at $\Delta\varphi = 0, 2\pi, 4\pi$, etc. In this case, a variety of options appear, provided that the following condition is satisfied:

$$2\pi(n-1) = 5.068 \times 10^2 E_\gamma d \frac{(1-\beta)}{\beta}, \qquad (6)$$

where n is the harmonic order. Different values of β and E_γ can satisfy Eq. (6) with $n \geq 2$.

An essentially relativistic energy of the projectile would, nevertheless, be a necessary condition, as would some limitation of the emitted photon energy. These restrictions arise due to many additional requirements, not only due to the phase condition. The nuclei in the atomic string should be excited sequentially, and a flat trajectory for high-energy channeling is appropriate to achieve this effect. Far-impact excitation with a reasonable probability takes place only at $\xi \longrightarrow 0$, i.e., again at a high energy of the projectile. For correlated Mössbauer emission, the crystal phonon spectrum should not be perturbed, and the known restriction of $E_\gamma \leq 100$ keV naturally arises. In quantum theory, channeling is considered as a Mössbauer-type process, because for distant collisions the crystal-lattice vibrations (phonons) remain without perturbation.

In addition, radiation damage of crystals is strongly reduced when channeled particles have high energies, allowing crystal targets to withstand irradiation for longer times. Ionization energy losses of heavy projectiles decrease in inverse proportion to their energy. At the same time, radiative energy losses are insignificant, unlike the case for a high-energy electron beam. Nevertheless, the possibility of correlated coherent γ emission under Mössbauer conditions in a crystal might be questioned in the case of the discussed scheme of excitation by channeled projectiles. Fortunately, a similar type of emission has already been experimentally observed [10] from ^{57}Fe nuclei in a crystal exposed to synchrotron radiation at the resonance energy.

It is necessary to select a candidate nucleus that is appropriate for the coherent Coulomb excitation scheme. The best one appears to be the stable ^{161}Dy isotope, contained in ^{nat}Dy with an abundance of 19%. Its level scheme is shown in Fig. 4. The first excited (5/2$^-$) and third excited (3/2$^-$) levels are connected with the 5/2$^+$ ground state by $E1$ transitions that are characterized by moderate $B(E1)$ strengths. The transitions are partially converted, but the photon-emission branch remains competitive, being near 30%. The transitions have energies of E_γ = 25.65 keV and 74.57 keV that are potentially useful for the discussed scheme.

An $M1$ multipolarity can be found in many nuclei, but the Coulomb excitation $M1$ cross-section is much lower than that for $E1$ transitions, although it also grows drastically at $\xi \longrightarrow 0$. The ^{161}Dy nuclide may be unique suited to this scheme among stable isotopes, with $E1$ multipolarity of the useful transitions, with the exception of ^{181}Ta. But the latter nuclide has transitions characterized by much lower $B(E1)$ values. Dysprosium can exist in the form of single crystals, either in hexagonal symmetry as a metal crystal or in cubic as Dy_2O_3 oxide.

It is useful to numerically evaluate examples for coherent excitation of the 25.65 keV level in ^{161}Dy via the basic harmonic (n = 1) and the 74.57 level via the second harmonic (n = 2). For better definition, it is assumed here that the Dy crystal is exposed to relativistic ^{208}Pb ions. Some magnitude of phase shift on the order of $\Delta\varphi$ = 5 mrad should be acceptable for each atom, because the total phase shift after consequent excitation of 100 nuclei along the string reaches a value of only 0.5 rad, or ±14°.

Inserting into Eq. (5) the values $\Delta\varphi$ = 0.005, E_γ = 0.02565 MeV, and typical crystallographic d = 4 Å, one deduces $(1 - \beta) \approx 10^{-4}$, i.e., $\gamma \approx 71$ and a kinetic energy of $E_k \approx 66$ GeV/nucleon. In this essentially relativistic case, the collision parameter remains relatively high, $\eta \approx 5.0$, and the Coulomb excitation parameter is close to zero at $\xi = 2.5 \times 10^{-8}$. As discussed above, the cross-section of $E1$ Coulomb excitation should be very high for such values of these parameters. The coherent radiation of 100 nuclei should be significantly enhanced in addition.

The channeling wavelength and photon absorption for a crystal of finite thickness must also be evaluated. The half-absorption length for 25 keV photons in Dy material is about 20 μm, and a crystal of comparable thickness should be applicable. Using Eqs. (1) and (2), one deduces a channeling wavelength of $\lambda \approx 6.5$ μm. This means that three full oscillations will occur in the crystal. Consequently, six trajectory maxima can serve as sources of coherent radiation. The total yield of radiation is thus enhanced due to many factors, although absolute estimates are still difficult. Counter-productive interference corresponds to a radiation phase-shift

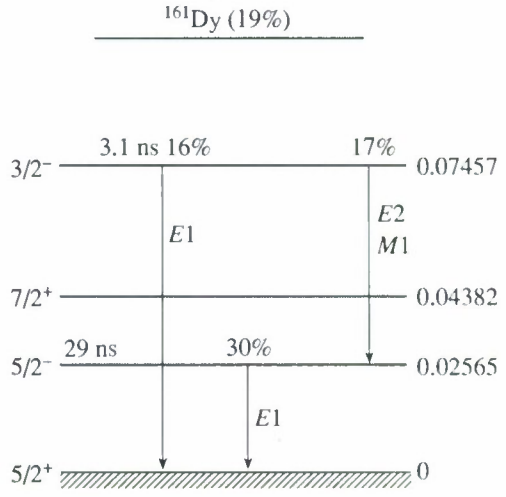

Fig. 4. Partial energy-level scheme of the ^{161}Dy nucleus showing the ground state and three lowest excited levels. Energies are in megaelectronvolts and spin, parity, half-life, multipolarity and γ-emission branches are given.

range of $\pi \le \Delta\varphi \le 2\pi$, but this will appear only at distances of about thousands of atomic layers.

The Mössbauer correlations probably do not survive over such distances anyway. Even in the case of perfect correlations, one point should be discussed. Although radiation absorption does not significantly restrict the described scheme, there arises the question of whether the radiation is transmitted through the crystal layer, or whether the nuclear mode excitation is bound to the string of atoms and is emitted from matter only at the surface of the crystal and the photon is emitted to the outside. In the latter variant, the absorption does not suppress the radiation at all, and only the positive and negative phases along the string are important. This may restrict the target thickness even more than the absorption conditions.

The $(1 - \beta)$ value for the excitation of the third level in ^{161}Dy at 74.57 keV with the second harmonic (n = 2) has been estimated using Eq. (6). A resonance kinetic energy of E_k = 2.42 GeV/nucleon and the corresponding relativistic parameter γ = 3.58 were deduced. The channeling wavelength in this case decreases to 1.4 μm, or about 3.5×10^3 atomic layers. The condition of consequent multiple excitation of nuclei in the string still holds, and many trajectory maxima take place on the projectile's path through the crystal. Negative phases do not arise in this case, because the phase shift becomes a multiple of 2π. The crystal can be as thick as about 100 μm because of the significantly lower absorption coefficient for 75 keV photons as compared to 25 keV.

Mössbauer conditions are relatively good for 75 keV photons in a heavy Dy crystal if kept at liquid nitrogen temperature. The disadvantage of the scheme with exci-

tation of the third level in ^{161}Dy at second harmonics arises due to the increased radiation damage of the crystal at lower projectile energy: 2.42 GeV/nucleon instead of 66 GeV/nucleon as needed for the first level. The energy transferred to the lattice and to electron excitations is also increased, which may disturb the Mössbauer emission of radiation. However, this problem can be solved only after experimental studies. The yield of radiation would also be unknown until measured experimentally.

A kinetic energy of heavy ions near 1 GeV/nucleon is available at GSI, Darmstadt; such an experiment can be arranged within reasonable expenses. The 74.57 keV transition should be resonantly excited at the fourth harmonic by a projectile with a kinetic energy of about 1.110 MeV/nucleon. It would be interesting to test experimentally whether or not Mössbauer conditions in a crystal survive at such energies. The concrete details of properties for Dy crystals are significant, but in the present work only a general scheme is discussed for a new type of experiments on coherent Coulomb excitation of nuclei in a crystal lattice by relativistic heavy projectiles. A technical proposal can be developed later.

CONCLUSIONS

New possible applications of nuclear Coulomb excitation are discussed. In the first scheme, a radioactive ion-beam facility should be used for acceleration of ions containing isomeric ^{178m2}Hf to study triggering levels in this nuclide that may cause a release of the isomer energy. The second scheme may be potentially promising to achieve lasing of nuclear radiation. We have considered coherent excitation and radiation of nuclei ensconced in a crystal lattice and exposed to a relativistic heavy-ion beam. The equations for resonance harmonics are formulated, and other peculiarities important for realization of such a process are discussed. Among them are the special cross-section behavior of the $E1$ Coulomb excitation, properties of radiation absorption, channeling trajectory parameters, and Mössbauer conditions for coherent emission. A realistic test experiment is formulated, linked to the existing possibilities at GSI, Darmstadt, for production of relativistic heavy-ion beams.

REFERENCES

1. Special Issue on Gamma-Ray Lasers, Hyperfine Interact. **107** (1997).
2. Y. T. Oganessian and S. A. Karamian, Laser Phys. **5**, 336 (1995).
3. J. J. Carroll, Laser Phys. Lett. **1**, 275 (2004).
4. D. Habs, Presentation at *LPHYS'02, Bratislava, 2002*.
5. Y. L. Pivovarov, Nucl. Instrum. Methods Phys. Res. B **145**, 96 (1998).
6. A. B. Hayes, D. Cline, C. Y. Wu, et al., Phys. Rev. Lett. **96**, 042505 (2006).
7. J. J. Carroll, S. A. Karamian, L. A. Rivlin, and A. A. Zadernovsky, Hyperfine Interact. **135**, 3 (2001).
8. K. Alder, A. Bohr, T. Huus, et al., Rev. Mod. Phys. **28**, 432 (1956).
9. A. Heinz, K.-H. Schmidt, A. R. Junghans, et al., Nucl. Phys. A **713**, 3 (2003).
10. U. Van Bürck, R. L. Mössbauer, E. Gerdau, et al., Phys. Rev. Lett. **59**, 355 (1987).

High-spin, multiparticle isomers in ^{121,123}Sb

G. A. Jones,[1,*] S. J. Williams,[1,2] P. M. Walker,[1] Zs. Podolyák,[1] S. Zhu,[3] M. P. Carpenter,[3] J. J. Carroll,[4] R. S. Chakrawarthy,[2] P. Chowdhury,[5] I. J. Cullen,[1] G. D. Dracoulis,[6] A. B. Garnsworthy,[1] G. Hackman,[2] R. V. F. Janssens,[3] T. L. Khoo,[3] F. G. Kondev,[7] G. J. Lane,[6] Z. Liu,[1] D. Seweryniak,[3] and N. J. Thompson[1]

[1]*Department of Physics, University of Surrey, Guildford GU2 7XH, United Kingdom*

[2]*TRIUMF, 4004 Westbrook Mall, Vancouver, British Columbia, V6T 2A3, Canada*

[3]*Physics Division, Argonne National Laboratory, Argonne, Illinois 60439, USA*

[4]*Department of Physics and Astronomy, Youngstown State University, Youngstown, Ohio 44555, USA*

[5]*University of Massachusetts Lowell, Lowell, Massachusetts 01854, USA*

[6]*Department of Nuclear Physics, RSPhysSE, Australian National University, Canberra 0200, Australia*

[7]*Nuclear Engineering Division, Argonne National Laboratory, Argonne, Illinois 60439, USA*

(Received 31 May 2007; published 25 March 2008)

Isomers in near-spherical $Z = 51$, antimony isotopes are reported here for the first time using fusion-fission reactions between ^{27}Al and a pulsed ^{178}Hf beam of energy, 1150 MeV. γ rays were observed from the decay of isomeric states with half-lives, $T_{1/2} = 200(30)$ and $52(3)\,\mu$s, and angular momenta $I = (\frac{25}{2})$ and $I^{\pi} = \frac{23}{2}^{+}$, in ^{121,123}Sb, respectively. These states are proposed to correspond to $\nu(h_{\frac{11}{2}})^2$ configurations, coupled to an odd $d_{\frac{5}{2}}$ or $g_{\frac{7}{2}}$ proton. Nanosecond isomers were also identified at $I^{\pi} = \frac{19}{2}^{-}$ [$T_{1/2} = 8.5(5)$ ns] in ^{121}Sb and $I^{\pi} = (\frac{15}{2}^{-})$ [$T_{1/2} = 37(4)$ ns] in ^{123}Sb. Information on spins and parities of states in these nuclei was obtained using a combination of angular correlation and intensity-balance measurements. The configurations of states in these nuclei are discussed using a combination of spin/energy systematics and shell-model calculations for neighboring tin isotones and antimony isotopes.

DOI: 10.1103/PhysRevC.77.034311 PACS number(s): 23.20.Lv, 23.20.En, 25.70.Jj, 27.60.+j

I. INTRODUCTION

Nuclei near closed shells represent an excellent opportunity to probe important facets of nuclear structure. Nuclides close to the $Z = 50$ shell closure are particularly good for such investigations, due to the experimental accessibility of many $Z = 50$, tin nuclei across the $N = 50$–82 shell. Of recent interest in this region is the energy evolution of spherical proton orbitals with increasing neutron excess, particularly $\pi d_{\frac{5}{2}}$, $\pi g_{\frac{7}{2}}$, and $\pi h_{\frac{11}{2}}$ [1,2]. These effects are best explored in antimony nuclei, with one proton outside a $Z = 50$ core. One of the first indications of this orbital evolution came from the observation of a change in the ground-state quantum number for antimony nuclei, from $I^{\pi} = \frac{5}{2}^{+}$ in ^{121}Sb to $\frac{7}{2}^{+}$ in ^{123}Sb [3]. The energy difference between the first excited $\frac{5}{2}^{+}$ and $\frac{7}{2}^{+}$ states changes by nearly 1.5 MeV in odd-A antimony nuclei from $117 \leqslant A \leqslant 133$, interpreted as a decrease in energy of the $\pi g_{\frac{7}{2}}$ orbital relative to $\pi d_{\frac{5}{2}}$ state [1]. This change in energy difference has been interpreted as a signature for the presence of a strong tensor force [4] or a decreasing spin-orbit interaction for the $d_{\frac{5}{2}}$, $g_{\frac{7}{2}}$, and $h_{\frac{11}{2}}$ levels with increasing neutron excess [1,2]. These are both consistent with an empirical reduction in relative energy between the $g_{\frac{7}{2}}$ and $h_{\frac{11}{2}}$ proton orbitals, which changes by $\sim$2 MeV over odd-A antimony nuclei with $117 \leqslant A \leqslant 133$ [1,2].

Nuclei near closed-shell boundaries are also a good place to simultaneously study both collective and multiparticle excitations. Strongly coupled rotational structures, built on $\pi h_{\frac{11}{2}}$ intruder and $\pi(g_{\frac{9}{2}})^{-1}$ excitations, are observed in odd-A antimony nuclei with $113 \leqslant A \leqslant 121$ [5–8]. As the neutron number increases and the closed $N = 82$ shell is approached, however, the excitation energy of these deformed states increases, and the rotational bands are no longer yrast; the $\pi \frac{9}{2}[404]$ state becomes nonyrast in ^{123}Sb ($N = 72$), increasing in energy to $E_x = 1337$ keV [9,10]. This simplifies the picture dramatically, because all states can be interpreted as spherical single or multiparticle excitations. In particular, many states can be described in terms of those observed in tin nuclei, coupled to an extra proton [11,12]. Nevertheless, the many valance particles make it difficult to perform detailed shell-model calculations, and comprehensive experimental data provide a benchmark against which to test the development of appropriate theoretical descriptions.

This article describes the identification of states in ^{121,123}Sb from the decay of previously unreported isomeric states.

II. EXPERIMENTAL PROCEDURE

The experiment was performed at Argonne National Laboratory using the Argonne Tandem Linear Accelerator System (ATLAS), which delivered a ^{178}Hf beam onto a ^{208}Pb target at a laboratory energy of 1150 MeV, to study long-lived isomeric states in hafnium-like nuclei (presented in Ref. [13]). This article reports results obtained from incidental fusion-fission reactions between the ^{178}Hf projectiles and a ^{27}Al frame supporting the ^{208}Pb target. Fission of the ^{205}At compound nucleus populated nuclei with large yields, from $_{34}$Se to $_{54}$Xe.

*gareth.jones2@barcap.com

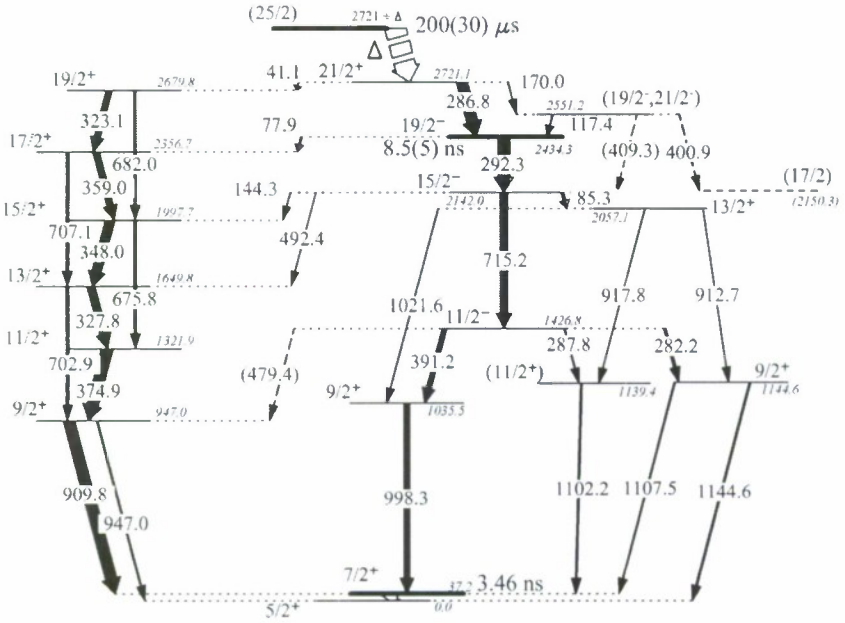

FIG. 1. Level scheme for transitions in ^{121}Sb, observed in the long-pulsing experiment from the decay of a $T_{1/2} = 200(30)\,\mu$s isomer. Widths of arrows indicate the intensity of particular γ-ray decays.

The resulting γ-ray decays from all reaction products were measured using the Gammasphere array [14], comprising 101 Compton-suppressed germanium detectors in this experiment. The beam was bunched into short pulses of width ~0.5 ns, separated by periods of 82.5 ns. This pulsing was utilized to deliver *short* and *long* pulsed-beam conditions, enabling the study of metastable states in the $10^{-9} \rightarrow 10^{-4}$ s range. In the short-pulsing experiment, 1 of 10 beam pulses was incident on the target, resulting in a 825-ns inspection period within which delayed γ-ray decays could be studied. Events where two or more coincident γ rays were detected within a 2-μs range were written to tape for subsequent off-line analysis. In the long-pulsing measurement, a 25-μs beam-on period preceded a 75-μs beam-off period during which the data acquisition system was triggered by single γ-ray events and time stamped using an external 10-MHz oscillator clock. Great care was taken to calibrate the HPGe detectors for γ-ray energy measurements, using a number of γ-ray sources.

III. DATA ANALYSIS

The nature of the fusion-fission reaction process leads to the detection of a large number of γ rays emitted from excited states in a broad range of nuclei, resulting in a highly complex data set. Due to this level of complexity, it was necessary to utilize multidimensional γ-ray coincidence techniques to correlate decays associated with particular nuclides. A number of coincidence cubes corresponding to different γ-ray time and energy coincidence conditions were created for both the short-pulsing and long-pulsing experiments. These were analyzed with software packages described in Refs. [15–17].

A combination of the high statistics obtained in this experiment and the high granularity of the Gammasphere detector array allow for a γ-γ angular correlation analysis to be performed on pairs of coincident transitions from the decay of isomeric states. Each of the detectors in the Gammasphere array is associated with angles (θ, ϕ) with respect to the orientation of the beam axis. Pairs of γ-ray coincidence events $(E_{\gamma_1}, E_{\gamma_2})$ were placed into symmetric matrices according to the angle between the detectors, δ, expressed by $\cos\delta = \cos(\phi_2 - \phi_1) \times \sin\theta_1 \sin\theta_2 + \cos\theta_1 \cos\theta_2$ [18]. The detector pairs were grouped into 11 bins with average angular differences of $\delta = 22°, 40°, 54°, 66°, 76°, 90°, 104°, 114°, 126°, 140°$, and 158°, each with $350 < N < 700$ combinations. The groups were chosen to evenly spread the number of detector combinations over a range of $\cos^2(\delta)$ values. The intensity of a given transition pair was measured for each of the groupings using the symmetric matrices, and normalized with the relative efficiency of the detector pairs. Angular-correlation coefficients (A_{kk}) were obtained from a fit to the intensities of the γ-$\gamma(\delta)$ coincidence events to the function:

$$W(\delta) = 1 + A_{22} P_2(\cos\delta) + A_{44} P_4(\cos\delta). \qquad (1)$$

where P_2 and P_4 are Legendre polynomials. Values of A_{kk} were compared with those calculated, using the procedure described in Ref. [19].

IV. RESULTS

A. ^{121}Sb

Transitions from the decay of a previously unobserved microsecond isomer were identified in the long-pulsing experiment. γ rays from the decay of states in ^{121}Sb were identified in projections of double coincidence gates placed on γ rays from Ref. [11]. The updated level scheme from the analysis of this experiment is illustrated in Fig. 1; three states at energy, $E_x = 2057.1$, 2150.3, and 2551.2 keV are reported for the first time. Table I provides a summary of all ^{121}Sb transitions observed in the measurement; asterisks (*) indicate transitions observed for the first time. The relative γ-ray intensities were established from spectra under different double-gating conditions.

TABLE I. Transitions observed in ^{121}Sb from the $T_{1/2} = 200(30)$ μs isomer in the long-pulsing experiment. Relative intensity measurements are provided for γ-ray decays in the rotational [$I_\gamma(R)$] and single-particle structures [$I_\gamma(S)$] on the left and right side of Fig. 1, respectively. The normalized ratio of the rotational to single-particle structure intensities is 0.7(1). Transitions observed for the first time are marked with asterisks (*).

E_γ (keV)	E_i (keV)	E_f (keV)	J_i^π	J_f^π	$I_\gamma(R)$	$I_\gamma(S)$
41.1(5)*	2721.1	2679.8	$21/2^+$	$19/2^+$	5.0(9)	–
77.9(3)*	2434.3	2356.7	$19/2^-$	$17/2^+$	9.4(10)	–
85.3(3)*	2142.0	2057.1	$15/2^-$	$13/2^+$	–	18(2)
117.4(3)*	2551.2	2434.3	$(21/2^-,19/2^-)$	$19/2^-$	–	2.5(3)
144.3(5)*	2142.0	1997.7	$15/2^-$	$15/2^+$	<1	<1
170.3(3)*	2721.1	2551.2	$21/2^+$	$(21/2^-,19/2^-)$	–	4.0(5)
282.2(3)	1426.8	1144.6	$11/2^-$	$9/2^+$	–	23(3)
286.8(3)	2721.1	2434.3	$21/2^+$	$19/2^-$	13.3(14)	100
287.8(4)	1426.8	1139.4	$11/2^-$	$(11/2^+)$	–	6.9(9)
292.3(3)	2434.3	2142.0	$19/2^-$	$15/2^-$	3.9(5)	98(9)
323.1(3)	2679.8	2356.7	$19/2^+$	$17/2^+$	53(5)	–
327.8(3)	1649.8	1321.9	$13/2^+$	$11/2^+$	70(7)	–
348.0(3)	1997.7	1649.8	$15/2^+$	$13/2^+$	84(9)	–
359.0(3)	2356.7	1997.7	$17/2^+$	$15/2^+$	58(6)	–
375.0(3)	1321.9	947.0	$11/2^+$	$9/2^+$	98(10)	–
391.2(3)	1426.8	1035.5	$11/2^-$	$9/2^+$	–	43(5)
400.9(4)*	(2551.2)	(2150.3)	$(21/2^-,19/2^-)$	(17/2)	–	5.8(7)
(409.3(6))*	2551.2	2142.0	$(21/2^-,19/2^-)$	$15/2^-$	–	1.7(4)
(479.4(4))*	1426.8	947.0	$11/2^-$	$9/2^+$	–	<1
492.4(4)*	2142.0	1649.8	$15/2^-$	$13/2^+$	3.0(4)	1.4(4)
675.8(3)	1997.7	1321.9	$15/2^+$	$11/2^+$	23(3)	–
682.0(3)	2679.8	1997.7	$19/2^+$	$15/2^+$	20(2)	–
702.9(3)	1649.8	947.0	$13/2^+$	$9/2^+$	20(2)	–
707.1(3)	2356.7	1649.8	$17/2^+$	$13/2^+$	21(2)	–
715.2(3)	2142.0	1426.8	$15/2^-$	$11/2^-$	–	72(7)
909.8(3)	947.0	37.2	$9/2^+$	$7/2^+$	100	–
912.7(4)*	2057.1	1144.6	$13/2^+$	$9/2^+$	–	3.7(5)
917.8(4)*	2057.1	1139.4	$13/2^+$	$(11/2^+)$	–	9.3(10)
947.0(4)	947.0	0.0	$9/2^+$	$5/2^+$	11.7(14)	–
998.3(4)	1035.5	37.2	$9/2^+$	$7/2^+$	–	51(5)
1021.6(5)*	2057.1	1035.5	$13/2^+$	$9/2^+$	–	5.2(7)
1102.2(5)	1139.4	37.2	$(11/2^+)$	$7/2^+$	–	15.9(17)
1107.5(3)	1144.6	37.2	$9/2^+$	$7/2^+$	–	10.8(12)
1144.6(3)	1144.6	0.0	$9/2^+$	$5/2^+$	–	15.3(17)

Two distinctly different structures are present in the level scheme of Fig. 1, linked by low-intensity transitions. The structure on the left side is the rotational band built on the $\pi\frac{9}{2}[404]$ orbital [8], also observed in lighter odd-A antimony isotopes with $113 \leqslant A \leqslant 119$ [5–8]. The spins and parities of these states are assigned accordingly. The order of states on the right side of Fig. 1 is indicative of noncollective, single, and multiparticle excitations.

Figure 2(a) provides the time projection from several γ-γ gates on transitions following the decay of the microsecond isomer. The half-life was measured to be $T_{1/2} = 200(30)$ μs. Spectra illustrating γ rays observed in the rotational and single-particle decay structures are provided in Figs. 2(b)–2(e).

The observation of the 41-keV transition [illustrated in Fig. 2(b)], which approaches the low-energy detection limit of Gammasphere, is a valuable link between the rotational band and the 2721.1-keV state. This 41-keV transition has a measured γ-ray intensity 13(8) times smaller than the 323-keV transition in the projection of a sum of double gates between the 359-keV and 348-, 328-, 375-, and 910-keV transitions. The difference between these γ-ray intensities indicates a conversion coefficient of $\alpha_{\text{tot}} = 12(8)$ for the 41-keV transition, which is consistent with $M1$ multipolarity. This evidence suggests a spin and parity of $I^\pi = \frac{21}{2}^+$ for the $E_x = 2721.1$ keV state. Intensity-balance measurements of this kind were used to infer other transition multipolarities, as summarized in Table II.

γ-γ angular correlation measurements were performed for pairs of transitions to gain an independent spin-parity assessment of the $E_x = 2721.1$ keV state. Figure 3 presents angular correlation measurements for a selection of transition pairs in ^{121}Sb, also summarized in Table III. Data are fitted using Eq. (1). These measurements are based on the $E2$, 1145-keV transition [20] as a primary gate; they are also consistent with the $M1+E2$, 998-keV γ-ray mixing ratio published in Ref. [20]. The spins and parities of the states

TABLE II. Experimental internal conversion coefficient measurements, α_{tot}, compared with calculated values for transitions, γ_1, of energy $E_{\gamma 1}$.

Nucleus	$E_{\gamma 1}$ (keV)	Gate	$E_{\gamma 2}$, $E_{\gamma 3}$ ... (keV)	α_{tot} (exp.)	α_{tot} (the.) [22]					Assignment ($E_{\gamma 1}$)
					$E1$	$M1$	$E2$	$M2$	$E3$	
^{121}Sb	41	{359}{348, 328, 375, 910}	323($M1$)	12(8)	2	8	43	198	2140	$M1(+E2)$
		{910, 375, 328, 348}	323($M1$),682($E2$)	15(3)						$M1+E2$
		{910, 375, 328, 348}	323($M1$),682($E2$)	15(3)						
	78	{359}{287}	348($M1$)	0.2(4)	0.4	1.3	4.2	17.1	62.5	$E1$
	85	{292}{1022}	998($M1$)	0.1(3)	0.3	1.0	3.0	11.8	40.3	$E1$
	117	{170}{998, 715, 391}	292($E2$)	0.47(17)	0.12	0.41	0.95	3.60	8.48	$M1$
	170	{117}{998, 715, 391}	292($E2$)	0.08(12)	0.04	0.14	0.26	0.94	1.54	$E1$ or $M1$
	287	{998}{391}	292($E2$)	0.02(5)	0.01	0.04	0.04	0.16	0.17	$E1$, $M1$, or $E2$
^{123}Sb	128	{1089}{956}	442($E2$)	0.85(15)	0.10	0.32	0.71	2.59	5.57	$E2$
		{1089}{442}	956($E2$)	0.75(14)						$E2$
		{956}{442}	1089($E2$)	0.69(13)						$E2$

on the right side of Fig. 1 are assigned on the basis of γ-γ angular correlations and intensity-balance measurements. The angular correlation measurements provide additional evidence for the $I^\pi = \frac{21}{2}^+$ spin parity of the $E_x = 2721.1$ keV state.

It is unlikely that the $E_x = 2721.1$ keV level is the origin of the long, $T_{1/2} = 200$ μs half-life. The Weisskopf single-particle transition rates for the 287- and 41-keV γ-ray decays, from an isomeric state with $T_{1/2} = 200$ μs, are $B(E1) = 3.5 \times 10^{-11}$ and $B(M1) = 6.8 \times 10^{-8}$ W.u., respectively. These are inconsistent with transition rates observed systematically [21] by at least four orders of magnitude. It follows that to account for the isomeric half-life another level must exist that decays to the $E_x = 2721.1$ keV state via an unobserved, low-energy, highly converted transition, expressed by Δ in Fig. 1. By considering typical Weisskopf transition rates [21], the efficiency of Gammasphere, and the magnitude of the internal conversion process, the energy and multipolarity of Δ can be restricted to $E_\Delta(E2) < 60$ keV or $E_\Delta(M2) < 80$ keV. Based on these limitations, the $E_x = 2721.1 + \Delta$ keV state is tentatively assigned spin $I = (\frac{25}{2})$.

A number of previously unobserved γ rays, shown in Fig. 2(c), reveal the existence of a state at $E_x = 2057.1$ keV. The 85-keV transition is in coincidence with 1022-, 918-, and 913-keV γ rays, which decay to the $E_x = 1035.5$, 1139.4, and 1144.6 keV states, respectively. Intensity-balance measurements, summarized in Table II, indicate $E1$ multipolarity for the 85-keV γ ray; the $E_x = 2057$ keV level is assigned a spin parity of $I^\pi = \frac{13}{2}^+$.

A state with energy $E_x = 2551.2$ keV is inferred from the observation of 117- and 170-keV γ rays [see spectra in Figs. 2(d) and 2(e)]. The tentative 409-keV transition to the $E_x = 2142.0$ keV level, illustrated in Fig. 2(e), suggests the ordering of the 117- and 170-keV γ rays. Using intensity-balance arguments, summarized in Table II, the 117- and 170-keV γ rays are provided with $M1$ and $M1$ or $E1$ multipolarity, respectively. This information indicates a spin parity of $I^\pi = (\frac{21}{2}^-)$ or $(\frac{19}{2}^-)$ for the $E_x = 2551.2$ keV state.

A 401-keV γ ray has been observed in coincidence with the 170-keV transition and in anticoincidence with the 117-, 292-, and 287-keV lines. The spectrum in Fig. 2(e) shows coincidences among the 401-keV and 170-, 391-, 715-, and

TABLE III. Angular correlations for pairs of transitions γ_1 and γ_2 with mixing ratios δ_1 and δ_2, respectively. A_{22} and A_{44} coefficients are calculated using the prescription of Ref. [19]. These calculated values are compared with experimental ones obtained from data fitted to Eq. (1).

Nucleus	Initial state	γ_2 (keV)	$J_i^\pi \rightarrow J_f^\pi$	δ_2	γ_1 (keV)	Assignment (γ_1)	A_{22}	A_{44}	δ_1
^{121}Sb	$11/2^-$	1145	$9/2^+ \rightarrow 5/2^+$	0	282	$11/2^- \rightarrow 9/2^+$	−0.08(5)	−0.01(7)	$0.01^{+0.19}_{-0.14}$
	$15/2^-$	391	$11/2^- \rightarrow 9/2^+$	0	715	$15/2^- \rightarrow 11/2^-$	−0.12(3)	0.02(4)	$-0.17^{+0.19}_{-0.08}$
	$19/2^-$	715	$15/2^- \rightarrow 11/2^-$	0	292	$19/2^- \rightarrow 15/2^-$	0.097(19)	0.05(3)	$0.02^{+0.09}_{-0.07}$
	$21/2^+$	1145	$9/2^+ \rightarrow 5/2^+$	0	287	$21/2^+ \rightarrow 19/2^-$	−0.11(5)	−0.04(7)	0.03(14)
		715	$15/2^- \rightarrow 11/2^-$	0			−0.048(19)	0.01(3)	−0.04(6)
		292	$19/2^- \rightarrow 15/2^-$	0			−0.099(13)	0.03(2)	0.05(4)
^{123}Sb	$15/2^+$	1089	$11/2^+ \rightarrow 7/2^+$	0	956	$15/2^+ \rightarrow 11/2^+$	0.15(4)	0.00(6)	$-0.10^{+0.17}_{-0.25}$
	$19/2^+$	1089	$11/2^+ \rightarrow 7/2^+$	0	442	$19/2^+ \rightarrow 15/2^+$	0.13(4)	−0.07(6)	$-0.08^{+0.14}_{-0.18}$
	$23/2^+$	1089	$11/2^+ \rightarrow 7/2^+$	0	128	$23/2^+ \rightarrow 19/2^+$	0.14(5)	−0.00(6)	$-0.06^{+0.18}_{-0.21}$

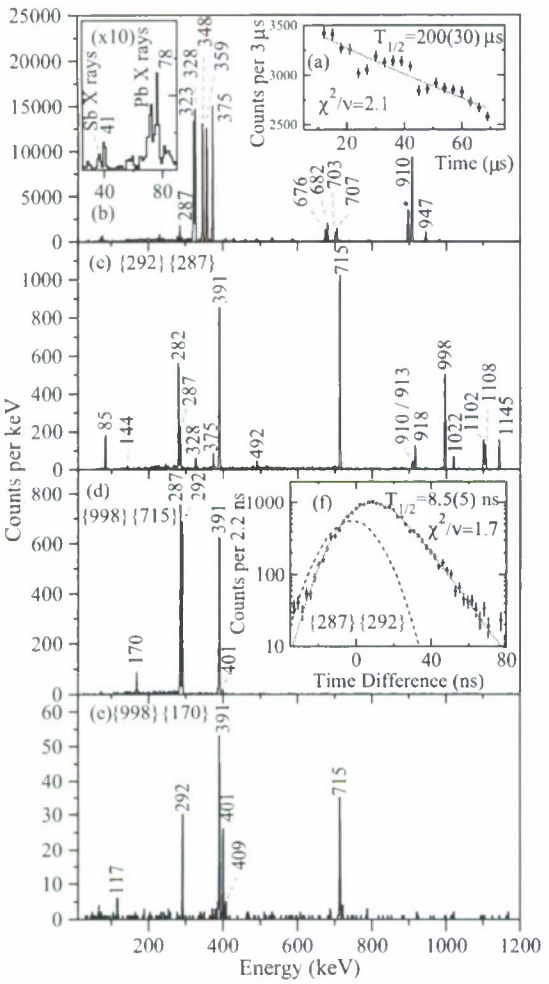

FIG. 2. (Color online) Panel (a) gives the time evolution of the $T_{1/2} = 200(30)$ μs isomer in ^{121}Sb, measured using summed double coincidence gates on all transitions. Panels (b)–(e) provide double-gated spectra; gates are given in parenthesis ($\{x\}\{y\}$) for each, except panel (b), which is a sum of double gates on all transitions in the rotational sequence of Fig. 1. Panel (f) illustrates the γ-ray time difference between the 287- and 292-keV transitions; the half-life is measured to be $T_{1/2} = 8.5(5)$ ns using a folded Gaussian plus exponential fit. The dashed line is the prompt Gaussian used in the fit [FWHM = 30(3) ns]. Contaminants from ^{204}Pb are indicated by asterisks (*). See text for further details.

998-keV transitions. The coincidence between the 401- and 715-keV γ rays implies that the 401-keV transition should be placed between the $E_x = 2551.2$ and 2142.0 keV levels. However, the energy of the γ ray does not match the difference between the states; a discrepancy of 8.3 keV remains. This provides evidence for another state at an energy of either $E_x = 2542.9$ or 2150.3 keV. Because it is less likely that an 8.3-keV transition of any multipolarity would compete with the 117- or 409-keV transitions (from the $E_x = 2542.9$ keV state), a tentative state of energy, $E_x = 2150.3$ keV is, therefore, assigned to ^{121}Sb.

In addition to the microsecond isomer, the $E_x = 2434.3$ keV, $I^\pi = \frac{19}{2}^-$ state was observed to be isomeric. Figure 2(f) provides the time difference between 287- and 292-keV γ rays. A folded Gaussian plus exponential fit of these data indicates a half-life of $T_{1/2} = 8.5(5)$ ns. The transition strengths for the 78-keV ($E1$) and 292-keV ($E2$) transitions are $B(E1) = (4.1 \pm 0.9) \times 10^{-6}$ and $B(E2) = 0.78(10)$ W.u., respectively. These are comparable with the transition strengths of the $E1$ and $E2\gamma$ rays decaying from the $I^\pi = \frac{19}{2}^-$, $E_x = 2553.6$ keV state in ^{119}Sb ($B(E1) = 7.3 \times 10^{-7}$ and $B(E2) = 0.026$ W.u., respectively [23]).

B. ^{123}Sb

The decay of two isomers has been observed for the first time. γ rays from the decay of states in ^{123}Sb were identified in projections of double coincidence gates placed on γ rays first reported in Ref. [11]. Figure 4 illustrates the partial level scheme of ^{123}Sb from the present experiments; Table IV provides a summary of all transitions observed.

1. $I = (27/2)\hbar$ isomer

The double-gated coincidence spectrum in the top panel of Fig. 5(a) shows the 1089-, 956-, 442-, and 128-keV transitions observed from the decay of a microsecond isomer. Figure 5(b) provides a time spectrum of transitions from the isomeric decay in the long-pulsing experiment; the half-life is measured to be $T_{1/2} = 52(3)$ μs.

Intensity-balance measurements (summarized in Table II) were performed for the 128-keV transition, providing strong evidence for $E2$ multipolarity. γ-γ angular correlation measurements between the 1089-keV and 956-, 442-, and 128-keV transitions are presented in Fig. 6 and summarized in Table III. The correlation between the 1089- and 128-keV transitions indicated either pure quadrupole (probably $E2$) or mixed dipole/quadrupole (probably $M1/E2$) character for the 1089-keV γ ray, which is consistent with the evaluation in Ref. [24]. Angular correlations summarized in Table III indicate pure quadrupole or mixed dipole/quadrupole character for the 442- and 956-keV transitions. In addition to angular correlation measurements, the nonobservation of transitions linking the $E_x = 2044.4$, 2486.3, and 2614.1 keV states to the (negative-parity) states on the left side of Fig. 4, indicated differences in angular momenta of $\Delta I \geqslant 2$. On the basis of these arguments, the $E_x = 1088.6$, 2044.4, 2486.3, and 2614.1 keV states are assigned spins and parities of $I^\pi = \frac{11}{2}^+$, $\frac{15}{2}^+$, $\frac{19}{2}^+$, and $\frac{23}{2}^+$, respectively.

The $T_{1/2} = 52(3)$ μs half-life appears to derive from the $E_x = 2614.1$ keV level, decaying via the 128-keV transition. This corresponds to a single-particle transition rate of $B(E2) = 5.3(1) \times 10^{-3}$ W.u. This is approximately 5 times smaller than that of the $I^\pi = \frac{21}{2}^-$ state in ^{121}Sb and 10 times smaller than the $I^\pi = \frac{21}{2}^-$ state in ^{119}Sb [12]. In regard to the discrepancy in transition strength, it is noted that the $T_{1/2} = 52$ μs half-life may derive from a state higher in energy than the $E_x = 2614.0$ keV level, decaying via an unobserved, low-energy, highly converted transition.

TABLE IV. A summary of γ-ray energies, E_γ in ^{123}Sb between states with spin and parity, J_i^π and J_f^π, and energy, E_i and E_f. γ-ray intensities for transitions on the right and left side of Fig. 4 are given by I_γ(R) and I_γ(L) from the long-pulsing and short-pulsing experiments, respectively.

E_γ (keV)	E_i (keV)	E_f (keV)	J_i^π	J_f^π	I_γ(R)	I_γ(L)
127.8(3)	2614.1	2486.3	$23/2^+$	$19/2^+$	60(5)	–
160.3(5)	160.1	0.0	$5/2^+$	$7/2^+$	–	25(3)
201.0(4)	2239.1	2038.2	$(19/2^-)$	$(15/2^-)$	–	104(18)
381.7(4)	2038.2	1656.5	$(15/2^-)$	$(11/2^-)$	–	114(15)
396.0(5)	1656.5	1260.7	$(11/2^-)$	$9/2^+$	–	29(3)
441.9(3)	2486.3	2044.3	$19/2^+$	$15/2^+$	109(11)	–
567.7(4)	1656.5	1088.6	$(11/2^-)$	$11/2^+$	–	14(3)
626.1(4)	1656.5	1030.3	$(11/2^-)$	$9/2^+$	–	94(7)
955.8(3)	2044.3	1088.6	$15/2^+$	$11/2^+$	112(9)	–
1030.3(4)	1030.3	0.0	$9/2^+$	$7/2^+$	–	100(8)
1088.6(3)	1088.6	0.0	$11/2^+$	$7/2^+$	100	–
1100.9(5)	1260.7	160.1	$9/2^+$	$5/2^+$	–	18(4)
1260.9(7)	1260.7	0.0	$9/2^+$	$7/2^+$	–	7(2)

2. $I^\pi = (19/2^-)$ and $(15/2^-)$ isomers

Transitions from the decay of the $E_x = 2239.1$ keV isomeric state (initially reported in Ref. [11] with $T_{1/2} = 110(10)$ ns) were observed in the short-pulsing experiment. The double-gated coincidence spectra in Figs. 5(c) and 5(d) show γ-ray decays from this isomer, which are summarized in Table IV. Figure 5(e) illustrates a time spectrum, double gated on delayed transitions from the isomeric $E_x = 2239.1$ keV level; relative to the accelerator RF signal, the half-life of the decay is measured as $T_{1/2} = 190(30)$ ns. With regard to the large discrepancy between the value observed in this work and that presented in Ref. [11], timing calibration was extensively checked with the accurate measurement of other, previously observed, isomeric states.

The $E_x = 2038.1$ keV state was also observed to be isomeric; Fig. 5(f) provides a time difference spectrum between the 201-keV transition, and those from the decay of states below the isomer. The half-life of the state was measured to be $T_{1/2} = 37(4)$ ns using a folded Gaussian plus exponential fit.

Due to insufficient statistics, it was not possible to assign spins and parities to the states populated from the decay of the $T_{1/2} = 190$ ns isomer, using angular correlations. Tentative spins and parities are, therefore, adopted from the systematic arguments proposed in Ref. [11].

Transition strengths for the 201- and 382-keV γ rays are $B(E2) = 0.22(2)$ and 0.048(2) W.u., respectively, which are consistent with those of other $E2$ transitions observed locally [12,25].

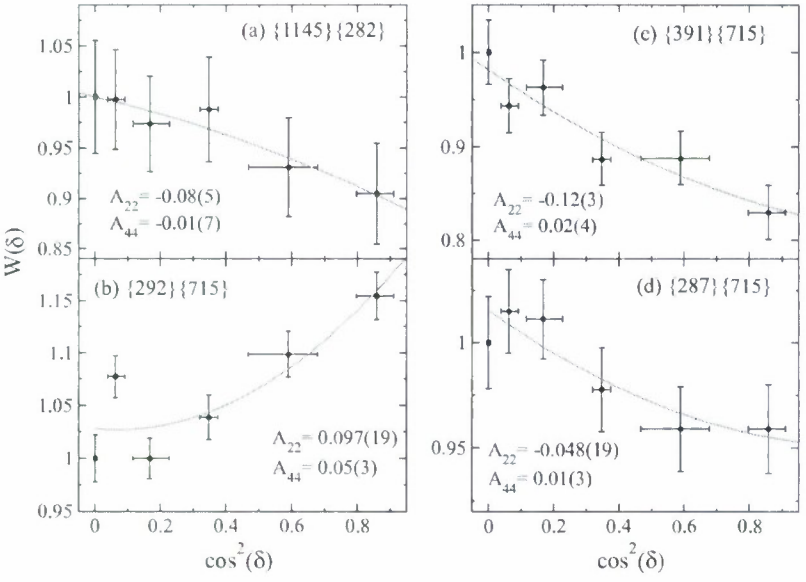

FIG. 3. (Color online) Representative angular correlation measurements for transitions in ^{121}Sb. Information on the γ-γ coincidences (E_x, E_y) involved is provided in each case by $\{x\}\{y\}$.

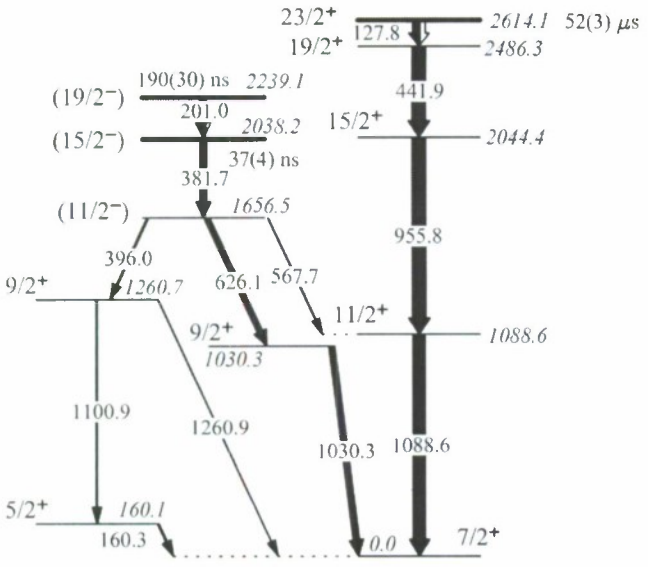

FIG. 4. Level scheme for transitions in ^{123}Sb observed in this experiment from the decay of $T_{1/2} = 190(30)$ ns and 52(3) μs isomers.

V. DISCUSSION

When the levels schemes for ^{121,123}Sb are compared (Figs. 1 and 4, respectively), one observes a number of differences in the distribution and decay of nuclear states. This is due to a combination of the change in quantum number for the respective ground states between ^{121}Sb and ^{123}Sb and the fact that the rotational band built on the $\pi\frac{9}{2}[404]$ intruder state (observed in $^{113-121}$Sb [5–8]) becomes nonyrast in odd-A antimony nuclei with $123 \leqslant A \leqslant 131$. Despite these differences, the multiparticle level structure of these nuclei is well described by considering neutron states in neighboring tin nuclei coupled to the extra proton [11,12].

Figure 7 illustrates a systematic correlation between the yrast states in ^{121,123}Sb and their tin isotones, ^{120,122}Sn. The $I^\pi = 10^+$ state, present in even-tin nuclei from $116 \leqslant A \leqslant 130$, is interpreted as a pure $\nu(h_{\frac{11}{2}})^2$ excitation [12,25]. Similarly, the $I^\pi = \frac{25}{2}^+$ levels in ^{117,119}Sb are associated with a $d_{\frac{5}{2}}$ proton maximally aligned to the $I^\pi = 10^+$ states in the neighboring isotones ^{116,118}Sn [12]. The $I^\pi = (\frac{25}{2}^+)$ spin parity of the isomeric state in ^{121}Sb is systematically consistent with the spin of the isomeric states in ^{117,119}Sb. As such, the configuration of the isomer is adopted tentatively as $\pi d_{\frac{5}{2}} \otimes \nu(h_{\frac{11}{2}})^2$. However, it is noted that because the energy between the $d_{\frac{5}{2}}$ and $g_{\frac{7}{2}}$ proton orbitals is so small (~50 keV [1]), there is likely to be a significant $\pi g_{\frac{7}{2}}$ admixture in the wave function of these states.

It is important to note a limitation with this assessment, based on energy/spin systematics in nearby Sn isotones, because there are large discrepancies between the transition rates in these nuclei: the 197-keV transition in ^{120}Sn (from the $I^\pi = 7^-$ state) is approximately 200 times faster than the analog $E2$ transition in ^{121}Sb (from the $I^\pi = \frac{19}{2}^-$ state), whereas the 163-keV transition in ^{122}Sn (from the $I^\pi = 7^-$ state) is approximately 15 times faster than the 201-keV

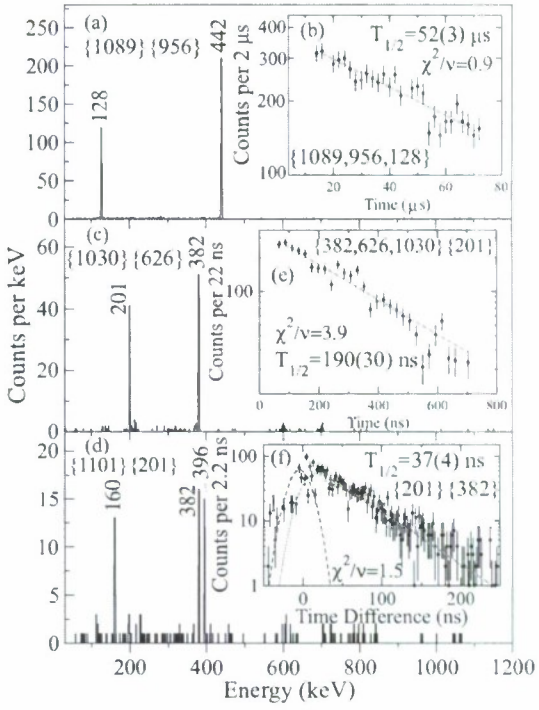

FIG. 5. (Color online) The spectrum in panel (a) illustrates γ rays from the decay of a microsecond isomer in ^{123}Sb. The time evolution of its decay is given in spectrum (b). From double gates on all transitions from its decay, the half-life is measured to be $T_{1/2} = 52(3)$ μs. Double-gated spectra in panels (c) and (d) show γ rays from the decay of an isomer identified in the short-pulsing experiment. The time evolution of its decay is provided in panel (e); the half-life is measured to be $T_{1/2} = 190(30)$ ns using a folded Gaussian plus exponential fit. Spectrum (f) illustrates the γ-ray time difference between the 201-keV transition and those from the decay of states below the isomeric $E_x = 2038.2$ keV state; the half-life is measured to be $T_{1/2} = 37(4)$ ns using a folded Gaussian plus exponential fit. The dashed line is the prompt Gaussian used in the fit [FWHM = 30(3) ns]. Gates for each spectrum are provided in parenthesis ($\{x\}\{y\}$).

transition [from the $I^\pi = (\frac{19}{2}^-)$ state] in ^{123}Sb. On the basis of the current data we are unable to identify the physical origin of such differences; the discrepancies may reflect significant differences in wave function between these states. Given the paucity of an exact theoretical description for these states, such as that provided by shell-model calculations with a physical model space, such assignments should be made with caution. Nevertheless, the correlation between the energies/spins of states in neighboring Sn and Sb nuclei is striking, for which, in the absence of such theoretical examination, it may seem sensible to draw these comparisons.

Shell-model calculations have been performed for ^{127,129,131}Sb and ^{126,128,130}Sn using the model space and Hamiltonian described in Ref. [26], with the shell-model codes OXBASH [27] and ANTOINE [28]. It was not possible to perform calculations for lighter antimony nuclides without severely truncating the model space. Experimental level energies are well reproduced by shell-model calculations, in most cases

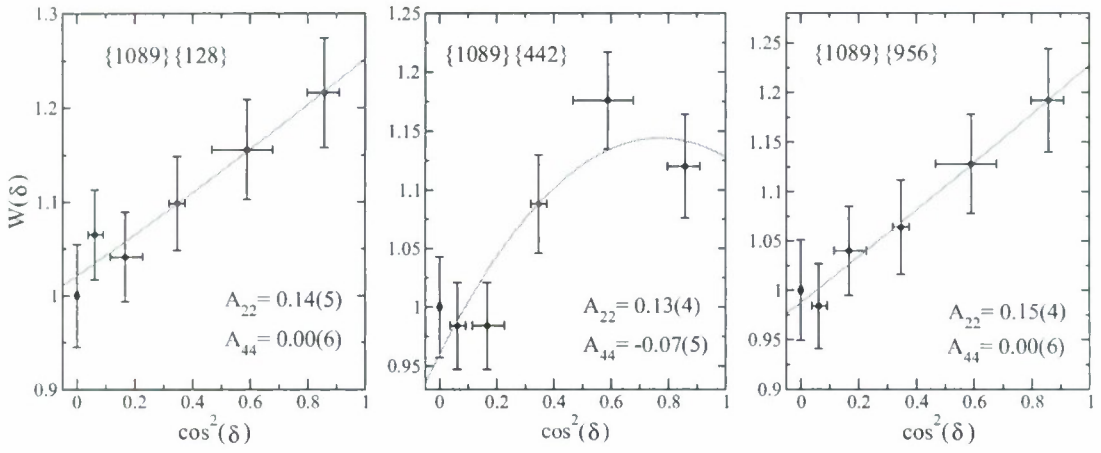

FIG. 6. (Color online) Representative angular correlation measurements for transitions in ^{123}Sb. Information on the γ-γ coincidences (E_x, E_y) involved is provided in each case by $\{x\}\{y\}$.

to within 200 keV. Figure 8 provides a comparison between empirical and calculated energies for the first-excited $I^\pi = \frac{23}{2}^+$, $\frac{19}{2}^-$, and $\frac{15}{2}^-$ states. A noteworthy feature of this plot is the indication of a $I^\pi = \frac{23}{2}^+$ level in ^{127}Sb that has not been observed experimentally, due probably to the paucity of spectroscopic data for this neutron-rich nucleus. The $I^\pi = \frac{23}{2}^+$ isomer in ^{123}Sb is interpreted as the isotopic analog of the states in ^{127,129,131}Sb. The orbital occupation numbers for each of these calculated states is provided in Table V; a leading $\pi g_{\frac{7}{2}} \otimes \nu(h_{\frac{11}{2}})^{-2}$ configuration is associated with the $I^\pi = \frac{23}{2}^+$ states.

The configurations of the 5^- and 7^- levels in even-A tin nuclei involve a neutron in the intruder $h_{\frac{11}{2}}$ orbital, coupled to an even-parity orbital from the $N = 4$ harmonic oscillator shell, with leading neutron configurations of $\nu(h_{11/2} \otimes d_{3/2})$ and $\nu(h_{11/2} \otimes s_{1/2})$, respectively [29]. The $I^\pi = \frac{15}{2}^-$ and

TABLE V. Wave function occupation numbers taken from shell-model calculations discussed in the text.

Nucleus		Occupation numbers						
	I^π	$\nu d_{\frac{5}{2}}$	$\nu g_{\frac{7}{2}}$	$\nu d_{\frac{3}{2}}$	$\nu s_{\frac{1}{2}}$	$\nu h_{\frac{11}{2}}$	$\pi g_{\frac{7}{2}}$	$\pi d_{\frac{5}{2}}$
^{130}Sn	10^+	8.00	6.00	4.00	2.00	10.00		
	7^-	7.99	5.99	3.02	2.00	11.00		
	5^-	7.99	5.98	3.42	1.60	11.00		
^{131}Sb	$\frac{23}{2}^+$	8.00	6.00	4.00	2.00	10.00	0.98	0.01
	$\frac{19}{2}^-$	7.98	5.98	3.05	2.00	11.00	0.99	0.01
	$\frac{15}{2}^-$	7.99	5.99	3.19	1.84	11.00	0.99	0.00
^{128}Sn	10^+	7.87	5.83	3.05	1.74	9.51		
	7^-	7.87	5.83	2.79	1.76	9.76		
	5^-	7.87	5.80	2.85	1.50	9.99		
^{129}Sb	$\frac{23}{2}^+$	7.87	5.82	2.86	1.67	9.78	0.98	0.01
	$\frac{19}{2}^-$	7.85	5.80	2.68	1.64	10.04	0.98	0.01
	$\frac{15}{2}^-$	7.85	5.77	2.59	1.36	10.43	0.98	0.01
^{126}Sn	10^+	7.72	5.66	2.59	1.53	8.50		
	7^-	7.71	5.66	2.40	1.48	8.75		
	5^-	7.71	5.63	2.39	1.32	8.96		
^{127}Sb	$\frac{23}{2}^+$	7.69	5.62	2.47	1.43	8.80	0.98	0.01
	$\frac{19}{2}^-$	7.68	5.63	2.22	1.39	9.08	0.98	0.01
	$\frac{15}{2}^-$	7.69	5.61	2.29	1.18	9.23	0.97	0.01

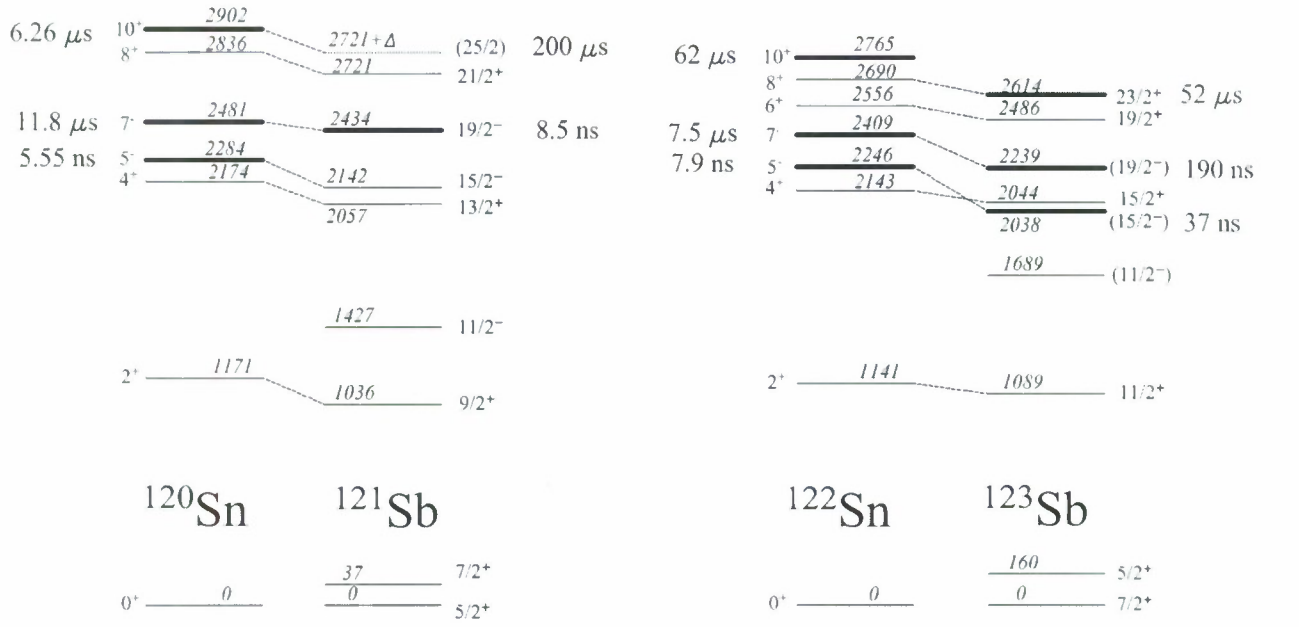

FIG. 7. Comparison of states in ^{121,123}Sb with those in isotonic tin neighbors, ^{120,122}Sn. Levels connected with dashed lines are interpreted as states with the same leading neutron configurations.

$\frac{17}{2}^-$ states in odd antimony nuclei with $113 \leqslant A \leqslant 131$ are associated with these configurations, coupled to a $d_{\frac{5}{2}}$ or $g_{\frac{7}{2}}$ proton [11,12]. Orbital occupation numbers from shell-model calculations (provided in Table V) are consistent with the configuration assignments for these states.

The top panel of Fig. 9 shows the energy of the $I^\pi = 5^-$ and 7^- states in even-A tin nuclei with increasing neutron excess, in comparison to the $I^\pi = \frac{15}{2}^-$ and $\frac{19}{2}^-$ in odd-A antimony nuclei. One can see that the excitation energy of these states steadily decreases with the addition of neutrons. There also appears to be a bifurcation of the antimony and tin state energies, with the antimony states becoming more bound with increasing neutron excess, relative to the corresponding tin states. The bottom panel of Fig. 9 plots the difference in energy between negative-parity states in antimony and tin with the same neutron configuration. A noteworthy feature of this picture is the asymptotic behavior of both plots, which

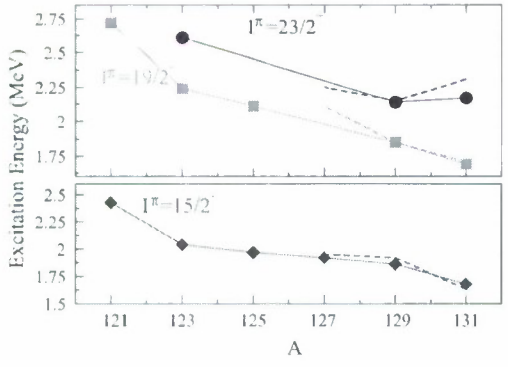

FIG. 8. (Color online) Energy of states from shell-model calculations (dashed lines) compared with those observed empirically from this work and Refs. [12,30,31].

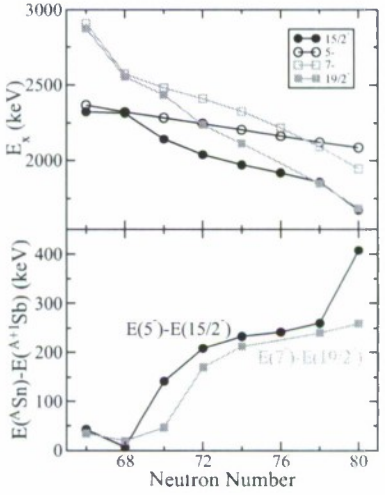

FIG. 9. (Color online) The top panel illustrates the evolution of negative-parity states in antimony and tin nuclei with $N = 66$–80 taken from Refs. [12,30,31]. Open square symbols (red) represent $I^\pi = 7^-$ states in tin nuclei, whereas filled squares (red) show $\frac{19}{2}^-$ states in antimony. Open circle symbols (black) represent $I^\pi = 7^-$ states in tin nuclei, whereas filled circles (black) show $\frac{19}{2}^-$ states in antimony. The bottom panel provides the energy difference between these states; the square symbols (red) show the energy difference between the $I^\pi = 7^-$ (Sn) and $\frac{19}{2}^-$ (Sb) states, whereas circles (black) illustrate the difference between the $I^\pi = 5^-$ (Sn) and $\frac{15}{2}^-$ (Sb) levels.

approach a limit of ~250 keV (excluding the $N = 80$ data point for the $\frac{15}{2}^-/5^-$ energy difference).

The difference in energy between the tin and antimony negative-parity states must derive from the addition of the additional proton, i.e., from the neutron-proton residual interaction. According to Fig. 9, the $I^\pi = \frac{15}{2}^-$ and $\frac{19}{2}^-$ states in odd-antimony nuclei are lowered by up to $E \sim 250$ keV. The occupation numbers for the wave functions of the $I^\pi = \frac{15}{2}^-$ and $\frac{19}{2}^-$ levels in ^{127,129,131}Sb, from Table V, illustrate the dominance of the $\pi g_{\frac{7}{2}}$ orbital. The monopole energy shift of the $\pi g_{\frac{7}{2}}$ level has been interpreted as a signature of a strong tensor force between the $h_{\frac{11}{2}}$ neutron and $g_{\frac{7}{2}}$ proton orbitals with increasing neutron excess in the $\nu h_{\frac{11}{2}}$ subshell [4]. The systematic (~250 keV) energy difference between states in tin and antimony, illustrated in the bottom panel of Fig. 9, is interpreted here as the manifestation of this residual interaction between the $g_{\frac{7}{2}}$ proton and $h_{\frac{11}{2}}$ neutron. In Fig. 9 the energy difference is reduced to almost zero as neutron number approaches $N = 68$, the inversion point of the $g_{\frac{7}{2}}$ and $d_{\frac{5}{2}}$ protons. At this point, the $d_{\frac{5}{2}}$ proton would be expected to have a significant contribution to the wave function of the $I^\pi = \frac{15}{2}^-$ and $\frac{19}{2}^-$ states. The energy difference here thus illustrates a reduction in the residual interaction between the $\nu h_{\frac{11}{2}}$ and $\pi d_{\frac{5}{2}}$ particles indicated in Ref. [4].

VI. SUMMARY

In conclusion, high-spin states have been identified in the stable nuclei, ^{121,123}Sb following fusion-fission reactions between ^{178}Hf and ^{27}Al. Multidimensional γ-ray coincidence techniques have been used to identify a number of previously unreported states, including four isomers. Angular correlation measurements have been used with intensity-balance techniques to identify spins and parities of states in these nuclei. The states observed in these nuclei are interpreted as multiparticle states formed from the coupling of a $d_{\frac{5}{2}}$ or $g_{\frac{7}{2}}$ proton with $\nu h_{\frac{11}{2}}$, $\nu s_{\frac{1}{2}}$, and $\nu d_{\frac{3}{2}}$ excitations, observed in neighboring tin nuclei.

The energies of negative-parity states have been compared in tin and antimony nuclei. The difference in these energies has been interpreted as the manifestation of the proton-neutron residual interaction, recently associated with a strong tensor force.

Shell-model calculations have been performed for ^{126,128,130}Sn and ^{127,129,131}Sb. The calculated excitation energies of states in these nuclei compare favorably with those observed empirically and predict the existence of a low-lying $I^\pi = \frac{23}{2}^+$ state in ^{127}Sb. Using systematic arguments, a $I^\pi = \frac{23}{2}^+$ state is also expected in ^{125}Sb, as the isotopic analog of $I^\pi = \frac{23}{2}^+$ states in odd-A antimony nuclei from $123 \leqslant A \leqslant 131$.

Shell-model calculations provide an accurate description for excited states around the "doubly magic" ^{132}Sn core. However, as the number of valence particles/holes increases, the resources required to perform such calculations increases exponentially. The spectroscopic results obtained in this work have contributed to the data available for $Z = 51$ nuclei between stability and the closed-shell at $N = 82$ and provide an empirical benchmark for which to test the development of these theoretical descriptions.

ACKNOWLEDGMENTS

The author acknowledges helpful discussions with R. Orlandi, B. A. Brown, and P. H. Regan. This work is supported by the US Department of Energy, Office of Nuclear Physics, under contract number DE-AC02-06CH11357 (ANL); US AFOSR under contract number F49620-02-1-0187; the AWE (UK); and the EPSRC (UK).

[1] M.-G. Porquet, S. Peru, and M. Girod, Eur. Phys. J. A **25**, 319 (2005).
[2] J. P. Schiffer, S. J. Freeman, J. A. Caggiano, C. Deibel, A. Heinz, C.-L. Jiang, R. Lewis, A. Parikh, P. D. Parker, K. E. Rehm, S. Sinha, and J. S. Thomas, Phys. Rev. Lett. **92**, 162501 (2004).
[3] R. B. Firestone and V. S. Shirley, *Table of Isotopes*, 8th ed. (Wiley, New York, 1996).
[4] T. Otsuka, T. Matsuo, and D. Abe, Phys. Rev. Lett. **97**, 162501 (2006).
[5] D. R. LaFosse, D. B. Fossan, J. R. Hughes, Y. Liang, H. Schnare, P. Vaska, M. P. Waring, and J.-Y. Zhang, Phys. Rev. C **56**, 760 (1997).
[6] C.-B. Moon, C. S. Lee, J. C. Kim, J. H. Ha, T. Komatsubara, T. Shizuma, K. Uchiyama, K. Matsuura, M. Murasaki, Y. Sasaki, H. Takahashi, Y. Tokita, and K. Furuno, Phys. Rev. C **58**, 1833 (1998).
[7] R. S. Chakrawarthy and R. G. Pillay, Phys. Rev. C **54**, 2319 (1996).
[8] W. F. Piel, Jr., P. Chowdhury, U. Garg, M. A. Quader, P. M. Stwertka, S. Vajda, and D. B. Fossan, Phys. Rev. C **31**, 456 (1985).
[9] M. Conjeaud, S. Harar, M. Caballero, and N. Cindro, Nucl. Phys. **A215**, 383 (1973).
[10] K. Heyde, Phys. Rep. **102**, 291 (1983).
[11] M.-G. Porquet, Ts. Venkova, R. Lucas, A. Astier, A. Bauchet, I. Deloncle, A. Prevost, F. Azaiez, G. Barreau, A. Bogachev, N. Buforn, A. Buta, D. Curien, T. P. Doan, L. Donadille, O. Dorvaux, G. Duchene, J. Durell, Th. Ethvignot, B. P. J. Gall, D. Grimwood, M. Houry, F. Khalfallah, W. Korten, S. Lalkovski, Y. Le Coz, M. Meyer, A. Minkova, I. Piqueras, N. Redon, A. Roach, M. Rousseau, N. Schulz, A. G. Smith, O. Stezowski, Ch. Theisen, and B. J. Varley, Eur. Phys. J. A **24**, 39 (2005).
[12] S. Lunardi, P. J. Daly, F. Soramel, C. Signorini, B. Fornal, G. Fortuna, A. M. Stefanini, R. Broda, W. Meczynski, and J. Blomqvist, Z. Phys. A **328**, 487 (1987).
[13] G. A. Jones, Ph.D. thesis, University of Surrey, 2006.
[14] I-Y. Lee, Nucl. Phys. **A520**, 641c (1990).
[15] W. Urban *Ana Software* (private communication).
[16] D. Radford, Nucl. Instrum. Methods A **361**, 297 (1995).
[17] D. Radford, Nucl. Instrum. Methods A **361**, 306 (1995).
[18] B. Fornal, S. Zhu, R. V. F. Janssens, M. Honma, R. Broda, B. A. Brown, M. P. Carpenter, S. J. Freeman, N. Hammond,

F. G. Kondev, W. Krolas, T. Lauritsen, S. N. Liddick, C. J. Lister, S. Lunardi, P. F. Mantica, N. Marginean, T. Mizusaki, E. F. Moore, T. Otsuka, T. Pawlat, D. Seweryniak, B. E. Tomlin, C. A. Ur, I. Wiedenhover, and J. Wrzesinski, Phys. Rev. C **72**, 044315 (2005).

[19] G. D. Dracoulis, G. J. Lane, F. G. Kondev, A. P. Byrne, T. Kibedi, H. Watanabe, I. Ahmad, M. P. Carpenter, S. J. Freeman, R. V. F. Janssens, N. J. Hammond, T. Lauritsen, C. J. Lister, G. Mukherjee, D. Seweryniak, P. Chowdhury, and S. K. Tandel, Phys. Rev. C **71**, 044326 (2005).

[20] T. Tamura, Nucl. Data Sheets **90**, 107 (2000).

[21] P. Endt, At. Data Nucl. Data Tables **26**, 47 (1981).

[22] F. Rosel, H. M. Fries, K. Alder, and H. C. Pauli, At. Nucl. Data Tables **21**, 91 (1978).

[23] S. Ohya and K. Kitao, Nucl. Data Sheets **89**, 345 (2000).

[24] S. Ohya, Nucl. Data Sheets **102**, 547 (2004).

[25] R. Broda, R. H. Mayer, I. G. Bearden, Ph. Benet, P. J. Daly, Z. W. Grabowski, M. P. Carpenter, R. V. F. Janssens, T. L. Khoo, T. Lauritsen, E. F. Moore, S. Lunardi, and J. Blomqvist, Phys. Rev. Lett. **68**, 1671 (1992).

[26] B. A. Brown, N. J. Stone, J. R. Stone, I. S. Towner, and M. Hjorth-Jensen, Phys. Rev. C **71**, 044317 (2005); Erratum-*ibid.* **72**, 029901(E) (2005).

[27] B. A. Brown, A. Etchegoyen, N. S. Godwin, W. D. M. Rae, W. A. Richter, W. E. Ormand, E. K. Warburton, J. S. Winfield, L. Zhao, and C. H. Zimmerman, MSU-NSCL report number 1289 (2004).

[28] E. Caurier and E. Nowacki, Acta Phys. Pol. B **30**, 705 (1999).

[29] K. Krien, B. Klemme, R. Folle, and E. Bodenstedt, Nucl. Phys. **A228**, 15 (1974).

[30] J. A. Pinston and J. Genevey, J. Phys. G **30**, R57 (2004).

[31] D. S. Judson, A. M. Bruce, M. J. Taylor, G. D. Dracoulis, T. Kibedi, A. P. Byrne, K. H. Maier, P. Nieminen, and J. N. Orce, J. Phys. G **31**, S1899 (2005).

APPENDIX B

PLENARY AND INVITED PRESENTATIONS DURING GRANT PERIOD

"Nuclear structure, induced depletion of isomers and the gamma-ray laser," Peking University, China June 9, 2006. **INVITED**

"Nuclear structure and the search for induced energy release from metastable isomers," International Conference on Frontiers of Nuclear Structure (NS 2006), Shanghai, China, June 12 – 17, 2006. **INVITED**

"Induced energy release from nuclear isomers and the role of nuclear structure," Coherent Control of Fundamental Processes in Optics and X-ray Optics, Nizhny Novgorod, Russia, June 29 – July 3, 2006. **PLENARY**

"Nuclear structure and the search for induced energy release from isomers," Conference on the Application of Accelerators in Research and Industry (CAARI) 2006, Ft. Worth, Texas, August 20 – 25, 2006. **INVITED**

"Basic research and induced depletion of isomers," Defense Threat Reduction Agency, Ft. Belvoir, Virginia, December 12, 2006. **INVITED**

"Studies of nuclear isomer depletion," Winter Colloquium on the Physics of Quantum Electronics, Snowbird, Utah, January 2 – 6, 2007. **PLENARY**

"Photon-induced isomer depletion," Workshop on Next Generation Isomers, Institute of Physics Division meeting on Nuclear and High-Energy Physics, University of Surrey, U. K., April 2 – 5, 2007. **INVITED**

"Everything you wanted to know about nuclear isomers, but were afraid to ask," Science and Engineering Apprentice Program, Army Research Laboratory, Adelphi, Maryland, July 26, 2007. **INVITED**

"Status of research into isomer depletion reactions," Spring 2008 Meeting of the Deutsche Physikalische Gesellschaft, Darmstadt, Germany, March 10 – 14, 2008. **PLENARY**

APPENDIX C

CONTRIBUTED PRESENTATIONS DURING GRANT PERIOD

"Initial search for triggered energy release from ," American Physical Society, Division of Nuclear Physics Fall Meeting, Kapalua, Hawaii, September 18 – 22, 2005.

"Tests of photon-induced depletion of via (γ, γ') reactions," Nuclear Structure: New pictures in the extended isospin space, Kyoto, Japan, June 11 – 14, 2007.